BERICHTE
aus dem Fachbereich Geowissenschaften
der Universität Bremen

No. 261

Bohrmann, G., T. Pape, and cruise participants

REPORT AND PRELIMINARY RESULTS OF R/V METEOR CRUISE M72/3, ISTANBUL – TRABZON – ISTANBUL, 17 MARCH – 23 APRIL, 2007.

MARINE GAS HYDRATES OF THE EASTERN BLACK SEA.

Berichte, Fachbereich Geowissenschaften, Universität Bremen, No. 261, 176 pages, Bremen 2007

ISSN 0931-0800

The "Berichte aus dem Fachbereich Geowissenschaften" are produced at irregular intervals by the Department of Geosciences, Bremen University.

They serve for the publication of experimental works, Ph.D.-theses and scientific contributions made by members of the department.

Reports can be ordered from:

Monika Bachur

Forschungszentrum Ozeanränder, RCOM

Universität Bremen

Postfach 330 440

D 28334 BREMEN

Phone: (49) 421 218-65516

Fax: (49) 421 218-65515

e-mail: MBachur@uni-bremen.de

Citation:

Bohrmann, G., T. Pape, and cruise participants
Report and preliminary results of R/V METEOR Cruise M72/3, Istanbul – Trabzon – Istanbul,
17 March – 23 April, 2007. Marine gas hydrates of the Eastern Black Sea.
Berichte, Fachbereich Geowissenschaften, Universität Bremen, No. 261, 176 pages. Bremen, 2007.

ISSN 0931-0800

R/V METEOR
Cruise Report M72/3

Marine gas hydrates of the Eastern Black Sea

M72, Leg 3a
Istanbul – Trabzon, 17 March – 3 April, 2007

M72, Leg 3b
Trabzon – Istanbul, 3 – 23 April, 2007

Cruise within the framework of the BMBF/DFG
special programme GEOTECHNOLOGIEN:
"METRO – Methane and methane hydrates within the Black Sea: Structural analyses, quantification and impact of a dynamic methane reservoir"

Edited by

Gerhard Bohrmann and Thomas Pape

with contributions of cruise participants

The cruise was performed by
the Research Center Ocean Margins, University of Bremen, Germany

Universität Bremen

rcom bremen
research center ocean margins

R/V METEOR Cruise Report M72/3

Table of contents

Appendix

PREFACE

Starting the journey from Istanbul, Turkey on 17 March, R/V METEOR was scheduled for interdisciplinary work on gas hydrates in the Black Sea. During the first leg, the ship operated in two areas named the Sorokin Trough in Ukraine and the Gurian Trough in the Exclusive Economic Zone (EEZ) of Georgia. After a mid-leg stop in the harbour of Trabzon, Turkey on 3/4 April, the research vessel started the second leg again in Georgian waters (Fig. 1). Research work was performed in the southwestern part of Gudauta Ridge southwest of Suchumi followed by activities on Kobuleti Ridge in the Gurian Trough area (Fig. 1) west of Batumi and Poti. On the way to the Sorokin Trough, seep exploration was conducted on the deeper part of Andrusov Ridge in Turkish waters. Final research activities in Ukrainian waters were focused on Dvurechenskii mud volcano and the southwestern continental margin of the Kerch Strait (Fig. 1). The research cruise ended on 23 April in the harbour of Istanbul.

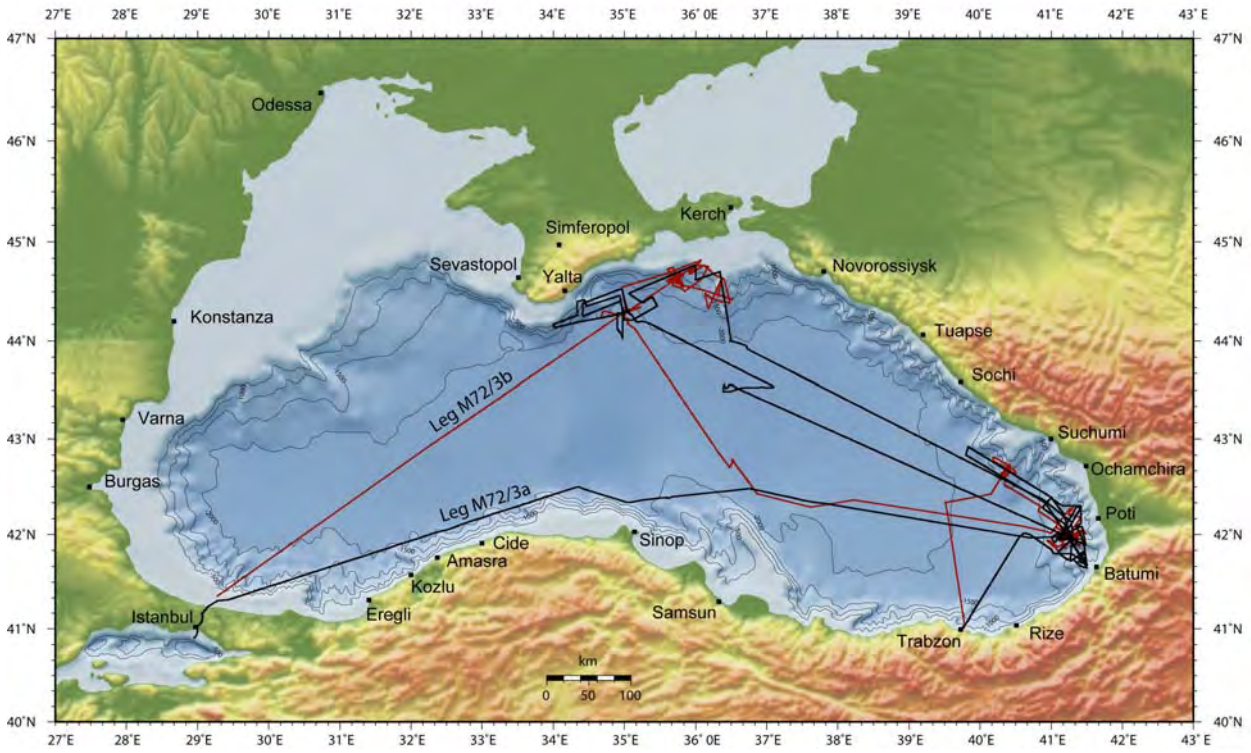

Fig. 1: Cruise track of R/V METEOR cruise M72/3.

The overarching goal of the research activities during Legs M72/3a and 3b was a better understanding of the distribution and dynamics of methane and gas hydrates in sediments of the Black Sea, as well as the origin of methane and its fluxes from the sediment to the water column. The main focus was laid on the gas hydrate transition zone, i.e. in water depths of about 750 m and deeper, where the boundary of the methane hydrate stability field and the sea floor overlap. However, the results of pre-examinations demonstrated that gas hydrates might even develop in sediments of mud volcanoes in the deep Black Sea very close to the gas hydrate stability curve, since elevated heat fluxes and the presence of relatively saline waters lead to a shift of the gas hydrate stability field.

The main program that had been set up was the BMBF joint project METRO, “Methane and methane hydrates within the Black Sea: Structural analyses, quantification and impact of a dynamic methane reservoir”, funded in the framework of the special programme ‘Geotechnologies’ within the subject area

'Methane in the geo-/biosystem'. The project METRO is also embedded in the German-Russian agreement on 'Co-operations on the realm of marine and polar research'. The activities of MARGASCH II are based on former expeditions with R/V POSEIDON P317/4 and R/V PROFESSOR LOGACHEV TTR-15 in 2004 and 2005, respectively, and represent the terminal phase of data acquisition.

Fig. 2: Research vessel METEOR. View from outside (*left*) and view from the bridge to the working deck (*right*).

R/V METEOR cruise M72/3 was a highly interdisciplinary approach which brought together an international group of scientists from institutions within Germany and countries around the Black Sea (Turkey, Ukraine, Georgia, Russia). The cruise and research programme were planned, coordinated, and carried out by the Earth Sciences Department and the DFG-Research Center Ocean Margins at University of Bremen. Detailed knowledge on local distribution and behaviour of the seeps was contributed by Prof. Michael K. Ivanov and his group from Moscow State University. The German embassies in Tbilisi, Ankara and Kiev and the Ministry of Foreign Affairs in Berlin helped in obtaining the permissions necessary to work in Georgian, Turkish and Ukrainian waters of the Black Sea. Thanks to all of them.

Fig. 3: Images taken during R/V METEOR cruise M72/3 in the Black Sea: ROV "QUEST4000m" on the working deck during a pre-dive check before deployment (left), CT-laboratory (right).

The cruise was financed in Germany by the German Federal Ministery of Education and Science (Bundesministerium für Bildung und Forschung, BMBF; grant 03G0604A)) and by the German Research Foundation (DFG). The shipping operator (Reederei F. Laeisz GmbH, Bremerhaven) provided technical support on the vessel in order to accommodate the large variety of technical challenges required for the complex sea-going operations. We would like to especially acknowledge both masters of the vessel,

Niels Jakobi and Uwe Pahl, and her crew for their continued contribution to a pleasant and professional atmosphere aboard R/V METEOR.


Fig. 3, continuation: Positioning of the multichannel seismic streamer (*left*); maintenance of the Dynamic Autoclave Piston Corers (*right*).

Personel aboard R/V METEOR M72/3

Table 1: Scientific crew.

Name	Working group	Affiliation	Participation
Friedrich Abegg	Autoclave team	RCOM, Bremen	Leg 3b
Sarah Althoff	Hydroacoustic team	RCOM, Bremen	Leg 3a & b
Yuriy G. Artemov	Hydroacoustic team	IBSS, Sevastopol	Leg 3a & b
Marlene Bausch	Geochemical team	RCOM, Bremen	Leg 3b
André Bahr	Geology team	NIOZ, Texel	Leg 3b
Gerhard Bohrmann	Chief scientist	RCOM, Bremen	Leg 3a & b
Anke Bleyer	Geochemistry team	IFM-GEOMAR, Kiel	Leg 3b
Markus Brüning	Hydroacoustic team	RCOM, Bremen	Leg 3a & b
Baris Bozkaya	Geochemistry team	TPAO, Ankara	Leg 3a
Steven Bucklew	ROV team	CSSF, Sidney,	Leg 3a
Klaus Dehning	Autoclave team	MARUM, Bremen	Leg 3b
Bettina Domeyer	Geochemistry team	IFM-GEOMAR, Kiel	Leg 3b
Noemi Fekete	Seismic team	RCOM, Bremen	Leg 3b
Phillip Franke	ROV team	MARUM, Bremen	Leg 3a
Sascha Fricke	Seismic team	RCOM, Bremen	Leg 3b
Phillip Forte	ROV team	WHOI, USA	Leg 3a
Kornelia Gräf	Autoclave team	RCOM, Bremen	Leg 3b
Hasan Güney	Seismic team	TPAO, Ankara, Turkey	Leg 3b
Savas Gürcay	Hydroacoustic team	TPAO, Ankara	Leg 3b
Gregor von Halem	Autoclave team	RCOM, Bremen	Leg 3a & b
Hans-Jürgen Hohnberg	Autoclave team	RCOM, Bremen	Leg 3a & b
Daniel Hüttich	ROV team	MARUM, Bremen	Leg 3a
Bettina Domeyer	Geochemistry team	IFM-GEOMAR, Kiel	Leg 3b
Deniz Karaca	Geochemistry team	IFM-GEOMAR, Kiel	Leg 3a
Stephan A. Klapp	Geology team	RCOM, Bremen	Leg 3a & b

Table 1, continuation: Scientific crew.

Name	Working group	Affiliation	Participation
Hanno Keil	Seismic team	RCOM, Bremen	Leg 3b
Ingo Klaucke	Sidescan sonar team	IFM-GEOMAR, Kiel	Leg 3b
Elena Kozlova	Sedimentology team	MSU, Moscow	Leg 3a
Stephanie Kusch	Geochemistry team	AWI, Bremerhaven	Leg 3b
Anh Hoang Mai	Autoclave team	MARUM, Bremen	Leg 3a
Vasileios Mavromatis	Geochemistry team	IFM-GEOMAR, Kiel	Leg 3a
Aneta Nikolovska	Hydroacoustic team	RCOM, Bremen	Leg 3a
Thomas Pape	Geochemistry team	RCOM, Bremen	Leg 3a & b
Benedikt Preu	Seismic team	RCOM, Bremen	Leg 3b
Janet Rethemeyer	Geochemistry team	AWI, Bremerhaven	Leg 3a
Michael Reuter	ROV team	MARUM, Bremen	Leg 3a
Heiko Sahling	ROV mapping	RCOM, Bremen	Leg 3a
F. Schmidt-Schierhorn	Geology team	RCOM, Bremen	Leg 3a
Thorsten Schott	Sidescan sonar team	OKTOPUS	Leg 3b
Florian Scholz	Geochemistry team	IFM-GEOMAR, Kiel	Leg 3a
Shouye Yang	Hydroacoustic team	TJU, Shanghai	Leg 3b
Christian Seiter	ROV team	MARUM, Bremen	Leg 3a
Volkhard Spiess	Seismic team	RCOM, Bremen	Leg 3b
Regina Surberg	Geochemistry team	IFM-GEOMAR, Kiel	Leg 3b
Klaus Wallmann	Geochemistry team	IFM-GEOMAR, Kiel	Leg 3a
Marcel Zarrouk	ROV team	MARUM, Bremen	Leg 3a
Anna Zotova	Hydroacoustic team	MSU, Moscow	Leg 3b
Beka Zebedashvilli	Hydroacoustic team	TSU, Tbilisi, Georgia	Leg 3b

Fig. 4: Groups of scientists and technicians sailed during Legs M72/3a (*left*) and M72/3b (*right*).

Participating institutions

AWI	Alfred-Wegener-Institut für Polar- und Meeresforschung, 27570 Bremerhaven, **Germany**
CSSF	Canadian Scientific Submersible Facility, Sidney, **Canada**
DEU	Dokuz Eylul University, Depart. of Geophysics and Institute of Marine Sciences and Technology, Baku Bulvari No. 32, 35340 Izmir, **Turkey**

DWD	Deutscher Wetterdienst, Geschäftsfeld Seeschiffahrt, Bernhard-Nocht-Straße 76, 20359 Hamburg, **Germany**
IBSS	A. O. Kovalevsky Institute of Biology of the Southern Seas, Ukrainian Academy of Scienes, 2 Nakhimov Av., 99011 Sevastopol, **Ukraine**
IFM-GEOMAR	Leibniz-Institut für Meeresforschung an der Christian-Albrechts-Universität, Wischhofstr. 1-3, 24148 Kiel, **Germany**
MSU	Geology and geochemistry of fuel minerals, Geological faculty Moscow State University, Vorobjevy Crory, Moscow, **Russia**
NIOZ	Royal Netherlands Institute for Sea Research P.O.Box 59, 1790 AB Den Burg, Texel, **The Netherlands**
OKTOPUS	Oktopus GmbH, Kieler Str. 51, 24594 Hohenweststedt, **Germany**
TJU	Tongji University, State key laboratory of marine geology. Shanghai 200092, **China**
TPAO	Turkish Petroleum Company, Exploration Group, Mustafa Kemal Mah. 2.cad. No: 86, 06520 Ankera, **Turkey**
TSU	Faculty of Geography, Seismometrical Laboratory, Tbilisi State University, Chavchavadeze str. 1, Tbilisi, **Georgia**
RCOM/MARUM	MARUM / DFG-Forschungszentrum Ozeanränder University of Bremen, Postfach 30440, 28334 Bremen, **Germany**
WHOI	Woods Hole Oceanographic Institutions, Woods Hole, MA 02543-1050, **USA**

Table 2: Crew members onboard R/V METEOR.

Name	Work onboard	Name	Work onboard
Niels Jakobi	Master	Volker Hartig	Chief Engineer
Uwe-Klaus Klimeck	Officer	Uwe Schade	Engineer
Thomas Wunderlich	Officer	Ralf Heitzer	Engineer
Stefan Räbisch	Officer	Rudolf Freitag	Electrician
Jörg Walter	Chief Electronics	Joachim Stenzler	Fitter
Olaf Willms	Electronics	Carsten Heitmann	Motorman
Katja Pfeiffer	System operator	Frank Sebastian	Motorman
Alexander Ruhtke	Surgeon	Uwe Szych	Motorman
Uwe Pahl	Master	Michael Both	Chief steward
Eugen Müller	Meteorologist	Rainer Götze	Steward
Thorsten Truscheit	Weather technician	Jan Hoppe	Steward
Peter Hadamek	Boatswain	Peter Eller	Steward
Kai Rabenhorst	Seaman	Franz Grün	Chief cook
Bernd Neitzsch	Seaman	Willy Braatz	Cook
Matthias Pomplun	Seaman	Seng-Choon Ong	Launderer
Björn Pauli	Seaman	Robin Fischer	Trainee
Günther Stänger	Seaman	Hartmut Guse	Seaman
Günther Ventz	Seaman	Wolf-Thilo Ochsenhirt	Weather technician
Jonathan Gröhnke	Trainee	Alexander Reuss	Trainee

Participating companies

Reederei F. Laeisz GmbH	"Haus der Schiffahrt", Lange Straße 1a, D-18055 Rostock, **Germany**
FIELAX	Gesellschaft für wissenschaftliche Datenverarbeitung mbH, Schifferstrasse 10 – 14, 27568 Bremerhaven, **Germany**

1 Introduction and geological background

(G. Bohrmann)

1.1 Objectives

Methane is twenty times more effective as a greenhouse gas than CO_2, however, its concentration within the atmosphere is much smaller. In contrast, methane generated by microbial decay and thermogenic breakdown of organic matter seems to be a large pool in geological reservoirs. Numerous features such as shallow gas accumulations, pockmarks, seeps, and mud volcanoes are present in a wide variety of oceanographic and geological environments (Judd, 2003). Release and uptake of methane by such sources may provide positive and negative feedback to global warming and/or cooling and are therefore focal points of current research (Kvenvolden, 1998).

Studying methane emission sites will elucidate how stable these reservoirs are and how the pathways to the atmosphere are working. Because of their high methane density, gas hydrates are of special interest, when they occur close to the seafloor. Previous investigations have shown that hydrates generate extremely high and variable fluxes of methane to the overlying water column due to their exposed position close to the sediment/water interface. Not only do they influence their immediate environment, but they may also contribute substantially to the transfer of methane to the atmosphere.

Shallow gas hydrates, potentially associated with free gas, are known from sediments in several areas and are of specific interest in the Black Sea where a large number of active methane emission sites exist. New investigations on mud volcanoes have shown that even deep at the stability field in 2,000 m depth hydrates are very close to their stability limit and may serve as emission sites (Bohrmann et al., 2003). Most of the few studies dealing with this phenomenon were made without using appropriate pressurized sampling techniques and are therefore of limited value. Because of the sensitivity of gas hydrate stability and the connection of methane to environmental change, pressurized autoclave sampling technology and investigations and experiments under *in situ* conditions are essential for constraining the potential of environmental hazards from methane in sediments. The technical application of the autoclave tools was performed to better understand the dynamics of gas and gas hydrates within the Black Sea. Furthering our understanding using the autoclave technology was the focus of this cruise and this aided several subprojects in accomplishing their specific research objectives.

The focus of the METRO program is to investigate near-surface methane and methane hydrates in the Black Sea in order to understand their origin, structure, and behavior as well as their interaction with the sedimentary and oceanic environment. This is critical for evaluating and quantifying their importance in the global carbon cycle. Research activities of METRO are concentrated in the Black Sea for various reasons. It is the largest anoxic basin with much higher methane concentrations than in any other marginal sea. Sediments of 10-19 km thickness reveal a large potential reservoir for methane generation and hundreds of methane emission sites are known from water column investigations performed by our Russian and Ukrainian colleagues. In addition, fluid venting, active mud volcanoes pockmarks, and gas-bearing sediments have been discovered and reported in the literature (Ivanov et al., 1998; Bouriak and Akhmezjanov, 1998). It was in the Black Sea and Caspian Sea that samples of gas hydrates were first recovered from marine sediments (Yefremova and Zhizchenko, 1974). Based on the stability field of methane hydrate, areas deeper than 750 m water depth are of particular interest.

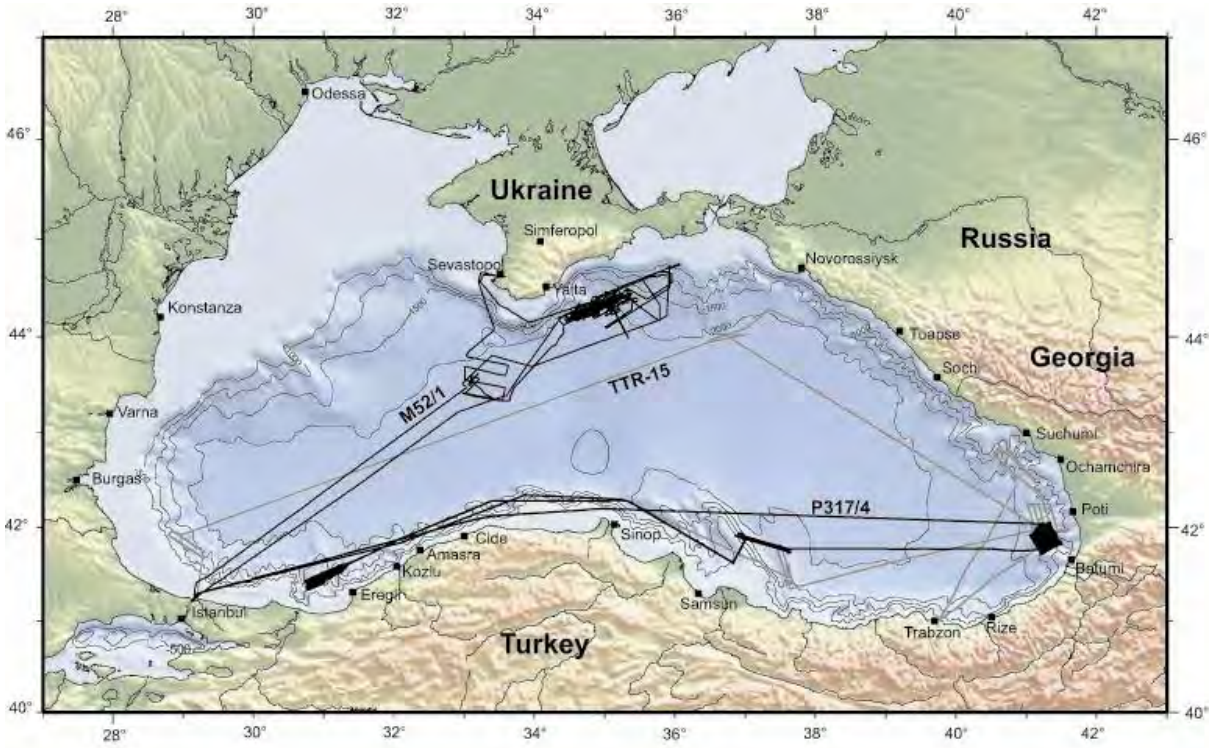

Fig. 5: Black Sea map with track lines of former gas hydrate cruises R/V METEOR M52/1, R/V POSEIDON cruise P317/4 and R/V PROFESSOR LOGACHEV cruise TTR-15.

R/V METEOR cruise M72/3 followed several other research cruises (Fig. 5) to the Black Sea conducted over the course of the last couple of years and it was the last cruise within the BMBF initiatives OMEGA and METRO. Using different techniques of seafloor mapping (multibeam bathymetry, deep-towed sidescan sonar, and video observation), the aim of the METRO project was to identify and map various facies and environments that are related to near-surface gas hydrates and methane seeps off the coast of Georgia, Ukraine, Russia, and Turkey. Besides the need for quantification of the total amount of methane bound in gas hydrates, it is important to determine the portion of gas hydrates and free gas that are reactive. Hydrates occur in the subseafloor from several tens of meters below the sediment surface down to the base of the methane hydrate stability field, which is reached around 500 m sediment depth in the deep Black Sea area (Bohrmann et al.; 2003). Gas released from the seafloor or hydrate outcrops are known from a few locations, where they may interact with the ocean or even reach the atmosphere in the form of gas bubbles. The determination of the extent of these 'reactive' locations and understanding their formation is crucial in assessing the potential impact of gas hydrates and their dissociation on the isotopic chemistry of the ocean and on climate.

Previously, mud volcanoes in the central part of the Black Sea and the Sorokin Trough were investigated during R/V METEOR cruise M52/1 (MARGASCH I, January 2002). In addition, other seeps, like gas and oil seeps in various geological settings, were investigated in the Gurian Trough area (Sahling et al., 2004, Klaucke et al., 2005; Akhmetzhanov et al., 2007). During METRO-cruises we used pressurized sampling techniques and remotely operated vehicles (ROVs). Since gas hydrates react rapidly to changes in pressure and temperature, pressurized autoclave sampling technology, and investigations and experiments under *in situ* conditions are essential. Beside the Ocean Drilling Program, the technical development of these capabilities were first shown by the former project OMEGA and the applications of the autoclave technology greatly improved the understanding of gas hydrate dynamics (Abegg et al., 2003).

Because the Black Sea water is anoxic at ~ 100 m below sea level, seep sites below that water depth show no colonization by chemosynthetic clams or tube worms because of the lack of oxygen, which these organisms need for their symbiotic metabolism with bacteria. Other seep manifestations that help to identify active venting are bacterial mats and carbonate buildups (Fig. 6, right), which form at seep sites because of increased rates of anaerobic methane oxidation (Michaelis et al., 2002).

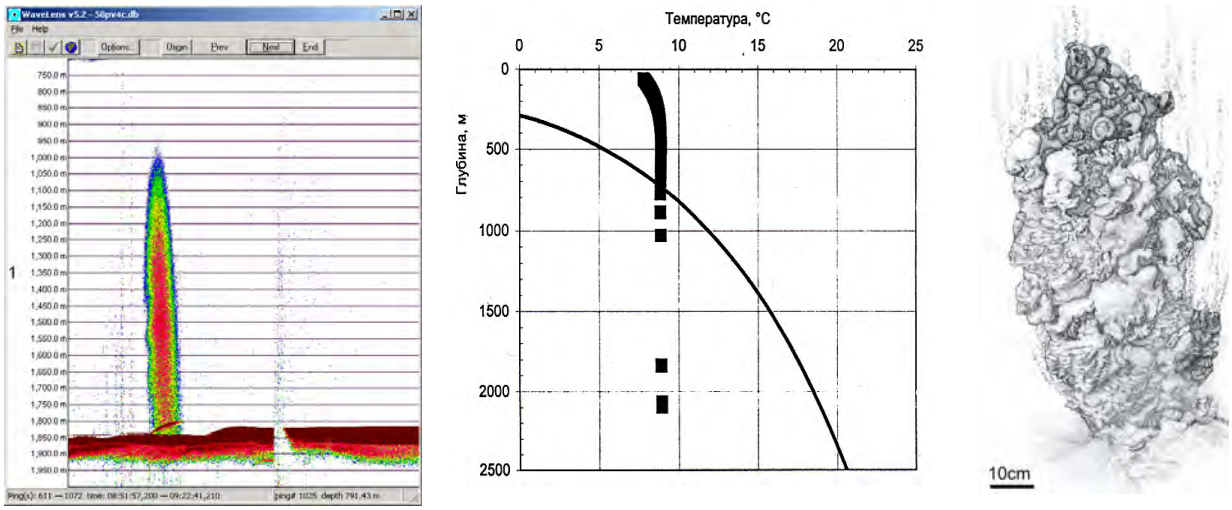

Fig. 6: Acoustic image from a gas bubble stream located in the Black Sea abyssal plain (*left*); depth locations of gas flares detected and methane hydrate stability field in the Black Sea (*middle*; from Egorov et al., 2003); metre-sized carbonate tower grown on a gas bubble site in the GHOSTABS-field (*right*; from Reitner et al., 2005).

During the last few years, gas bubble emanating from the seafloor were increasingly observed predominately in shallow water areas like the GHOSTABS-field in the Dneper paleo-delta (Artemov et al., 2007). Free-gas releasing seeps were typically identified by hydroacoustic plumes in the water column that show strong backscatter signals with flare-like shapes detected by single-beam echosounders (Fig. 6, left). Those flares are often rooted at the seafloor where the gas seeps from the sediment deposits (Artemov et al., 2007).

1.2 Black Sea overview

The Black Sea is located north of Turkey and south of Ukraine and Russia. To the west it is bordered by Romania and Bulgaria and to the east by Georgia. It is a marginal ocean with a water depth of 2-2.2 km. The Black Sea is surrounded by Cenozoic mountain belts like the Great Caucasus, the Pontides, and the Balkanides (Fig. 8; Robinson, 1997). Two deep basins, the western and eastern Black Sea basins, are underlain by oceanic or thinned continental crust with a sediment cover of 10-19 km thickness (Tugolesov et al., 1985).

The basins are separated by the Andrusov Ridge which is formed from continental crust and overlain by only 5-6 km of sediment. The origin of the Black Sea is interpreted as a back-arc basin evolved during late Cretaceous times (Nikishin et al., 2003).

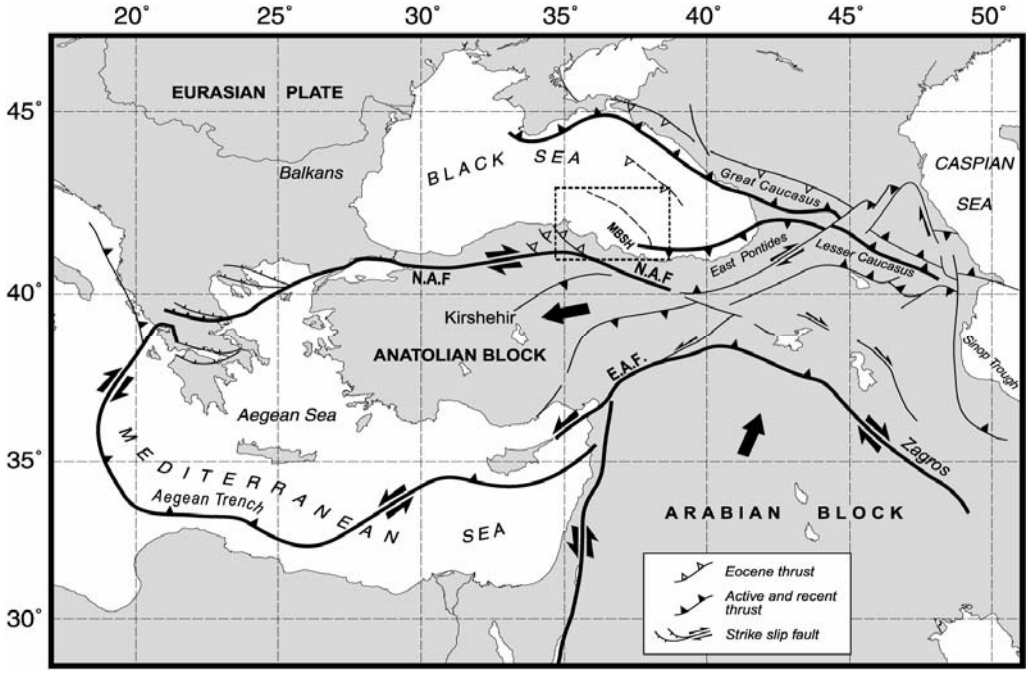

Fig. 7: Simplified tectonic map of the Arabia/Eurasia collision zone (from Rangin et al., 2002). The Eastern Black Sea Basin is located directly north of the tectonic escape of Anatolia.

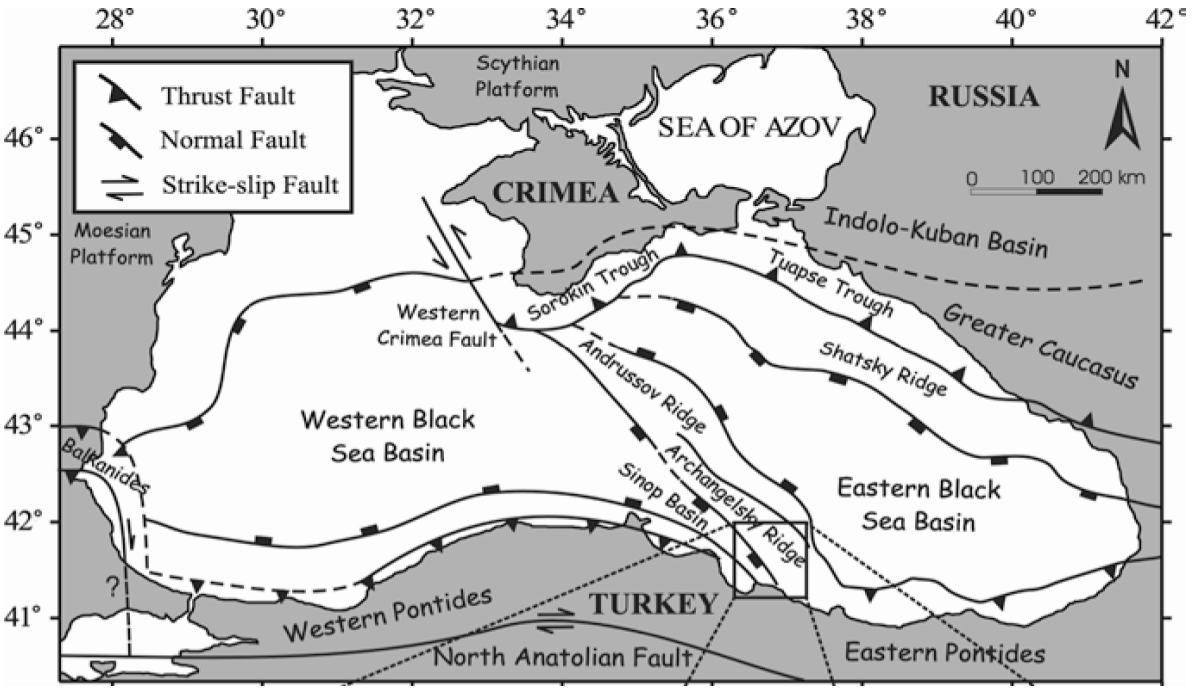

Fig. 8: Simplified tectonic map showing the major tectonic elements of the Black Sea (from Çifçi et al., 2003).

The area changed to a compressional regime during the Eocene and the tectonic evolution of the basin is characterized by a subsidence history that resulted in the separation of the two basins (Nikishin et al., 2003). Modern stress field observations from structural data, earthquake foci, stress field measurements onshore in the Crimean and Caucasus regions, and GPS data show that the Black Sea region is still in a dominantly compressional environment (Reilinger et al., 1997; Nikishin et al., 2003). The general source of compression is the collision between the Arabian, Anatolian, and the Eurasian plates (Fig. 7).

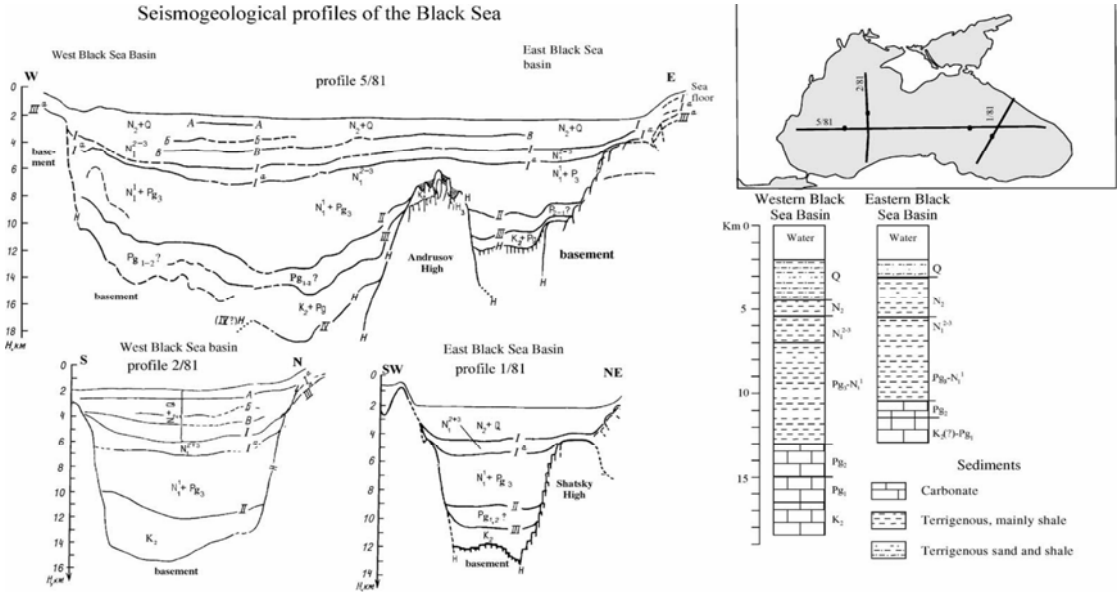

Fig. 9: Cross-sections through the West and East Black Sea basins, location map and stratigraphic columnar sections for both basins from Nikishin et al., 2003).

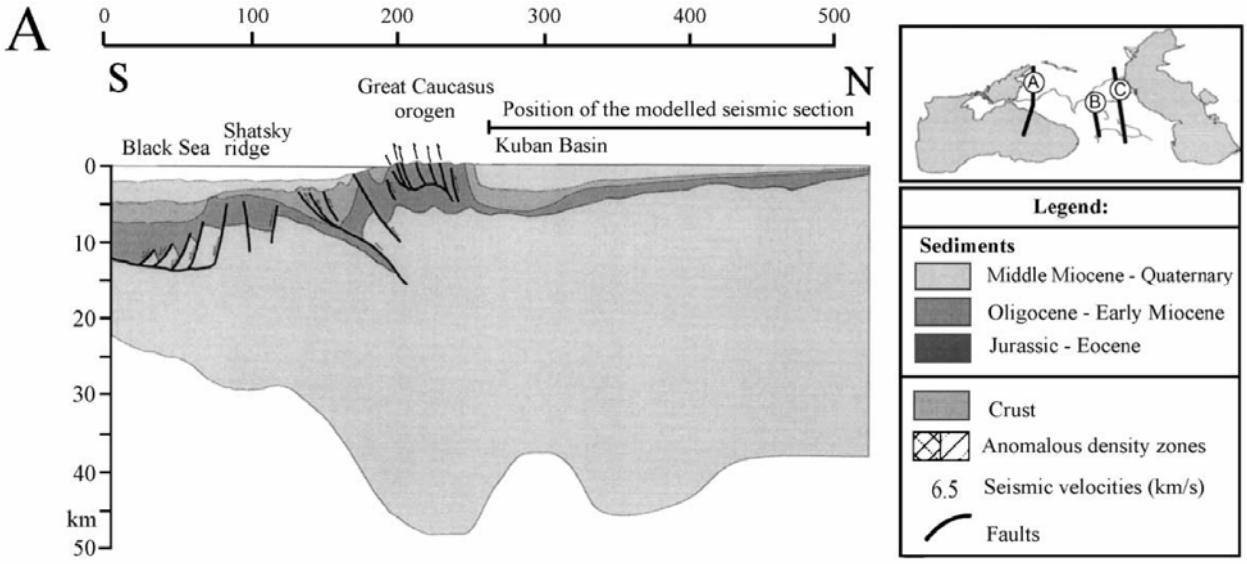

Fig. 10: Crustal section through the Western Caucasus to the Eastern Black Sea. The profile is marked by letter A in the map (from Ershov et al., 2003).

The Sorokin Trough is a foredeep basin of the Crimean Mountains belonging to the eastern basin of the Black Sea. It forms a large depression, which is 150 km in length and 50 km in width southeast of the Crimean Peninsula (Tugolesov et al., 1985). A large number of its mud volcanoes evolved from diapiric zones in a compressional regime between the Cretaceous to Eocene blocks of the Tetyaev Rise and the Shatskiy Ridge (Tugolesov et al., 1985). The sediments extruded in the mud volcanoes are clay-rich deposits from the Maikopian Formation that forms an Oligocene-Lower Miocene sequence of 4-5 km in thickness. The Maikopian Formation is overlain by at least 2-3 km thick Pliocene to Quaternary sediments (Fig. 9). A second foredeep basin specially filled with thick Maikopian sediments forms the Tuapse Trough which strikes parallel to the northeast coast of the Black Sea. Similar to the Sorokin Trough, the basin was compressed between the Shatsky Ridge and the Greater Caucasus (Nikishin et al., 2003). Sediments from the Caucasus fold belt are overthrusting deposits of the Tuapse basin to the west (Fig. 10).

2 Cruise narrative and weather

2.1 Cruise narrative

(G. Bohrmann)

R/V METEOR sailed from the pier in Ambarli / Istanbul, Turkey at 8 a.m. local time on March 17, one day later than planned. Before leaving Istanbul, R/V METEOR stayed 4 days in the port of Ambarli where scientists and scientific equipment were exchanged. Scientists from Germany (from IFM-GEOMAR, AWI, and the University of Bremen), USA, Canada, Turkey, Ukraine, and Russia embarked during March 14 and 15, and the time before the ship left port was used to install all the new equipment in the laboratories of the vessel. Unfortunately, two containers had been delayed for two days, which postponed the start of the cruise for at least one day. On Saturday, March 17, everything happened very quickly. After we passed the Bosporus Strait, we had a two-day transit along the northern Turkish Coast to the easternmost area of the Black Sea. We started station and mapping work on Monday, March 19, at the continental margin of Georgia (station list in the Appendix). After collecting new multibeam bathymetry data during the night, we started our first dive with the remotely operated vehicle (ROV) on Tuesday, March 20, at Colkheti seep in 1100 m water depth (Fig. 11). During the past few days many repairs on ROV "QUEST4000m" had been carried out by the ROV team.

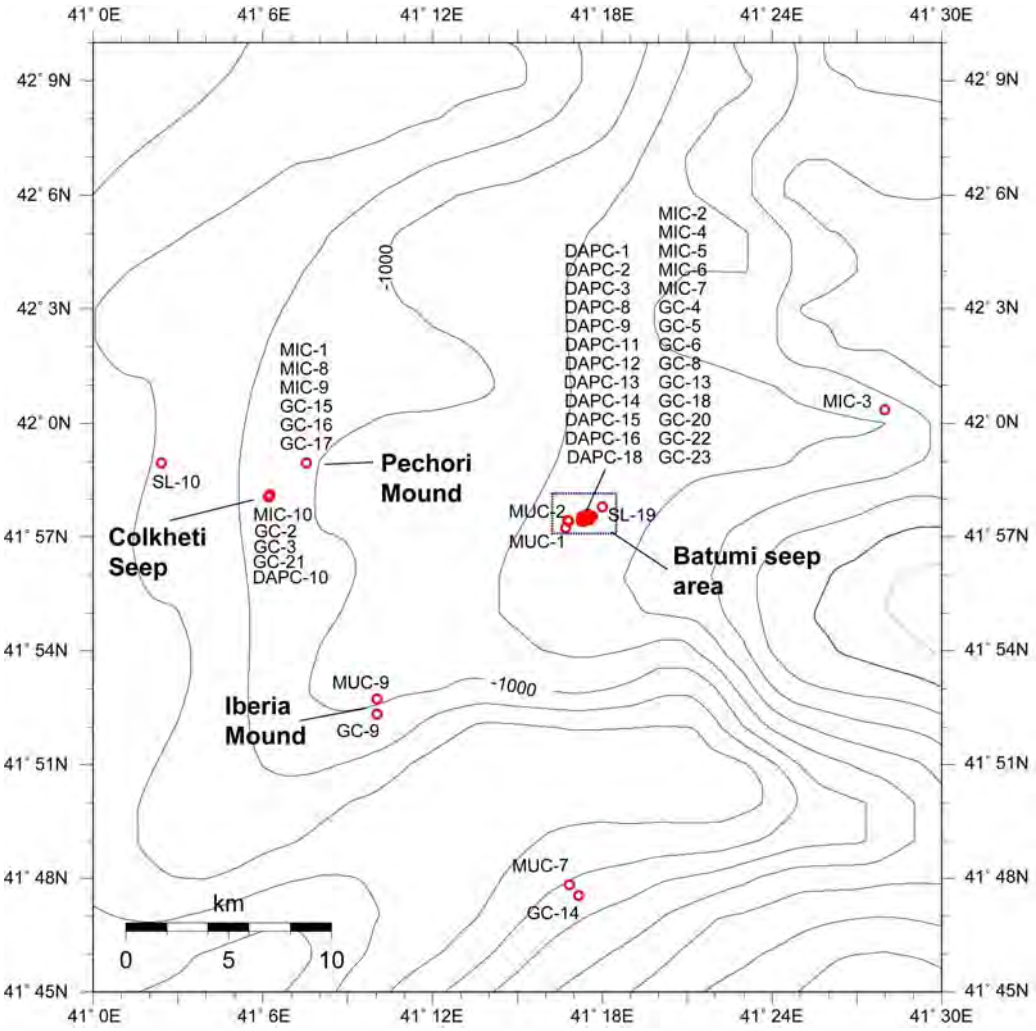

Fig. 11: Map of Kobuleti Ridge showing locations of sampling (ROV sampling stations are not included).

The first ROV dive on Colkheti Seeps was successful and two further dives were run during the following two days at locations in the area of Batumi seeps in 850 m water depth (Fig. 12). After finishing the diving program with ROV "QUEST4000m" and the geological work at the Georgian continental margin, R/V METEOR sailed north on a 28-hour-long transit to Ukrainian waters. We took advantage of the transit to overcome a period of bad weather. We reached our area in Ukrainian waters on Friday, March 23, and started with a survey south of Kerch Strait. Kerch Strait connects the Black Sea with the Sea of Azov between the Kerch (Ukraine) and Taman (Russian) peninsulas. Free methane forms methane hydrate in water depths greater than 750 m (i.e. within the gas hydrate stability field) or the gas escapes into the water column in areas shallower than 750 m. Therefore, many sites where gas escapes from the seafloor, like in the Batumi area, have been detected by the 18 kHz signal of the Parasound system.

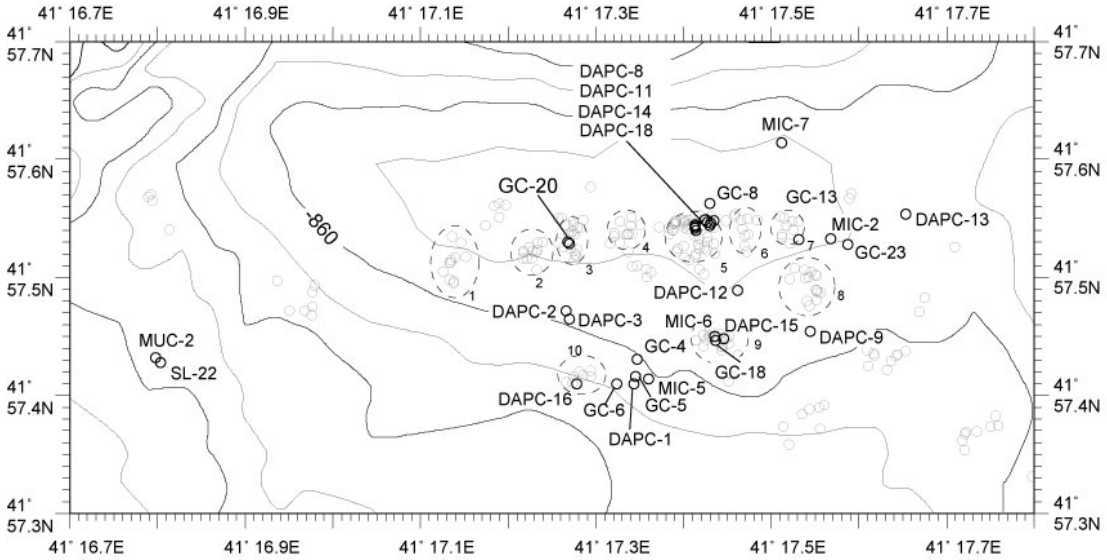

Fig. 12: Map of Batumi seep area on Kobuleti Ridge showing locations of sampling (without ROV sampling). The flares detected by the Kongsberg EM 710 multibeam echosounder are shown by small circles. Flare clusters are defined by larger circles and a number.

The dive on Sunday, March 25 was on Dvurechenskii mud volcano (DMV) in the central Sorokin Trough (Fig. 13). This program included a long-term experiment with a mooring on the seafloor in order to measure temperature changes (Fig. 14). The mooring was deployed during the previous cruise M72/2 on March 7, and during our re-visit three weeks later we recovered one of the temperature data loggers. The second data logger is planned to measure temperature changes of the mud volcano over 3-4 years, in order to understand long-term variations in the mud flow activities of the DMV. The temperature data measured during the three week period already revealed temperature changes at the mud volcano and let us forecast interesting results on temperature variations at the mud volcano for the future.

Besides the recovery of the date logger, push cores and temperature measurements with the T-stick were taken along transects over the mud volcano. In order to establish a geological map, we performed video documentation continuously and searched for gas emission sites, which have not been found. In addition to the ROV work, the sediments of the mud volcano were sampled by the autoclave piston corer. This tool takes a sediment core of up to 2.5 m length and keeps the gas and gas hydrate inside the sediments under *in situ* pressure conditions. The autoclave tool also allows for a controlled degassing of the cores, which enables us to quantify the amounts of gas and gas hydrate in the sediments. A gravity corer on the

Vodyanitskii mud volcano (VMV), which is located close to DMV (Fig. 13), recovered the first gas hydrate specimen, and so we decided to perform a one-day dive program on this structure on Wednesday March 28. This dive was exciting in many aspects. One accomplishment of the dive was that we could capture the first images of gas bubble release in 2000 m water depth in the Black Sea.

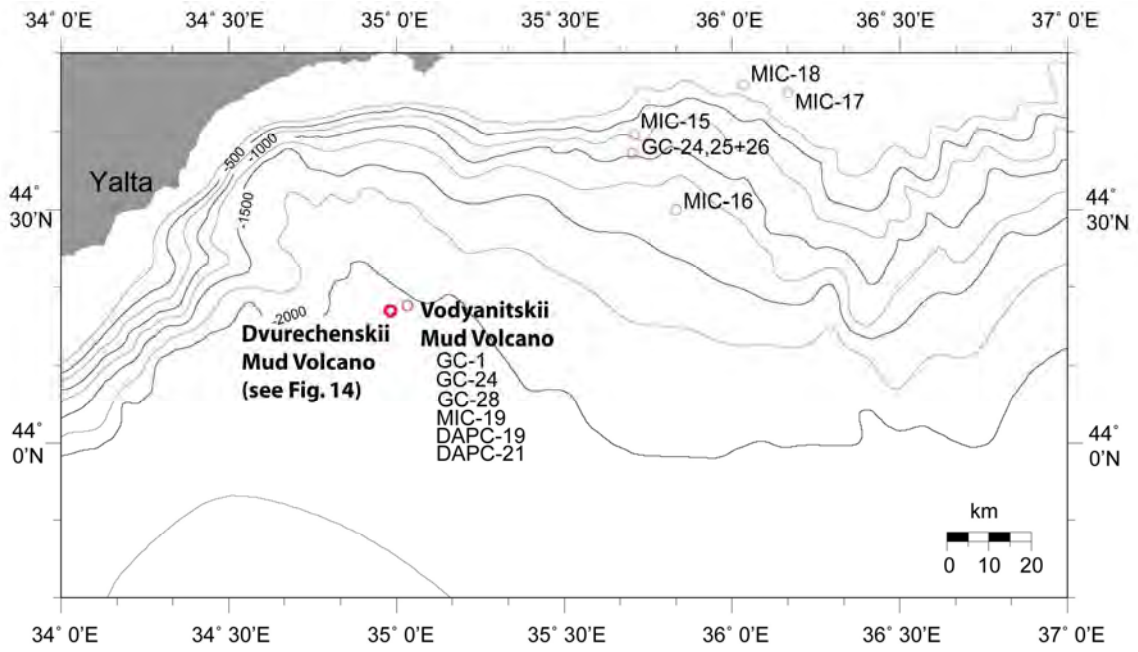

Fig. 13: Map of Sorokin Trough southeast of the Crimean Peninsula showing sampling stations of cruise M72/3.

After one day of sailing from the Ukrainian Sorokin Trough to the Georgian continental margin offshore Batumi we reached the area of Batumi seeps. In particular the EM710 multibeam system was used during the first week at this location to detect gas bubble emanations over the entire 2-km wide swath. By using this method, 150-250 individual gas seeps, which were clustered at 10 locations, were identified in an area of 1.2 x 0.9 km at the Batumi seeps (Fig. 12). For the purpose of using the same names for locations, we used numbers to identify these clusters (# 1 to # 10). During the dives in the Batumi seeps area, all ten clusters were inspected and at each of them temporal changes in seepage activity were identified.

Besides regional mapping of bubble streams using all the systems of the ROV and the hull-mounted echosounder systems on the ship, quantification of the gas emission amount from single bubble streams was only possible by using the ROV "QUEST4000m". We therefore used various sizes of plastic bags with known volumes to quantify gas release from a site. The bags were put on the bubble stream with the aperture facing down, so that the upward moving gas was collected in the bag. After the ninth dive of the ROV, the diving program of Leg M72/3a was concluded with a total bottom time of 80 hours. This successful diving program included many highlights and gave us essential new insights into the fluid and gas circulation on the sea bed of the Black Sea. The last two days of Leg 3a were dedicated to sample sediment core collection from specific sites of interest.

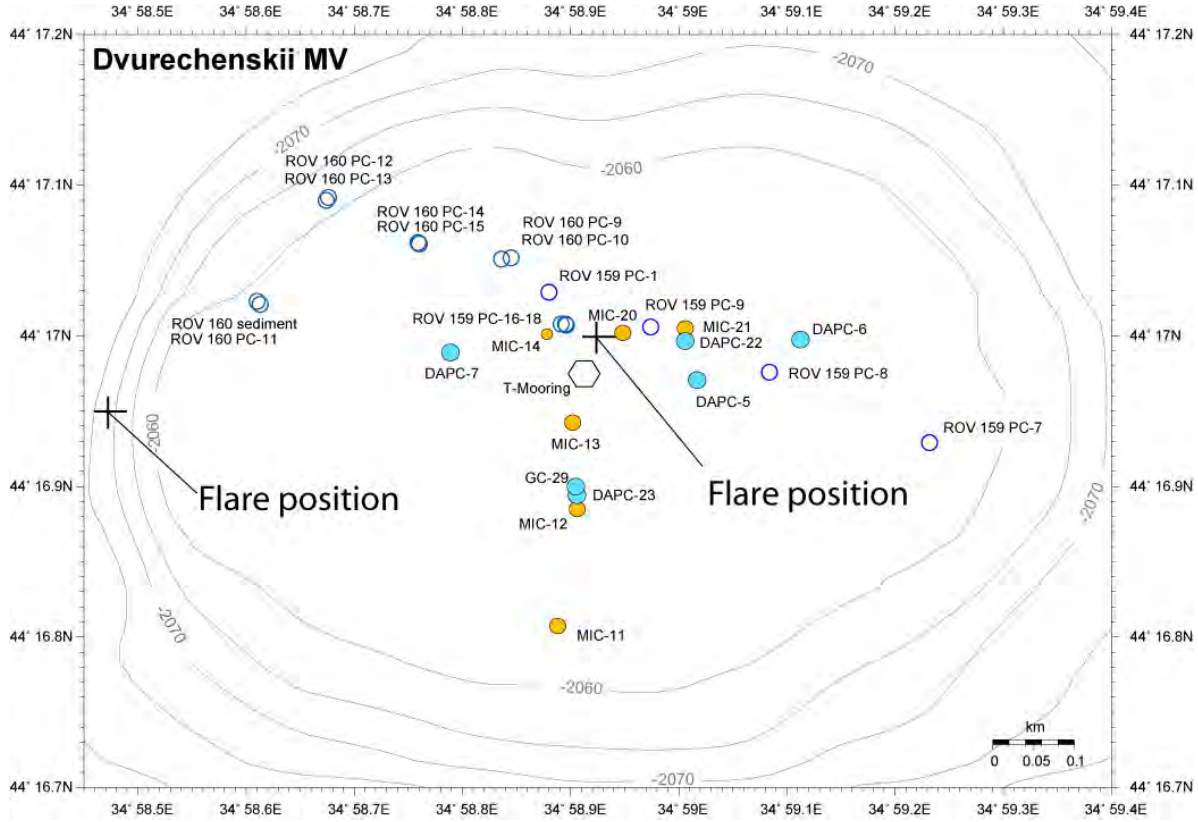

Fig. 14: Sample locations taken during R/V METEOR cruise M72/3 on Dvurechenskii mud volcano. Two flare locations were detected at the end of the cruise.

At the end of Leg M72/3a R/V METEOR came to the port of Trabzon, Turkey on Tuesday, April 3, 2007 at 8:00 a.m. local time. Eighteen scientists, technicians, engineers, and ROV pilots disembarked in Trabzon, and four containers including ROV "QUEST4000m" and its equipment were unloaded. Among the equipment we took on board was a 13-m-long, 4-m-high and 22-ton heavy trailer, which contained two completely installed labs for running medical computer-tomography (CT) scans. The CT-scanner was used for imaging small-scale structures of gas-hydrate samples within the autoclave chambers. The work in the port of Trabzon was finished by the end of the day and R/V METEOR started sailing with a new scientific party at the end of that same day.

On Thursday, 5 April, mapping of sediments and bathymetry by Parasound and the EM120 started along the Georgian continental margin, followed by a multichannel seismic survey over the Gudauta Ridge. Acoustic anomalies (flares) had been detected in the water column during Leg M72/3a when bathymetric profiling was carried out in this area. Further mapping revealed numerous flares on the summit and partly along the flanks of the ridge. Flare locations and the bathymetric map of the area were used to establish a plan for seismic profiling. Beside the seismic equipment, the deep-towed sidescan sonar from Kiel (DTS-1) was used and showed seafloor anomalies at the flare locations. We also recovered a sediment core highly saturated with gas from 690 m water depth, which based on temperature and pressure is not deep enough to form gas hydrate (Fig. 15). Since all the flares that had been found occur above the stability conditions of gas hydrates, we left Gudauta Ridge area on Friday evening and started to record an overview multichannel seismic profile on the way to the Batumi seeps.

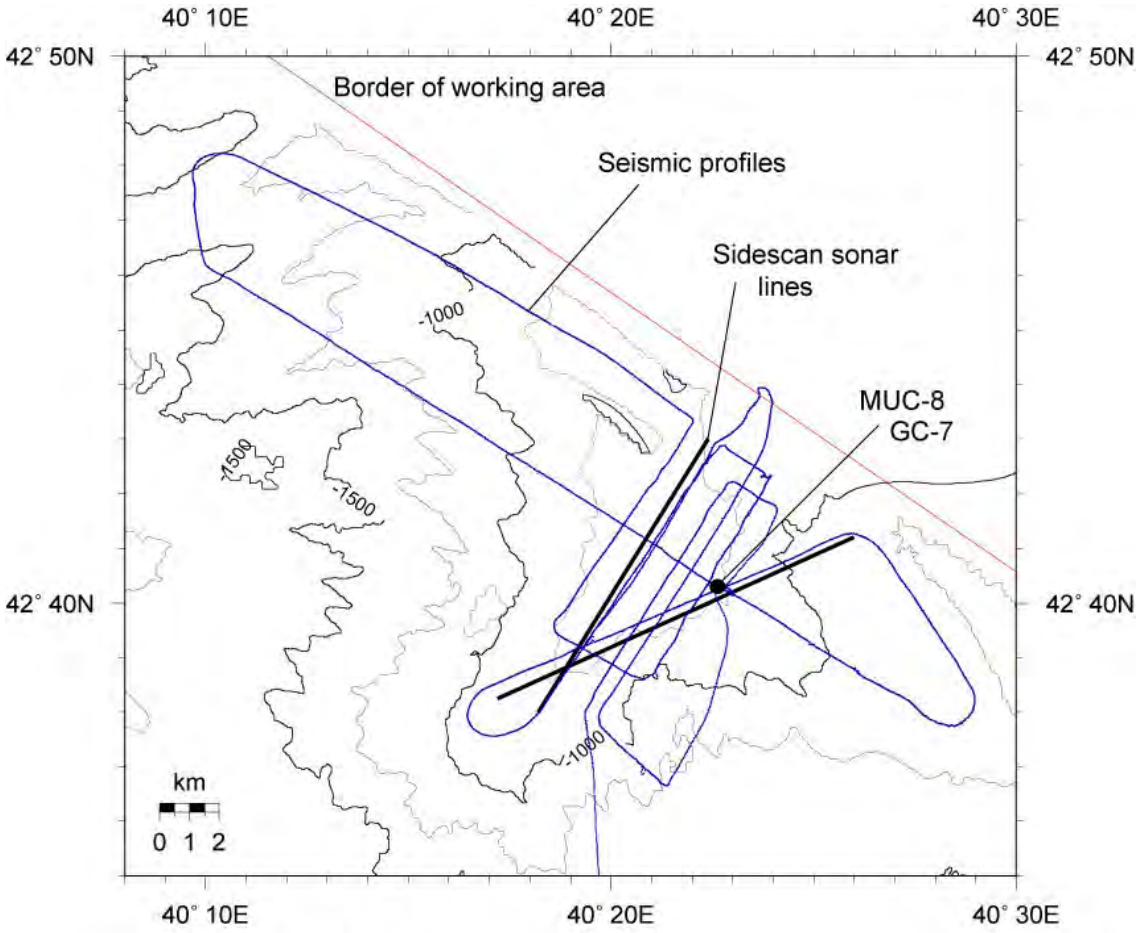

Fig. 15: Profiles (Seismic and Sidescan Sonar) and sample locations during R/V METEOR cruise M72/3 on Gudauta Ridge.

The gravity corer and both autoclave piston corers were used to sample gas hydrates at distinct locations of flare clusters mapped during Leg M72/3b. Gravity coring during the afternoon on the Iberia mound was successful (Fig. 11). During the night, high resolution sidescan sonar mapping using the 410 kHz and 75 kHz frequencies were carried out in the Batumi seep area. On Easter Sunday , April 08, we sampled a further seep area, which is known as Pechori mound. Pechori mound is a pronounced seafloor elevation with a diameter of about 3 km and stands approximately 50 m above the seafloor in 1100 m water depth. Gravity coring successfully retrieved seep sediments from Pechori mound in which dispersed gas hydrates were present (Fig. 11). In contrast to pure white hydrate the staining of oil leads to a more yellowish colour of the Pechori hydrates. Sediment sampling in areas rich in gas hydrates was performed daily during the day time, while seismic and sidescan sonar work was conducted during the night. A detailed, high-resolution seismic survey with profiles only 25 m apart was started for 30 hours until Easter Monday, April 09. This seismic data will be an important base for a future drilling campaign in the Batumi seep area using the portable mobile drilling device MeBo developed at Bremen University.

On Friday, April 13, a last comprehensive sampling program along the Georgian continental margin was run at Pechori mound, and at Colkheti and Batumi seeps (Fig. 11). The second part of the leg was planned to investigate areas in Turkish and Georgian waters of the Black Sea. On Sunday afternoon we reached the Sorokin Trough, where we first planned to combine a sidescan sonar survey together with a multichannel seismic measurement over DMV. Since there was an increase in wind speed up to Beaufort 6 within a short time of only 2 hours, we had to cancel the sidescan sonar deployment and run the seismic lines

alone. In contrast to previous seismic profiles, these seismic records document very interesting details of the inner structure of the mud volcano.

The following day was again dedicated to an extensive sediment sampling program on top of two mud volcanoes (Fig. 13). After this working program was successfully finished we moved to the eastern Sorokin Trough south of the Kerch Peninsula. To date there is no information on the presence of gas hydrates in this area. A first survey using the hull-mounted sonar systems of R/V METEOR and seismic profiling found evidence for gas expulsion. Gas flares were found in varying numbers and densities along the entire continental slope above 750 m water depth. A maximum amount of flare activity occurred in the western part. In order to tackle our gas hydrate questions we were mainly interested in finding flares along the deeper parts of the slope below 750 m water depth. In the night from Wednesday, April 18 to Thursday, April 19 a flare of more than 400 m height above the sea floor was found in 900 m water depth.

This location, which we called Kerch Flare, lies certainly within the gas hydrate stability field, meaning that methane hydrates can form in the sediments. A first attempt in sampling gas hydrates using the gravity corer was not successful, which can be explained by a non-homogenous distribution of gas hydrates at the seep site. On Friday, April 20 and the following Saturday we had a very busy program, because some scientific goals had not yet been reached, but needed to be reached before the return transit to Istanbul. Unfortunately, gas hydrate sampling failed at the Kerch Flare site, and so, because of the short remaining time, we decided to sample hydrates on VMV and DMV.

At these locations, we were immediately successful in sampling gas hydrates. Besides gravity core sampling of gas hydrate specimen, which will be analyzed later in the lab, both dynamic autoclave piston corers (DAPC I and DAPC II; Fig. 14) were used. These coring systems keep the samples under *in situ* pressure conditions and so no gas is lost and no gas hydrates decompose on their way up through the water column. Besides DAPC-I, which has been already successfully used in the past as well as during the current cruise, the DAPC-II was a new development which allows us to subsample the 2.30-m-long sediment core into several segments while maintaining the pressure. The advantage of subsampling the core is that the subsamples allow quantifying the gas and gas hydrates for segments of the core. We were able to cut the core under pressure for the first time, which represents a valuable achievement of project METRO during the cruise. In addition the subsamples could be analyzed under pressure within the CT-lab. The CT scanner which we loaded in the port of Trabzon was used intensively during the cruise. More than 10,000 scans of gas hydrate samples were made.

Major goals for the CT-lab analyses were to inspect the internal fabric and the distribution of gas hydrates within natural marine sediments. In the past it was believed that gas hydrates are distributed more or less homogenously. Though in recent times there are more and more indications for different fabrics within hydrates, which are not yet well documented. R/V METEOR cruise M72/3 obtained many new results in this field. Among other things we could show vertical gas hydrate alignments over longer depth levels. These alignments probably formed by the rise of free gas vertical to the bedding planes. The gas hydrates filling the pathway of the gas ascent appear as long plates cutting through the sediments.

Furthermore, in the night between Friday and Saturday we could use the sidescan sonar again, which had problems with one of its transducers after the first three deployments and was then in repair during the last couple of days. Thanks to the effort and experience of our sidescan sonar technician the instrument could be used again and we were able to map the DMV. Surprisingly, two flares have been detected by sidescan sonar on DMV in areas that showed no gas flares a day before on Parasound recordings. A new Parasound profile run after the sidescan sonar survey confirmed the presence of two active flares. The flare on the centre of DMV reached a height of 1100 m above the seafloor (Fig. 14). The flares have not been active within the last 8 weeks, when R/V METEOR visited the mud volcano several times, but a major change in activity apparently happened just a day before. This new finding provoked many discussions among the cruise participants about the activity of the mud volcano, such as the intensity of mud flows, the frequency of gas expulsions, and many other questions.

Since we had to start our way back to Istanbul around midnight there was no more chance to extend our investigations of DMV. On Monday we left the Black Sea around 13:00 when we entered the Bosporus Strait under nice, sunny skies. We passed along the old city of Istanbul and entered the Sea of Marmara and the port of Ambarli.

2.2 Weather

M72/3a (17 March – 03 April, 2007)
(E. Müller)

The R/V METEOR Leg M72/3a was characterized by rather windy conditions, especially during the first eleven days. From 17 March to 27 April at least temporary strong winds (e.g. wind speed of Bft 6-7) could be observed on every day. During one day (23 March) the wind speed exceeded Bft 8. In comparison to the climatology it was unusually windy. From 28 March to 03 April the winds were weaker, mostly between Bft 3-4 with a few exceptions due to the local nocturnal east wind (Bft 5-6) off the coast of Georgia.

On 17 March, when R/V METEOR left Instanbul, a weakening high pressure ridge over the Atlantic provided sunshine and weak southwesterly winds of Bft 3-4, so good conditions for passing the Bosporus Strait. But on the next day the weather changed significantly. A cold front passed the Black Sea from west to east. It caused strong northwesterly winds up to Bft 7 and maximum waves of 3.5 m, which of course supported the eastward travel of R/V METEOR. On 19 March, when the first working area, the Batumi seep area, was reached, a new high pressure system built up over the Black Sea and caused a rapid drying and stabilizing of the troposphere. The weak southwesterly wind shifted to a moderate easterly wind until the evening. On the following days the anticyclone became stationary and was transformed in a so called “omega-situation”, which blocked the frontal systems coming from the west. With the strong subsidence the air temperature rose to 15 ºC. At the same time upstream of R/V METEOR, the coastal stations of Georgia measured 20 ºC. With the easterly winds the air cooled down when it flowed over the relatively cold sea surface (8.6 ºC). Simultaneously with the strengthening anticyclone over West Russia, a strong pressure gradient developed along the east coast of the Black Sea that persisted till 22 March. During the night, a strong easterly wind of Bft 6-7 blew and waves developed up to 3 m for a short time.

In the morning the wind decreased to Bft 3-4 and in the following night it increased again. This interesting phenomenon could be observed every night in the Batumi seep area. The strong pressure gradient forced an ageostrophic wind down the valley from the Georgian capital Tiflis to the coast. Probably an additional katabatic effect was also involved. On 23 March R/V METEOR left the Batumi seep area for transit to the "Sorokin Trough" area southeast of the Crimean Peninsula. A fast, deepening low pressure system moved from Greece to the Balkans against the blocking high over West Russia (Fig. 16). Therefore the pressure gradient over the Black Sea increased significantly and the easterly winds grew rapidly up to Bft 8 in the evening. On the following night, a wind speed of Bft 9 was measured for a short time and waves of 4 m height were observed.

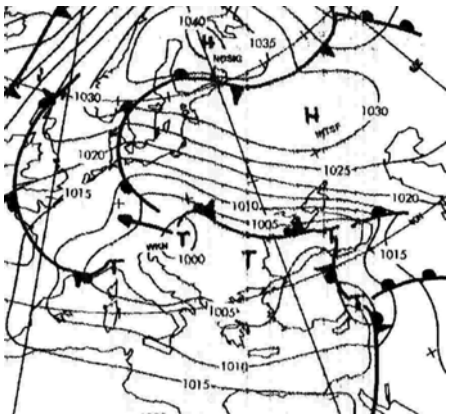

Fig. 16: Surface analysis (extract) of 24 March 2007, 00:00 UTC (DWD Hamburg).

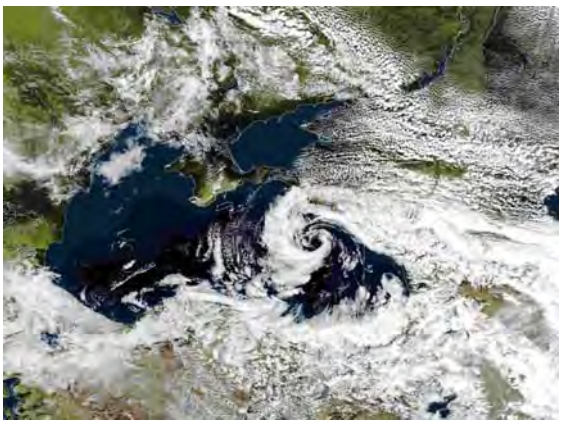

Fig. 17: Satellite image of NOAA-18, 27 March 2007, 10:18 UTC.

On the 24 March, the storm decreased rapidly down to Bft 4 in the morning. A swell of 2.5 m was left. Very similar to the weather situation on 05 March during M72/2 a small secondary cyclone developed near the Crimea peninsula on 25 March. The southwesterly wind Bft 5 shifted to northwest when the centre of the low crossed the R/V METEOR position in the evening. On 26 March, the cyclone moved further eastward and R/V METEOR came on the backside of the low. The wind turned to northeast and increased up to Bft 7 inducing waves of 3 m height. With the colder continental air from Russia the temperature dropped down to 4.5 ºC. On 27 March, the cyclone with its closed circulation was over the eastern Black Sea. Therefore, the northeasterly winds persisted, but weakened to Bft 5. The cloud vortice could be well recognized on the satellite picture (Fig. 17).

On 28 March, the small cyclone over the Black Sea moved slowly westwards along the southern edge of the Russian high pressure system and filled up. As a consequence the strong northeasterly wind of Bft 7 in the early morning decreased rapidly. At midday it was only Bft 4 and in the late evening Bft 2. On the 29th of March, the day of transit to the Batumi working area off the coast of Georgia, the stationary anticyclone over West Russia dominated the weather of the Black Sea, but with weak pressure gradients. Therefore only weak westerly winds of Bft 2-3 could be observed. This weather situation did not change significantly on 30 March. It resulted in a sunny day with very weak northwesterly winds and a sea almost as smooth as glass. The water temperature in the Batumi area was 9.5 ºC. On 31 March, the West Russian high lost its influence on the Black Sea and a low pressure system over south Italy extended to Turkey. Therefore, the cloudiness increased successively and the temperature rose up to 16 ºC. On the following three days, until the end of M72/3a in Trabzon (01 - 03 April 2007), a secondary low, which developed

over the relatively warm eastern Black Sea, dominated the weather in the working area off Georgia. It was mostly cloudy and rained from time to time. The prevailing wind direction was southwest with a wind speed around Bft 4. The temperature decreased from 10 ºC to 8 ºC.

M72/3b (04 - 23 April, 2007)
(W.-T. Ochsenhirt)

R/V METEOR left the port of Trabzon in the evening of 04April heading for the eastern Black Sea. The synoptic situation was characterized by a high over eastern Turkey with a ridge over southeastern Ukraine, causing southeasterly winds about 3 Bft.
A low pressure system coming from southern Italy moved eastwards north of the working area of R/V METEOR. The associated weather conditions encountered were some hours of rain and southeasterly winds of 3 or 4 Bft veering westerly.
During the following days, under high pressure influence, the weather in the area of investigation off Georgia was mainly calm and sunny with variable winds between 1 and 3 Bft and an extraordinary calm sea. On 12 April, a coldfront crossed R/V METEOR causing rain for a longer period first, then showers, but the wind speed did not exceed Bft 4. The same happened from 13 to 14 April with the passage of a frontal trough of a low over Northwest Russia. R/V METEOR left this area heading for another area north of Samsun. During the same day, the cruise was continued to the north where R/V METEOR arrived in the evening. Shortly before arrival, a thick band of clouds brought heavy rainshowers for about 2 hours and a northerly wind of 6 to 7 Bft. When the shower belt had moved away, the wind decreased to 2-3 Bft.
R/V METEOR remained in the area off the Crimean peninsula under high pressure influence with very low wind speeds and a calm sea. The cloudiness was variable, sometimes short precipitation was observed. On 19 April, the situation changed once more for a short time. A secondary depression over Romania crossed our area and moved to the Caucasus. The northerly wind increased to 5 Bft associated with showersqualls. On 21 April, the wind decreased again slowly and a new high pressure situation became established. Thus the cruise to Istanbul was effected during calm weather. The voyage ended on 23 April.

3 Multibeam swathmapping

(M. Brüning, S. Althoff, Y.G. Artemov, A. Nikolovska)

The Kongsberg Simrad EM120 and EM710 multibeam echosounders installed on R/V METEOR were used to survey the working areas in Georgia, Ukraine, and Turkey. Nighttime breaks in the sampling and dive program during Leg M72/3a were used for surveys, and during Leg M72/3b the sonars ran parallel to seismics and sidescan sonar profiles. The main parts of the working area in Georgia (Figs. 18 and 19), and parts of the Ukrainian (Fig. 20) and Turkish (Fig. 21) areas are covered now by these new maps.

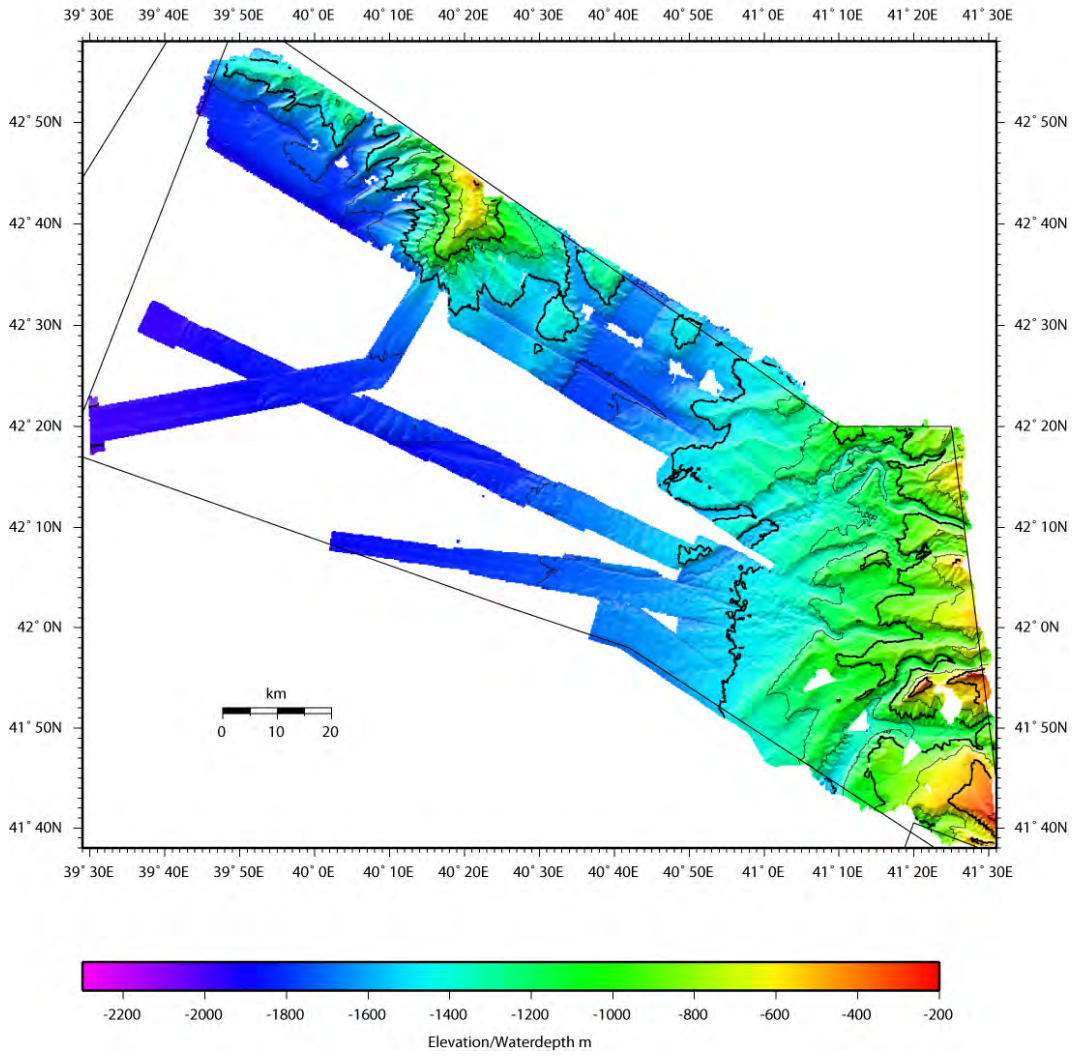

Fig. 18: Bathymetry of the Georgian working area. EM120 data of Cruise M72/3a and 3b processed with IFREMER Caraibes software.

The ship speed during the large scale surveys was 8 kns. The opening-angle of the EM120 (12 kHz) multibeam echo sounder was usually 140°. The system allows a setting in which the coverage is limited whether by angle or the swath-width on the seafloor. This setting gave better results than the angle control mode alone. Especially in deep water, the backscatter strength of the sediments was too weak to give exact depth discriminations for wide angle returns. The limitation to a certain value in metres allowed excluding those inaccurate returns in deep water, while a large angle allowed for a good coverage of the seafloor in shallow water. This is because the swath-width is narrower due to the smaller distance between the ship and the seafloor. Coverage limits were chosen based on the backscatter quality and varied between 3 and

10 km. The 191 beams available were distributed to yield an equidistant spacing on the seafloor. Simrad provides a yaw correction, which directs the beams according to the mean heading. This decreases the actual beam number slightly for the optimization of full coverage along and across the track. On transits with speeds up to 12 kns the EM120 was running, but gave rather bad results, especially for the outer beams. The wider the angle of the beams, the larger was the shift downwards.

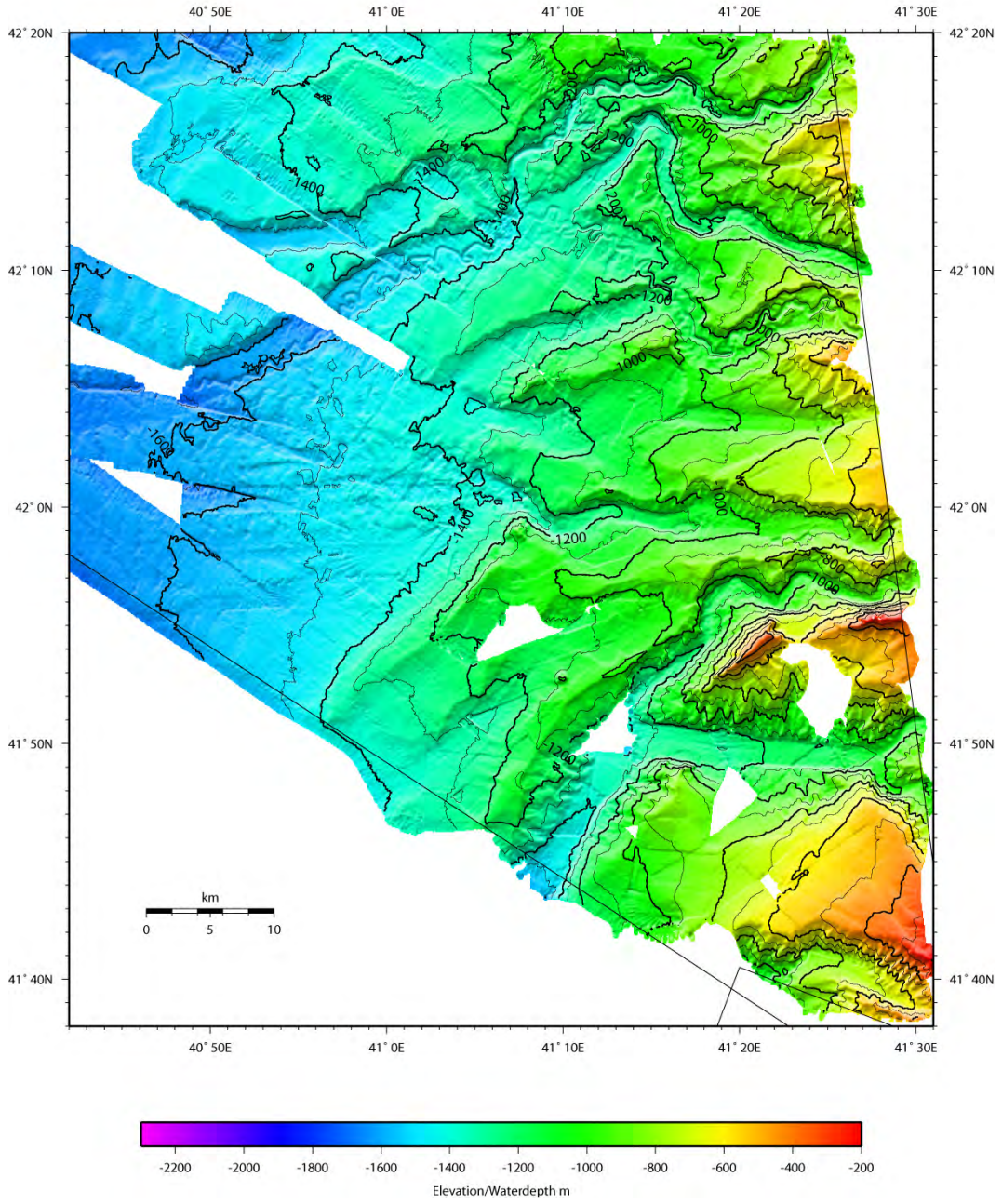

Fig. 19: Detailed bathymetry based on EM120 data of the working area offshore southern Georgia.

The EM710 (70 – 100 kHz) sonar ran down to a water depth of about 1200 m parallel to the EM120 profiling. The maximum coverage was 4000 m or 150 degrees with 256 beams. As the EM710 is optimized for shallower water, the coverage does not overlie the working areas.

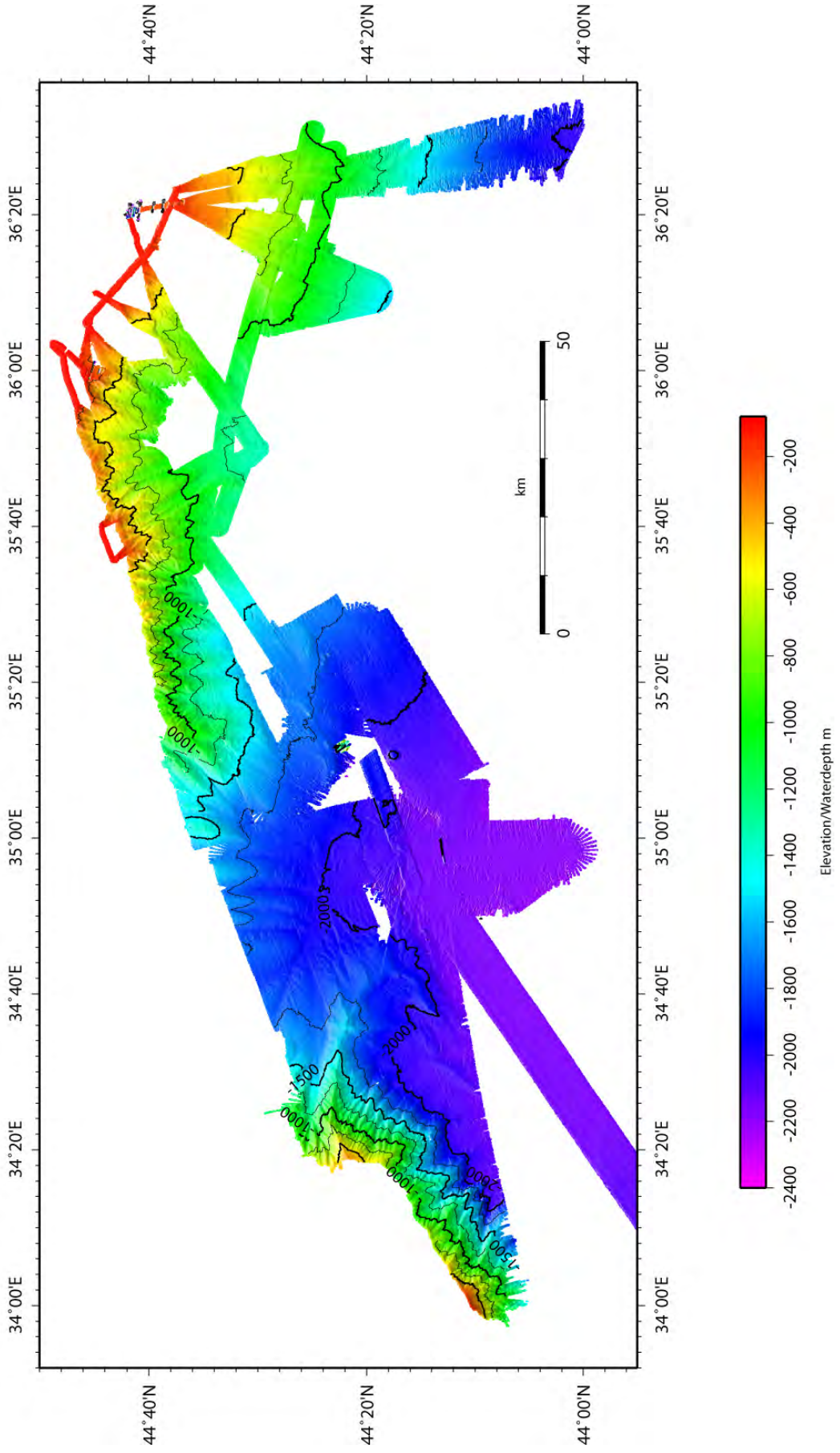

Fig. 20: Bathymetry of the Ukrainian working area based on EM120 measurements.

Data processing

The IFREMER Caraibes software served as the processing tool for the Simrad data. The DGPS navigation data were manually edited and then interpolated. Early bathymetric data were recalculated with the ROV's CTD's sound velocity profile until the Simrad computers included those sound profiles. Raw bathymetry data was cut by depth-thresholds adjusted to the surveyed area. A very rough manual editing, sometimes followed by a filter, removed the few spikes out of the generally good data set. The filter used a reference-grid, calculated with relatively large grid-spacing, to eliminate spikes in the soundings. Two runs of the filter were performed. The sensitivity in recognition of spikes was increased in the second run. Data-points of the outer beams, especially recorded during high speed transits and of obviously too deep depths, were erased rigorously. Soundings were gridded with 60 m grid-resolution and merged with available data (e.g. R/V POSEIDON cruise 317/4, R/V METEOR cruise 52/1, provided by W. Weinrebe, or Gebco). The EM710 data were much noisier than the EM120 data, and were only partly or not processed onboard. The maps shown were generated with the Generic Mapping Tool (GMT, Wessel and Smith, 1998).

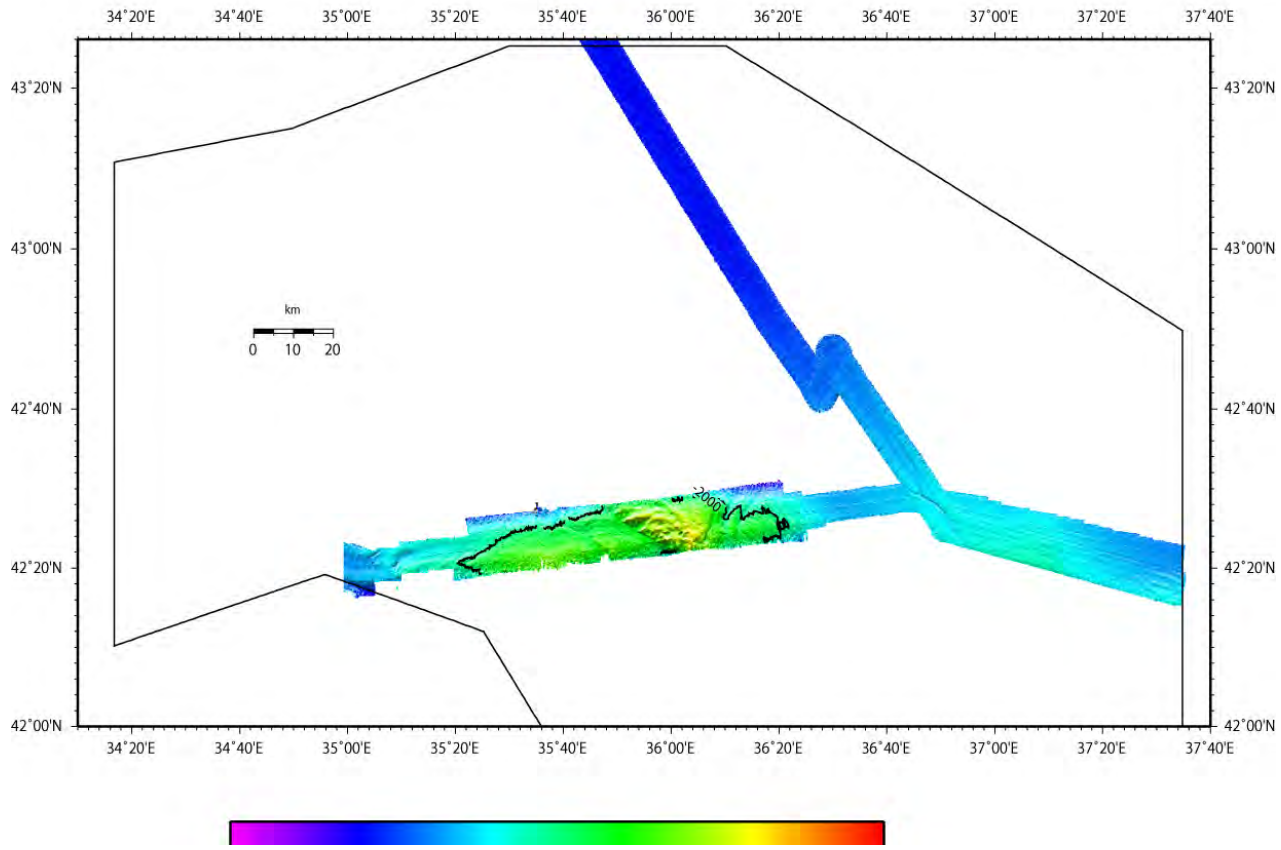

Fig. 21: Bathymetry of the Turkish working area. EM120 data.

4 Subbottom profiling and plume imaging

(A. Nikolovska, Y.G. Artemov, H. Sahling, M. Brüning, S. Althoff)

4.1 Introduction

During the R/V METEOR cruise M72/3 integrated hydroacoustic techniques were used in order to detect, localize and quantify methane fluxes as well as the subbottom composition in the working areas.

4.2 Methods

The following acoustic systems were used:

- Parasound, deep sea single beam echosounder, operating at primary high frequency (PHF) of 18 kHz, and secondary low frequency (SLF) of 4 kHz, this system is ship mounted,
- Kongsberg EM710, mapping multibeam echosounder, operating at 75 kHz (ship mounted),
- Kongsberg digital telemetry, multibeam obstacle avoidance horizontally looking sonar, operating at 675 kHz, mounted on the ROV "QUEST4000m",
- Benthos, sidescan sonar, operating at 325 kHz (mounted on the ROV "QUEST4000m"),

Due to the difference in the operating frequencies and the range capabilities, these acoustic systems were used for investigation of different seep parameters (in the water column and in the subbottom). In the following sections details of the operation are illustrated of the first three systems. The multibeam echosounder EM120 was used only for the bathymetry mapping. During the plume imaging in the Batumi area, the seep flares were visible on the backscatter of EM120 and were displayed as clouds of 'noise' above the seafloor. This was also a case with the Benthos sidescan sonar, i.e. the seeps were evident in the water column, and also in a form of high intensity backscatter patches on the seafloor backscatter. More details of the operation of these two systems are given in Chap. 3.

PARASOUND

A schema of the operation of Parasound is illustrated in Fig. 22. The sound beam of this system has an opening angle of $\alpha = 2°$, and the pinging rate is controlled by the depth of the water column where it is operating. The Hydrocontrol of Parasound was set to the following effective settings. In the sounder environment the system depth was either manually set to a value measured with the EM120, or it was automatically calculated on the basis of the water depth detected with the PHF. The C-Mean was manually set to 1500.00 m/s, and the C-Keel was also manually set to 1570.00 m/s. The depth search mode was set to variable min./max. depth limit with minimum depth of between 200 and 600 m and maximum depth set between 1500 and 2000 m (these values were determined by the expected minimum and maximum depth of the survey areas).

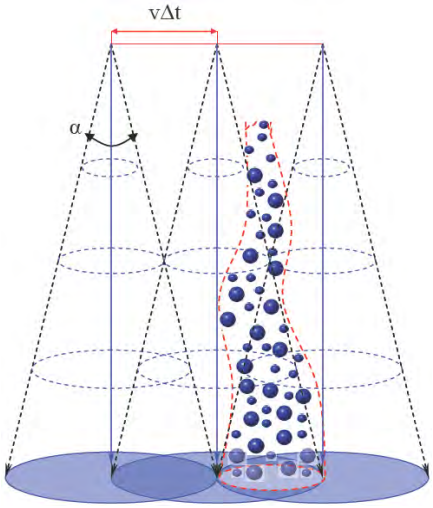

Fig. 22: Example echograph recorded in the water column in the Batumi seep area.

Transmission sequence during the plume surveys was set to single pulse. In the Batumi seep area, assessment of the performance of the pulse train mode for water column visualization was obtained (the time interval between the pulses was set 1000 ms, this is equivalent to the pulse two way travel time in 860 m water depth). It was observed that the pulse train mode allowed better control on the pinging interval, and also displayed better visualization through the water column, but the horizontal resolution was reduced. However, during the plume surveys, the water depth varies significantly causing interference (or delays) between subsequent pulse trains, thus producing a second seafloor multiple that interfered with the data from the water column. The system source level was fixed to 146.0 V, i.e. 241.86 dB. The transmitted pulse is 'Continuous Wave' with rectangular shape and length of 5.00 ms (2 periods per pulse).
The receiver band width for the PHF and the SLF was manually selected; for the PHF the output sample rate was set to 12.2 kHz with 66 % output sample rate, the same settings were also applied to the SLF. The receiver amplification for the PHF was ‘manually’ set to 30 dB (manual gain, for deep areas under 800 m) or 15 dB (for the shallower areas above 800 m), and to 12 dB for the SLF. The water column imaging and the subbottom profiling was conducted simultaneously. Examples of these surveys are given in Fig. 23 and Fig. 24.

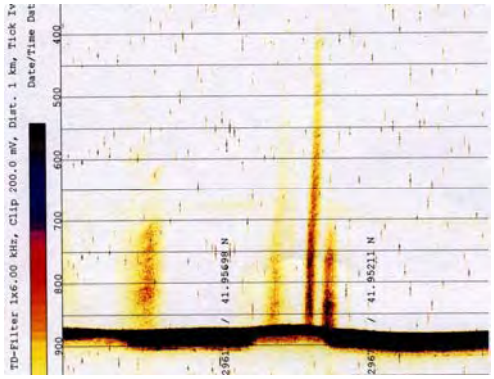

Fig. 23: Example echograph recorded in the water column in the Batumi seep area.

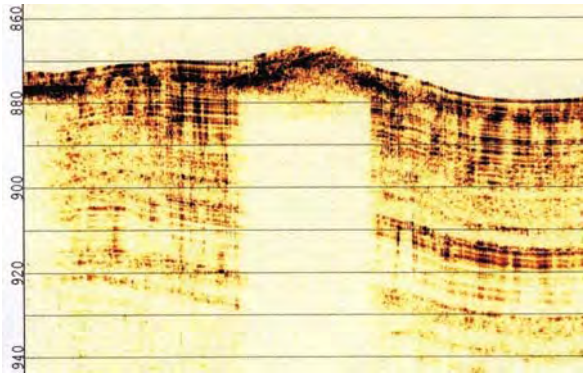

Fig. 24: Example subbottom echograph recorded at the same time as in Fig. 23, Batumi seep area.

The echosounder profiles were registered at ship speeds of ~7 and ~10 kns when mapping the area, and at ~0.5 to ~1.5 kns when surveying plume areas. At high ship speeds, the detection of seep flares was very difficult. The data quality was affected by high noise from the ship’s thrusters, which made it impossible to visualize weak scattering produced by bubbles in the water column. The combination of low ship speeds and the above mentioned echosounder settings allowed a very clear visualization of bubble plumes passed during the survey. This enabled an acquisition of reliable information about the distribution and location of bubble plumes within the areas where their existence has not been detected before. In the sub-bottom profiles there is a clear indication of the acoustic blanking effect at seep sites, due to the suspended gas/gas hydrate in the sediment.
A subbottom example from the Batumi seep site is illustrated in Fig. 24. This effect was observed on all sites where the gas seepage was detected in the water column. Nonetheless, the acoustic blanking was observed in areas where there was no evident gas escape.

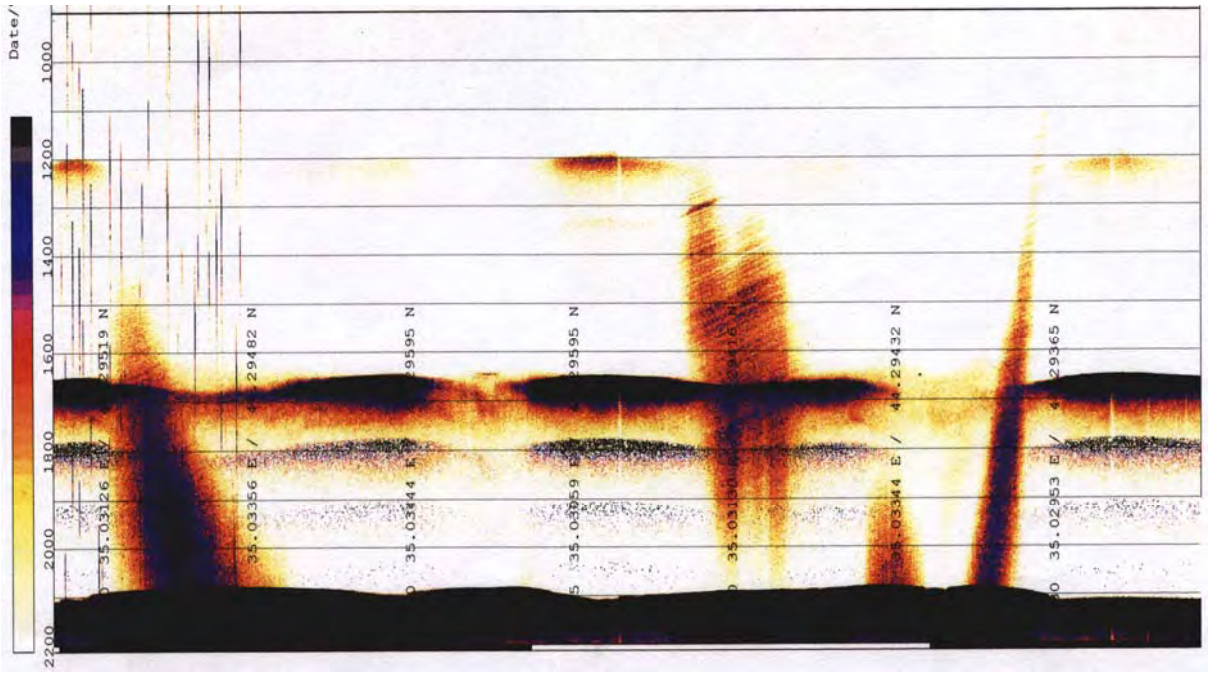

Fig. 25: Image aquired during M72/3 during survey in the Vodyanitskii mud volcano area (track on the seafloor is shown in Fig. 26).

The Parasound system was also used for localizing the gas flares once they were detected during the mapping surveys. This powerful system was particularly useful while operating in the deep sea environment (up to 2100 m). An example case from the Vodyanitskii mud volcano (VMV) area is illustrated in Figs. 25 and 26.

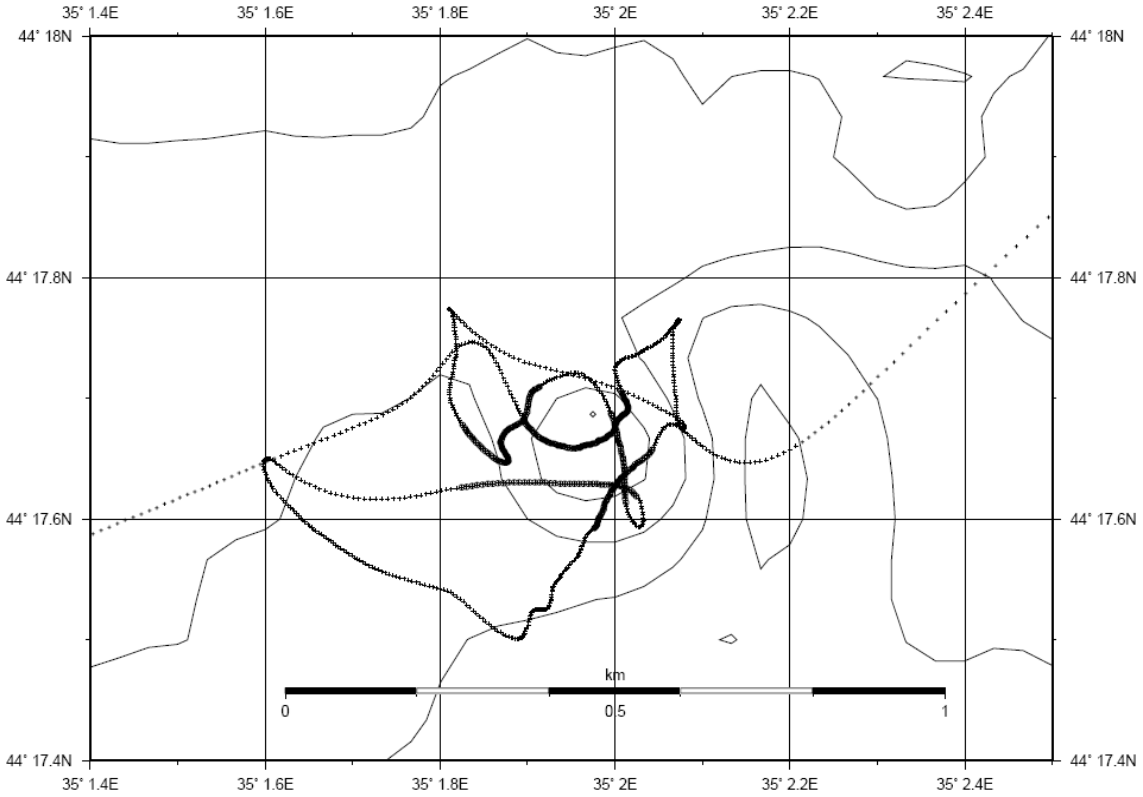

Fig. 26: Ship track during plume localization survey (see Fig. 25).

During the localization survey, the ship was set in a drifting mode. The ship track for the case illustrated in Fig. 25 is plotted in Fig. 26; the thick lines indicate the position of the track when a plume backscatter was occurring on the echograph. Based on the concentration of these lines, the area on the seafloor where the plume appeared was determined. The exact pinpointing of the plume centre is difficult to be obtained, mainly due to the fact that in deep water the beam footprint is very large. For example, in the VMV area at a depth of 2030 m the beam footprint is roughly 140 m in a diameter, thus the position of the plume centre can appear anywhere in this footprint. Nonetheless, when the coverage is obtained through different directions this uncertainty is much lower.

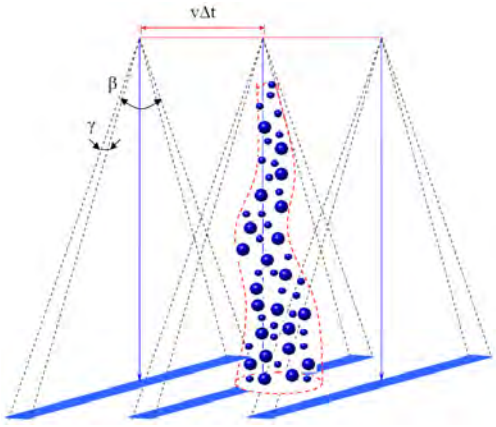

Fig. 27: Schematic drawing of the operation of Kongsberg EM710.

Kongsberg EM710

The multibeam echosounder EM710 is intended for shallow water bathymetry mapping (up to 800 m water depth). The beam spread angle is $\beta = 75°$ and $\gamma = 1°$, as illustrated in Fig. 27. The seafloor coverage depends on the water depth and for the investigated area is in the range of 1800 m up to 2000 m (across). This coverage was obtained with simultaneous pinging of 240 to 260 beams.

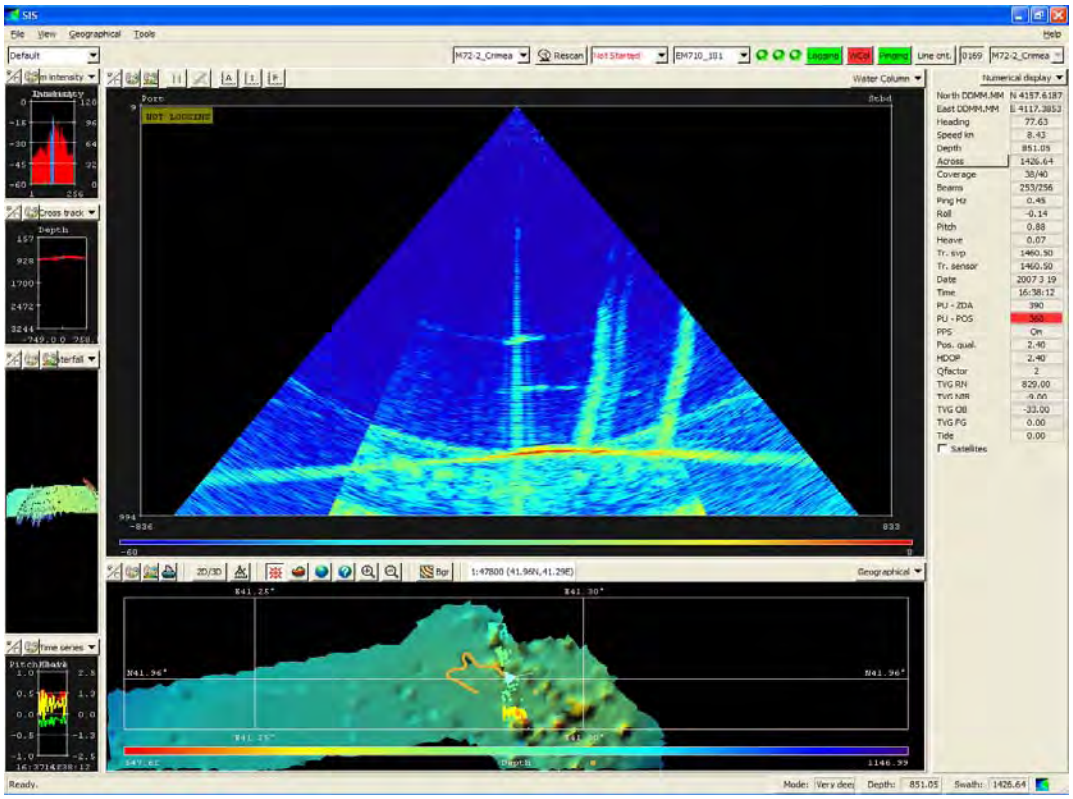

Fig. 28: EM710 water column display while localizing gas plumes, Batumi seep area.

The ping rate was set to a manual setting of 0.5 Hz, thus allowing sufficient time for analysing the on-line screen records. One of the additional features of echosounder is its ability to display the backscatter through the whole water column. The 'water column' display shows a graphical representation of the beam formed data for the entire water column for each ping. The display can be useful for debugging and for habitat monitoring. This feature was successfully used for detecting and localizing the gas plumes. An example of these records is given in Fig. 28. These measurements allowed for very good localization of the gas escaping point on the seafloor. The main parameters that were used for the localization purpose are: the ship position, the position of the transducer, the heading of the ship, the beam spread angle, and the centre point of the detected plumes (i.e. their location at the sea floor line).

These records were postprocessed and plotted on the bathymetry maps, thus allowing clear statistical concentration of the gas escape points. A summary of one survey at the Batumi seep area is illustrated in Fig. 29. The black dots indicate the centre of the flares as observed on a sequence of images (as the one in Fig. 28).

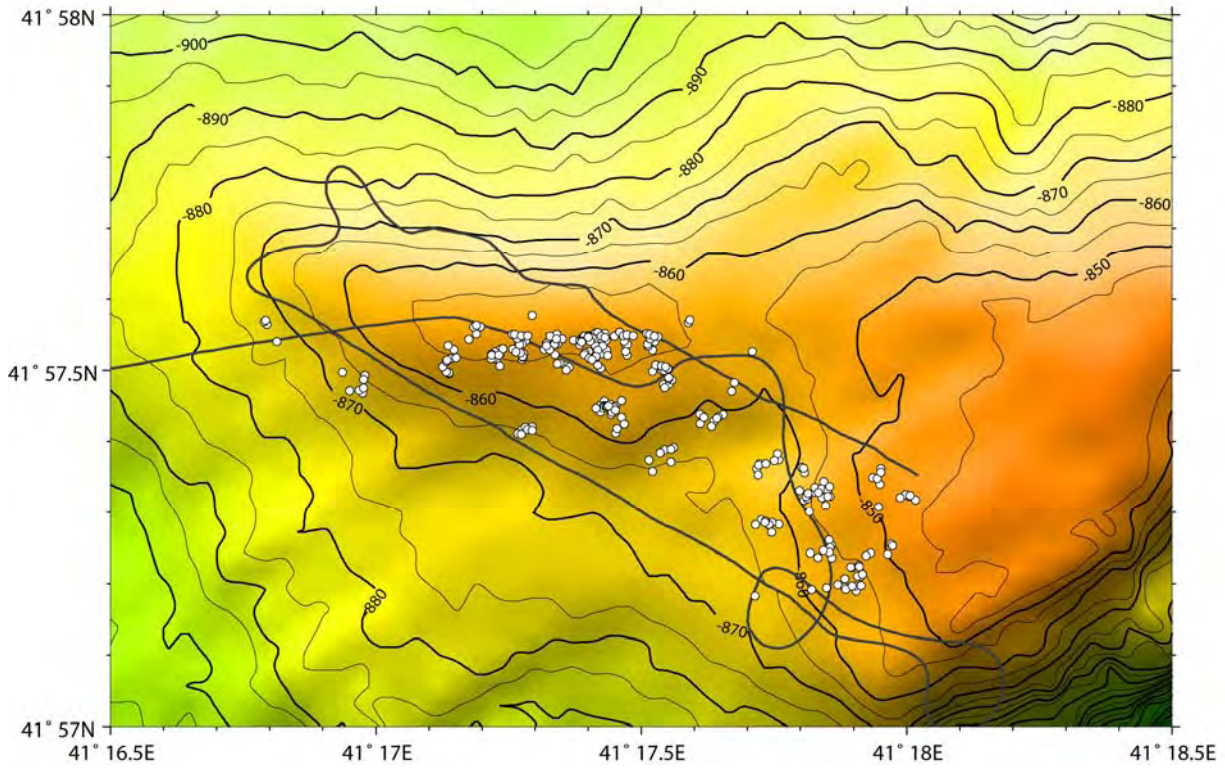

Fig. 29: Concentration of the seep flares detected during the EM710 plume localization survey in the Batumi seep area. The ship track during flare localization survey is indicated.

Kongsberg Digital Telemetry

High frequency (675 kHz) sonar was also used in the 'close up' investigation of the gas plumes. The perspective of this sonar is in a horizontal plane (through the seep flares) and it was proven to have the capability for differentiating single gas outlets on the seafloor. A drawing of the operation of this sonar is given in Fig. 30. The vertical opening angle of the sonar is fixed to $\delta = 90°$ and the horizontal beam angle is 1.4°. The transmitted sound pulse is in an interval between 23 µs and 35 µs, depending on the selected maximum range. When close to the seafloor (20 m to 30 m) the range of the sonar is limited to 20 m to 30 m; above these values the backscatter from the seafloor is too strong and the recognition of the gas

seeps becomes difficult. Thus, when surveying larger areas, the scanning was conducted at roughly 30 m ROV altitude, allowing 50 m scanning range. The positioning of the sites detected with this sonar was obtained through the navigation system, Posidonia, and the heading of the ROV "QUEST4000m". An example of the close range scan (~15 m) during the Batumi seep survey is illustrated in Fig. 31. It was visually noted that the plumes were tilted due to the influence of the water currents, thus, causing an elliptical-shaped backscatter. The centre of the plume had stronger backscatter that weekend in the direction of the current.

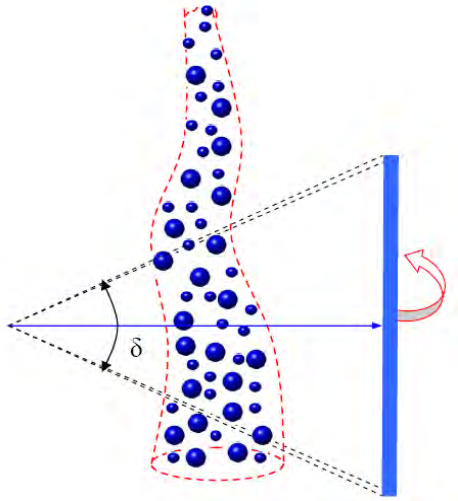

Fig. 30: Example schema of the operation of Kongsberg MS1000.

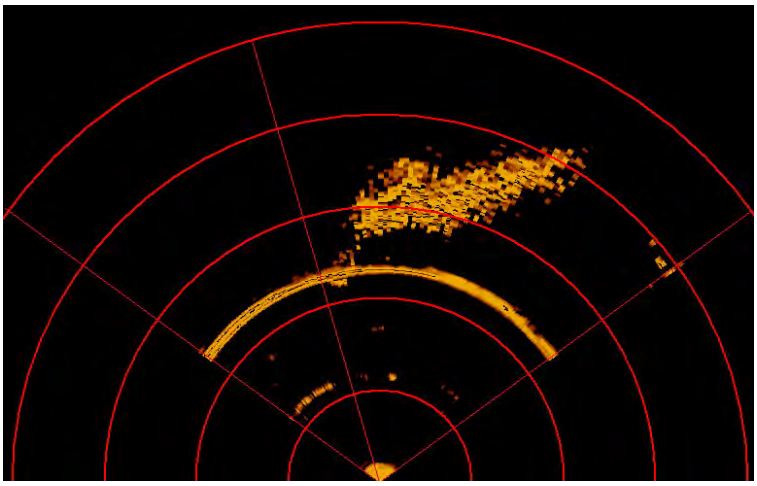

Fig. 31: Example scan from Kongsberg MS1000, fine resolution plume backscatter in a range of 20 m.

With Kongsberg DT sonar there are four operational scanning modes:

- Extra low resolution (high scanning speed mode), which was used for locating and tracking the seeps sites while the ROV is in motion.
- Low resolution (moderate speed mode), used while approaching a detected site, and/or while moving from one seep cluster to another.
- Fine resolution (slow scanning speed), used while scanning area for quantification purpose.
- High resolution (extra slow speed), used also while scanning area for quantification purpose and also for exact pin-pointing and resolving single densely packed bubble outlets.

The sonar measurements will be incorporated into a numerical model for determining the effective gas volume flux. Additional work is planned for integrating the existing sonar systems for the purpose of estimating the total volume gas fluxes in the areas where the high resolution sonar scanning is not available.

4.3 Flare imaging during M72/3b

During the R/V METEOR Leg M72/3b, the flare imaging survey using Parasound acoustic system was continued. In contrast to Leg M72/3a, the duration of transmitted sound pulse was decreased by the factor of 20, down to 0.250 ms (1 period per pulse). This improved the spatial resolution of flare imaging and subbottom profiling observations, so that even single gas bubble tracks in the water column as well as thin sediment layers could be steadily detected in PHF and SLF echograms, respectively.

Acoustic data, collected by the ATLAS PARASTORE V2.12b acquisition software into PS3 data files, were routinely post-processed with the use of WaveLens software (Artemov, 2006), aiming to provide the detailed analysis of echo returns from gas flares at 18 kHz. As the PS3 data format has been slightly changed since the Parasound system onboard R/V METEOR was upgraded to the new DS-3 version in February 2006, some corrections were made to the WaveLens – PS3 format interface, initially developed during cruise M52/1 (MARGASH) in 2002. When applied for processing Parasound data, WaveLens ran raw samples through the bandpass filter, performed the Hilbert transform, decreased sample rate, introduced the TVG correction, and converted PS3 data into the internal PARADOX database table. This was appropriate for the full set of WaveLens tools, except for split-beam operations (Artemov, 2006). Shown in Fig. 32, acoustic images (echograms) of Pechori, Kerch, and Dvurechenskii seeps illustrate the full sampling range echo signals processed by the WaveLens software.

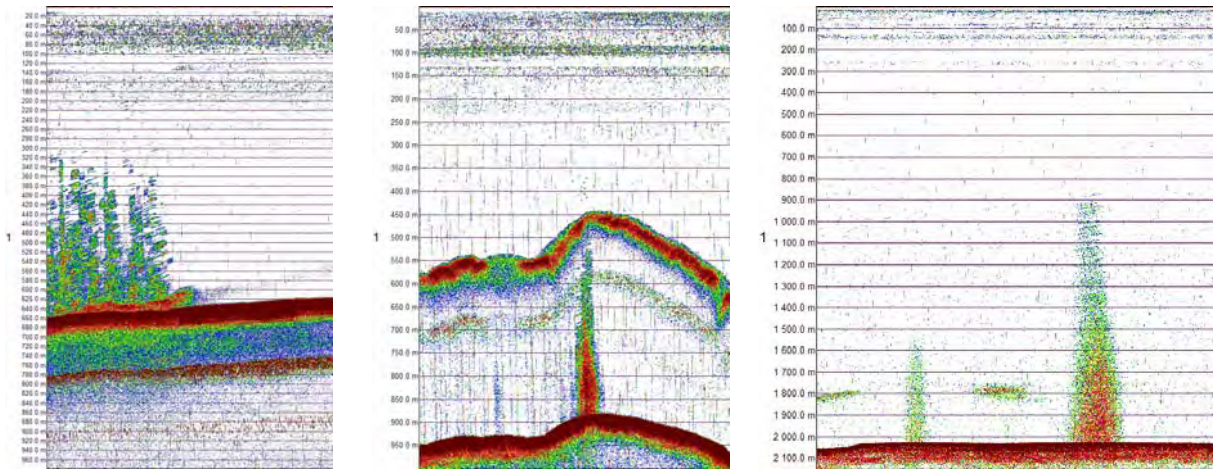

Fig. 32: Echograms of flares detected at Pechori mound (*left*), in the Kerch Strait area (*middle*), and at the Dvurechenskii mud volcano (*right*) during M72/3.

Based on Parasound PS3 data files and WaveLens data processing techniques, positions and heights of observed seepage flares were determined in targeted areas, including Georgian Pechori and Gudauta seep sites, Kerch Strait, and Sorokin Trough. The summary of obtained data is presented in Tabs. A.2.1 to A.2.4 in the Appendix. The mapped seeps in Kerch Strait area are shown in Fig. 33.

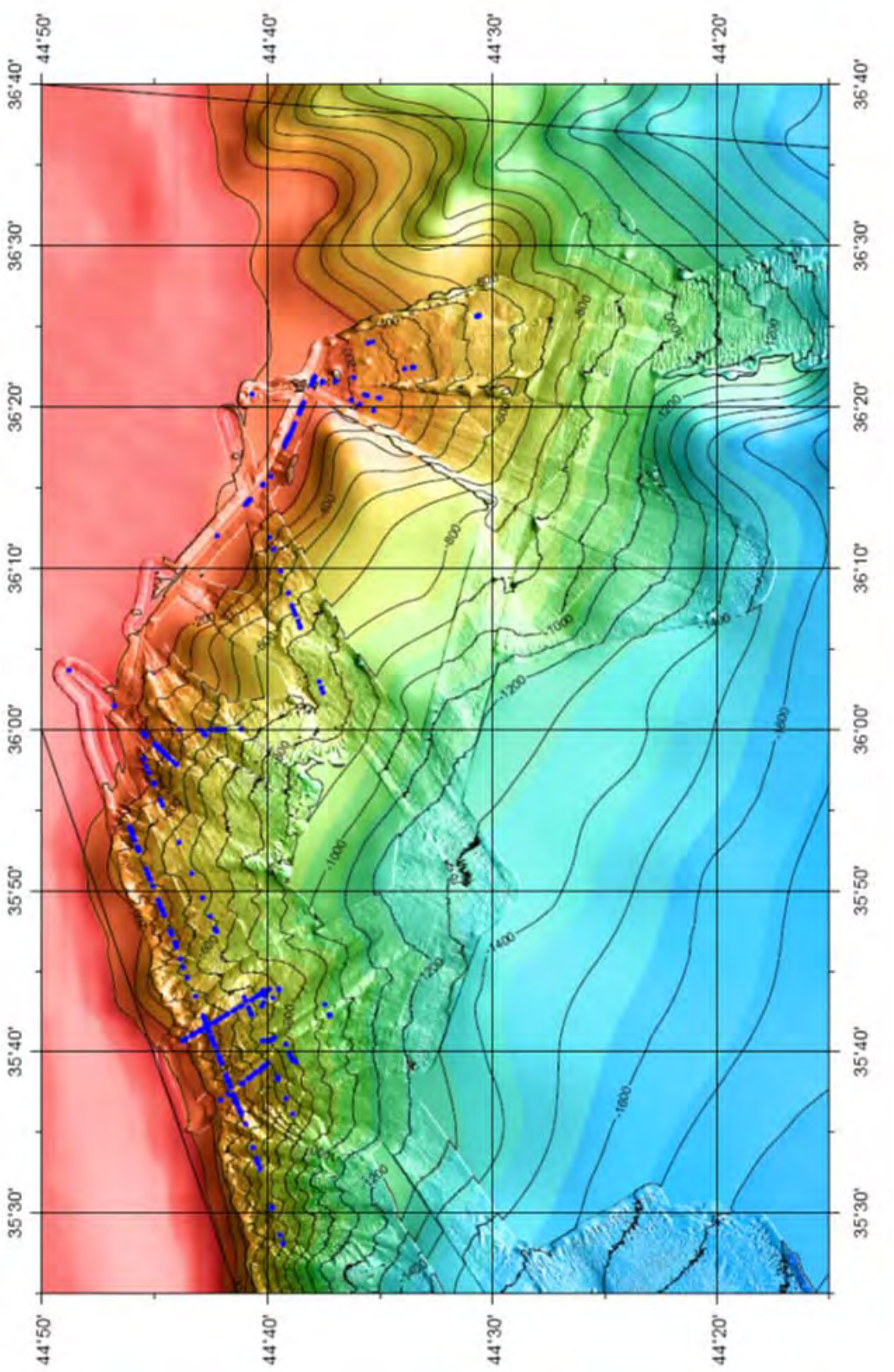

Fig. 33: Map illustrating positions of seeps (as dots) in the Kerch Strait area.

5 Sidescan sonar operations

(I. Klaucke, M. Brüning, A. Zotova, T. Schott, G. von Halem, and watchkeepers)

5.1 Objectives

Deployments of the DTS-1 sidescan sonar were targeted at two different objectives. First, standard 75 kHz profiles were run in order to image yet unknown portions of the continental margin off Georgia, as well as the continental slope off Kerch Strait and the Sorokin Trough on the Ukrainian margin. In addition, high-resolution 410 kHz profiles were run at sites already imaged during previous cruises in order to obtain very detailed images of gas seeps in the Black Sea.

5.2 Methods

Detailed geoacoustic mapping of mud volcanism and related fluid-escape structures have been targeted using the DTS-1 sidescan sonar system (Fig. 34) operated by IfM-GEOMAR, Kiel. The DTS-1 sidescan sonar is a dual-frequency, chirp sidescan sonar (*EdgeTech Full-Spectrum*) system employing both 75 and 410 kHz centre frequencies. The 410 kHz sidescan sonar emits a pulse of 40 kHz bandwidth with a duration of 2.4 ms (giving a range resolution of 1.8 cm), while the 75 kHz sidescan sonar provides a choice between two pulses of 7.5 and 2 kHz bandwidth with a pulse length of 14 and 50 ms, respectively. They provide a maximum across-track resolution of 10 cm. With typical towing speeds of 2.5 to 3.0 kns and a range of 750 m for the 75 kHz sidescan sonar, maximum along-track resolution is on the order of 1.3 m. In addition to the sidescan sonar sensors, the DTS-1 contains a 2-16 kHz chirp subbottom profiler, which provides a choice of three different pulses of 20 ms pulse length each. The 2-10 kHz, 2-12 kHz, or 2-15 kHz pulses each gives a nominal vertical resolution between 6 and 10 cm. The sidescan sonar and the subbottom profiler can be run with either, internal, external, coupled or gated trigger modes. Coupled and gated trigger modes also allow specifying trigger delays. The sonar electronics provide four serial ports (RS232) to attach up to four additional sensors. One of these ports is used for a *Honeywell* attitude sensor providing information on heading, roll, and pitch. A second port is used for a *Sea&Sun* pressure sensor. Finally, there is the possibility of recording data directly in the underwater unit through a mass-storage option with a total storage capacity of 30 GByte (plus 30 Gbyte emergency backup).

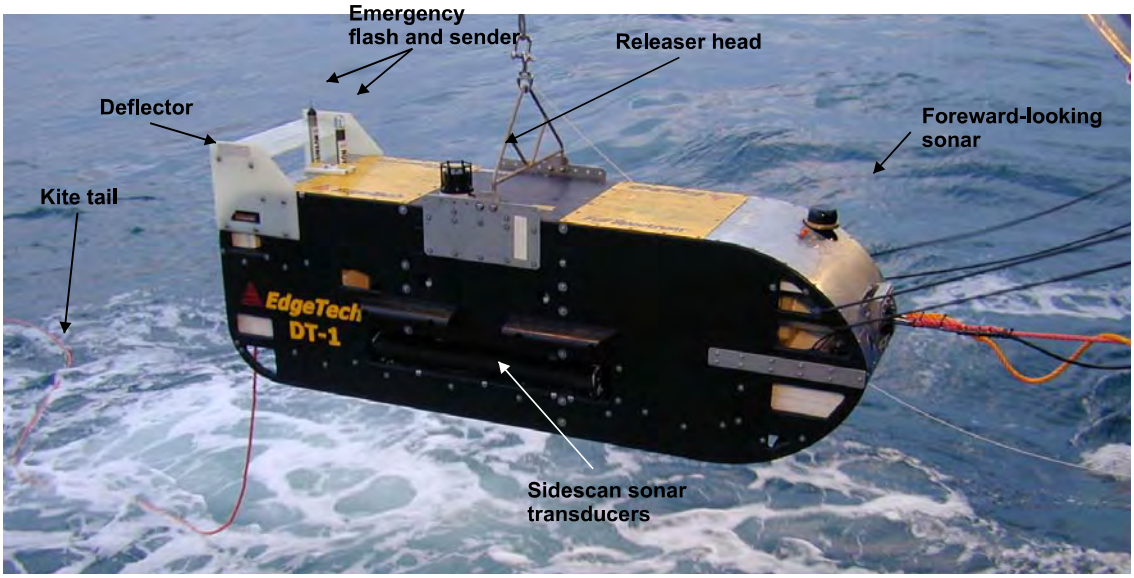

Fig. 34: Picture of the DTS-1 sidescan sonar towfish. The forward-looking sonar is no longer mounted.

The sonar electronic are housed in a titanium pressure vessel mounted on a towfish of 2.8 m x 0.8 m x 0.9 m in dimension (Fig. 34). The towfish houses a second titanium pressure vessel containing the underwater part of the telemetry system (*SEND DSC-Link*). In addition, a releaser capable of working with the USBL positioning system *POSIDONIA (IXSEA-OCEANO)* with a separate receiver head and an emergency flash and radio beacon (*NOVATECH)* are included in the towfish. The towfish is also equipped with a deflector at the rear in order to reduce the negative pitch caused by the weight of the depressor and buoyancy of the towfish.

The towfish is connected to the sea cable, via the depressor, through a 45-m long umbilical cable (Fig. 35). The umbilical cable is tied to a buoyant rope that takes up the actual towing forces. An additional rope has been taped to the buoyant rope and serves to pull in the instrument during recovery.

The main operations of the DTS-1 sidescan sonar are run using *HydroStar Online*, the multibeam bathymetry software developed by *ELAC Nautik GmbH* and adapted to the acquisition of *EdgeTech* sidescan sonar data. This software package allows onscreen presentation of the data, including the tow fish's attitude and the tow fish's navigation when connected to the *POSIDONIA* USBL positioning system. It also allows to set the main parameters of the sonar electronics, such as pulse, range, power output, gain, ping rate, and range of registered data. *HydroStar Online* also allows activating data storage either in XSE-format on the *HydroStar Online* PC or in JSF-format on the full-spectrum deep-water unit *FS-DW*. Simultaneous storage in both XSE and JSF-formats is also possible. Accessing the underwater electronics directly via the surface full-spectrum interface-unit FS-IU and modifying the sonar.ini file of the *FS-DW* allows changing additional settings such as trigger mode. The *FS-IU* also runs *JStar*, a diagnostic software tool that allows running some basic data acquisition and data display functions. *HydroStar Online* creates a new XSE-file when a file size of 20 MB is reached, while a new JSF-file is created every 40 MB. How fast this file size is accumulated depends on the amount of data generated, which hinges on the use of the high-frequency (410 kHz) sidescan sonar. The amount of data generated is also a function of the sidescan sonar, subbottom pulses, and the data window that is specified in the initialisation file (sonar.ini) on the *FS-DW*. The data window specifies the range over which data are sampled.

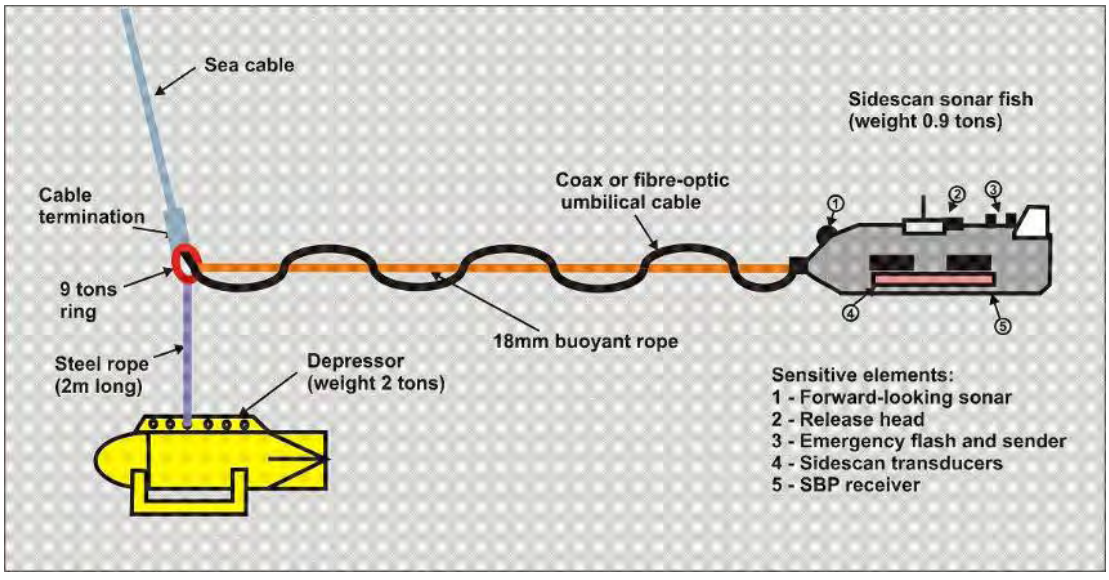

Fig. 35: The DTS-1 towing configuration.

5.3 Deployments

Three deployments of the DTS-1 were run in Georgian and Ukrainian waters. The first deployment, occuring on April 5, 16:00 to 22:30 UTC was designed to image several newly discovered gas flares on Gudauta Ridge. The second and third deployments were targeted at high-resolution surveys of the Batumi seep area. During the first survey, the 75 kHz profile obtained during the R/V Poseidon cruise 317/4 in November 2004 was repeated in order to detect possible changes in seafloor backscatter intensities during the last 2 and a half years and to better locate the sidescan sonar imagery by taking advantage of the *Posidonia* USBL system onboard R/V METEOR. The second survey had become necessary in order to fill gaps in the original analysis due to strong bottom currents, which caused the towfish to drift sideways away from the designed ship-track (Fig. 36). Navigation of the towfish with a precision of 100 m proved quite difficult. Unfortunately, the Posidonia USBL system does not work beyond 4000 m in range, which limits its use to water depths of less than 2000 m during towed sonar operations.

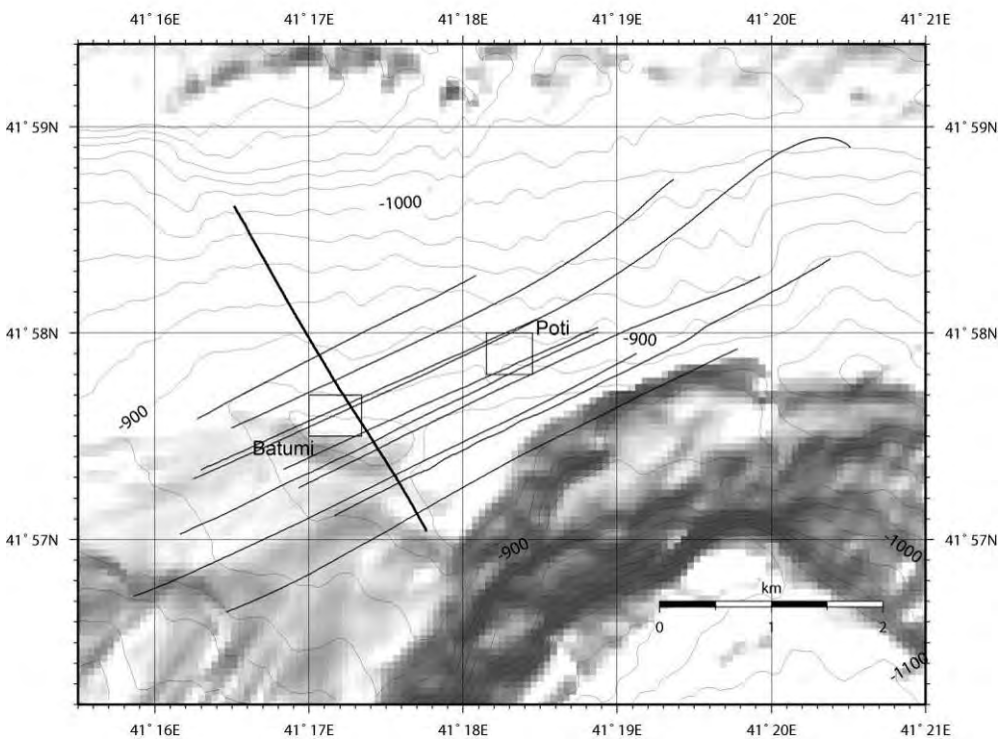

Fig. 36: Cruise tracks of high-resolution sidescan sonar deployments over Batumi seeps. The thick line shows the track of a 75 kHz track designed to repeat data from R/V POSEIDON cruise P317/4.

In the area of Kerch Strait, one survey had to be cancelled just after deployment of the instrument because of faulty cable connections conjunctly with current leakage in the port-side transducer resulting in loss of backscatter data on this channel.

Although repairs of the transducer are not possible, attempts to reduce the current leakage by further isolating the transducer from contact with seawater finally improved data from the port side channel. The 410 kHz option, however, remained unusable. A final deployment of the DTS-1 was run on April 21 from 00:45 to 10:05 UTC, over Vodyanitskii and Dvurechenskii Mud Volcanoes. A planned parallel track had to be called off because of strong winds and currents that would not allow proper navigation of the ship at towing speeds as low as 2.5 kns.

5.4 Preliminary results

The sidescan sonar data were processed onboard using the *Caraibes* software developed by IFREMER. This software package together with Posidonia navigation data allows quick and reliable georeferencing of the sidescan sonar images for subsequent sampling or first analysis onboard.

5.4.1 Gudauta Ridge

The deployment over Gudauta Ridge imaged several new cold seep sites. Some were already known from the Parasound and EM710 mapping of the area during Leg M72/3a, but some locations with similar high backscatter intensity, could be detected on the sidescan sonar images even though they lacked a gas flare in the water column (Fig. 37). The sites are too shallow to contain gas hydrates near the seafloor, but they will subsequently allow a good comparison of the backscatter facies of cold seeps with and without gas hydrate presence.

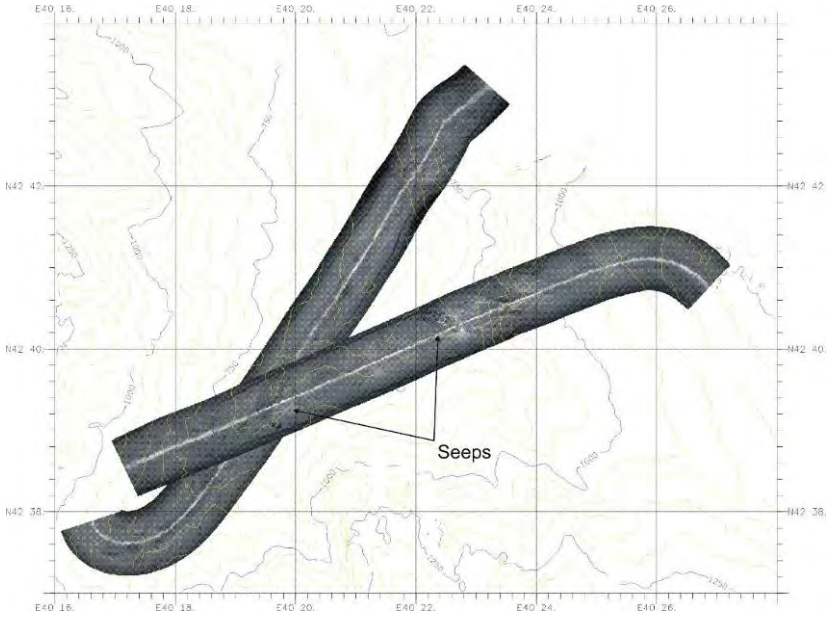

Fig. 37:
Mosaic of 75 kHz sidescan sonar profiles over Gudauta Ridge (Georgia) showing several seep sites characterised by high backscatter intensities (dark tones on the image).

5.4.2 Batumi Seeps

The standard 75 kHz profile over the Batumi and Kobuleti seeps showed an expected strong similarity between the image obtained during the R/V POSEIDON cruise P317/4 in 2004 (Klaucke et al., 2006) and the image obtained during the present cruise. Direct comparison is not yet possible since both images were processed with different software packages, but it is already evident that several high backscatter patches, north of Kobuleti seep, are no longer visible. The original idea that the alignment of high backscatter patches in the 2004 image could be the result of pulsating gas flares can be supported by these findings.

The subsequent high-resolution sidescan survey underlined important differences between the 75 kHz sidescan image and the 410 kHz sidescan image of the same area. The 410 kHz signal does not penetrate into the seafloor and mostly images very small scale relieves such as the faults of the Batumi seeps area (Fig. 38). The 75 kHz signal does penetrate the seafloor to a certain degree (a few tens of centimetres probably) and allows imaging of near-surface gas hydrates and gas bubbles.

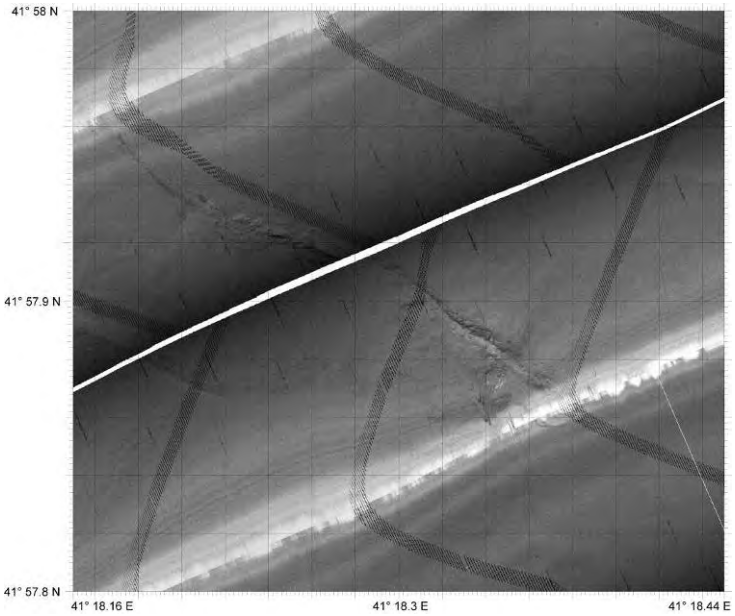

Fig. 38:
Two adjoining 410 kHz sidescan sonar profiles of the centre of Poti seep showing several faults, but generally lacking the high backscatter intensities visible on 75 kHz sidescan images from the same area (high backscatter is dark).

Surprisingly, the 410 kHz raw sidescan sonar images also show gas flares within the water column. Due to the high frequency of the sound signal, these gas bubbles must be extremely small. This might be an alternative explanation why the 410 kHz sidescan images do not reproduce the high-backscatter signatures of the 75 kHz sidescan images. The gas bubbles contained in the uppermost sediments might be too large to become resonant with a 410 kHz signal (Greinert and Nützel, 2004). On the other hand, the 410 kHz images allow detection of small-scale relief in great detail (Fig. 39), which can be subsequently compared with the results from dives with the remotely operated vehicle (ROV) and video observations. Concurrently with the 410 kHz signal, the 75 kHz sidescan transducers were also operating. While a towing altitude of 15-20 m is too low for correct imaging of the seafloor and interferences with the 410 kHz signal alter the images, the very lateral angle of incidence of the 75 kHz signal nicely allows imaging of gas plumes (Fig. 40) and a reliable correlation of the flares with specific backscatter facies on the seafloor.

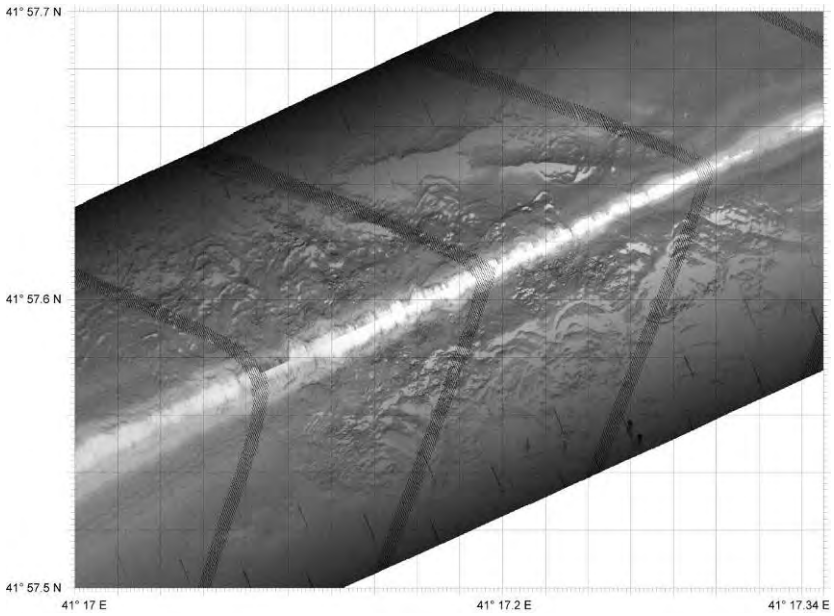

Fig. 39:
High-resolution (410 kHz) sidescan sonar profile over Batumi seep showing many overlapping, concentric rings that indicate strong morphological alteration of the seafloor. These zones correspond to an area of very high backscatter intensity on 75 kHz images (Klaucke et al., 2006) and could result from the decomposition of gas hydrate or the floating-up of slabs of hydrates leaving these craters behind.

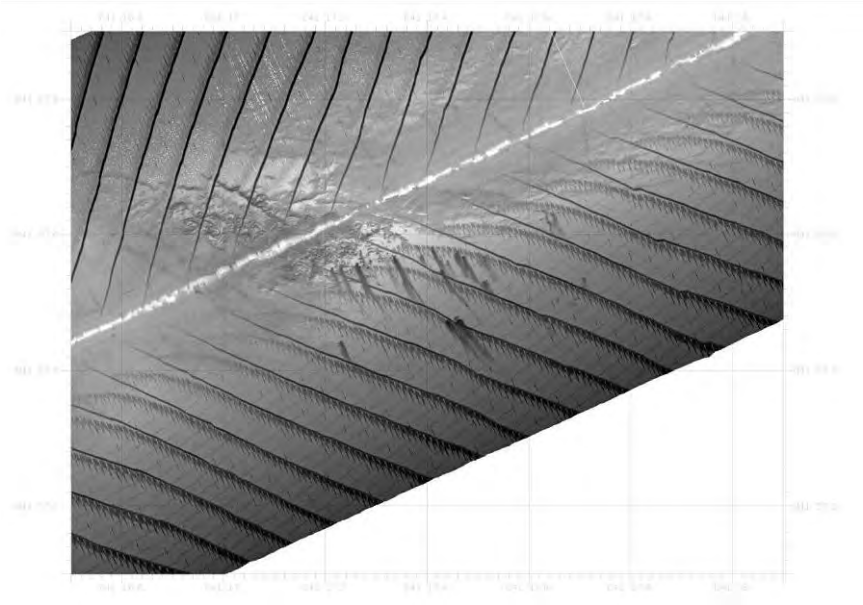

Fig. 40:
75 kHz sidescan sonar image of Batumi seep obtained during the high-resolution survey when the instrument was towed very closely to the seafloor. The lateral incidence nicely shows the location of gas flares on the seafloor. Interference patterns visible on the image result from the concurrent use of 75 kHz and 410 kHz sensors. High backscatter is dark.

5.4.3 Dvurechenskii Mud Volcano

The profile run across Dvurechenskii Mud Volcano (DMV) crossed at least five different mud volcanoes that show quite a diverse range of characteristics from mud pies to cone-shaped, rounded structures. Although processing of the data is only possible using a layback method that takes into account cable length and towing speed, correlation of the image with bathymetry will ultimately allow proper positioning of the images. One important result was the detection of three flares in the raw sonar data (one on Vodyanitskii MV) that was imaged during the previous leg and two on DMV that had not been seen, neither during the ROV dives of Leg M72/3a nor during flare imaging while coring on Leg M72/3b; Fig. 41). Subsequent flare imaging using the Parasound system confirmed the presence of the flare.

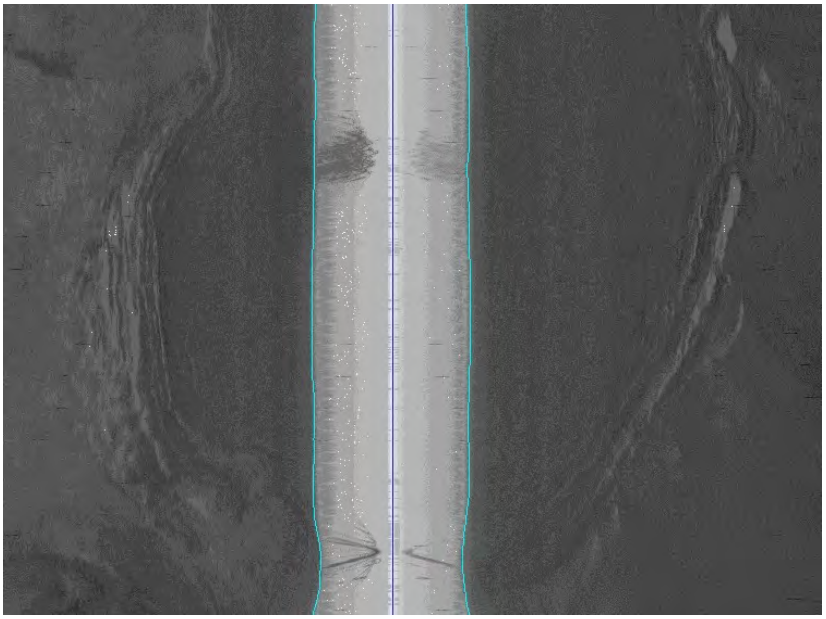

Fig. 41:
Raw sidescan sonar image showing the presence of two flares on Dvurechenskii mud volcano. One flare is located close to the temperature maximum on the mud volcano; the other is present at the rim.

The processed 75 kHz sidescan sonar data over DMV shows the flat-topped structure with creep folds visible near the rim (Fig. 42). Whether these creep folds are only present at the outer rim, or whether these structures only become visible at lateral incidence is not yet clear. There is a small backscatter anomaly

with elevated backscatter near the thermal maximum area of the mud volcano. In addition, a recent mud flow showing high backscatter intensity is visible at the southern flank of the mud volcano. To the northwest of DMV, another mud volcano structure is located with a rougher surface than the former. Here again, elongated zones of high backscatter intensity to the south of the structure point towards recent mud flow activity.

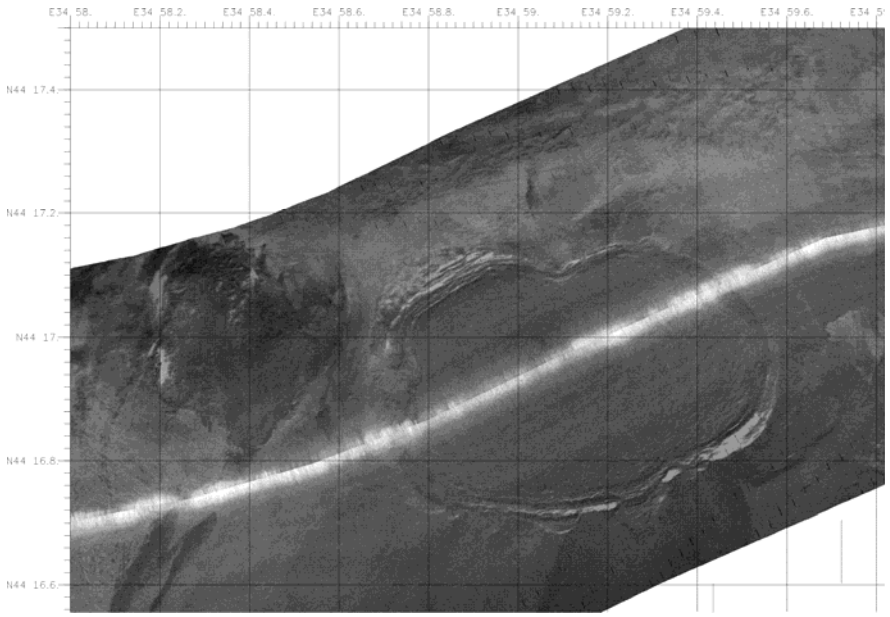

Fig. 42:
75 kHz sidescan profile crossing Dvurechenskii mud volcano. High backscatter intensity is dark.

6 Seismic investigations

(V. Spiess, N. Fekete, S. Fricke, S. Gürcay, H. Keil, B. Preu, A. Zotova)

6.1 Objectives

High resolution multichannel seismic data, acquired during the cruise, were collected to investigate the shallow and deeper subsurface structures in the vicinity of seep locations. As the migration of hydrocarbons is associated with signal attenuation by gas as well as by gas accumulations with higher reflectivity, the detailed imaging of seismic amplitudes will reveal the distribution of gas and the associated migration pathways. In particular, the widespread presence of gas flares in the Black Sea may be associated with an efficient and continuous supply of free gas, which is temporarily trapped at very shallow depth within the gas hydrate stability zone and below.

Seismic surveying during the cruise shall reveal the distribution of free gas and gas hydrate in the upper 10 to 50 m of the sea floor. This information will be related to the surface investigations carried out with other geophysical methods (sidescan sonar, sediment echosounder), and the results from coring, video, and observations with the remotely operated vehicle (ROV). Surveys in the Gudauta Ridge area, the Andrusov Ridge, and the Kerch Strait were of reconnaissance type, while the wider Batumi seep area and the Dvurechenskii mud volcano (DMV) had been subject to previous seismic studies (R/V METEOR M52/1 and R/V PROFESSOR LOGACHEV TTR15). Because of this, a refinement of existing data sets was intended.

6.2 Multichannel seismic equipment

With the GeoB high-resolution multichannel seismic equipment (Fig. 43), small-scale subsurface structures, usually unresolveable with conventional seismic systems, are imaged on a meter to sub-meter scale.

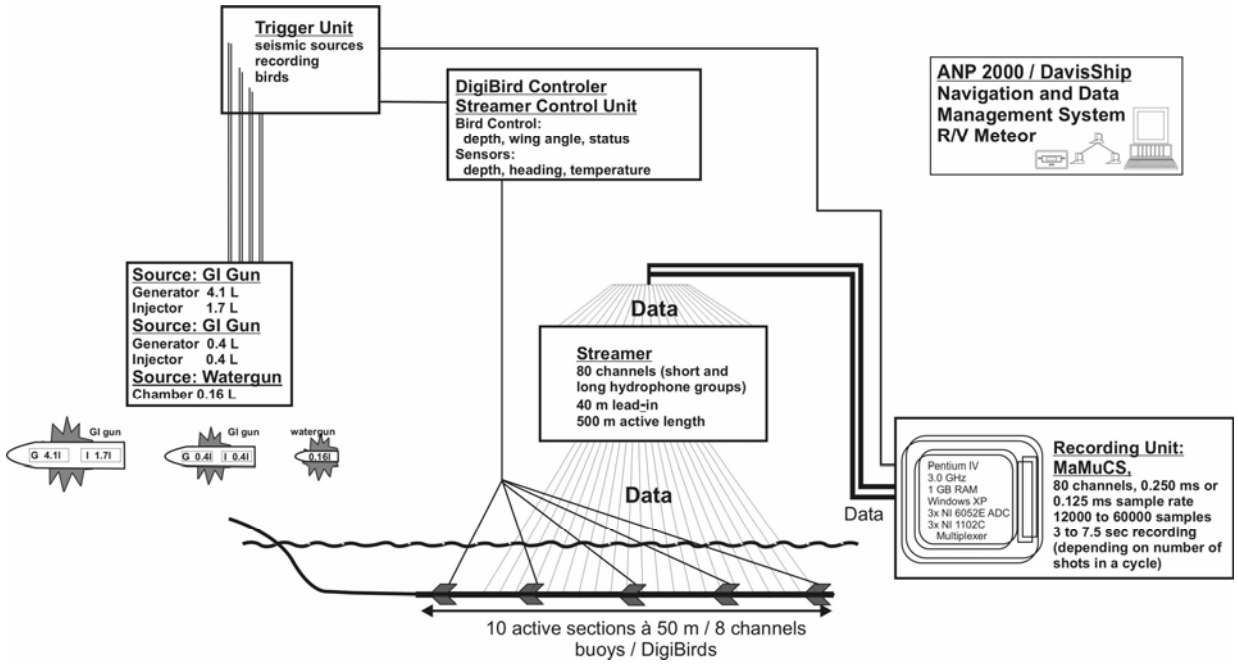

Fig. 43: System setup during Leg M72/3b.

Seismic sources

Three seismic sources were used in various combinations during R/V METEOR cruise M72/3b. One Sodera Generator-Injector (GI) airgun with extended chamber volume (4.1 L generator and 1.7 L injector,

frequency range ca. 30-300 Hz) was towed 7 m below the water surface on the starboard side of the ship. Another GI-gun with reduced chamber volumes (0.4 l both, frequencies between 100 - 800 Hz signal frequency) was towed on the port side in 1.5 m water depth. Both GI guns were operated in harmonic mode (injector volume does not exceed generator volume). At specially selected sites, namely at the Batumi seeps offshore Georgia and the DMV near the Crimean Peninsula (profiles GeoB07-023-095 and GeoB07-104-124), a 0.16 l chamber watergun (Sodera S-15; 0.16 L, 200-1600 Hz) was towed at 0.5 m depth and operated simultaneously with the smaller GI-gun. In these two areas, two simultaneous seismic data sets were acquired, which are characterized by greater depth penetration (GI gun source) and by higher vertical resolution (watergun). During the above profiles, one shot from each of the two sources at a time difference of 0.7 s or 1.5 s in the respective research areas was recorded in one common seismogram. An exception was made during profiles GeoB07-104 to GeoB07-106, where one seismogram contained 3 consecutive watergun shots and a GI gun shot with 800 ms separation inbetween. Shot rates varied from 4 s to 9.5 s, which achieved an approximate shot distance of 10 to 25 m at the usual profiling speed of 5 kns. Profiling simultaneously with the sidescan sonar at an average speed of 2.5 kns (Gudauta Ridge area, profiles GeoB07-002b to GeoB07-005, as well as profiles GeoB07-135 and GeoB07-136 near the Kerch Strait), the shot distance was approximately 8 m. The sources were shot at an air pressure of approximately 150 bar provided by the compressor container. For detailed information about the operation schedule of the sources, see the profile list (Tab. A.3) in the appendix.

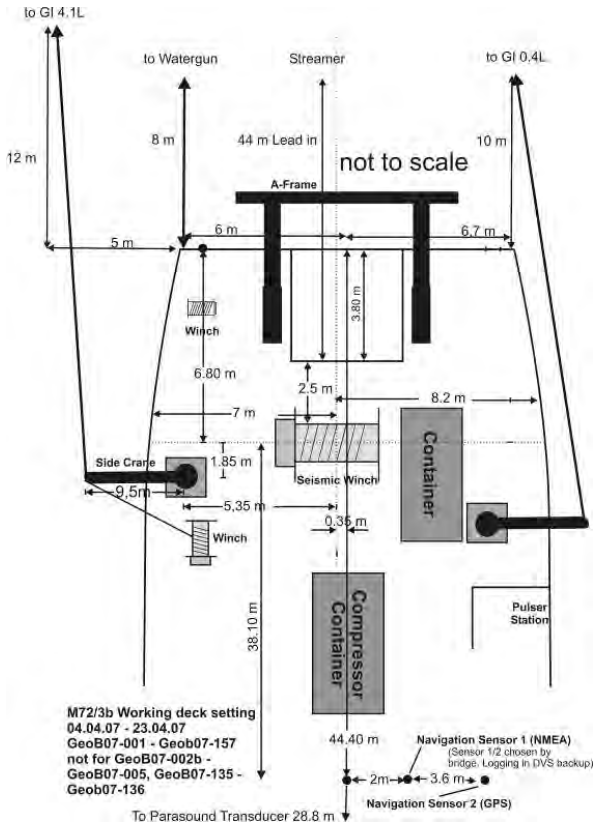

Fig. 44a:
Deck setting and towing geometry during profiling without sidescan sonar.

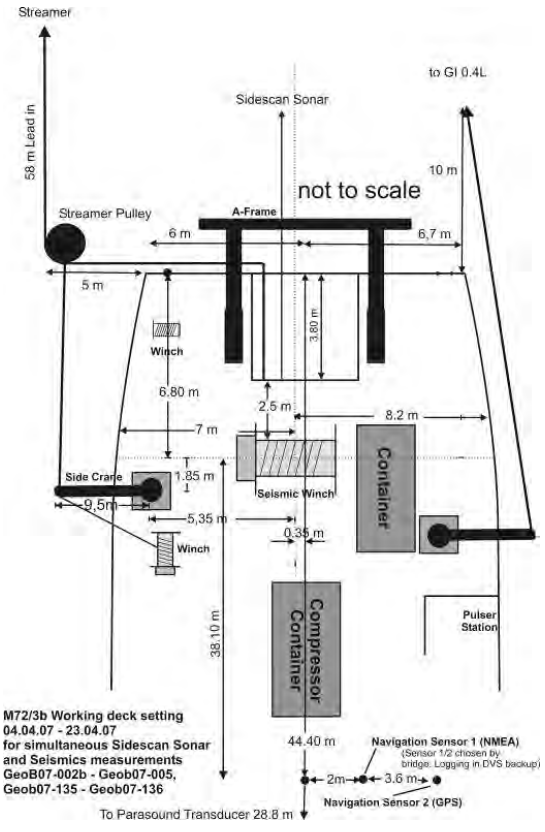

Fig. 44b:
Deck setting and towing geometry during simultaneous profiling with sidescan sonar (profiles GeoB07-002b to GeoB07-005 and GeoB07-135 to GeoB07-136).

The horizontal towing geometry of the seismic sources was unchanged during the cruise and is shown in Figs. 44a and 44b. The large GI gun was towed with the help of a crane on the starboard side approximately 5 m to the side and 12 m behind the ship. The watergun was deployed on the same side from the side wall of the ship and towed 8 m behind the stern. The small GI gun was operated from the port side crane and was approximately 10 m behind the port side wall. The lateral separation between the two latter guns was approximately 13 m, depending on the ship's course and the directions of wind and current. The towing depth of each source was controlled by a buoy tied to the towing cable. Two additional small buoys were fixed to the tail end of the large GI and served to stabilize it within the water column.

Multichannel surface streamer

The multichannel seismic streamer (SYNTRON), used during R/V METEOR cruise M72/3b, included a lead-in, 44 m of which was let out to connect the active streamer sections to the streamer winch, and ten active sections of 50 m length. A 30 m long Meteor rope with a buoy at the end was connected to the tail swivel, resulting in a total tow length of 574 m. A 30 m long deck cable connected the streamer to the recording system.

The streamer's active sections each contained 8 hydrophone groups (Fig. 45). Each of the 6.25 m long hydrophone groups was subdivided into 5 subgroups of different length. One was a single high-resolution hydrophone with a pre-amplifier. A programming module distributed the subgroups of 4 hydrophone groups, i.e. a total of 20 groups, to 5 channels. Every second 6.25 m hydrophone subgroup was completely used with all 13 hydrophones, whereas the two additional channels were reduced in length to 2.2 m and 3.3 m, respectively. All 80 channels were connected to the MaMuCS recording system, independent from the hydrophone group length. Single hydrophones were not recorded. Irrespective of the location within the 25 m units, programming modules were hardwired with the two long groups as first and second channel, at 12.5 m spacing, and the shorter groups as third and fourth channel. Accordingly, channels needed to be rearranged for proper offset assignment, i.e. in every group of 4 channels, the central two needed to be swapped before data processing.

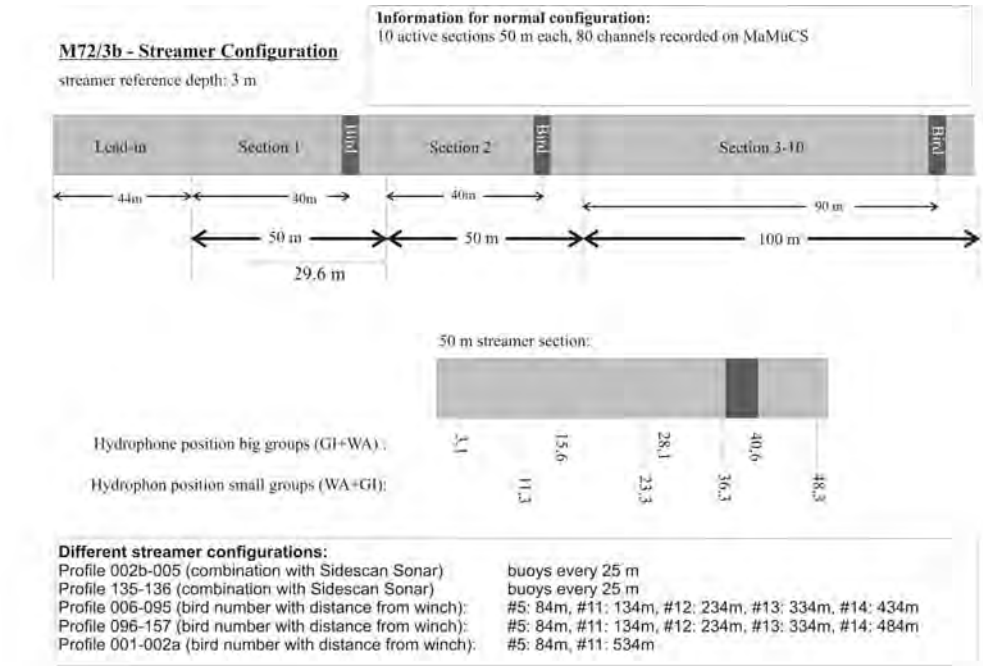

Fig. 45: Streamer setup during Leg M72/3b; streamer reference depth with birds was 3 m, with buoys, 1 m.

During investigations carried out only with the seismic equipment, the streamer was kept at 3 m depth below the surface with the help of 5 Digi birds and was towed midship. Fig. 45 summarizes bird locations relative to the streamer winch. During measurements combined with backscatter profiling (profiles Geo B07-002b to GeoB07-005 and GeoB07-135 to GeoB07-136), a set of 21 buoys took over the task of the birds, keeping the streamer at a depth of 1.5 m, and a specially manufactured pulley was used to lead the streamer to the starboard side. The length of lead-in was adjusted such that only the crosstrack position of the hydrophone groups changed. The along-track distance of the streamer sections behind the point of reference stayed the same as in the case of midship tow.
Because of hardware failure, several changes had to be undertaken during the cruise. The sections #2 and #4 were refilled with isopar oil after profile GeoB07-005, which resulted in an increased signal quality from channels 9 - 16 and 25 - 32. Section #7 had to be moved to the end position due to cable damage at the farther end, which caused deteriorating data quality from behind channel 64 in profiles after GeoB07-006. However, changing the streamer section sequence after profile GeoB07-095 seemed to solve this problem.

Bird Controller

In most profiles, streamer position was controlled and monitored through so-called birds. The system consisted of a controller computer and several Remote Units (RU). Each RU included a depth and a heading sensor as well as adjustable wings. Controller and RUs communicate via communication coils nested within the streamer. A twisted pair wire within the deck cable connected controller and coils.
Five DigiBird RUs (numbers 5, 11, 12, 13, and 14) were available and could be configured using the bird controlling unit. Birds were distributed along the streamer such that the control of streamer attitude was maximized (Fig. 45).
Each trigger signal started the bird's scan of water depth, wing angle, and heading data. The momentary location of the streamer could be displayed as a depth profile on a screen. Bird parameters including date and time were digitally stored on the trigger PC through a hyperterminal.
Before the streamer was deployed, each RU was programmed in the seismic lab to keep an operating depth of 3 m. The RUs thus forced the streamer to the chosen depth by adjusting the wing angles accordingly. Possible depth variations of the streamer could be checked later during preliminary data processing. Depth control appeared to be successful upon further review.

Data acquisition system

For data recording, the custom-designed and PC-based 96-channel seismograph MArine MUltiChannel Seismics (MaMuCS) was used. It is based on a Pentium IV PC (3 GHz, 1 GB RAM) with Windows XP operating system and was operated at a highest sampling rate of 0.125 ms at 16 bit resolution. It is equipped with three 32-channel multiplexers (NI 1102C) and three analogue-to-digital convertors (NI 6052E). The seismograph provides online data display of shot gathers as well as a brute stack section of the range of channels of the user's choice. It stores data in SEG-Y format on the internal hard disk drive. Back-up copies were created during intervals of no seismic activity on an external disk.
Data were recorded at a sampling frequency of 4 kHz (without watergun) or 8 kHz (with watergun) over time intervals of 3 to 7.5 s, resulting in up to 80 x 60000 samples at 4 byte per sample. Anti-aliasing was fixed to 10 kHz on the AD converter. Gain for each channel was set to 100 (measurement range 0.1 V). A filter of 55 to 400 Hz was applied to the displayed data during acquisition with the 4.1 L GI gun and one

of 200 - 1600 Hz was used to visualize watergun shots. However, this did not influence the raw seismic recordings. A connection failure between one of the multiplexers and the recording PC forced recording to be restricted to 56 channels in the profile interval of GeoB07-027 to GeoB07-077. However, the connection was successfully repaired during the next maintenance break.

Radio clock

A crucial part of the seismic data acquisition was that all components ran on exactly the same time, within an error of milliseconds. For this purpose, GPS time was used, which was directly acquired from the satellites through a Hopf GPS-DCF77 radio clock apparatus. The apparatus consisted of a GPS aerial, a radio clock (Hopf modul 6870), a multi-aerial amplifier (modul 4446), and a radio clock PC card (modul 6039). This last item was built into the trigger PC (see Section "Trigger unit"), making it the time server of the seismic acquisition system. GPS time was then distributed via LAN, and all other PCs were synchronized through the NTP (network time protocol) service. Larger time offsets were adjusted "smoothly" within a few minutes rather than in steps, but subsequently clocks were set every second.

Trigger unit

The custom trigger unit used during R/V METEOR Leg M72/3b controls seismic sources, seismographs, and bird controller. The unit was set up on an IBM compatible PC with a Windows NT 4.0 operating system and included a real-time controller interface card (SORCUS) with 16 I/O channels, synchronized by an internal clock. The unit was connected to an amplifier unit and a gun amplifier unit. The PC ran a custom software, which allowed it to define arbitrary combinations of trigger signals. This data was used to optimize the available recording time for two seismic sources and to minimize shot distance.

Trigger times could be changed at any time during the survey. Through this feature, the recording delay could be adjusted to water depth without interruption of data acquisition. The amplifier unit converted the controller output to positive or negative TTL levels. The gun amplifier unit, which generated a 60V / 8A trigger level, controlled the magnetic valves of the individual seismic sources. This was placed in the pulser station close to the gun pressure controls, wich enabled an emergency shutdown of gun operation.

Since the specific working areas did not include large water depth variations, the trigger scheme could be kept relatively simple throughout the whole cruise. Individual survey segments were acquired with a constant time delay between shots and the start of recording, mostly 0 s. The delay was set to 2 s above the Andrusov Ridge (profiles GeoB07-102 and GeoB07-103) and during part of the measurements above the DMV (profiles GeoB07-104 - GeoB07-124). It was increased to 2.4 s in profiles GeoB07-104 through GeoB07-106 until a watergun failure. The trigger scheme for the single operation of 4.1 L GI gun consisted of 6 s cycles, the first 5.5 s were recorded in seismic traces and the remaining time was assigned for the communication between bird RU’s and the bird controller PC (profiles GeoB07-007 to GeoB07-014, GeoB07-016 to GeoB07-022, GeoB07-096 to GeoB07-101, most of profile GeoB07-102, and profile GeoB07-103: Batumi overview lines, Pechori area, Iberia mound and Colkheti area). Data at the Kerch Strait (starting with profile GeoB07-125) were acquired in 4 s cycles with 3 s (up to profile GeoB07-143) or 3.5 s of recording time (starting at profile GeoB07-144).

Seismic lines acquired only with the 0.4 L GI source were triggered every 4 s with 3.5 s (Gudauta area, profiles GeoB07-001 to GeoB07-006; Colkheti seep, profile GeoB07-015) or 3 s of recording (simultaneous sidescan profiles in the Kerch Strait area GeoB07-135 and GeoB07-136).

The combined operation of the small GI gun with the watergun was feasible in 4.5 s cycles with recordings of 1 shot from each gun. Within one seismogram over 3.7 s the watergun was shot 0.7 s after

the GI gun (Batumi area, profiles GeoB07-023 to GeoB07-095). Also, 5-s-cycles with recordings of the last 3 s in each cycle were employed, during which the watergun shot 1.5 s after the small GI gun (DMV, profiles GeoB07-107 to GeoB07-124).
Several test profiles provide an exception to the above described trigger schemes. During profile GeoB07-007, the two GI guns were shot alternatingly every 6 s, with a recorded length of 5.5 s (one shot per seismogram). The same was repeated during profile GeoB07-102 with first a 9.5 s shot rate, then a 7.5 s shot rate, and a delay of 2 s before the start of recording. These tests served the assessment of best shot strategy concerning resolution and penetration of the different gun volumes. During profiles GeoB07-104 to GeoB07-106, three watergun shots followed by a GI shot were recorded in one 5-s-long seismogram. The delay between shots was 0.8 s and the time between the first shot and the start of recording was 24 s. This was done in order to achieve a high lateral resolution in the watergun data while still being able to fully repressurize the GI gun in each cycle (too high of shot rates have a negative influence on the signal strength). This strategy was abandoned when the watergun failed. Apart from its main task, the trigger PC was also used to record navigation data, bird status reports, and act as time server.

Data quality and statistics

Altogether, a set of 157 multichannel seismic profiles were acquired during Leg M72/3b, six of them simultaneously with sidescan sonar measurements. Apart from overview profiles, one complete 3D box of data was recorded at the Batumi seeps offshore Georgia with a line separation of 25 m. A high-density grid was shot above the DMV with a line separation of 40 m. Each seismic source shot over 50 000 times, creating approximately 700 GB of raw data. The sources functioned very reliably. Despite some problems with the streamer and the recording apparatus, data quality was good to very good, and due to the high shot rates, high lateral resolution has been achieved.

Onboard Seismic Data Processing

Onboard processing of seismic data was carried out with the commercial software package VISTA for Windows (Seismic Image Software Ltd.). A large portion of data underwent preliminary processing during the cruise. Brute stack profiles were recorded in real-time during data acquisition (stacked channels were 5-20) and were filtered and debiassed subsequently in order to help select an optimal profiling strategy. This enabled evaluation of data quality and gave a first impression of the subsurface geology. Raw data were processed at important locations within each study area. Acquisition geometry was set up based on estimations.

6.3 Preliminary results

6.3.1 Gudauta Seep Area

Seismic profiling of Leg M72/3b began on the Gudauta Ridge (Fig. 46), where Parasound surveying had revealed active gas flares in the water column and promising seep sites were expected. A short multichannel seismic program started just 24 hours after departure from the port of Trabzon. Four of the seven profiles (GeoB07-002b through -005) were shot concurrently with the sidescan sonar system DTS-1 at an average speed of 2.5 knots, while normal survey speed on the other lines was chosen to be 5 knots. A small GI Gun was used with 2 x 0.4 L chamber volumes.

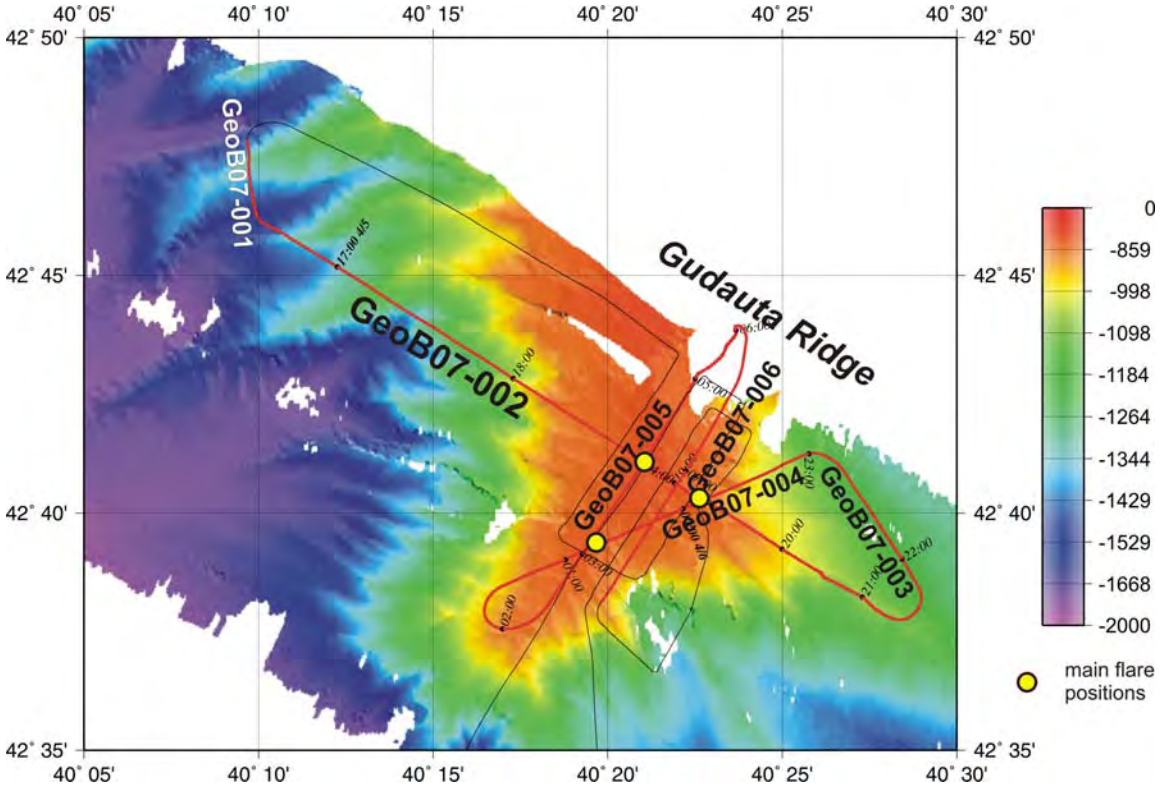

Fig. 46: Track chart of seismic survey on Gudauta Ridge. Major flare locations are indicated by circles. Lines GeoB07-003 through -005 were acquired parallel with the DTS-1 sidescan sonar system at approx. 2.5 knots survey speed.

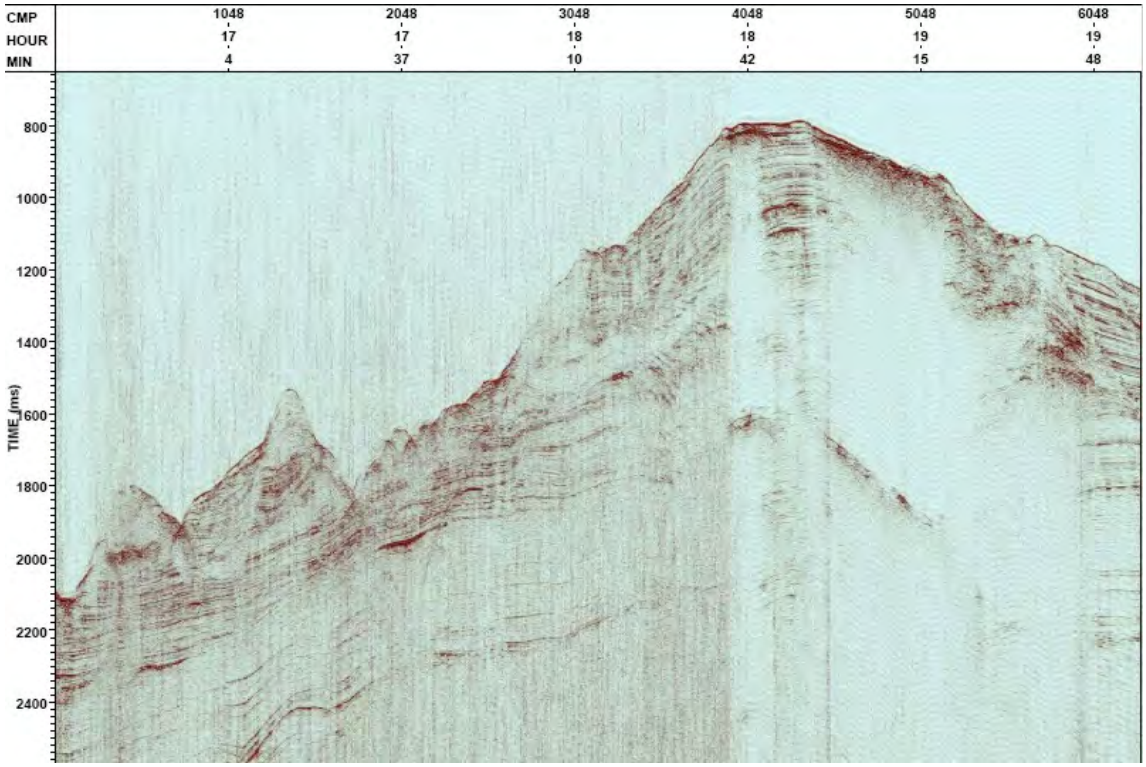

Fig. 47: Multichannel seismic Line GeoB07-002 across Gudauta Ridge. Two distinct zones of columnar blanking are located beneath gas flares in the water column, which were documented with the Parasound 18 kHz signal.

The first long Line GeoB07-002 (Fig. 47) confirmed the presence of flares in the water column. Seismic images also revealed distinct blanking zones, which might indicate massive gas accumulations just a few meters subbottom depth. The flare positions are shallower than the predicted depth of the gas hydrate stability field within the sediments, and so a sealing by gas hydrate bearing sediments can not be expected. The blanking zone was oriented approximately coast-parallel (NW-SE) and perpendicular to the ridge, which would be surprising for a structure that might have originated from diapiric uplift. In the vicinity, sediment structures reveal uniform deposition at depth, but near-surface sediments are more disturbed and show erosional truncation and slumping.

While the first lines suffered in data quality from technical problems in streamer connectors, it improved during the parallel towing of sidescan sonar and MCS when noise was reduced due to lower speed. Furthermore, short shot distances (4 seconds equivalent to 5.1 m) improved stacking results, and seismic images showed finer details of the shallow gas accumulations.

6.3.2 Batumi Seep Area

The Batumi seep area remained one of the focus areas of Leg M72/3b for more than a week, with an alternating sampling program during the daytime and geophysical surveying with MCS and sidescan sonar at night. A mixed seismic program with overview profiles, few lines across known seep sites as Pechori, Colkheti, and Iberia, as well as a three dimensional seismic survey around the Batumi seep were carried out (Fig. 48).

Seismic lines across the Pechori, Colkheti, and Iberia seeps revealed a complex to chaotic reflection pattern, and pronounced blanking zones beneath the top of the elevated seep locations (Fig. 49). Onboard processing showed that even after migration, the top of the seep area remained chaotic with numerous small scale and small offset faults. In addition, higher amplitudes may hint to shallow gas accumulations and/or gas hydrates. The origin of the seepage at depth could not be imaged due to the limited energy and the high frequency optimization of the streamer system (not recording frequencies below 40 Hz).

The main objective of the Batumi seep survey was the detailed investigation of the small scale structure of the seep. Also, the gas and gas hydrate distribution at the surface and identification of migration pathways and feeder channels were examined. Furthermore, potential future drilling with MeBo will require a sufficiently accurate subsurface imaging, which can only be provided by multichannel seismics due to the limited penetration of the Parasound sediment echosounder signal in the very gassy sediments.

Therefore, we carried out a 3D seismic survey with 25 m line spacing, which covered 1.5 days with 72 seismic lines an area of 1.7 nm in length across the 1.0 nm wide seepage area of Batumi, Kobuleti, and Poti seep (Fig. 50). A course of 27° was chosen to basically measure perpendicular to the main fractures observed at the surface in sidescan sonar data. A 0.4 L GI gun and a 0.15 L watergun, shooting both at a rate of 4.5 seconds with a delay of 0.7 sec, were combined to optimize surface resolution and gain deeper penetration through the shallow gas.

Figs. 51 and 52 show parts of Line GeoB07-008, which crosses both the Batumi and Kobuleti seep in NW-SE direction. Clearly a bottom simulating reflector (BSR) can be identified, where higher amplitude gas accumulations are trapped approx. 200 ms beneath the sea floor by gas hydrates. This gas pocket is restricted to the vicinity of Batumi seep and very likely feeds the observed gas flares at the sea floor.

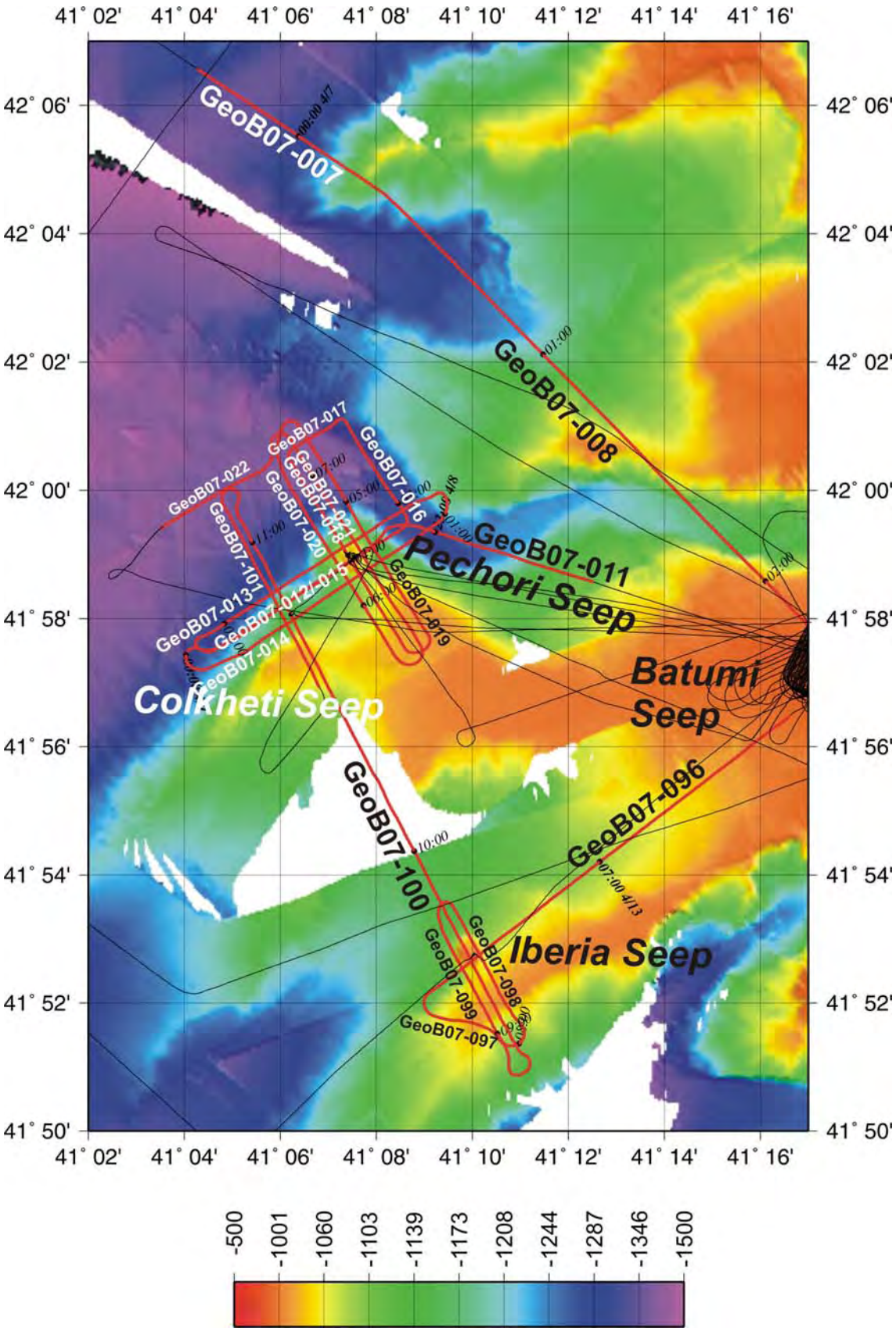

Fig. 48: Track chart of seismic surveys in the wider area of the Batumi seep on Kobuleti Ridge. To study the vicinity of Pechori, Colkheti, and Iberia seeps, between two and four parallel lines were shot with a 4.1 L GI Gun.

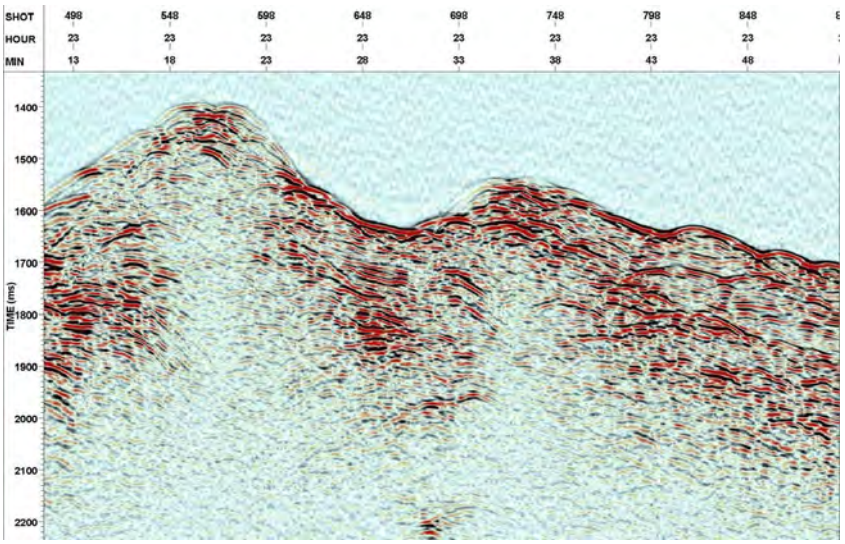

Fig. 49: Multichannel seismic Line GeoB07-012 across Pechori (left) and Colkheti seep (right). On the top of both mounds, high reflection and scatter amplitudes were observed, which might be derived from both shallow gas and gas hydrate accumulation. The surface sediment in the vicinity appeared heavily deformed. Shot distance is approx. 15 m.

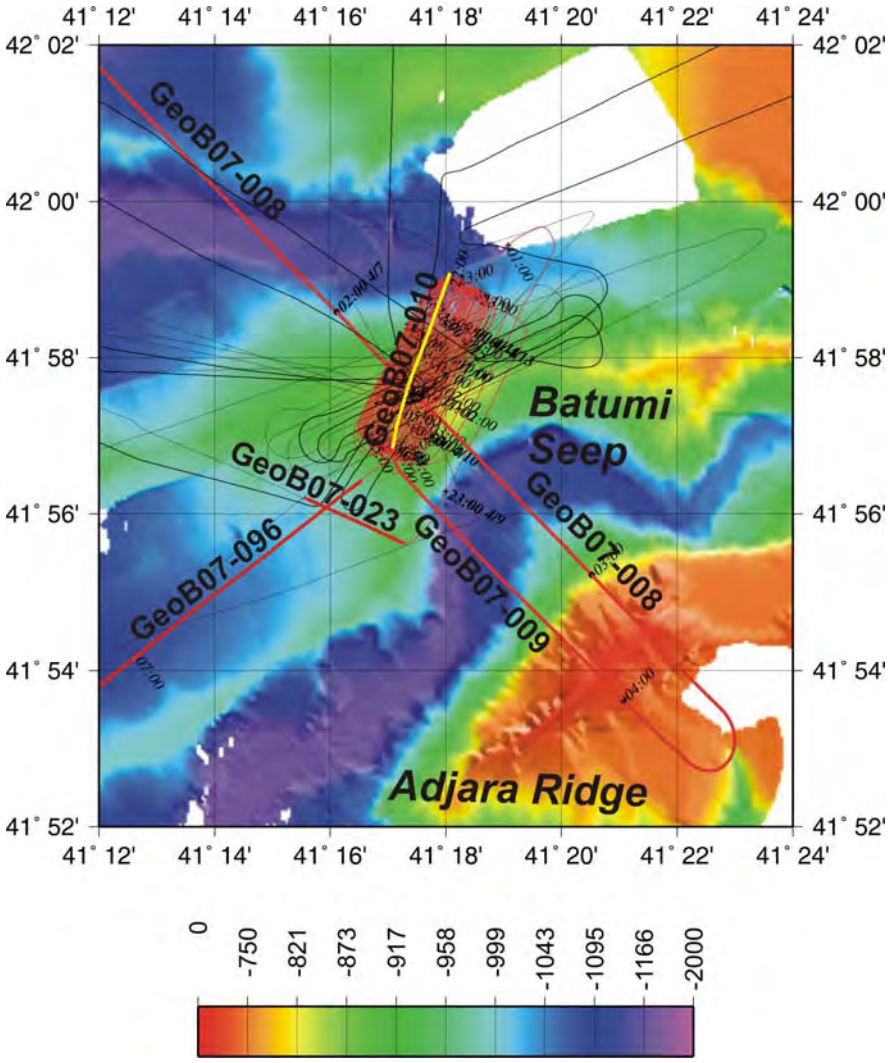

Fig. 50: Track chart of seismic surveys in the vicinity of the Batumi seep. Regional lines were shot with 4.1 L volume (GeoB07-008 and -010), while the 3D survey was carried out with a 0.15 L watergun and a 2 x 0.4 L GI Gun.

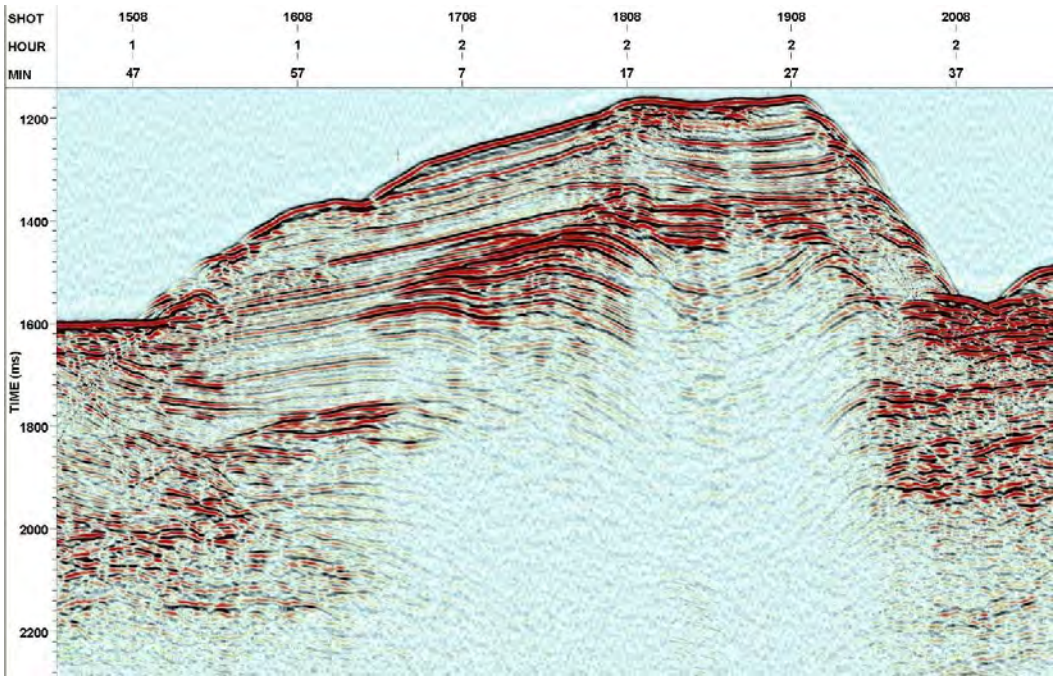

Fig. 51: Multichannel seismic Line GeoB07-008 across Batumi and Kobuleti seeps. A BSR is seen approx. 200 ms beneath the sea floor. Shot distance is approx. 15 m.

A closer look (Fig. 52) also reveals the fine structure beneath the sea floor. High amplitude reflections appear approx. 10-40 ms beneath the sea floor, indicating either a shallow gas reservoir or massive gas hydrate accumulations. The columnar blanking zone is less pronounced than at Gudauta Ridge, probably due to a limited gas supply within the GHSZ.

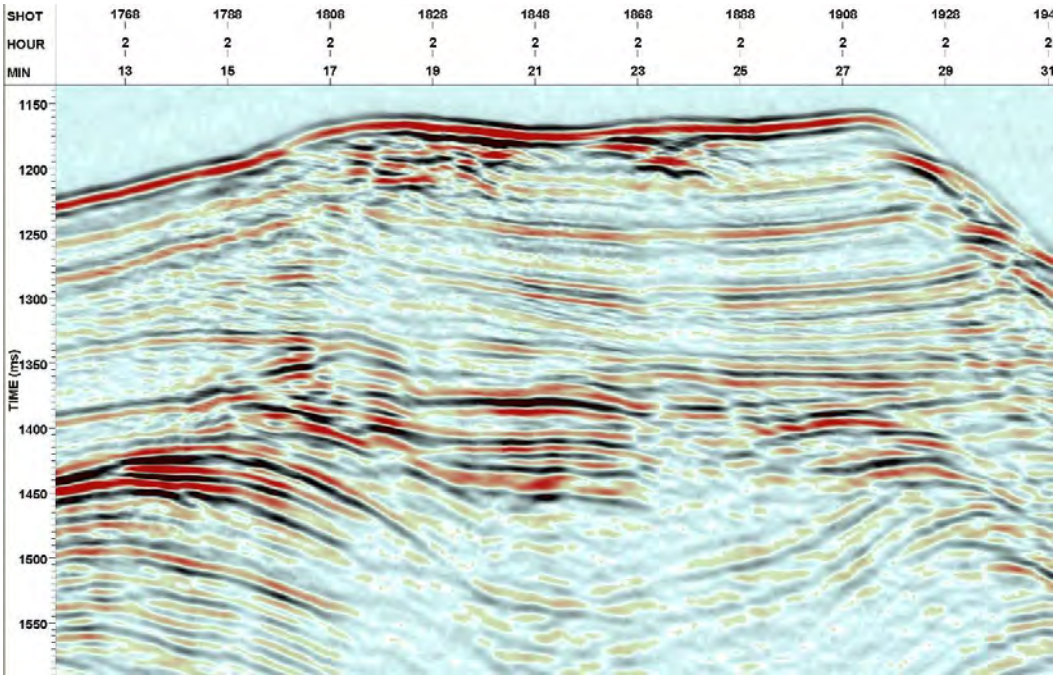

Fig. 52: Close-up of multichannel seismic Line GeoB07-008 across Batumi (left) and Kobuleti seeps (right) with blanking zones beneath and high amplitude patches in the shallow subseafloor. Shot distance is approx. 15 m.

6.3.3 Andrusov Ridge

The Andrusov Ridge is completely covered with a thick sediment package with mostly turbiditic sedimentation occurring in recent times. Accordingly, sediment structures were very uniform across the investigated area. Based on information from the Turkish Petroleum Company (TPAO), several locations had been proposed for further surveying to find indications of seepage. A short bathymetric and seismic survey was carried out, as shown in Fig. 53. And although a few faults had been identified, no further indications of sea floor seepage could be identified.

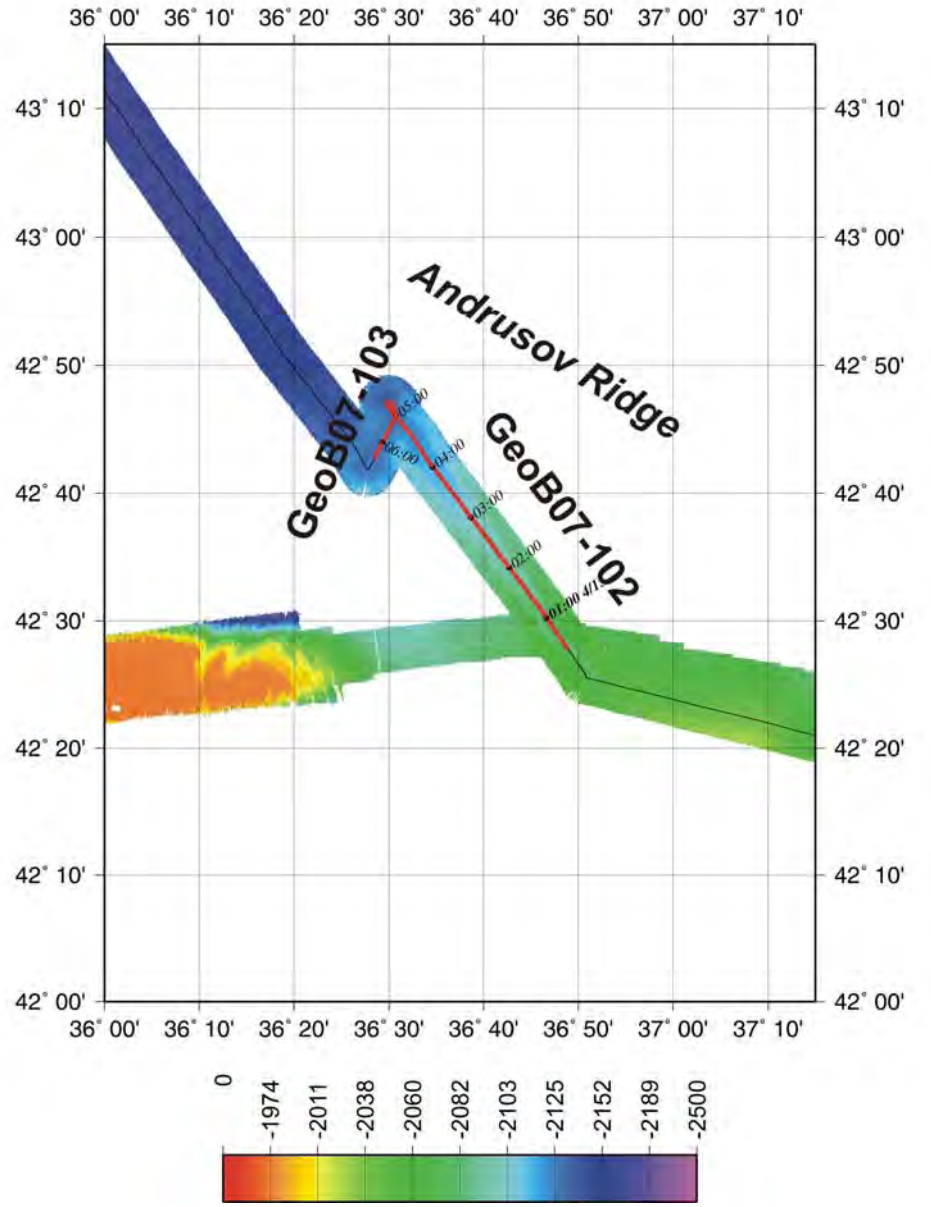

Fig. 53: Track chart of the seismic surveys on Andrusov Ridge, carried out with a 4.1 L GI Gun.

The seismic Line GeoB07-102 (Fig. 54) could not resolve in detail that the track was partially following a few meters deep channel, which was seen in swath mapping data and caused the near-surface diffractions. Also, bright spots and two major faults were found, but the complete absence of shallow gas reservoirs or mud volcano type of structures led to the decision to abandon operation before the deployment of the side-scan sonar.

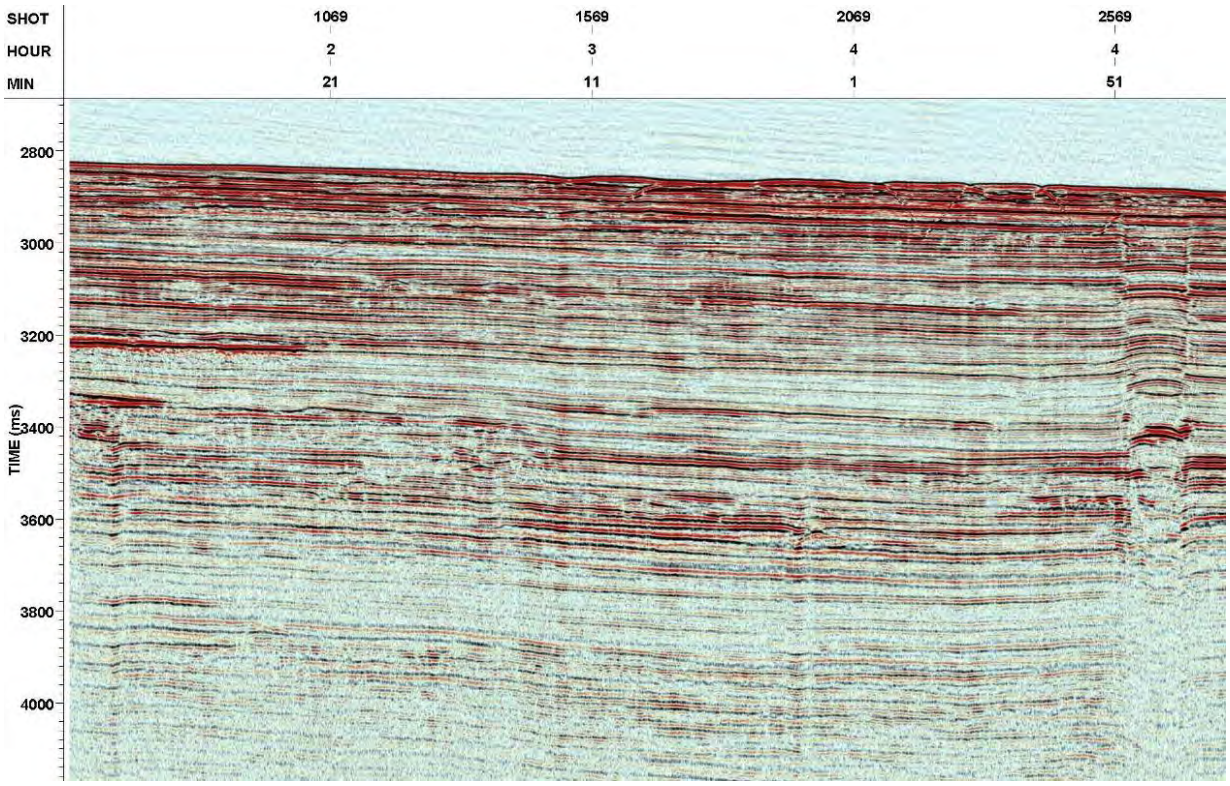

Fig. 54: Multichannel seismic Line GeoB07-102 on Andrusov Ridge. Shot distance is approx. 15 m.

6.3.4 Dvurechenskii Mud Volcano

The Dvurechenskii mud volcano (DMV) had been a focus area during Leg M72/3a for ROV investigations, and during Leg M72/3b, further work was planned for sampling and surveying. As there had already been regional seismic lines collected during R/V METEOR cruise M52/1, we concentrated on the imaging of the internal structure of DMV in particular near the sea floor (Fig. 55).

DMV is one of the few known seeps in the deep sea which produced a significant gas flare. Also, its shape is distinctive from other, conical mud volcanoes in the region. It has revealed a significant temperature anomaly, which confirms its ongoing activity with respect to mud and heat transport. Accordingly, both shallow gas and gas hydrates can be expected. Since high frequency systems such as the Parasound sediment echosounder cannot penetrate the seafloor, only seismic work is suitable to image the surface of its gas-charged flat top.

Altogether 20 lines have been shot in a dense grid, 15 of them across DMV itself, to map the shallow subsurface reflectors, which may be related to the gas flare activity or the temperature anomaly. Fig. 56 shows a seismic example from the center of DMV. Shallow reflectors of both positive and negative polarity are seen, but difficult to interpret from just a stack section. Diffractions at depth may be related to a transport pathway, accumulations of mud clasts, or gas hydrate, but only the spatial image may confirm the meaning of different features. In other lines, clear indications for shallow faults are seen as well as a strong positive amplitude anomaly, which may be explained by a widespread gas hydrate layer.

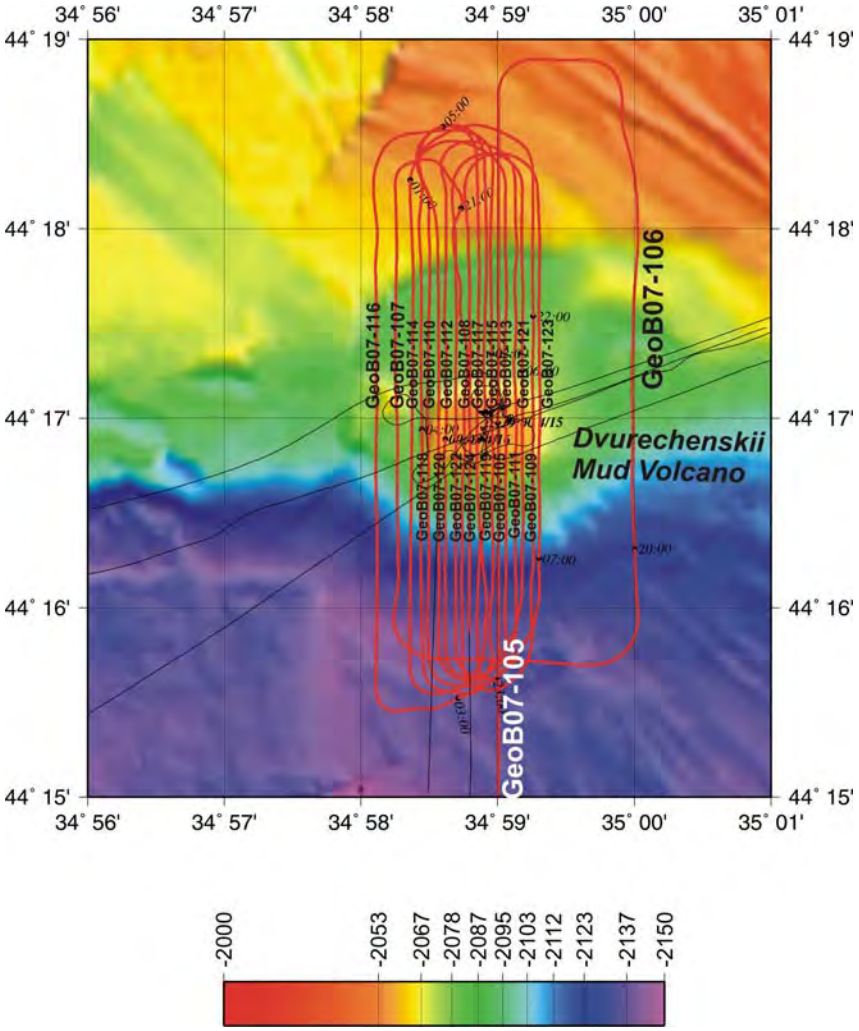

Fig. 55: Track chart of a detailed seismic survey in the vicinity of Dvurechenskii mud volcano, carried out with a 0.4 L GI Gun and a 0.15 L watergun. Line spacing was between 0.05 and 0.075 nm.

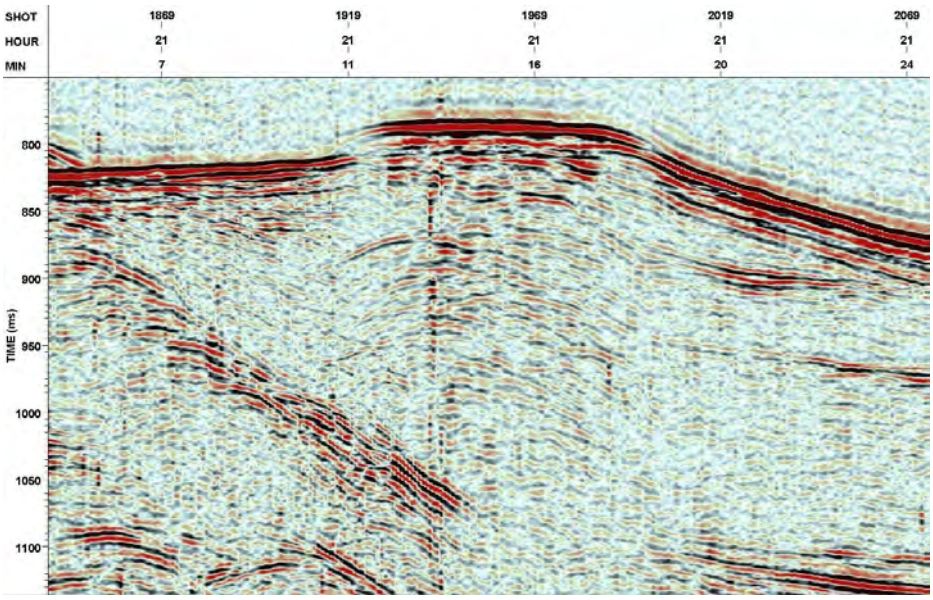

Fig. 56: Multichannel seismic Line GeoB07-108 across Dvurechenskii mud volcano. Several reflectors diffractions are observed in shallow depth beneath the flat top, which may indicate shallow gas or hydrate accumulations. Shot distance is approx. 12.5 m.

6.3.5 Kerch Strait

The combined seismic, bathymetric, and sediment echosounder investigations on the southwestern margin of the Kerch Strait had exploratory character. So far, the only available sources of information were flare investigations carried out by our Ukrainian and Russian colleagues and during Leg M72/3a.

Accordingly, the profiles were located to serve the need for an improved mapping of gas flares, a complete bathymetric coverage, and a first look at subsurface structures with Parasound and multichannel seismics. Altogether 43 seismic lines were shot both perpendicular and parallel to the margin to search for the origin of the intense flare activity in the region and to gain an overview about the tectonic and sedimentary regime.

Fig. 57 shows a track chart from the surveys carried out between station works. Since the sampling work was restricted because of two ammunition dumping sites, surveys concentrate on the northern and the southeastern part of the working area.

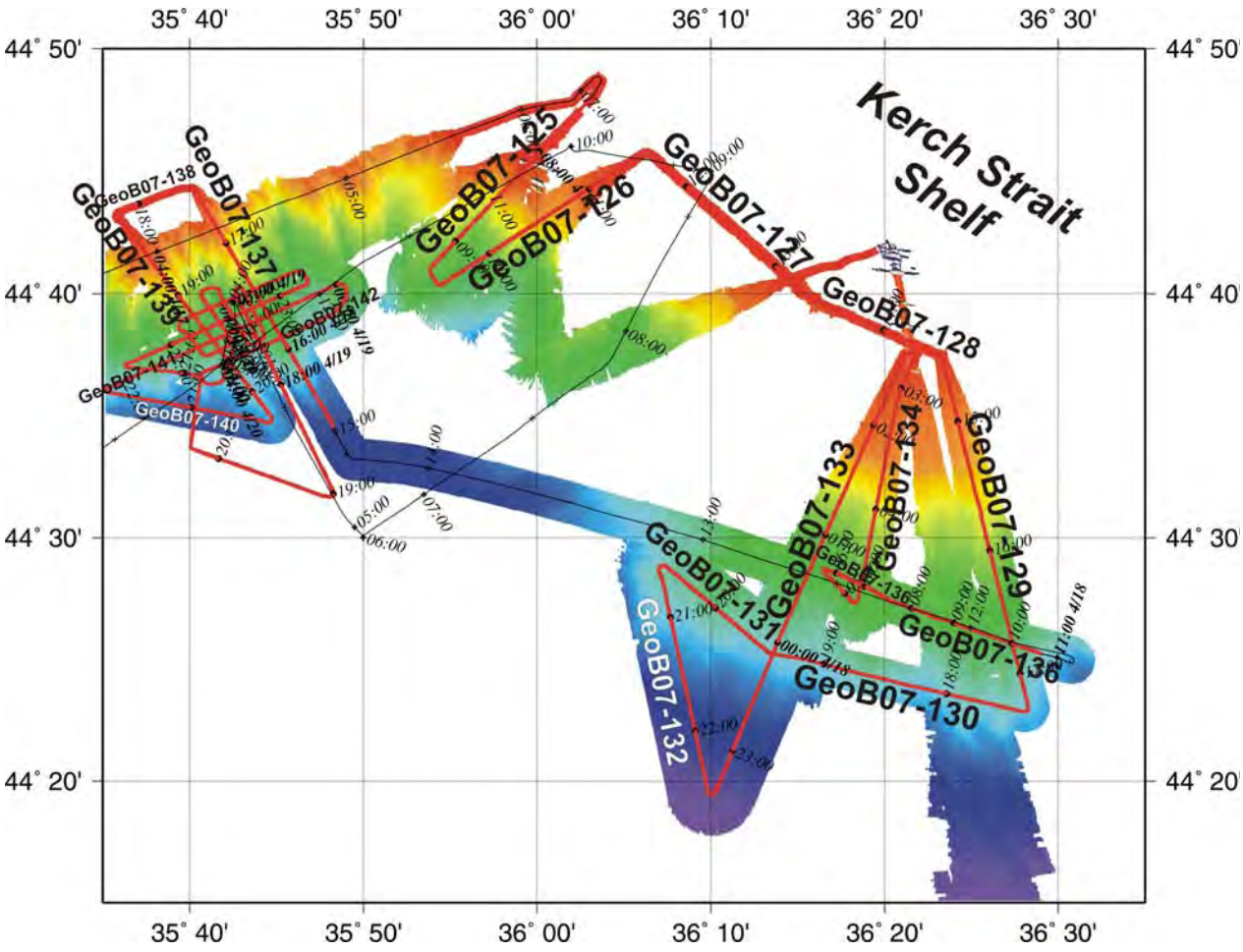

Fig. 57: Track chart of Kerch Strait area, carried out with a 4.1 L GI Gun.

Fig. 58 illustrates the depositional style, which is characterized by uniformly and distinctly layered sediment packages in the upper 300 to 700 ms. Beneath, more chaotic deposits appear, but structural elements are difficult to identify. Probably, a higher energy environment, as within a river-dominated slope fan, has shaped the region. Within the lower unit, numerous high amplitude anomalies can be identified, but clear indications for gas release to the sea floor, at least in water depths greater than 750 m, the upper boundary of the gas hydrate stability field in the Black Sea, were not found. In shallower water, gas flares could be documented by Parasound investigations, and seismic data shows numerous bright spots.

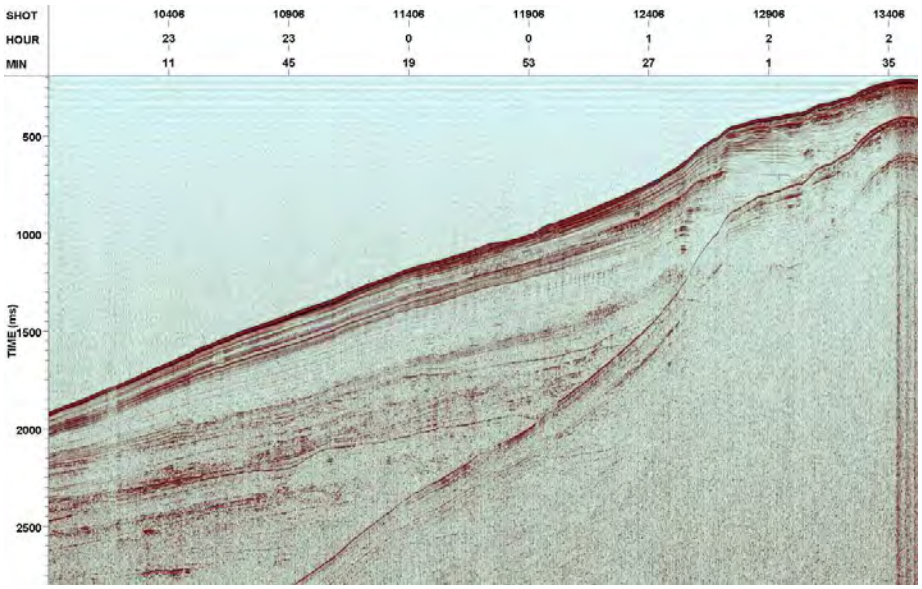

Fig. 58: Multichannel seismic Line GeoB07-133 across the slope of the Kerch Strait area in the southeastern corner of the working area. Here, thick hemipelagic deposits dominate the surface sediments. Shot distance is approx. 10 m.

As a consequence of these observations, we decided to continue our survey in the northern part of the area, where gas flare activity was much more intense. Fig. 59 shows a zoom into the track chart of this survey centered around a deep flare position in 890 m water depth, which we encountered during multichannel seismic Line GeoB07-139 (Fig. 60).

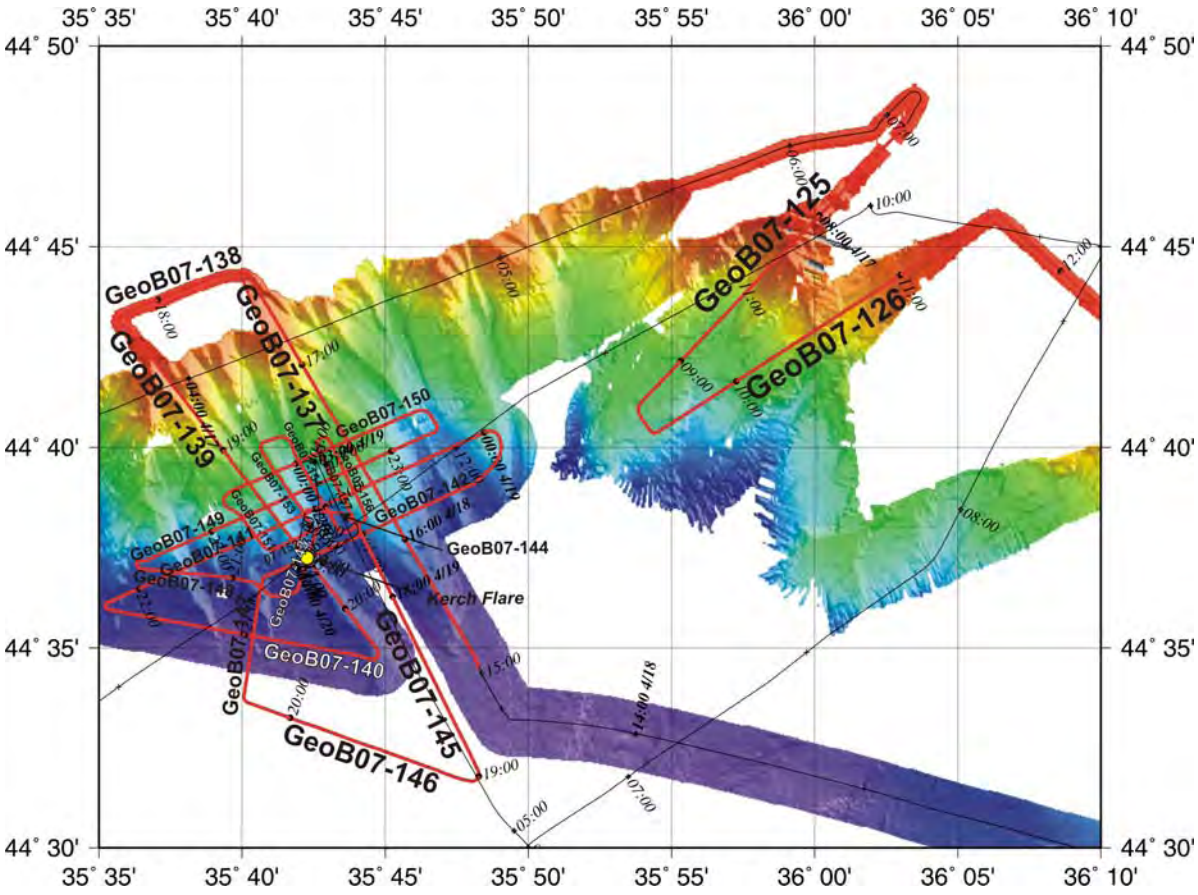

Fig. 59: Track chart of the northern part of the Kerch Strait area, carried out with a 4.1 L GI Gun.

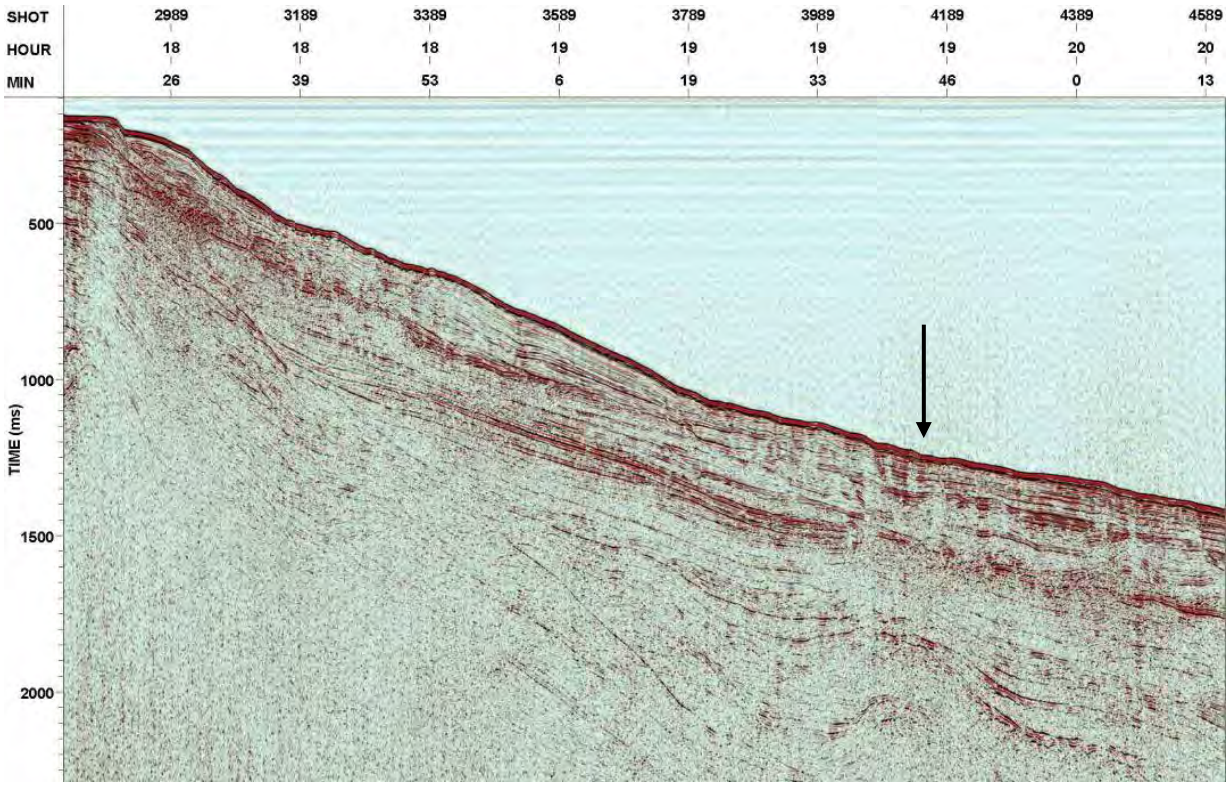

Fig. 60: Multichannel seismic Line GeoB07-139 across the northern slope of the Kerch Strait area. Here, a deep flare was encountered in 890 m water depth. Shot distance is approx. 10 m.

This line also shows a hemipelagic sediment cover, but thinner than in the Southeast. Underneath, chaotic units with amplitude anomalies occur, probably a result of the charge of free gas. In the vicinity of the flare, the deeper high amplitude unit is absent, but anomalies appear at shallower depth and also near the flare position.

Also in this region, traces of a BSR were found in depths shallower than 1000 meters, which motivated us to run a more detailed survey in the water depth interval between 700 and 1000 meters to learn more about the role of a thin GHSZ and its function in sealing the gas exchange with the sea water. Upslope of approx. 750 m water depth, flares appear frequently, and so the absence of flares must be related to shallow gas hydrate seals. Shore based work will reveal details of the collected data, since careful processing and improved resolution are required.

7 Remotely operated vehicle (ROV)

7.1 Technical performance

(C. Seiter, S. Bucklew, P. Forte, P. Franke, D. Hüttich, M. Reuter, M. Zarrouk)

During Leg M72/3a, the remotely operated vehicle (ROV) "QUEST4000m" (Fig. 61) was used aboard R/V METEOR on its 15th scientific mission. ROV "QUEST4000m" is operated by and housed at MARUM - Center for Marine Environmental Sciences at the University of Bremen, Germany. Designed and built by Schilling Robotics, Davis, USA, ROV "QUEST4000m" is the fifth model of Schilling Robotics' electrical work class ROV QUEST series, which is specially adapted to operational use in water depths down to 4000 m for MARUM.

Besides the "QUEST4000m" vehicle, the system includes a full control and handling periphery consisting of 20' control van, 20' workshop van, MacArtney Cormac electrical driven storage winch with 5000 m of 17.6 mm NSW umbilical, and two specially designed transportation vans for the 16 t winch and the 3.3 t vehicle. With an overall weight of 45 t, the Marum QUEST system is well adapted for use on R/V METEOR. During cruising time, the ROV was situated on the aft deck of R/V METEOR. From here launch and recovery of the vehicle was performed with a custom built launch and recovery system (LARS) installed on the A-frame of R/V METEOR.

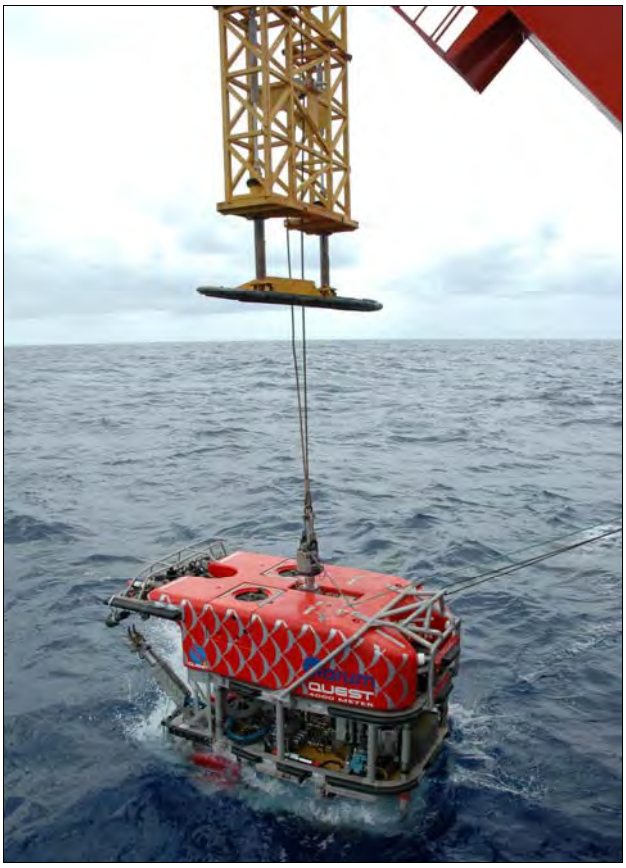

Fig. 61: MARUM ROV "QUEST4000m" deployed from the A-frame mounted custom built launch and recovery system (LARS) behind the stern of R/V METEOR.

The free-flying ROV "QUEST4000m" is standardly equipped with an RDI 1200 Hz Doppler Velocity Log (DVL), which in conjunction with both the 75 kW maximum electrical propulsion power from the seven electric ring thrusters in the latest Schilling Robotics design and the auto control functions (i.e. "Stationkeep", "Auto-heading") provides a relative positioning accuracy for the vehicle within decimeters. In further performance with the ship's stationary mounted IXSEA Posidonia USBL positioning system, an absolute GPS positioning accuracy of ~1 m could be obtained during Leg M72/3a at water depths of 800 m, and around 2 m at water depths of 2000 m. The analogue software tool, DVLNav with display of vehicle, ship, and bathymetry map underlay, allows highly efficient cooperation between ROV pilots and the ship's bridge staff concerning safe vehicle-umbilical-ship-system handling. All relative and absolute vehicle positioning data as well as heading and relative motion data are time coded and stored in a real-time database system (DAVIS-ROV).

During Leg M72/3a, the ROV "QUEST4000m" telemetry and power supply system SeaNet with its vehicle installed two HUBs provided 8 video/ RS-232, 40 RS-232, and 12 RS-485 data channels. Video/ data transfer and communication, control data to the vehicle as well as sensor, diagnostics, and video data from the vehicle, was done via three single mode optical fibers and can be observed and controlled during operation. SeaNet telemetry also provides a convenient implementation and quick handling of third party equipment on the vehicle. The topside control system allows transparent access to all RS-232 and video channels. Via the TCP/IP from the control van net work/database to the ship's net work real-time data distribution to nearly all laboratories on the ship is possible. Sensor data interpretation and processing is possible during dive operation, regardless of the original raw-data format and hardware interface.

The basic "QUEST4000m" vehicle set up includes on the port side a 5-function hydraulic manipulator ("Rigmaster") and on the starboard side a 7-function master arm controlled hydraulic slave manipulator ("Orion") for the handling and performance of operation tasks requiring sampling tools and devices (Fig. 62). Two hydraulically driven, toolskid mounted drawers with boxes and/or custom built mounting frames for cameras and equipment provide the accessibility and storage of these tools and devices as well as of samples.

During Leg M72/3a, the vehicle's front upper porch installed light suite included two Schilling Robotics 10 W HID lights, two DSP&L SA 400 W HMI lights, two DSP&L DML 150 W dimmable lights, two DSP&L DML 500 W lights, and one DSP&L SSA5500 150 W flood light. This light suite illuminated the area in front of the vehicle up to a range of about 10 m depending on the water turbidity. Within this range, detailed high resolution imaging and camera filming was possible with the vehicle's upper pan&tilt mounted color zoom video camera, InsitePacific planar optic PEGASUS. The lower pan&tilt mounted color zoom video camera, InsitePacific dome port PEGASUS, and the 3.34 megapixel digital still camera, Insite Pacific SCORPIO, with two upper front porch installed strobes, and also the near-bottom on drawer mounted InsitePacific ATLAS, has a broadcast quality 870 TVL 3CCD video camera. During Dives 155 and 156, the HD-TV camera InsitePacific ZEUSPLUS, was used on the starboard side toolskid drawer on scientific demand, then it was replaced by the InsitePacific ATLAS due to technical malfunctions. In addition, the overall camera set up contained three InsitePacific AURORAs, which are wide-angle fix-focus color cameras for tool and device handling observation tasks. All camera signals are standardly distributed in the control van for digital video time coded recording, for IFREMER ADELIE software frame grabbing, to the pilot's head up display for navigating, to the ship's bridge supporting the ship's navigators, and also to a ship's laboratory for the most efficient cooperation between pilots, observers, and scientists in the laboratory. Pan&tilt data of both, upper and lower units, are time-coded stored in the real-time database.

Further equipment standardly installed on the vehicle front includes two 532 nm, 5 mW lasers for dimension measuring, a Sea&Sun CTD with additional turbidity sensor, a Sonardyne ROV HOMER acoustic beacon finder for site marking and/or positioning, and a Kongsberg 625 Hz forward looking scanning sonar for mapping and safety reasons in steep and dangerous environments. CTD sensor data are time coded stored in the real-time database.

The stationary toolskid mounted, Benthos model 7381-06, two frequency (123 and 382 kHz) sidescan sonar system was used for online microbathymetry mapping during several dives on Leg M72/3a.

Post-cruise data archives will be hosted by the information system PANGAEA at the World Data Center for Marine Environmental Sciences (WDC-MARE), which is long-term operated by MARUM and the Foundation Alfred-Wegener-Institute for Polar and Marine Research (AWI), Bremerhaven.

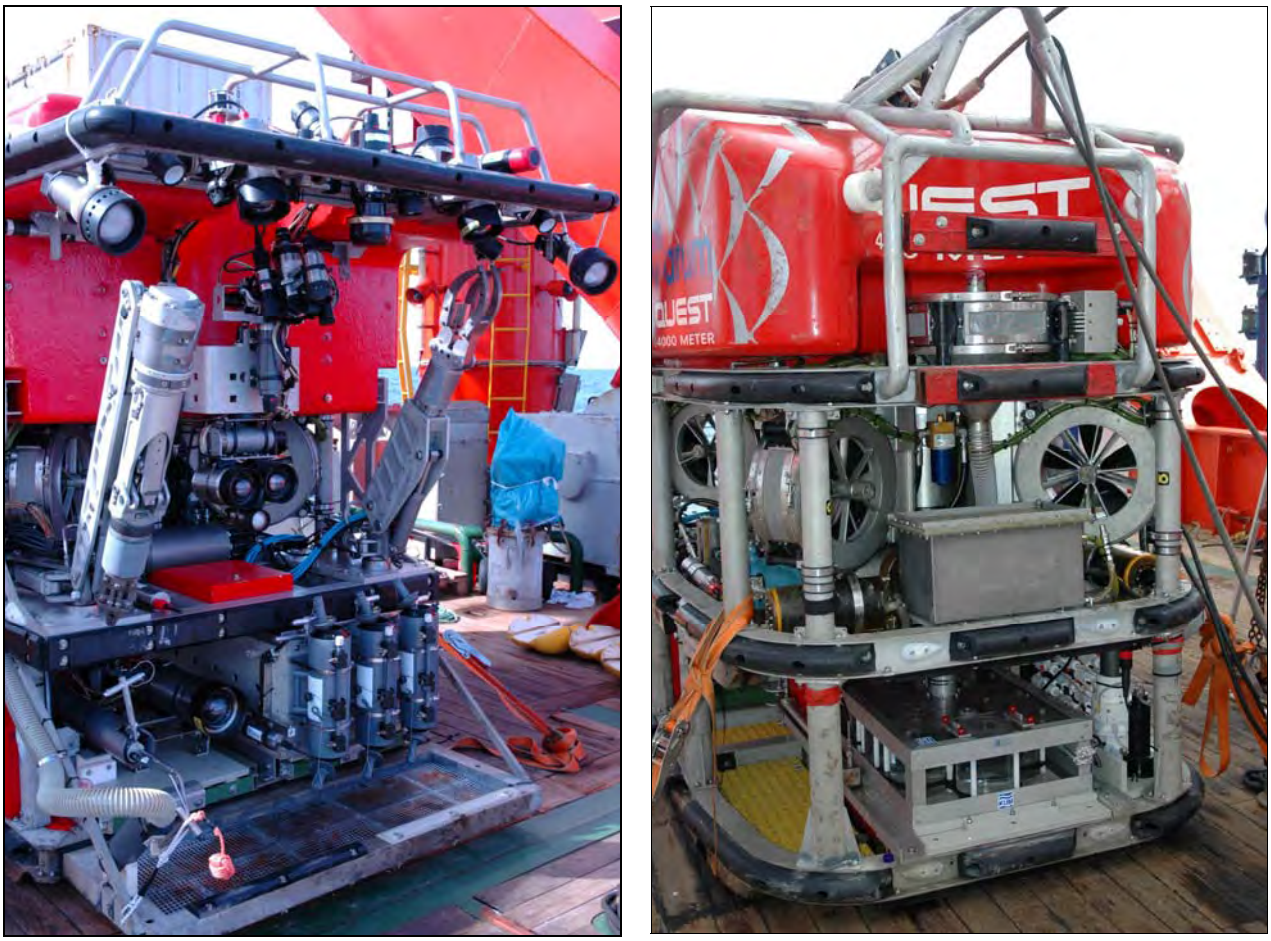

Fig. 62, *left*: ROV "QUEST4000m" front view (from top to bottom): upper porch with lights, strobes, sonar, beacon finder, InsitePacific AURORA cameras, and USBL transducers; upper pan&tilt with light, InsitePacific planar optic PEGASUS, and lasers; lower pan&tilt with InsitePacific dome port PEGASUS and SCORPIO still camera, and light; Orion manipulator on left, Rigmaster manipulator on right; two forward lateral thrusters (FS, FP) on behind; on toolskid from left to right suction/flush hose (for rotary sampler, not used during M72/3a), KIPS fluid sampling nozzle and high temperature sensor (not used during M72/3a), InsitePacific ATLAS, tool/sample box with three Niskin bottles; lower porch with grating

right: ROV "QUEST4000m" aft view (from top to bottom): syntactic foam block with aft guard; thruster vertical aft (VA) frequently in suction pump function with suction hose adapter (not used during M72/3a); two aft lateral thrusters (AS, AP) with 4 kW high power lights transformer and two compensators; toolskid with rotary sampler (not used during M72/3a) in the middle and KIPS pump and valve pack to the right (not used during M72/3a)

During cruise M72/3a, ROV "QUEST4000m" performed 9 dives. All dives were planned in cooperation with the science team, using underlay maps produced and processed by the team from the DFG-Research Center Ocean Margins (RCOM) at Bremen University, Germany. A total dive time of 99 hrs 08 min including 79 hrs 35 min bottom time was achieved with a highly efficient operational quality.

7.2 Dive observations and protocols

(G. Bohrmann, H. Sahling, G. von Halem, M. Brüning, S.A. Klapp, S. Althoff, Y.G. Artemov, B. Bozkaya, E. Kozlova, A. Nikolovska, V. Mavromatis, T. Pape, J. Rethemeyer, F. Schmidt-Schierhorn, K. Wallmann)

We performed 9 ROV dives during R/V METEOR cruise M72/3a in Ukrainian (4 dives) and Georgian waters (5 dives). Details of the dives are listed in Tab. 3. For each dive we developed a detailed dive plan based on the scientific objectives. The following tools were primarily handled and/or released with the 7-function "Orion" slave manipulator, and if necessary supported by the 5-function "Rigmaster" manipulator: (1) gas bubble sampler (GBS) for *in situ* high pressure gas samples, (2) gas bubble catcher (GBC) for estimating gas quantifications at flare sites, (3) T-probe for *in situ* T measurements, (4) autonomous T-logger, stationarily mounted to ROV frame and toolskid, and (5) push cores for sediment sampling. Additionally, the Kongsberg 625 Hz forward looking scanning sonar was used to provide high resolution sonar recordings and screen shots with bitmap-export for gas flare identification and quantification. "QUEST4000m" was also used for inspection of a gravity core mooring, deployed during the previous cruise M72/2, and for recovering an autonomous long term T-logger from there. During M72/3a, ADELIE-GIS (Geographic Information System) from Ifremer was used to post process the ROV "QUEST 4000m" navigation data. *Adelie GIS* offers the possibility of filtering and smoothing the navigation. First the "raw" navigation data are filtered by the criteria's depth and speed, so that descend and ascend as well as navigation points which have an unrealistic speed are filtered (Fig. 63). Finally the navigation curve was smoothed out using Gaussian smoothing and the smoothed data table was exported as an Excel file and merged with the dive protocol file (Fig. 63).

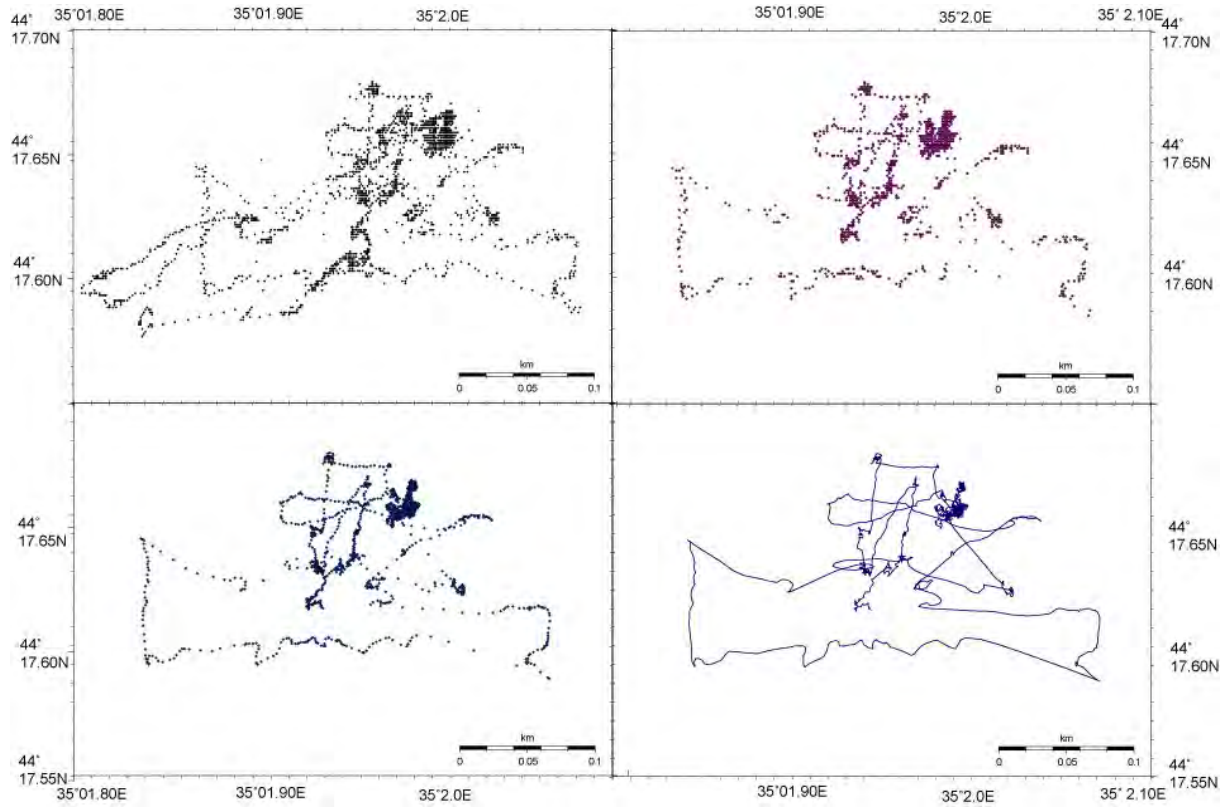

Fig. 63: Four plots showing the post dive navigation processing; (*upper left*) raw data, (*upper right*) depth and speed filtered, (*lower left*) smoothed and finally (*lower right*) converted to a line.

Table 3: Overview about ROV dives performed during M72/3 including major meta data and dive characteristics.

Dive number/GeoB	**Dive 155 / 11901**	**Dive 156 / 11904**	**Dive 157 / 11907**	**Dive 158 / 11908**	**Dive 159 / 11910**	**Dive 160/ 11915**	**Dive 161/ 11917**	**Dive 162/ 11919**	**Dive 163/ 11921**	**Total 9 dives**
Area	Colkheti Seep	Batumi Seep	Batumi Seep	Egorov Seep	Dvurechenskii MV	Dvurechenskii MV	Vodyanitskii MV	Batumi Seeps	Batumi Seeps	**Ukraine 4 Georgia 5**
Scientist	Bohrmann	Sahling	Brüning	Pape	Klapp	Bohrmann	Sahling	von Halem	Brüning	
Date	20 March 2007	21 March 2007	22 March 2007	24 March 2007	25 March 2007	27 March 2007	28 March 2007	30 March 2007	31 March 2007	
Start at bottom (UTC)	07:52	08:20	11:42	14:50	08:05	08:08	13:30	12:35	05:47	
End at bottom (UTC)	17:05	18:15	20:27	18:54	17:58	16:45	22:30	19:05	19:25	
Bottom time (h:m)	09:13	09:55	08:45	04:04	09:53	08:37	09:00	06:30	13:36	**79:35**
MiniDVD tapes	10 x A = Pegasus 10 x B = DSPL	10 x A = Pegasus 10 x B = DSPL	7 x A =Atlas 7 x B = DSPL/ Pegasus	3 x A = Atlas 3 x B = DSPL/ Pegasus	11 x A =Atlas 11 x B = DSPL/ Pegasus	9 x A =Atlas 9 x B = DSPL/ Pegasus	8 x A =Atlas 8 x B = DSPL/ Pegasus	7 x A =Atlas 7 x B = DSPL/ Pegasus	14 x A =Atlas 14 x B = DSPL/ Pegasus	158 tapes
HDCam tapes	2	3								
Minfilms ROV	Pegasus + Zeus	Pegasus + Zeus	Atlas	Atlas	Atlas	Atlas	Atlas	Atlas	Atlas	
Tools/ Measurements										
Push cores (no.)	-	2	4		4	10	1			21
Gas bubble sampler	1 (#1)	2	2				1	1	1	8
Bubble catcher small		6	2					1	1	
Bubble catcher large		2								
Sediment sample	1					1				2
Temperature stick	2	3	1		8	11	1			26
Marker /Special		1 Marker 1 (No. 1)	2 Marker (No.2 + 3)		T-string recovery					

7.2.1 *Dive 155 (GeoB 11902)*

Area:	Colkheti seep, western Kobuleti Ridge, Georgia		
Responsible scientist:	Gerhard Bohrmann		
Date:	Tuesday, 20 March 2007		
Start at Bottom (UTC):	07:52		
End at Bottom (UTC):	17:05		
Total bottom time:	9 hours and 13 minutes		
Start at the bottom:	41°57.945'N	41°06.197'E	1093 m water depth
Start ascend:	41°58.071'N	41°06.197'E	1112 m water depth

Scientist schedule:

07:53 – 10:00	Markus Brüning / Gerhard Bohrmann
10:00 – 12:00	Elena Kozlova / Heiko Sahling
12:00 – 14:00	Aneta Nikolovska / Heiko Sahling
14:00 – 17:05	Stephan A. Klapp / Gerhard Bohrmann

Table 4: Instruments/tools during Dive 155.

GeoB	Tool/instrument	Start	End	Lat. [°N]	Long. [°E]
11902-1	gas bubble sampler -1	10:20	10:52	41:96.785	41:10.329
11902-2	temperature stick-1	11:28	11:40	41:96.785	41:10.328
11902-3	temperature stick-2	11:42	11:53	41:96.786	41:10.328
11902-4	sediment sample-1	16:37	16:40	41:96.786	41:10.329

Waypoints:	Start:	41°57.95'N	41°06.20'E
	WP 1:	41°58.07'N	41°06.19'E (TTR-15 cruise)
	WP 2:	41°58.20'N	41°06.00'E
	WP 3:	41°58,40'N	41°06.20'E

Description of the dive

Colkheti seep is morphologically less evident than Pechori mound which lies about 2 km southwest of Pechori mound on the southwestern flank of Kobuleti Ridge. The structure forms a nose of 500 to 700 m in diameter with a highly structured surface at the flank of the ridge. It is oriented to the north. Oil slicks had been observed in satellite data and by visual observation during R/V PROFESSOR LOGACHEV in 2005 (TTR-15 cruise). During the cruise, a TV-grab was successfully deployed after several hours of sea-floor observations directly over a site where bubble release on the seafloor was observed in the video camera. The TV-grab contained huge amounts of yellow to brown methane hydrates closely associated with oil.

Based on this sampling, the site was chosen for seafloor observation in order to inspect the bubble release and to sample sediment and gas. In principle, a south to north transect was planned to cover the TV-grab site (WP1 in Fig. 64). The ROV reached the bottom approximately 220 m south of WP1 (Fig 64). After a short time inspecting the seafloor at the start point location, the ROV moved up to a survey depth about 25 m above the seafloor. While heading north, the forward looking sonar of the vehicle was used to detect bubble streams in the water column by anomalies in the sonar images. This goal was reached at WP1, where a single bubble stream was found after an acoustic anomaly had been observed and the ROV moved into a bubble stream in the water column. Bubbles were recorded by HDCAM and ROV "QUEST4000m" dived down to the bubble release spot on the seafloor. When the vehicle placed on the seabed, drops of oil have been observed. The gas bubble sampler was used (Fig. 65, left) and collected bubbles over

25 minutes. A clear hydrate formation around the bubbles was observed, although it was not clear how much free gas and gas hydrate existed in the funnel (Fig. 65, right). After enough free gas had been caught, the mixture of gas and gas hydrate was sucked into the pressure chamber by opening and closing the valve again. After we recognized that push core sampling was not possible (tools were incomplete), two T-stick measurements were taken, first 10 and then 20 cm away from the bubble site.

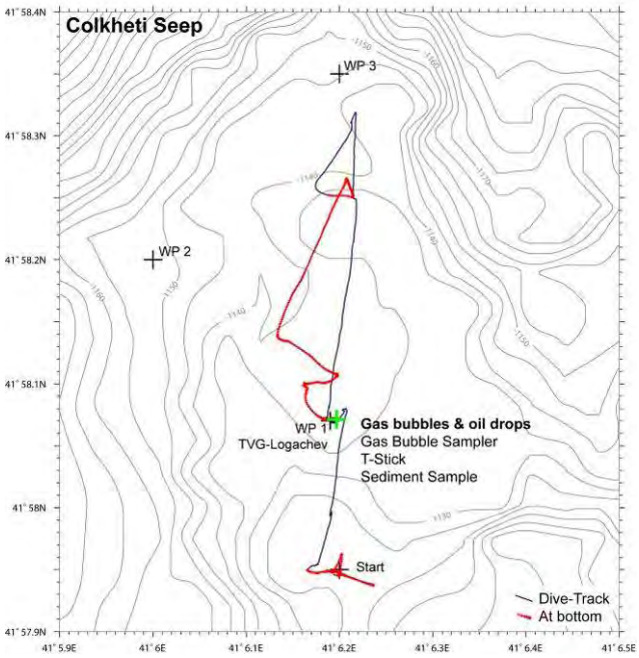

Fig. 64: Survey track over Colkheti seep during ROV Dive 155.

After this sampling program, a further sonar survey 25 m above the seabed to the north (heading to WP3) failed in finding more bubble sites and it was decided by the scientists to dive back to WP 1 during which seafloor observations were performed. 150 m north of WP1, another bubble inspection by sonar was started after the information from the bridge came about an acoustic anomaly observed by the multibeam system from the ship. The anomaly was first found in the forward looking sonar, however, the signal became weak after a while and the sonar signal of bubble stream from WP1 appeared again by heading to the southeast. A second inspection of the same site showed a clear additional bubble stream on the seafloor very close by the two other streams observed during the first time. After an oil-rich sediment sample was taken by a hand net, we poked in the sediment using a knife in the manipulator arm. Yellow to brownish hydrate pieces (oil-rich hydrates) floated immediately upwards from the site, where the manipulator arm of the ROV had poked. This was a clear indication that shallow gas hydrate was present. Ascent of the ROV started after 8 hours and 57 minutes of diving.

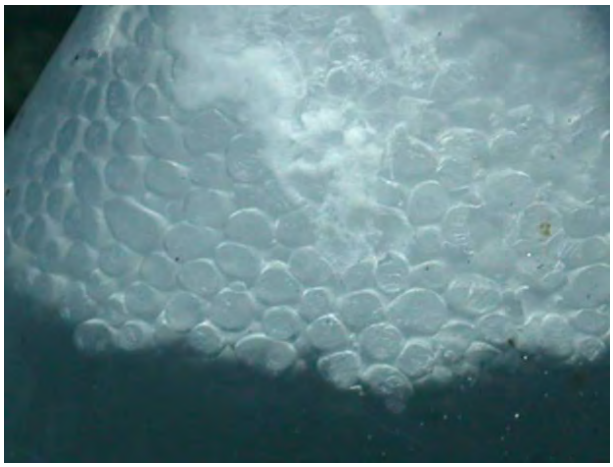

Fig. 65: *Left*: Gas bubble sampler used during ROV Dive 155. The uppermost part of the funnel is filled with a mixture of gas hydrate and probably free gas, before the valve of the pressure chamber was opened. The pressure chamber has atmospheric pressure, which sucked the gas hydrate/free gas into the chamber, after it was opened. *Right*: Detail of the funnel showing the bubble fabric of the hydrate, which developed during the procedure of collecting the bubbles.

7.2.2 *Dive 156 (GeoB 11904)*

Area:	Batumi seep, Georgia		
Responsible scientist:	Heiko Sahling		
Date:	Wednesday, 21 March 2007		
Start at Bottom (UTC):	08:20		
End at Bottom (UTC):	18:15		
Total bottom time:	9 hours and 55 minutes		
Start at the bottom:	41°57.945'N	41°17.108'E	812 m water depth
Start ascend:	41°57.565'N	41°17.507'E	824 m water depth

Scientist schedule:

08:15 – 09:45	Heiko Sahling / Aneta Nikolovska
09:45 – 12:00	Markus Brüning / Aneta Nikolovska
12:00 – 14:00	Heiko Sahling / Markus Brüning
14:00 – 16:00	Heiko Sahling / Gregor von Halem
16:00 – 18:00	Aneta Nikolovska / Gregor von Halem
18:00 – 18:10	Aneta Nikolovska / Gregor von Halem

Table 5: Instruments/tools during Dive 156.

GeoB	Tool/instrument	Start	Lat. [°N]	Long. [°E]	Water Depth [m]
Flare Cluster 3					
11904-1	bubble catcher small	12:17	41:57.529	41:17.272	835
11904-2	bubble catcher small	12:47	41:57.529	41:17.272	835
11904-3	bubble catcher small	12:50	41:57.530	41:17.271	835
11904-4	bubble catcher small	12:52	41:57.530	41:17.273	835
11904-5	bubble catcher small	12:56	41:57.529	41:17.272	835
11904-6	bubble catcher small	13:01	41:57.529	41:17.271	835
11904-7	gas bubble sampler II	13:17	41:57.529	41:17.272	835
11904-8	bubble catcher large	13:43	41:57.529	41:17.272	835
11904-9	bubble catcher large	13:54	41:57.529	41:17.273	835
11904-10	temperature Stick	14:15	41:57.529	41:17.271	835
11904-11	temperature Stick	14:27	41:57.528	41:17.270	835
11904-12	temperature Stick	14.35	41:57.529	41:17.271	835
11904-13	push core 47	15:02	41:57.529	41:17.270	835
11904-14	marker 1	15:16	41:57.528	41:17.271	835
Flare Cluster 5					
11904-15	push core 46	16:49	41:57.540	41:17.414	833
11904-16	gas bubble sampler I	17:33	41:57.541	41:17.413	833

Waypoints:	Start:	41°57.52'N	41°17.10'E
	WP 1:	41°57.55'N	41°17.60'E
	WP 2:	41°57.45'N	41°17.43'E

Description of the dive

Using the horizontal-looking sonar on the ROV we looked and found Flare Cluster No. 1 (Fig. 66). A few bubble streams were escaping through the "perforated but smooth" surface. Good images were captured with HD camera ZEUS, but shortly after that the camera failed and did not work again until the end of the cruise. The bubble streams were too small to cause a significant backscatter signal in the sonar, therefore, no scans were made and we did not try to quantify the bubble escape by use of the bubble catcher.

The next target was Flare Cluster No. 2, where sonar scans were used for quantification as we approached it. A short look around at seafloor showed that the bubbles were more vigorous compared to Flare Cluster No. 1, with several bubble streams. The seafloor was “Perforated and structured” with irregular surface and some chimney-like structures were found. We conducted no quantification by tools.

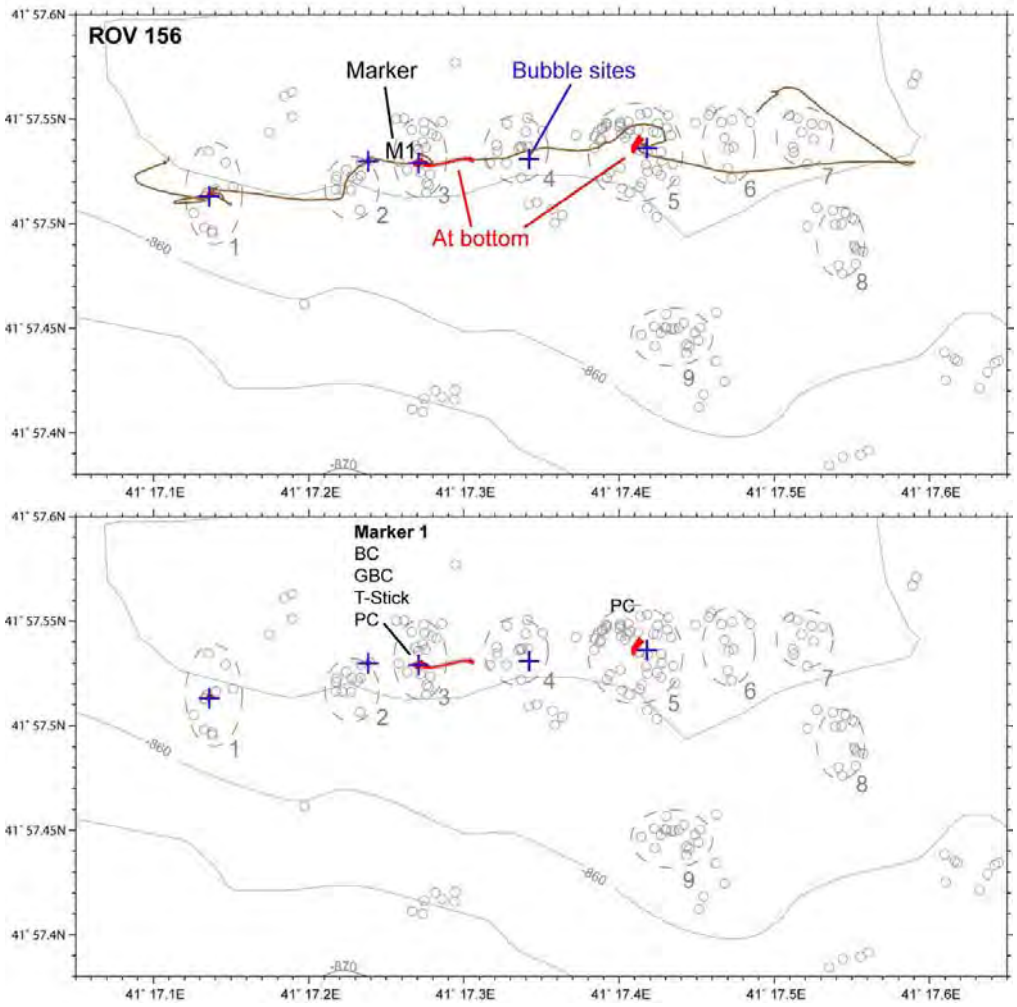

Fig. 66: Track of ROV Dive 156 (GeoB 11904) at Batumi seep and sampling stations. Crosses mark the exact positions, at which bubbles have been observed at the seafloor during the ROV dive.

Search for bubbles at Flare Cluster No. 3 with sonar revealed a very strong signal in the water column. Recordings with sonar were performed and bubbles were already seen in the water column. The seafloor was strongly “perforated-and-structured” and chimney-like structures occurred. Bubbles escaped vigorously from one central outlet. The ROV was set down and we spent the next hours observing and measuring bubble escape rates with the 5.5 l small bubble catcher, the gas bubble sampler, T-stick, and push corer. To our surprise, no gas hydrates formed from the collected gas in the gas bubble catcher. Later analyses of the gas (Chap. 12) revealed that a specific gas composition existed differing from that of the gas hydrates in the sediments. This gas composition is such that the expected gas hydrates are not stable at the water depth of around 860 m (Chap. 10.4). The repeated measurements of bubble flow with the gas bubble catcher revealed that more than 3.5 l of gas was released per minute.

The T-Stick was held in the bubble stream and subsequently placed inside the gushing hole. The ROV could only push the T-stick 30 cm down to the fourth temperature sensor. The recorded temperature

increased almost linearly and did not reach an asymptotical value after 8 min when we terminated the measurements too early, as was revealed later when reading the data. The probe registered a 0.1 °C gradient within the ~30 cm of penetration. During a second try to penetrate with the T-Stick just half a meter away from the gusher site, we encountered the same obstacle at depth that prevented penetration for more than 30 cm. As final action at this site, Marker 1 was placed.

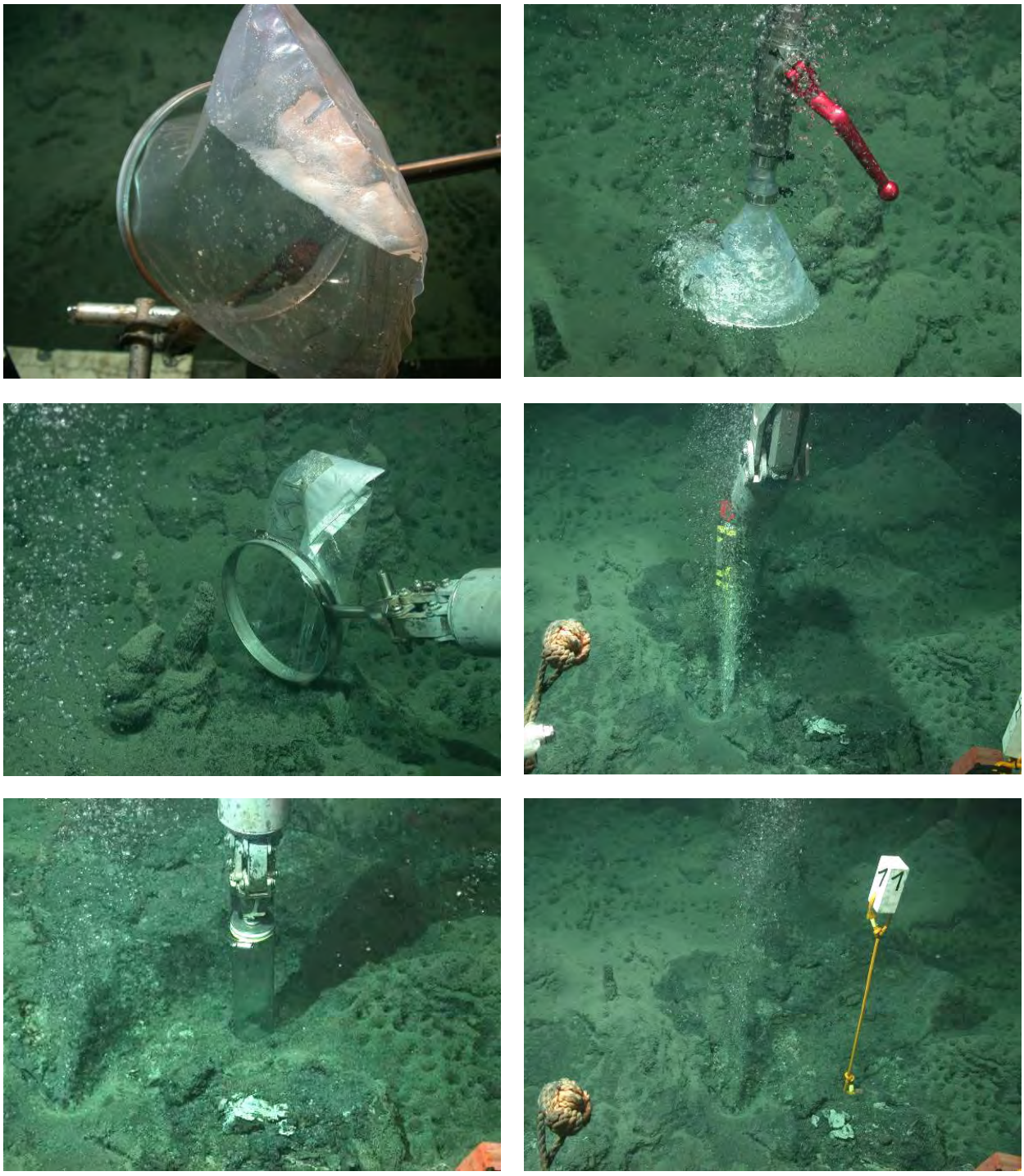

Fig. 67: Sampling at the gusher site, which actively released bubbles. It is the centre of Flare Cluster No. 3. *Top left:* Bubbles collected by the large bubble catcher do not form gas hydrates. *Top right:* Gas sample taken by the gas bubble sampler. *Middle left:* The two chimney-like structures shortly before scooped by the large bubble catcher. *Middle right:* The T-Stick deployed in the gusher. *Bottom left:* Pushcore taken 20 cm away from the gusher site. *Bottom right:* The site after sampling and deployment of Marker No. 1

At Flare Cluster No. 4, a strong flare was recorded in order to quantify the gas released. Following this, the ROV moved to Flare Cluster No. 5 and the sonar recorded a considerably high backscatter. The sea-floor in this area is "perforated but smooth". In addition to those fields of holes encountered earlier, some holes and the sediments in their vicinity looked blackish, and may indicate a more recent bubble activity. However, the actual escape sites have been the "regular" holes without these blackish rims. At least five holes or a group of holes emitted bubbles along a line. Even more escape sites are probably present in the background, but were not well imaged by the ROV camera system. A push core was taken at the bubble sites and the gas bubble sampler was held over the outlet. Unfortunately, the gas bubble sampler was not tightly closed, thus, no gas analyses could be performed.

7.2.3 *Dive 157 (GeoB 11907)*

Area:	Batumi seep, Georgia		
Responsible scientist:	Markus Brüning		
Date:	Thursday, 22 March 2007		
Start at Bottom (UTC):	11:42		
End at Bottom (UTC):	20:27		
Total bottom time:	8 hours and 45 minutes		
Start at the bottom:	41°57.520'N	41°17.100'E	812 m water depth
Start asciend:	41°57.542'N	41°17.412'E	824 m water depth

Scientist schedule:

11:00 – 13:00	Markus Brüning / Gregor von Halem
13:00 – 15:00	Gerhard Bohrmann / Yuriy G. Artemov
15:00 – 17:00	Gerhard Bohrmann / Baris Bozkaya
17:00 – 19:00	Markus Brüning / Aneta Nikolovska
19:00 – 20:30	Markus Brüning / Klaus Wallmann

Table 6: Instruments/tools during Dive 157.

GeoB	Tool/instrument	Start	Lat. [°N]	Long. [°E]	Water Depth [m]
Flare Cluster 7					
11907-1	bubble catcher, small	15:53	41.57.542	41.17.529	834
11907-2	gas bubble sampler	16:30	41.57.543	41.17.529	834
11907-3	T-stick	16:51	41.57.543	41.17.529	834
Flare Cluster 6					
11907-4	bubble catcher, small	18:21	41.57.546	41.17.473	835
11907-5	gas bubble sampler	18:33	41.57.544	41.17.472	835
11907-6	marker 2	18:59	41.57.544	41.17.472	835
Flare Cluster 5					
11907-7	push core 38	19:52	41.57.542	41.17.413	833
11907-8	push core 46	19:58	41.57.543	41.17.413	833
11907-9	push core 67	20:03	41.57.545	41.17.413	833
11907-10	push core 68	20.13	41.57.542	41.17.413	833
11907-11	marker 3	20:16	41.57.542	41.17.413	833

Waypoints:	Start:	41°57.52'N	41°17.10'E
	WP 1:	41°57.55'N	41°17.60'E
	WP 2:	41°57.45'N	41°17.43'E

Description of the dive

The key objective of the first part of the dive was to map the seafloor from west to east using the ROV-mounted sidescan sonar (Fig. 68). This operation worked very well and the ~550 m long transect was completed in one hour. During this profile the doppler log was constantly reset to the Posidonia position in order to achieve high quality DVL Nav location output. However, on the online screen this caused considerable jumps in the sidescan sonar images.

The second objective of this dive was to find and observe bubble emission sites at flare clusters that we have not surveyed before. Flare Cluster 8 was immediately found by scanning sonar and a scan record was saved for the purpose of quantification. At the seafloor two individual bubble streams were detected from a "perforated but smooth" seafloor. A bubble catcher was placed over the streams, but within a few minutes the amount of escaping bubbles decreased, therefore, the objective of quantification was abandoned.

In order to find more vigorous bubble outflows the ROV headed towards the position of Flare Cluster 7. After scan recordings, the small bubble catcher revealed that 1 l of bubbles are released in 10 min. A sample with the gas bubble sampler was caught, and the T-stick deployed in the bubble hole. When pulling out, whitish material was dragged out of the hole, too. These were probably layers of white coccolith ooze laminae.

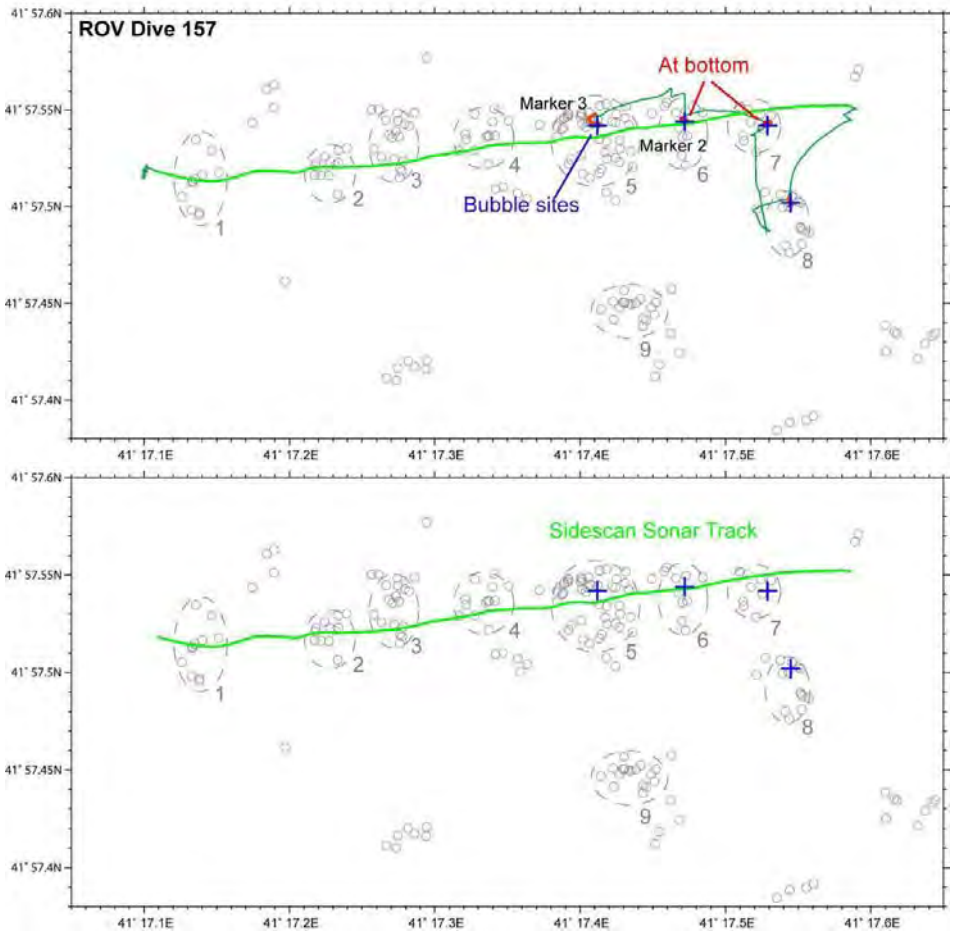

Fig. 68: Track plot of ROV Dive 157 (GeoB 11907) and the location of the sidescan sonar track at the seafloor. Crosses mark the exact positions at which bubbles have been observed at the seafloor with the ROV.

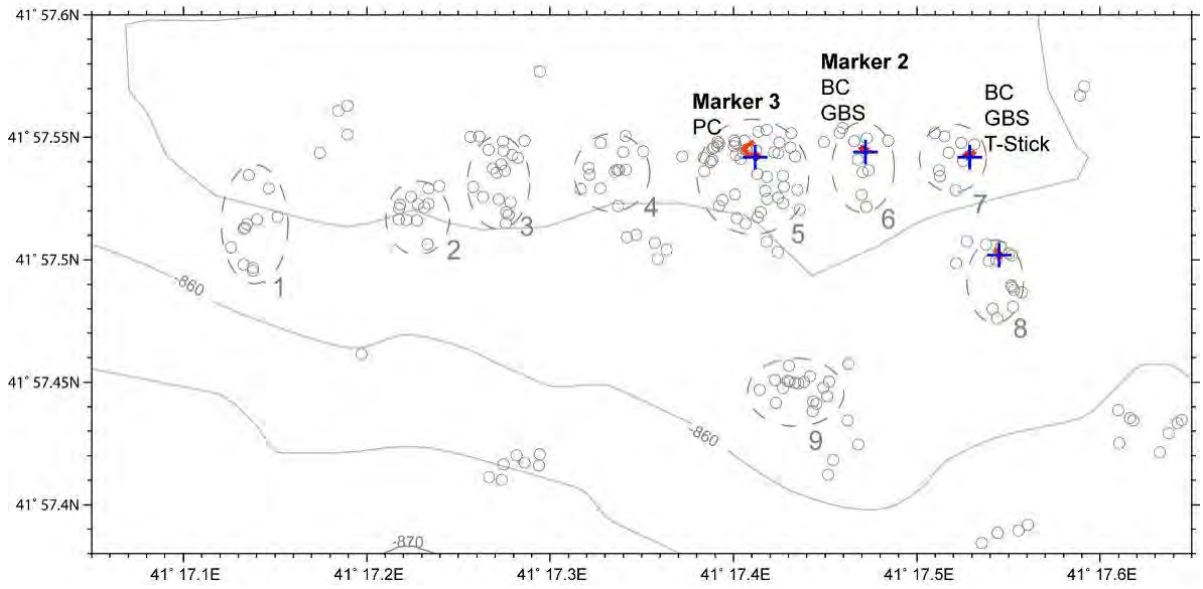

Fig. 68 continuation: Sampling sites at the seafloor during ROV Dive 157 (GeoB 11907). Crosses mark the exact positions at which bubbles have been observed at the seafloor with the ROV.

Meanwhile, the procedure of finding the flares with scanning sonar became a routine and Flare Cluster 6 was quickly found. The holes in the "perforated-but-smooth" seafloor slowly emit bubbles, which were collected by the small bubble catcher. It took ~12 min to catch one litre of gas. Gas was collected at this site with the gas bubble sampler. Following, there were some disturbances of the seafloor by the ROV operations in the course of which bubbles were released from the seafloor. As a last action, Marker 2 was deployed.

A push corer transect was taken at Flare Cluster 5. This cluster has been observed and sampled during the previous ROV Dive 156. Four push cores were taken at different distances to the bubble sites. Marker 3 was placed.

7.2.4 *Dive 158 (GeoB 11908)*

Area:	'Egorov Flare' Site, Sorokin Trough, Ukraine		
Responsible scientist:	Thomas Pape		
Date:	Saturday, 24 March 2007		
Start at Bottom (UTC):	14:50		
End at Bottom (UTC):	18:54		
Total bottom time:	4 hours and 4 minutes		
Start at the bottom:	44°23.548'N	35°15.499'E	1781 m water depth
Start ascend:	44.23°749'N	35°15.964'E	1750 m water depth
Scientist schedule:			
14:45 – 17:00	Thomas Pape / Gerhard Bohrmann		
17:00 – 19:00	Thomas Pape / Janet Rethemeyer		

Waypoints:	Start:	44°23.55'N	35°15.50'E
	WP 1:	44°23.617'N	35°15.609'E ('Egorov Flare' position)
	WP 2:	44°23.65'N	35°16.0'E
	WP 3:	44°24.00'N	35°15.70'E

Description of the dive

A very strong plume feature was imaged by Ukrainian scientists from the Institute of Biology of the Southern Seas (IBSS, Sebastopol) during R/V PROFESSOR VODYANITSKII cruise in 2002 and the flare image was published by Egorov et al. (2003). The seep was probably crossed by the seismic Line GeoB-012, which was measured during MARGASCH I cruise (M52/1) in 2002.

The ‚Egorov Flare' Site is located on the southern flank of a local depression encircled by a ridge from the northwest to northeast and elevated structures in the west to southwest. An area was found to be elevated about 40 m above its surrounding and located about 0.8 nm northeast of the 'Egorov Flare' position.

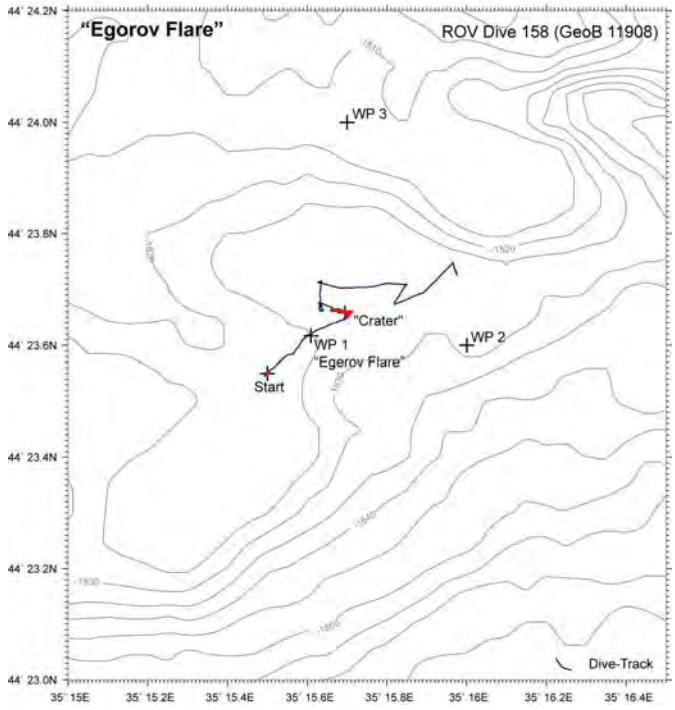

Fig. 70: Track of ROV "QUEST4000m" Dive 158, 'Egorov Flare' Site.

With respect to the initial results, a short-timed survey with ROV "QUEST 4000m" in this area was dedicated for exploration of potential gas seeps at the seafloor as well as bubble streams in the water column. The activities were predominantly carried out by the forward looking sonar mounted on the ROV and were completed by the R/V METEOR based Parasound system. In order to avoid significant sonar signals caused by rough seafloor morphology, the ROV primarily moved about 25 m above ground.

To explore a large area around the flare position, a transect covering three waypoints (WP) was planned during the ROV survey (Fig. 69). The seafloor was reached approx. 0.1 nm southwest of the 'Egorov Flare' site (WP1) in about 1781 m water depth. For detecting gas bubbles, the ROV was moved with 0.2 kns and a heading of 52° at about 25 m above the seabed, and the forward looking sonar was used. Since the altitude did not allow for seafloor observations through the water column beneath the vehicle, the video recording was interrupted during that time. WP 1 ('Egorov Flare' position) was reached about 30 min from the start of the transect. Since obvious gas bubble-related anomalies were not recognized in the sonar during that time, the ROV was directly moved towards a next target point, without any stopover and seafloor inspections at WP1. This target point, located approx. 0.2 nm WSW of WP2, was spontaneously defined during the dive. The heading was adjusted to 58° and the speed over ground was raised to about 0.3 kns. No sonar signals were observed during the subsequent flight and after 25 min it was decided to descend the vehicle for seafloor observations, and possibly for further investigations and samplings. At 44°23.65'N, 35°15.70'E a crater-like structure, characterized by a rough morphology, was found. Steep flanks, sharp crests, soft sediment boulders, several dm-deep incisions, and edges suggest that these morphological features were recently formed and only slightly subjected to erosion processes (Fig. 70). Thus, it seemed plausible to assume that the crater-like structure at this site was related to the 'Egorov Flare' located in 2002 somewhat to the SW. However, during the current dive gas bubbles were not visualized at this site.

Fig. 71: Impressions from a crater-like structure located at about 44° 23.65'N, 35°15.70'E. *Top left:* Edges at the crater like structure. *Top right*: Seafloor elevation of soft sediment. *Bottom left:* Sediment penetrated with the ROV's manipulator arm. *Bottom right:* Sediment upon treatment with the manipulator. Note the absence of gas bubbles during this experiment.

The most impressive morphological features at the crater-like structure were studied comprehensively by ground observations and video-recording. Further, the sediment consistency was checked by sticking in the ROV's manipulator. Unexpectedly, no gas bubbles were released during penetration of the sediment.
In order to proceed with the flare survey in the area, it was decided not to deploy further instruments at the crater-like structure. Based on putative gas streams in the water column imaged by the ship-based Parasound system at that time, ROV "QUEST4000m" was lifted to about 25 m above ground and moved to the NW (heading 305°). At a distance of about 0.07 nm NW of the crater-like structure, the forward looking sonar gave some slight signals in a southward direction. However, while moving the ROV to the south, the signals randomly came up and disappeared again. Although that site was exhaustively explored for the next 30 min, there were no clear indications of bubble streams in that area. Further, signals were also lost in the Parasound system and, thus, it was decided to investigate a relatively wide basin-like structure to the N (heading 355°). In that area – at about 44°23.71'N, 35°15.63'E – bubble flares were not observed and a W-E orientated transect was followed. Bubble streams were neither detected during that transect, nor during a short subsequent passage to the SW. Also no bubble streams were detected during a transect to the NE at the final stage of the dive. The dive was completed at about 18:54 and ROV "QUEST4000m" was lifted from 44°23.75'N, 35°15.96'E.

7.2.5 *Dive 159 (GeoB 11910)*

Area:	Dvurechenskii mud volcano, Sorokin Trough, Ukraine
Responsible scientist:	Stephan A. Klapp
Date:	Sunday, 25 March 2007
Start at Bottom (UTC):	08:05
End at Bottom (UTC):	17:58
Total bottom time:	9 hours 53 minutes

Start at the bottom:	44°16.901'N	34°59.292'E	2045 m water depth
Start ascend:	44°16.946'N	34°58.850'E	2042 m water depth

Scientist schedule:

2 h	ca. 08:00 – 10:00	Heiko Sahling / Stephan A. Klapp
2 h	ca. 10:00 – 12:00	Heiko Sahling / Friederike Schmidt-Schierhorn
2 h	ca. 12:00 – 14:00	Markus Brüning / Elena Kozlova
2 h	ca. 14:00 – 15:45	Stephan A. Klapp / Gregor von Halem
2 h	ca. 15:45 – 17:00	Stephan A. Klapp / Friederike Schmidt-Schierhorn
2 h	ca. 17:00 – 18:00	Gerhard Bohrmann / Gregor von Halem

Table 7: Instruments/tools during Dive 159.

GeoB	Tool/instrument	Start	Lat. [°N]	Long. [°E]
11910-1	T-stick-1	08:30	44:16.900	34:59.293
11910-2	T-stick-2	09:18	44:16.929	34:59.233
11910-3	push core 16	09:21	44:16.929	34:59.232
11910-4	T-stick-3	09:54	44:16.946	34:59.175
11910-5	T-stick-4	10:45	44:16.977	34:59.085
11910-6	push core 60	10:48	44:16.976	34:59.084
11910-7	T-stick-5	11:36	44:17.006	34:58.974
11910-8	push core 47	11:41	44:17.006	34:58.974
11910-9	T-stick-6	12:27	44:17.019	34:58.929
11910-10	T-stick-7	13:14	44:17.029	34:58.880
11910-11	push core 46	13:25	44:17.029	34:58.880
11910-12	T-string recovery	16:55	44:16.972	34:58.910
11910-13	T-stick 8	17:39	44:16.947	34:58.850

Waypoints:	Start:	44°16,9'N	34°59.30'E
	P1:	44°16,92'N	34°59.24'E (first push core)
	P2:	44°16.97'N	34°59.07'E (second push core)
	P3:	44°17.00'N	34°58.97'E (third push core)
	P4:	44°17.03'N	34°58.88'E (fourth push core)
	P5:	44°16.970'N	34°58.91'E (GC mooring)

Description of the dive

The Dvurechenskii mud volcano (DMV), located in the Sorokin Trough southeast of the Crimean Peninsula, has been target of several expeditions. On the previous leg of the ongoing M72 expedition (Leg M72/2), temperature anomalies of up to 14 °C were recorded in the central part of the pie-type mud volcano. Even 16 °C were reported during the M52/1 expedition in 2002 in the same area of the volcano. A mud flow on the southwestern flank was observed during TTR-6 by sidescan sonar imaging. Also, gas expulsion was observed during R/V PROFESSOR VODYANITSKII cruises by gas flares in the water

column. A gravity corer mooring containing two thermistor temperature strings were deployed during M72/2 and the recovery of one of them was an objective of ROV Dive 159 (GeoB 11910).

The major objective of the dive was to gain an overview of the mud volcano by running a transect from the eastern rim to the center where major temperature anomalies were reported and then further on to the southwestern mud flow. During this transect, 8 temperature measurements and 4 push cores were taken. Temperatures were recorded by a temperature stick comprising 8 sensors. The dive track (Fig. /!) ran from the southeastern rim of the mud volcano to the northern central part (where temperature anomalies were recorded earlier) along four waypoints and from there towards the mooring station south of Waypoint 4.

The ROV went down east of Waypoint 1 on the rim of the mud volcano; temperatures there are about the same as normal Black Sea water. The track was continued via Waypoints 2 and 3 towards WP 4. At each waypoint, a push core was taken and temperatures were measured next to the push core and in addition between waypoints.

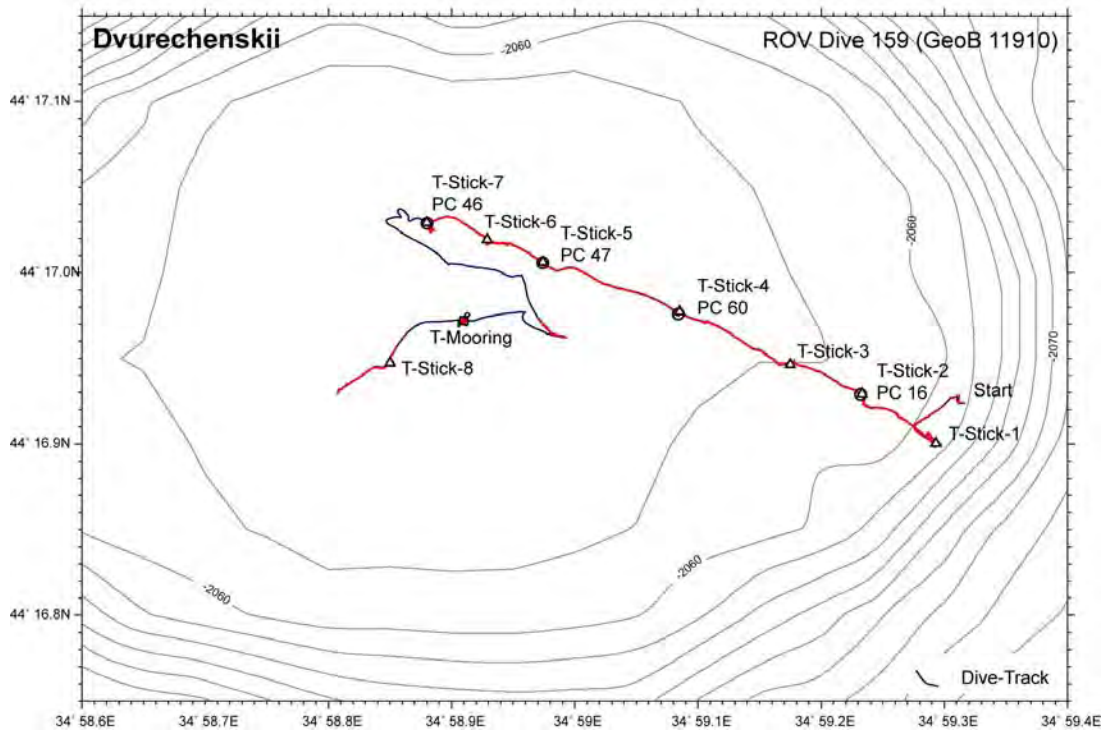

Fig. 72: Track of ROV Dive 159.

During the temperature and push core taking at Waypoint 4, a few bubbles were released. This was the only bubble site on this survey. It is not a seep site where bubble continuously stream out of the seafloor, but only upon sediment treatment by the tool. High temperature anomalies and bubbles indicate an active area of the mud volcano. Hence, from Waypoint 4 a short survey was conducted attempting to find bubbles by forward looking sonar, but no bubbles were found by sonar.

The sonar survey started at 40 m above the seafloor with a 50 m range and maximum gain. A 360° look was taken above Waypoint 4. The ROV then moved towards a spot between WP 4 and 3 because an anomaly appeared in the sonar. The anomaly vanished and no bubbles were discovered. The survey continued towards the mooring station, where the thermistor temperature string was recovered (Fig. 72, *right*). The state of the mooring station had neither changed nor had it been sucked into the sediment (Fig.72, *left*). One last temperature measurement was done in the vicinity of the mooring station.

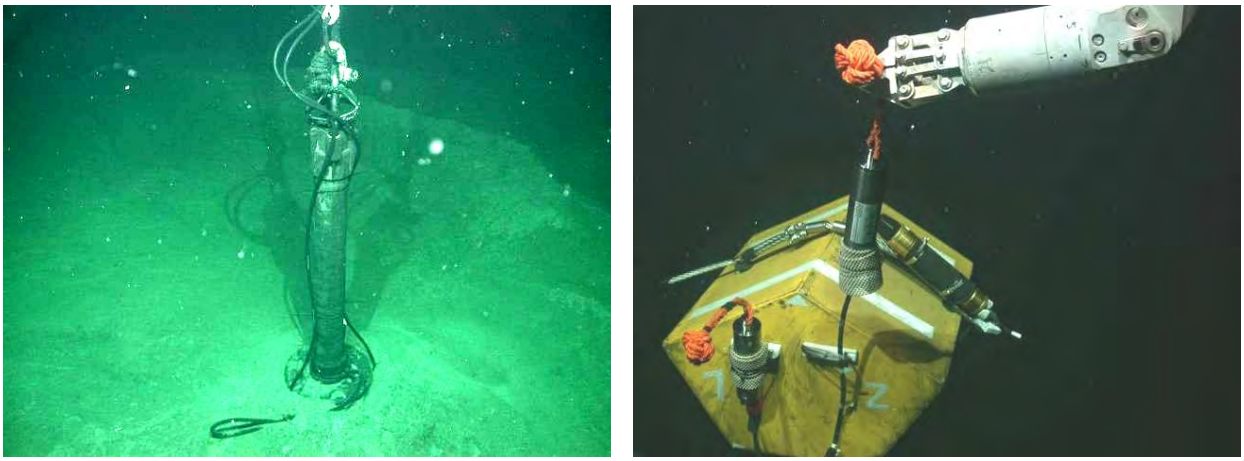

Fig. 73: *Left:* Mooring station upon a gravity core. *Right:* T-string recovery from the floating part of the mooring station.

The morphology of the structure employs two types of features, which can, in a first approximation, be assigned to the rim and to the central part. The rim appears rough and comprises many furrows, which interchange with little elevations. The furrows do not reach deeper than one meter, although this is difficult to say from video observation. Some of the furrows are covered by thin sediment layers and others have fairly fresh edges (Fig. 73). Furrows and hills look chaotic at some locations, but at others they appear to be oriented in a somewhat parallel fashion (44°16.916' N, 34°59.263' E, near Waypoint 1). The central part of the DMV is not flat, although the morphology looks in general much smoother. The rough rim structures change continuously over a broader distance to the gentler and smoother central part of the mud volcano. This is indicated by decreasing hill diameters and heights along with shallow furrows with soft edges. Every now and then during the survey, darker patches occurred on the sediment surface looking like a track. The origin of these sediment compounds is unclear, but it might be a shadow effect when light from the vehicles' spotlight shines on cracks in the mud volcano's sediment cover. The inspection of the DMV was not completed by this dive. In particular, the western parts of the mud volcano need to be further explored, since on the TTR-6 cruise a mud flow was detected over the southwestern flank.

Fig. 74: *Left:* Sediment-covered furrow. *Right:* Furrow with more or less fresh edges.

7.2.6 *Dive 160 (GeoB 11915)*

Area:	Dvurechenskii mud volcano, Sorokin Trough, Ukraine
Responsible scientist:	Gerhard Bohrmann
Date:	Monday, 26 March 2007
Start at bottom (UTC):	08:08
End at bottom (UTC):	16:45
Total bottom time:	8 hours and 37 minutes

Start at the bottom:	44°16.803'N	34°58.606'E	2060 m water depth
Start ascend:	44°17.089'N	34°58.968'E	2041 m water depth

Scientist schedule:

08:07 – 10:00	Gerhard Bohrmann / Gregor von Halem
10:00 – 12:00	Gerhard Bohrmann / Thomas Pape
12:00 – 14:00	Gregor von Halem / Klaus Wallmann
14:00 – 17:00	Markus Brüning / Klaus Wallmann
17:00 – 19:00	Heiko Sahling / Sarah Althoff

Table 8: Instruments/tools during Dive 160.

GeoB	Tool/instrument	Time (UTC)	Lat [°N]	Long [°E]	Water Depth (m)
11915-1	T-stick-1	08:31	44°16.802	34°58.596	2052
11915-2	T-stick-2	09:04	44°16.838	34°58.596	2043
11915-3	T-stick-3	09:37	44°16.893	34°58.709	2043
11915-4	T-stick-4	10:04	44°16.954	34°58.784	2041
11915-5	T-stick-5	10:39	44°17.002	34°58.889	2040
11915-6	T-stick-6	11:14	44°16.995	34°58.736	2042
11915-7	T-stick-7	11:49	44°17.024	34°58.612	2042
11915-8	push core-11	11:57	44°17.023	34°58.610	2042
11915-9	gas catcher-1,	12:12	44°17.021	34°58.613	2042
11915-10	T-stick-8	12:52	44°17.093	34°58.673	2043
11915-11	push core-12	12:59	44°17.090	34°58.674	2043
11915-12	push core-13	13:06	44°17.092	34°58.676	2043
11915-13	T-stick-9	14:21	44°17.054	34°58.759	2042
11915-14	push core-14	14:26	44°17.061	34°58.760	2042
11915-15	push core-15	14:31	44°17.062	34°58.759	2042
11915-16	T-stick-10	15:12	44°17.005	34°58.896	2040
11915-17	push core-16	15:14	44°17.007	34°58.896	2040
11915-18	push core-17	15:16	44°17.008	34°58.891	2040
11915-19	push core-18	15:21	44°17.008	34°58.895	2040
11915-20	T-stick-11	15:45	44°17.052	34°58.842	2041
11915-21	push core-9	15:48	44°17.051	34°58.836	2041
11915-22	push core-19	15.51	44°17.052	34°58.845	2041

Waypoints:	Start:	44°16.80'N	34°58.60'E	
	WP1:	44°16,92'N	34°59.24'E	
	WP2:	44°16.97'N	34°59.07'E	
	WP3:	44°17.00'N	34°58.97'E	
	WP4:	44°17.03'N	34°58.88'E	
	WP5:	44°16.97'N	34°58.91'E	(GC mooring)
	WP6:	44°16.84'N	34°58.65'E	
	WP7:	44°17.01'N	34°58.90'E	
	WP8:	44°17.04'N	34°58.83'E	

Waypoints, continuation:

WP9:	44°17.06'N	34°58.76'E
WP10:	44°17.09'N	34°58.68'E
WP11:	44°17.00'N	34°58.58'E

Description of the dive

Following ROV Dive 159 on Dvurechenskii mud volcano (DVM), ROV Dive 160 was planned to explore the western part of the flat top mud volcano and to extent the push core sampling and temperature measurement program. The dive started at the southwestern flank of the mud volcano, where a mud flow in the sidescan sonar pattern was seen during TTR-6 cruise (Woodside et al., 1997). After we reached the seafloor, ROV "QUEST4000m" moved upwards to the rim in a northeastern direction. The first T-stick temperature measurement was performed on the rim of the DMV. Exploring the seafloor structure towards the center close to the T-mooring station and from there to the western rim of DMV (Fig. 74), we performed 7 temperature measurements using the T-stick (for results see Chap. 8). The westernmost location was visited because a white patch was recognized on a TV-sled deployment during R/V METEOR cruise M52/1 (Bohrmann et al. 2003), which could not be sampled during that cruise. Beside the T-stick measurement, we took a push core and sampled the white material by using the gas catcher tool. After that work was finished, the ROV moved along the rim of the DMV and then from a northwestern position again back to the centre of the mud volcano. Two push cores at each site were taken at four sites and temperature measurements were performed (Fig. 74). During the dive, we checked the water column several times for gas bubbles by using the ROV forward looking sonar. However, no bubbles were observed. We recognised a slight depth change of about 2-4 m from the rim to the centre of the mud volcano, which seems to be the highest area. Other observations included cracks or parallel furrows on the sea floor, which probably are related to mud flows in the past (Fig. 75). Fresh mud flows have not been recognised.

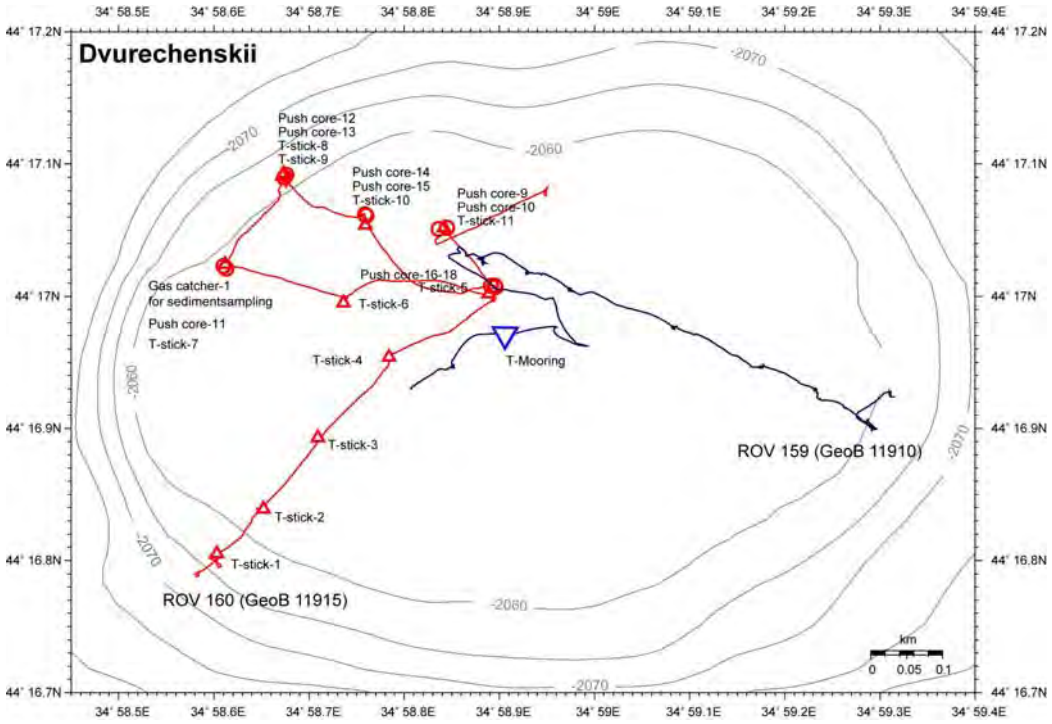

Fig. 75: Seafloor track of Dive 160 on Dvurechenskii mud volcano showing sites of sampling and T-Stick measurements (Dive 159 track is also shown). Contour lines on the map have slight offset in depth to the ROV depths.

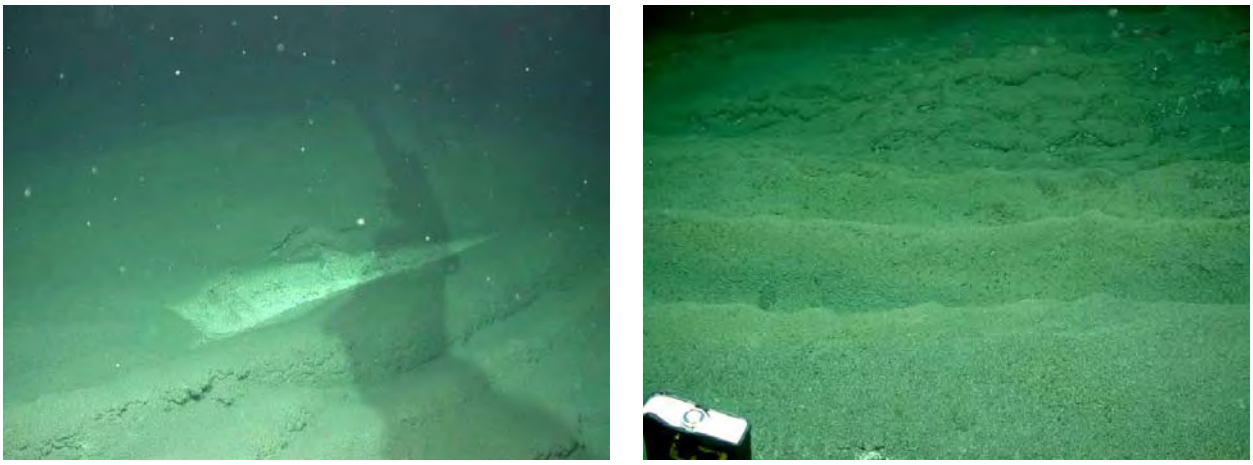

Fig. 76: Seafloor images from Dvurechenskii mud volcano taken during ROV Dive 160. The left image shows a white patch in a depression, where a sediment sample was taken using a gas catcher (GeoB 11915-9). The right picture illustrates the pattern of parallel cracks or furrows which are typically found in the western part of the mud volcano.

7.2.7 *Dive 161 (GeoB 11917)*

Area:	Vodyanitskii mud volcano, Sorokin Trough, Ukraine		
Responsible scientist:	Heiko Sahling		
Date:	Wednesday, 28 March 2007		
Start at Bottom (UTC):	12:30		
End at Bottom (UTC):	22:30		
Total bottom time:	9 hours		
Start at the bottom:	41°57.520'N	41°17.100'E	812 m water depth
Start ascend:	41°57.542'N	41°17.412'E	824 m water depth
15:20 – 17:00	Aneta Nikolowvska / Heiko Sahling		
17:00 – 19:00	Sarah Althoff / Heiko Sahling		
19:00 – 21:00	Yuri G. Artemov / Markus Brüning		
21:00 – 23:00	Gerhard Bohrmann / Thomas Pape		
23:00 – 00:30	Gregor von Halem / Heiko Sahling		

Table 9: Instruments/tools during Dive 161.

GeoB	Tool/instrument	Start	Lat. [°N]	Long. [°E]	Water Depth [m]
11917-1	gas bubble sampler-5	16:35	44:17.657	34:01.992	2032
11917-2	T-stick-1	18:02	44:17.657	35:01.992	2032
11917-3	push core-11	18:12	44:17.657	35:01.992	2032

Waypoints:	Start WP 1:	44°17.621'N	35°01.946'E, 2060 m (GC 11913)
	WP 2:	44°17.650'N	35°02.050'E
	WP 3:	44°17.720'N	35°01.950'E
	WP 4:	44°17.650'N	35°01.830'E

Description of the dive

The dive started at the deployment position of gravity corer GeoB 11913 (Fig. 76). The waypoints mark the extent of the footprint of flares recorded in Parasound during a survey conducted on the night from 25

to 26 March. Earlier cruises have shown with ship-based echosounder that gas flares are present at Vodyanitskii mud volcano (35°01.975'E, 44°17.687'N; Y.G. Artemov, pers. comm.).

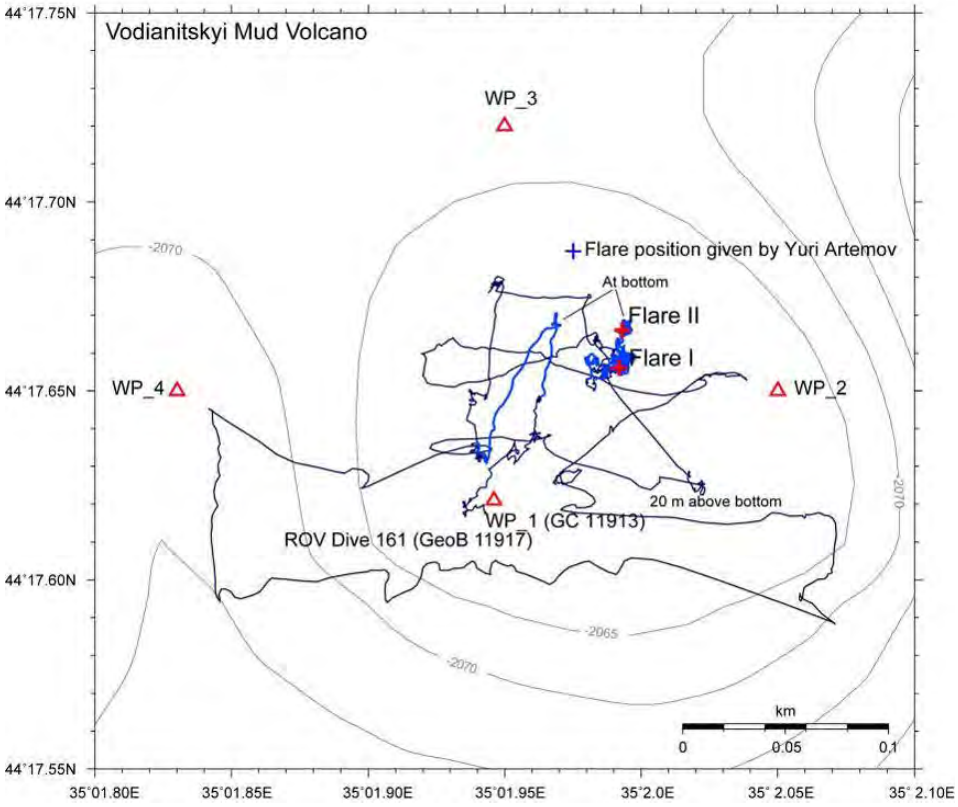

Fig. 77: Track of ROV Dive 161 at Vodyanitskii mud volcano.

A sonar survey heading NE in the water column about 20 m above ground revealed high backscatter anomalies that we misinterpreted for a while as gas flares. It turned out that we imaged the rising flank of the mud volcano, which showed in places high backscatter due to stronger bottom topography. At the northernmost part of this transect, the ROV moved to the seafloor and flew back to its start position. A second transect 20 m above ground was conducted west of the first one. At the northern end, a survey to the east revealed the first evidence for bubbles. At least two plumes were seen in the horizontal-looking sonar and recorded. At the bottom, two 0.5 m depressions connected to each other were observed. They had sharp edges exposing whitish layered sediments. The bottom of the hole looked like liquid mud filled. These were not the sites with bubble escapes. We continued to look around, but found no bubbles, maybe due to the stirring up of flocculent material by the ROV. After a second scan with the horizontal-looking sonar, two bubble sites were detected and located visually at the seafloor.

The spot with bubble release was about a 2 m large feature of disturbed sediments at 44°17.657'N, 34°01.992'E (Fig. 77, *top left*). It looked like a small sediment slide or a collapse structure. The sediments were disturbed with hard-looking cm to dm sized consolidated sediments lying around that resembled carbonates. Touching with the manipulator of the ROV revealed that these were soft and broke into pieces when grabbed. The bubbles escaped irregularly from an area of several decimetres around a central bubble stream. ROV movements induced additional bubble releases. Bubble sizes were small, maybe 0.5 cm or less. Bubbles were collected with the gas bubble sampler and hydrate formation was observed (Fig. 77, *bottom left*). Only a small portion of the bubble/hydrate mixture in the funnel was sucked into the sampler.

A T-stick was deployed and meanwhile a push corer was taken (Fig. 77, *top right*). The sediments close to the bubble outlet fell out, thus, a push corer about 1 m to the left of the stream was taken. After leaving this site, a sonar scan was recorded in order to allow quantification by acoustic means.
A lengthy survey in the water column started in order to find additional bubble sites with the horizontally looking sonar system, but this was unsuccessful. Thus, the known two bubble escape locations were revisited. With the horizontally-looking sonar, the presence of two bubble escape sites was confirmed. Following the bubbles to the seafloor, we re-discovered the "Flare I" location and proceeded to the second site. This was documented by video at the position: 44°17.666'N, 35°01.993E (Fig. 74, *bottom right*). Samples could not been taken due to a failure of the Orion 7-function arm. Video documentation as well as high-resolution sonar scan were conducted while the ROV-team tried to fix the problem. Unfortunately, a shut down of the entire deck unit led to a "dead vehicle". During ascent, the power supply was re-established and the vehicle was brought on deck successfully.

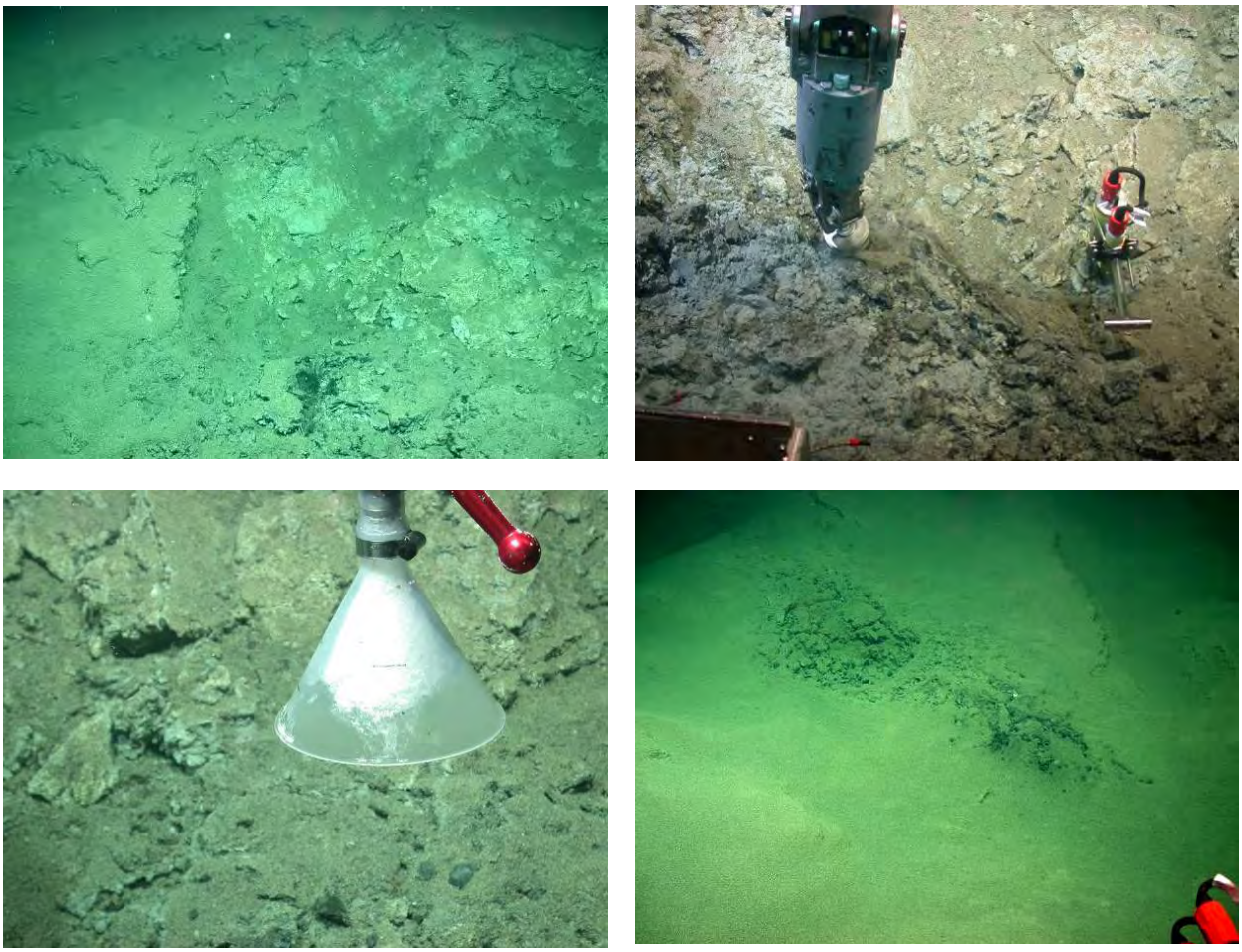

Fig. 78: *Top left:* Emission of small bubbles at Flare I, those are difficult to image on still photos. The outlet is the dark area in the centre of the image. *Top right*: Sediment sampling by push corer while T-stick measurements are conducted in the bubble site. *Bottom left:* Hydrate formation in the Gas Bubble Sampler. *Bottom right:* The seafloor at site Flare II. The bubbles escape from darkish area at the right hand side.

7.2.8 *Dive 162 (GeoB 11919)*

Area:	Batumi seep, Georgia
Responsible scientist:	Gregor von Halem
Date:	Friday, 30 March 2007
Start at Bottom (UTC):	12:35
End at Bottom (UTC):	19:05
Total bottom time:	7 hours

Start at the bottom:	41°57.531'N	41°17.342'E	814 m water depth
Start ascend:	41°57.401'N	41°17.273'E	847 m water depth

Scientist schedule:

2 h	ca. 14:00 – 16:00	Gregor von Halem / Markus Brüning
2 h	ca. 16:00 – 18:00	Deniz Karaça / Gregor von Halem
2 h	ca. 18:00 – 20:00	Sarah Althoff / Markus Brüning

Table 10: Instruments/tools during Dive 162.

GeoB	Tool/instrument	Start	Lat. [°N]	Long. [°E]	Water Depth [m]
Flare Cluster 4					
11919-1	bubble catcher small	15:12	41:57.544	41:17.337	833
Flare Cluster 3					
11919-2	gas bubble sampler	18:03	41:57.534	41:17.4266	835

Waypoints:

Start:	41°57.531'N	41°17.342'E
WP 1:	41°57.529'N	41°17.271'E
WP 2:	41°57.401'N	41°17.273'E

Description of the dive

Due to non-function of the ORION arm the tools used were limited to the small bubble catcher and one gas bubble sampler.

By using the horizontally-looking sonar on the ROV, we searched the area and found bubbles in the water column at Flare Cluster No. 4 (Fig. 78). A curtain of bubbles escaped along a linear trend with 8 individual bubble streams. The streams caused a significant backscatter signal on the sonar, therefore a sonar

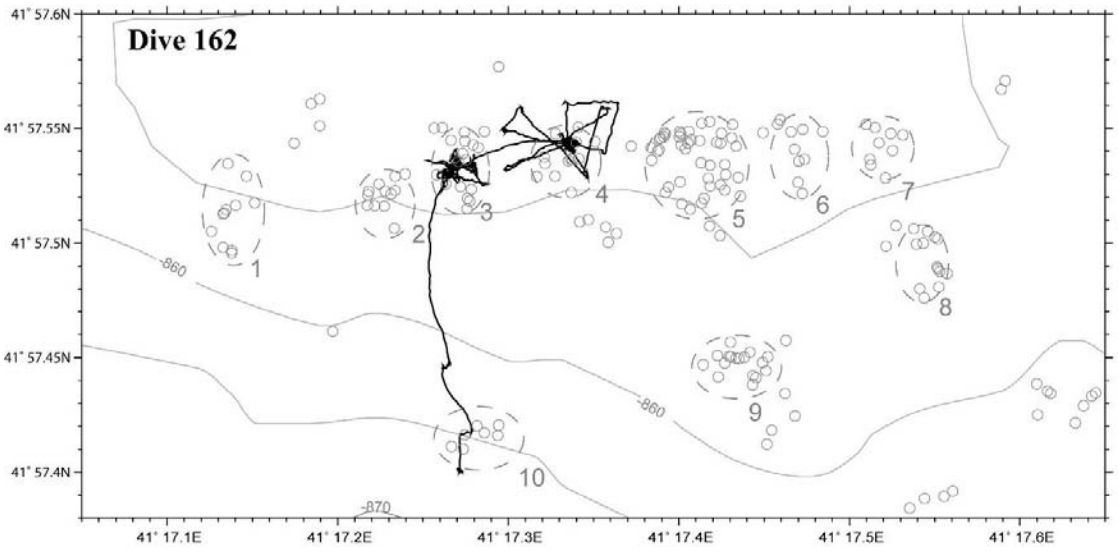

Fig. 78: ROV 162 Dive Track (GeoB 11919) at Batumi seep.

screenshot was taken. The next objective was a flight over Flare Cluster 4 at low altitude (Fig. 79). The seafloor looked “perforated and structured” around the bubble streams and linear depressions were present in the N, “not perforated and smooth” surface, without bubble escape sites, in the east, and a chimney-field SW of the bubble stream. Finally, the bubble stream was quantified with the bubble catcher.

The next target was Flare Cluster no. 3, Marker no. 1 (set during Dive 156) where we found the former very active “gusher” site inactive. Strong backscatter signals on the sonar in the close vicinity to Marker 1 guided us to another active bubble escape site where bubbles were emitted along a linear trend giving the impression of a fracture along which more than 10 individual bubble streams occurred. The next objective was a flight over Flare Cluster 3 at low altitude, before we sampled the newly discovered bubble escape site with the gas bubble sampler. Finally, heading south another active gas escape site was found at the “perforated and smooth” type Flare Cluster 10 before ascent.

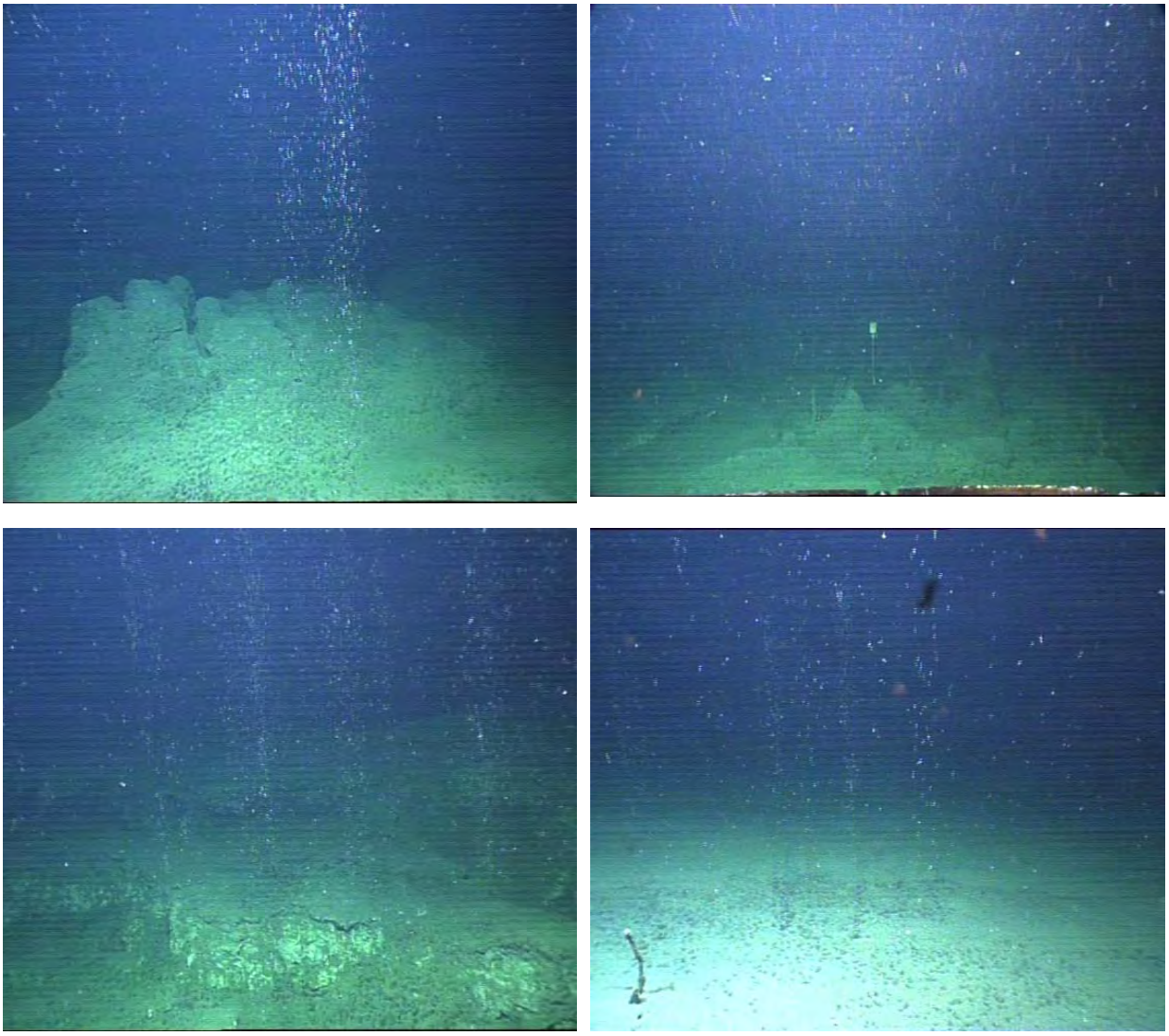

Fig. 79: Sampling and surveying at Flare Cluster 4, 3, and 10. *Top left:* “Perforated and structured” surface around the bubble escape site at Flare Cluster 4. *Top right*: “Dead” bubble escape site next to Marker 1 at Flare Cluster 3. *Bottom left:* “Curtain” of bubbles at Flare Cluster 3. *Bottom right:* “Perforated but smooth” type seafloor at Flare Cluster 10 and three bubble escape sites.

7.2.9 *Dive 163 (GeoB 11921)*

Area:	Batumi seep, Kobuleti Ridge, Georgia
Responsible scientist:	Markus Brüning
Date:	Saturday, 31 March 2007
Start at Bottom (UTC):	05:47
End at Bottom (UTC):	19:25
Total bottom time:	13 hours and 36 minutes

Start at the bottom:	41°57.400'N	41°17.267'E	844 m water depth
Start ascend:	41°57.542'N	41°17.840'E	833 m water depth

Scientist schedule

09:00 – 11:00	Markus Brüning / Heiko Sahling
11:00 – 13:00	Markus Brüning / Vasileios Mavromatis
13:00 – 15:00	Gregor von Halem / Elena Kozlova
15:00 – 17:00	Gregor von Halem / Gerhard Bohrmann
17:00 – 19:00	Heiko Sahling / Aneta Nikolovska
19:00 – 21:00	Thomas Pape / Markus Brüning

Table 11: Instruments/tools during Dive 163.

GeoB	Tool/instrument	Start	End	Lat. [°N]	Long. [°E]
11921-1	gas bubble sampler -1	18:07	18:33	41:57.530	41:17.266

Waypoints:	Start:	41°57.40'N	41°17.28'E (Flare cluster 10)
	WP 1:	41°57.45'N	41°17.43'E (Flare cluster 9)

Description of the dive

Dive 163 started at 05:47 at the southern rim of the Batumi seep as it is expressed in the 75 kHz DTS sidescan sonar image. The first target we explored was the Flare Cluster no. 10 of the Simrad EM710 flare imaging survey (Fig. 80). The bubble site observed during the dive before was found quickly. Several

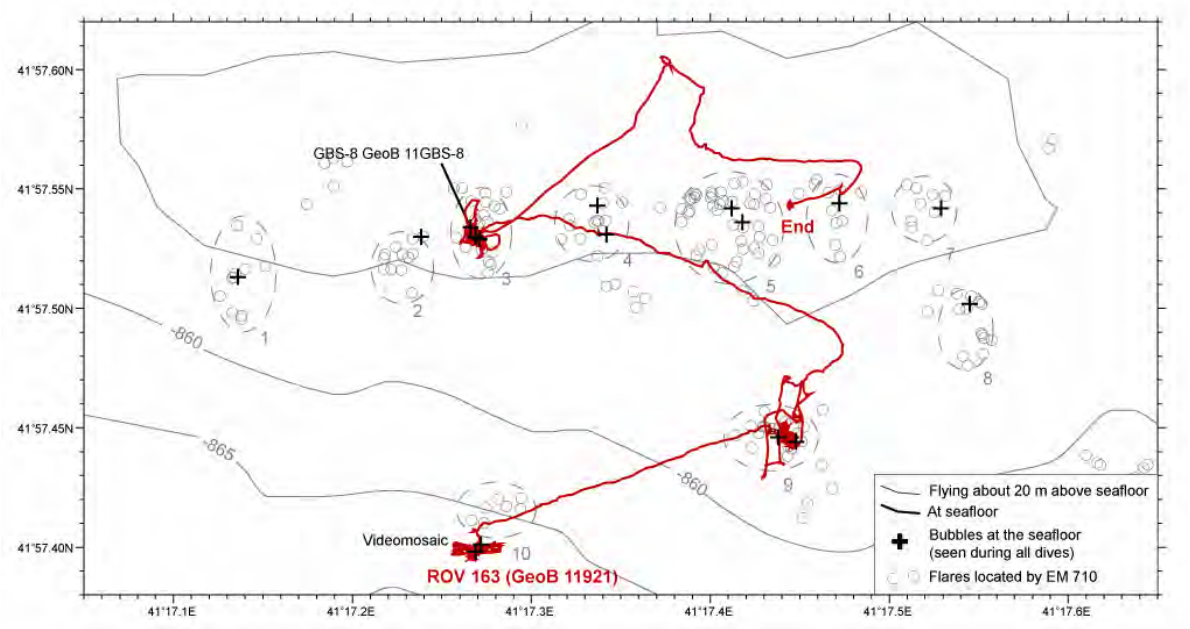

Fig. 80: Seafloor track of Dive 163 at the Batumi seep area.

scans with the forward-looking sonar were recorded at 25 m altitude. On the seafloor, bubble escaping was documented on video and with still images (Fig. 81). The site is very flat with many holes in the ground, of which some were actively bubbling. Escapes were lined up in an E-W trending direction of 3 m length. The larger number of escapes (6 to 8) was grouped at the eastern end, with some other weaker bubble streams located 5 to 7 m to the west. Two wooden sticks pinched out of the seafloor to a height of 50 cm. The flow rates of three of the bubble streams were quantified by collection of gas in the gas catcher. The sampled streams represent the strongest to weak streams. A second sonar scan was conducted at an altitude of 1.5 m resolving the different streams. The seafloor was finally mapped with the DSPL camera flying the ROV in 0.6 m altitude to create a mosaic from the videos. The five E-W trending 35 m long lines have a distance of 1.5 m. The sidescan sonar data were recorded during the mosaicing. An anomaly, 15 m north of the bubble escape site of Cluster 10, was passed when heading to Cluster 9, but did not show any expression on the seafloor.

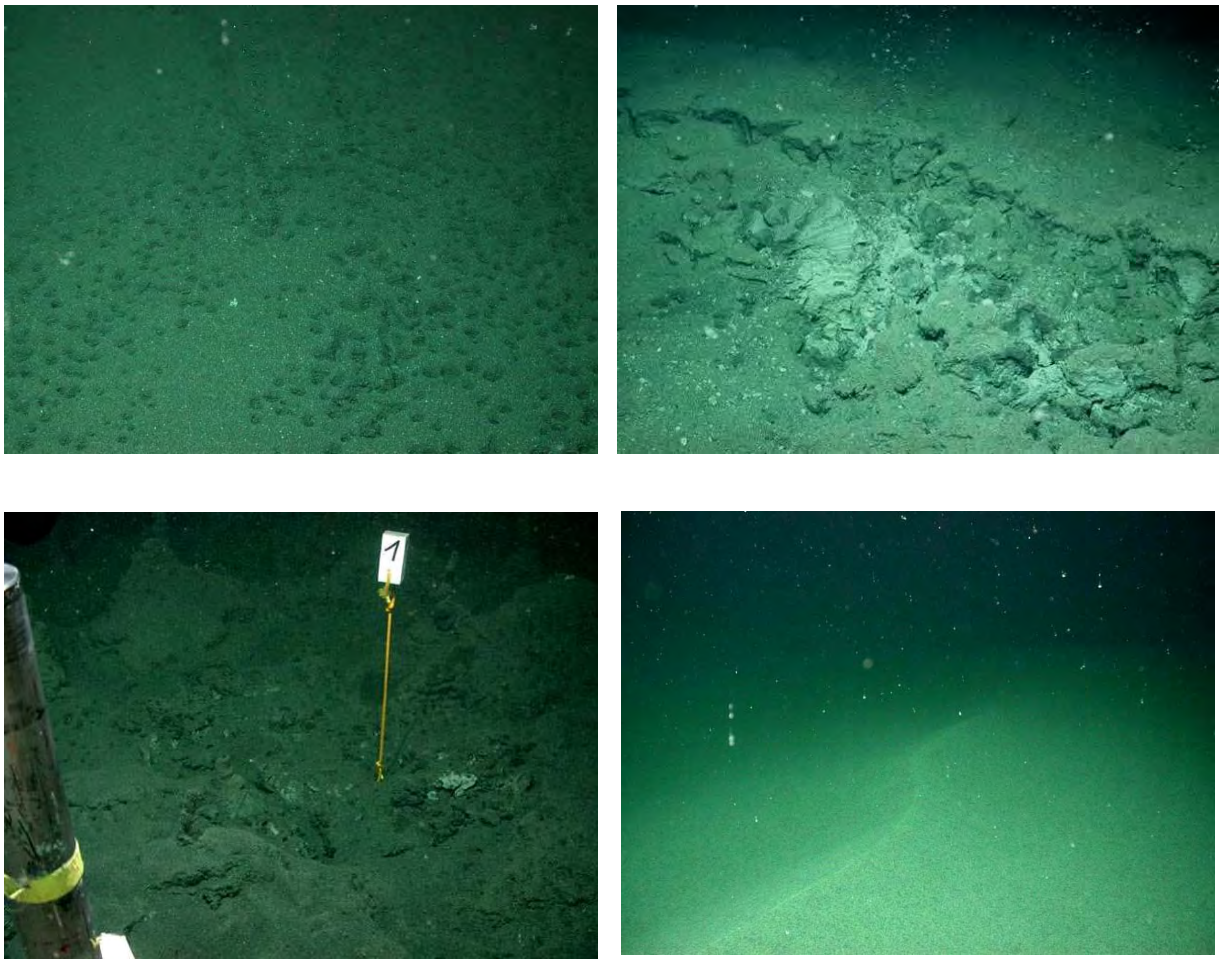

Fig. 81: *Top left:* Holes of bubble escapes at cluster 10. *Top right*: Bubble escape at cluster 9. *Bottom left:* Non-active bubble escape at cluster 3. *Bottom right:* Elongated dune proposed to cause linear features on side scan sonar images.

The flight close to the seafloor to Cluster 9 showed only plain sediments without signs of venting. Arriving at Cluster 9, the vehicle was lifted to 25 m altitude and the forward-looking sonar was deployed to find bubble streams in the water column. One strong and another weaker stream 25 m apart were discovered. Sounding was conducted to other directions, but no other flares were detected. High resolution sonar scans from four directions were made at 4.5 m altitude to separate single streams in the backscat-

tered signals. Close to the seafloor, escape flow rates were quantified with the gas bubble catcher. The about eight bubble streams are a few metres apart from each other. During the observation, the flow rate increased significantly. The seafloor around the escapes looks rough, with clasts, which are partly layered. Over the observed escape site, a block of 30 cm size has a white skin, a layering of 5 mm separation shined through.

Topographic undulations in the vicinity have a height up to one metre. Exploring the surrounding of Cluster 9, N-S trending grabens of about three to four metre depth and 10 m width were discovered. One sidewall housed a two metre deep hole with 40 cm diameter.

The transit to cluster 3 showed a hilly seafloor. At cluster 3, the objective was to take pictures of the gusher site next to marker 1, which was found inactive the day before. When turning the vehicle to match the angle of the Dive 156 image, bubble escape started again, first episodically, then continuous as it was observed the other day.

The next task was to collect one of the chimneys around marker 1 with the bubble catcher bag, but this failed in spite of many tries due to limited abilities of the Rigmaster arm holding the bubble catcher at the appropriate angle. The gas bubble sampler was filled on this spot successfully. Finished at Cluster 3, the ROV headed northeast to find a linear feature seen on all sidescan sonar images from that area. After flying along the line indicated on the 75 kHz sidescan-dive-map, heading south and then east again to find the structure by crossing the indicated location. The ROV's sidescan indicated the searched feature southwest of the dive maps position. Arriving on the spot, a kind of elongated dune was found. As the time for dive work was over, it was not possible to explore the feature anymore.

8 *In situ* sediment and bottom water temperature measurements

(F. Schmidt-Schierhorn, T. Feseker)

8.1 Introduction

The ascent of warm fluids and mud at cold seeps creates temperature anomalies close to the seafloor and in the bottom water. Detecting and quantifying these anomalies provides information on the nature and strength of fluid seepage. During Leg M72/3a, *in situ* temperature measurements were conducted over the course of the ROV dives at shallow sediment depths and in the bottom water in order to identify areas with active seepage. In order to investigate the temporal variability of the activity of Dvurechenskii mud volcano (DMV), a gravity corer equipped with thermistor strings had been deployed in the course of the previous cruise M72/2. The first temperature record was obtained during M72/3a, 18 days after the deployment. The sum of these measurements will be used to estimate flow rates and the depth of the gas hydrate stability zone.

8.2 Materials and methods

8.2.1 Long-term temperature observation using a gravity corer equipped with thermistor strings

A temperature lance equipped with thermistor chains was deployed at the geometrical centre of the DMV during M72/2. This lance consists of a regular gravity corer with a weight set of 200 kg and a 5.75 m long barrel. Two RBR thermistor chains were attached to the corer along the barrel. Each thermistor chain consists of eight sensor nodes distributed evenly over a length of 4.9 m. The thermistor chains are connected to two independent data loggers attached to a buoy floating approximately 3 m above the seafloor and may be recovered using the ROV while the lance remains in the sediment.

8.2.2 ROV-operated temperature lance

A novel temperature lance manufactured by RBR Ltd. (Fig. 82, *left*) was used during the ROV dives to obtain *in situ* sediment temperature measurements from up to 0.6 m below the seafloor. The lance consists of eight temperature sensors distributed over a length of 0.5 cm. During an entire dive, a reading from each sensor is stored in a central logging unit every ten seconds. The precision of the measurements is 0.002 °C. Using the manipulator arm of the ROV, the lance is lowered into the sediment (Fig. 82, *right*) to the maximum penetration depth of 0.6 m and left in place for at least ten minutes to allow the sensors to adjust to the sediment temperature. The real temperature value may be estimated by extrapolation from the

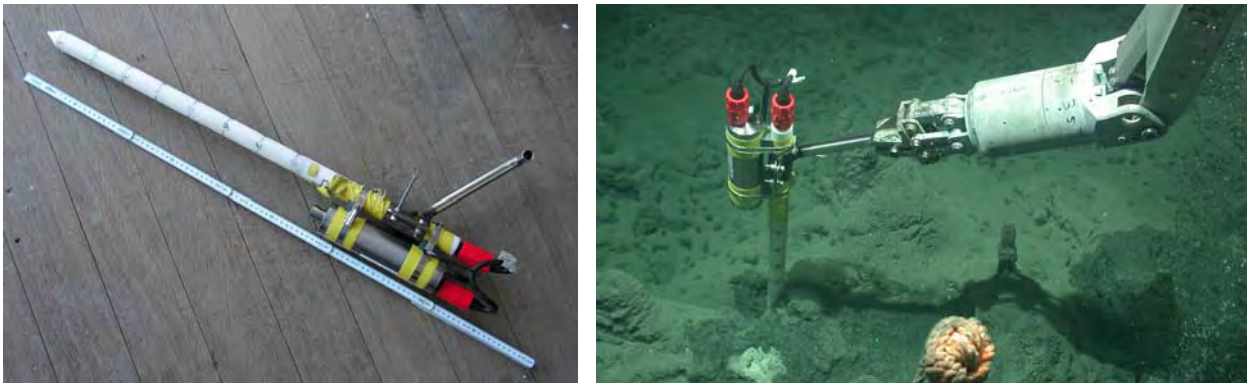

Fig. 82: Temperature lance. *Left:* on deck of R/V METEOR. *Right*: during its deployment at the seafloor (source: University of Bremen, MARUM)

recorded equilibration curve. During the cruise, first rough estimates of the equilibrium temperatures were obtained from visual analyses of the recorded curves.

8.2.3 Autonomous bottom water temperature loggers mounted on ROV "QUEST4000m"

For the measurements in the water column, two autonomous MTLs (miniaturized temperature data loggers) from ANTARES Datensysteme GmbH were attached to the frame of the ROV "Quest4000m" (Fig. 83). The MTLs were programmed to record one temperature reading every second during the entire dive. The resolution of the MTL sensors is 0.6 mK, allowing for highly accurate relative temperature measurements. However, the absolute precision amounts to ±1/10K, as the sensors were not calibrated with a high precision reference.

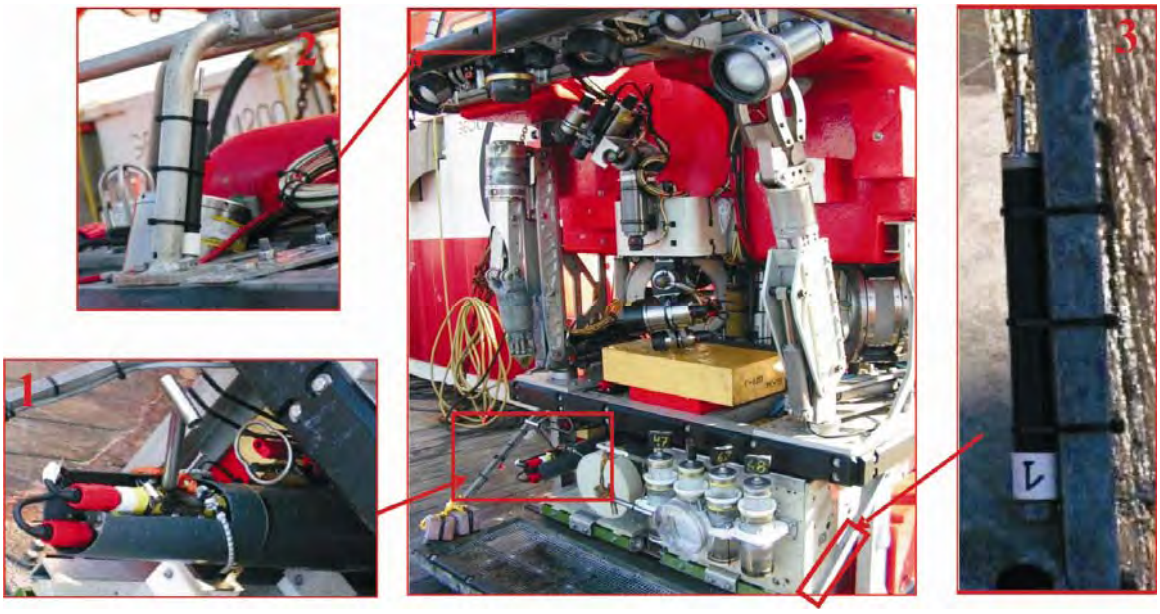

Fig. 83: *Positions of the different devices on the ROV. Left bottom:* Temperature Stick (XR-420). *Left top*: MTL (1854008A). *Right:* MTL (1854007A).

A list showing positions of areas investigated and measurement characteristics is given in Tab. 12.

Table 12: Overview of temperature measurements performed during M72/3a at Colkheti seep (CS), at the Batumi seep area (BS), at Dvurechenskii mud volcano (DMV), and Vodyanitskii mud volcano (VMV).

GeoB no.	ROV dive no.	Area	Lat [°]N	Long [°]E	Water depth [m]	Duration of deployment [min]	Penetration depth [cm]
11902-2	155	CS	41:96.785	41:10.328	1113	00:12	50
11902-3	155	CS	41:96.786	41:10.328	1113	00:11	56
11904-10	156	BS	41:57.529	41:17.271	835	00:09	
11904-11	156	BS	41:57.528	41:17.270	835	00:07	16,5
11904-12	156	BS	41:57.529	41:17.271	835	00:10	20
11907-3	157	BS	41:57.543	41:17.529	834	00:15	61
11910-1	159	DMV	44:16.900	34:59.293	2046	00:12	62
11910-2	159	DMV	44:16.929	34:59.233	2045	00:16	62
11910-4	159	DMV	44:16.946	34:59.175	2044	00:17	62
11910-5	159	DMV	44:16.977	34:59.085	2042	00:15	62
11910-7	159	DMV	44:17.006	34:58.974	2042	00:16	62
11910-9	159	DMV	44:17.019	34:58.929	2041	00:18	55
11910-10	159	DMV	44:17.029	34:58.880	2040	00:28	63

Table 12, continuation: Overview of temperature measurements

GeoB no.	ROV dive no.	Area	Lat [°]N	Long [°]E	Water depth [m]	Duration of deployment [min]	Penetration depth [cm]
11910-12	159	DMV	44:16.972	34:58.910	2036	*)	*)
11910-13	159	DMV	44:16.947	34:58.850	2042	00:11	60
11915-1	160	DMV	44:16.802	34:58.596	2052	00:14	58
11915-2	160	DMV	44:16.838	34:59.596	2043	00:11	58
11915-3	160	DMV	44:16.893	34:58.709	2043	00:12	60
11915-4	160	DMV	44:16.954	34:58.784	2041	00:17	66
11915-5	160	DMV	44:17.002	34:58.889	2040	00:12	61
11915-6	160	DMV	44:16.995	34:58.736	2042	00:12	62
11915-7	160	DMV	44:17.024	34:58.612	2042	00:13	64
11915-10	160	DMV	44:17.093	34:58.673	2043	00:23	53
11915-13	160	DMV	44:17.054	34:58.759	2042	00:26	53
11915-16	160	DMV	44:17.005	34:58.896	2040	00:12	51
11915-20	160	DMV	44:17.052	34:58.842	2041	00:18	53
11917-2	161	VMV	44:17.657	35:01.995	2032	00:28	54

*) Picking up thermistor from long-term temperature observation station at DMV.

8.3 Preliminary results

8.3.1 In situ sediment temperature measurements

Batumi Seep Area

In the course of two reconnaissance dives at the Batumi seeps site, four temperature measurements were obtained using the ROV temperature lance. The temperature values ranged between 8.94 and 9.17 °C. Compared to a bottom water temperature of approximately 9.1 °C, this suggests a relatively low temperature anomaly. Strongly irregular profiles with more than one relative minima and maxima (e.g. Fig. 84) may be related to gas ebullition associated with bottom water infiltration and circulation.

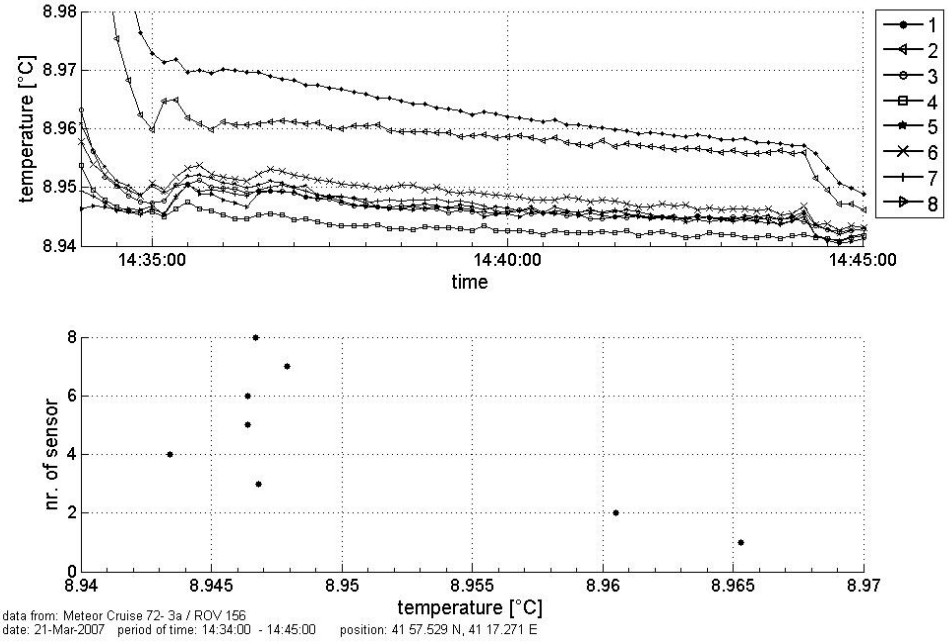

Fig. 84: Temperature measurement at ROV Dive 156, station 4 at the Batumi seep area. *Upper graph*: Different symbols represent the temperatures recorded by the eight individual sensors (1-8). *Lower graph*: The profile reveals a temperature decrease from sensor six to five, where it reaches a local minimum. From this point downward, the values increase again rapidly, reaching a maximum of about 8.966 °C at sensor 1.

Dvurechenskii Mud Volcano

Continuing the survey of sediment temperatures from the previous cruise leg, M72/2, 20 *in situ* temperature measurements were obtained during two dives at Dvurechenskii mud volcano (DMV; Tab. 12). Measurements were obtained at sites of push core sampling and along previously defined transects from the edges of the plateau towards the most active area NW of the geometrical center of the mud volcano (Fig. 85).

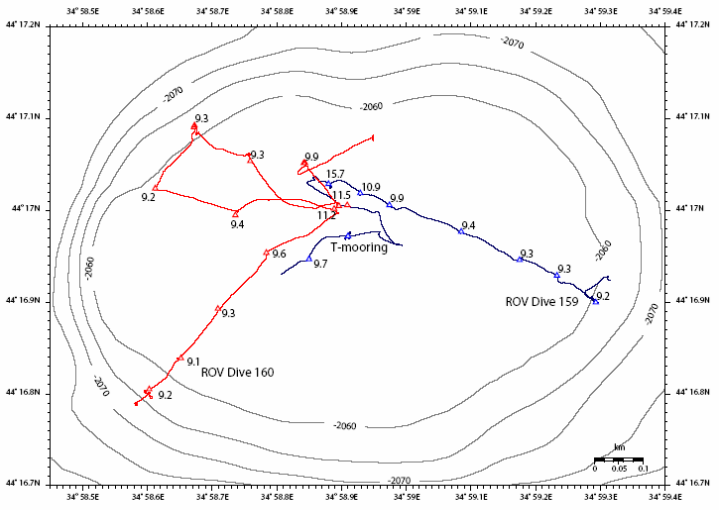

Fig. 85: Overview of the temperature measurements at Dvurechenskii mud volcano.

Measured sediment temperatures ranged between the bottom water temperature of 9.1 to more than 15 °C. The highest value of 15.7 °C was at approximately 0.6 m below the seabed during ROV Dive 159 at station 5 (position: 44°17.029' N, 34°58,88' E) This appears to be the active center of the mud volcano. The preliminary evaluation of the measured data suggests that all stations show a linear temperature increase with depth.

As an example, Fig. 86 shows the result of a measurement from ROV Dive 159 (25 March 2007, station 7) from DMV. In the upper graph, the lines of different colors represent the measurements obtained from the eight individual sensors. The lower figure presents the derived temperature profile over the length of the ROV temperature lance.

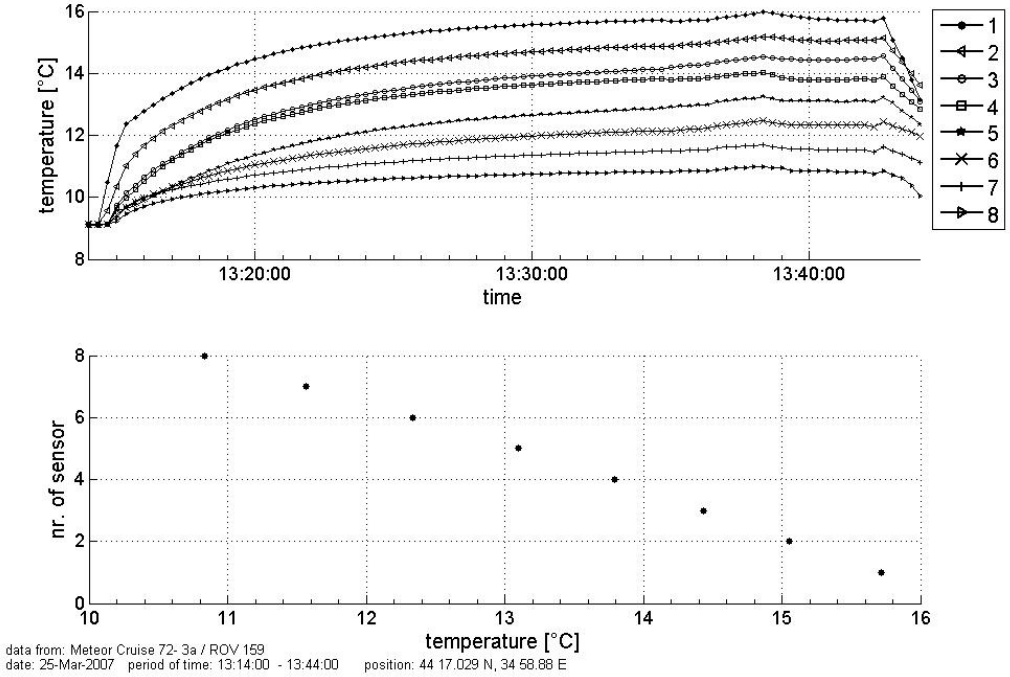

Fig. 86: Temperature measurement obtained during ROV Dive 159, station 7 at Dvurechenskii mud volcano.

Vodyanitskii Mud Volcano

At Vodyanitskii mud volcano only one measurement was obtained (Tab. 12). The corresponding profile reveals a linear temperature increase with depth, reaching a maximum of 10.09 °C at the deepest sensor.

Colkheti seep

Colkheti seep is a site situated near the Batumi seeps, where oil has been found at the seafloor. Using the ROV temperature lance, two measurements were obtained during one dive (Tab. 12). The measured values range from 9.00 to 9.24 °C, suggesting a relatively low temperature anomaly at this site.

At the first station (GeoB 11902-2), the measured profile is strongly nonlinear with a distinct temperature maximum at the second sensor (Fig. 87). In contrast, the profile obtained from the second station shows a linear temperature increase with depth (not shown here).

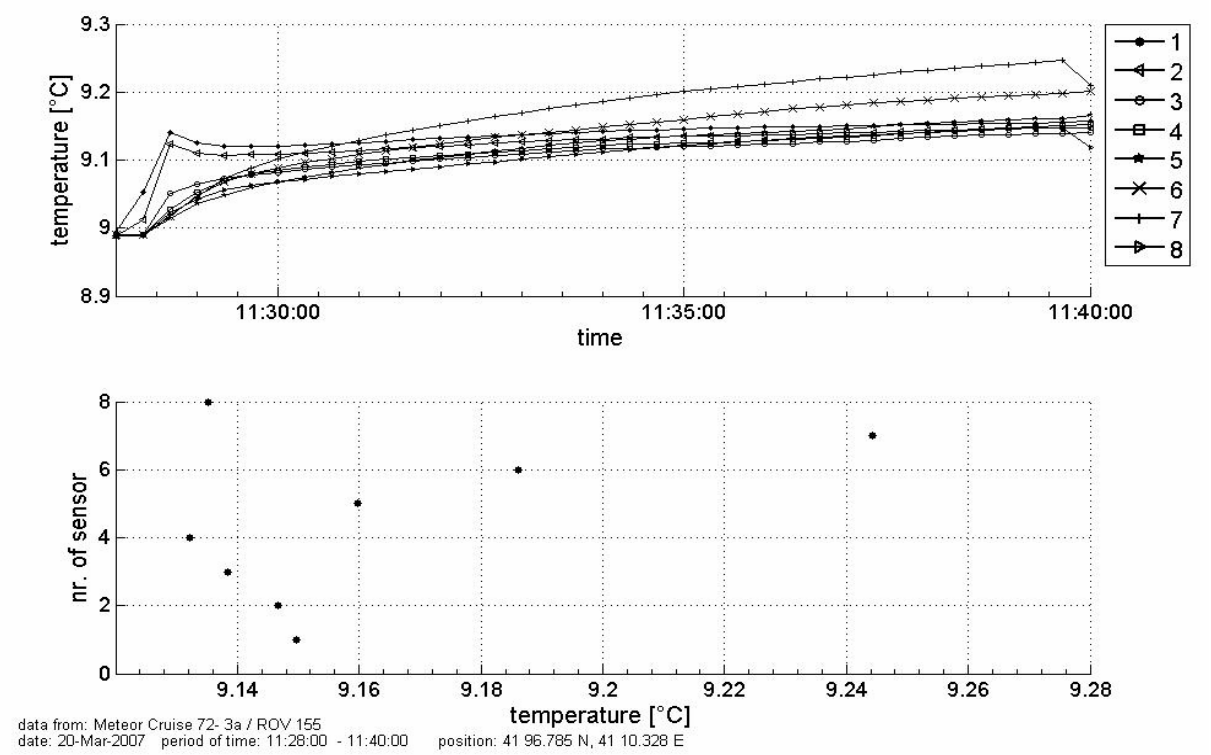

Fig. 87: Temperature measurement at ROV Dive 155, station 1 at Colkheti seep.

8.3.2 Bottom water temperature

Fig. 88 shows the comparison of data from the two MTLs and from the CTD recorded during ROV Dive 159 at DMV on 25.3.07. The relative measurements were very sensible and show a similar pattern, but the offset between the individual curves is obvious. Moreover, the time series recorded by MTL 2 shows large variability. As this logger was mounted at the top of the porch of the ROV, it may be suggested that this phenomenon is related to the temporal heating of the seawater by the lamps of the ROV. All loggers recorded the highest bottom water temperature when the highest subsurface temperature value was measured with the ROV lance. The corresponding time interval from 13:14 to 13:44 o'clock is marked by a black rectangle.

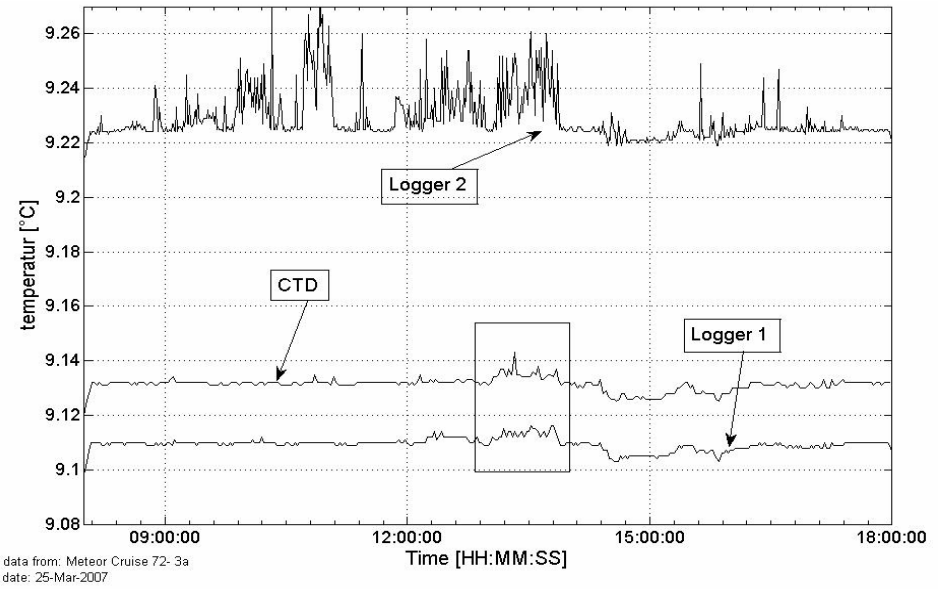

Fig. 88: Temperature measurement with MTLs in comparison to data from the CTD at ROV Dive 159 at Dvurechenskii mud volcano. Black rectangle: time interval while measuring maximum temperatures near the centre of DMV.

8.3.3 First results from the long-term temperature observation at Dvurechenskii Mud Volcano

One of the two data loggers from the long-term temperature lance was recovered 18 days after the deployment of the lance during the previous cruise Leg M72/2. The thermistor chain recorded one reading from each of the eight temperature sensors every 15 minutes. The corresponding time series are shown in Fig. 89. The largest temperature changes occurred during the first few days of the observation, suggesting that the temperature distribution in the sediment column was altered by the presence of the lance. At all sensors temperature decreased with time, but the first three sensors and the last one (sensor 8) showed less decline than the others.

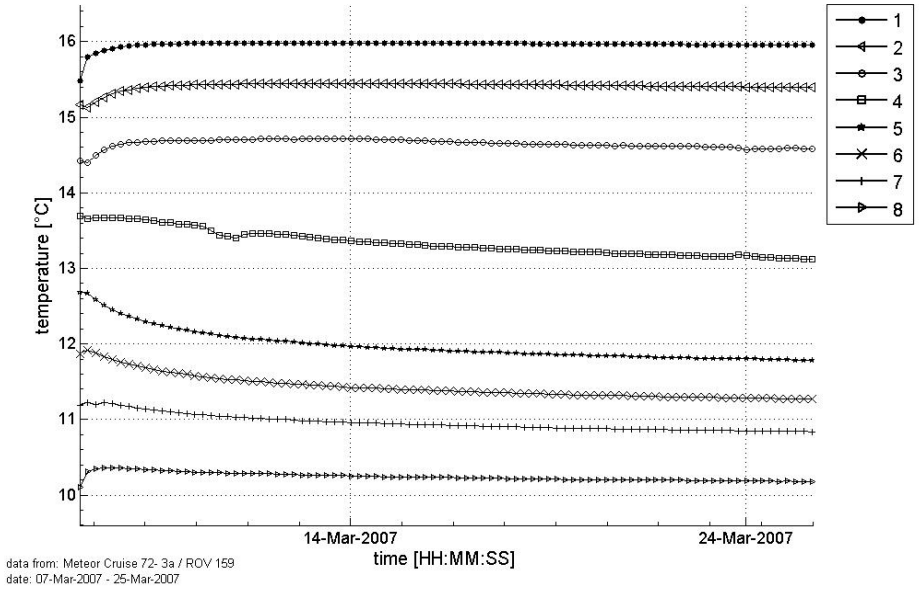

Fig 89: Results from the long-term temperature observation. Different symbols represent the different sensors.

9 Autoclave work

(H.-J. Hohnberg, F. Abegg, T. Pape, S.A. Klapp, K. Dehning, A.H. Mai)

9.1 Introduction

During M72/3, three autoclave tools for sampling-gas hydrate-bearing sediments and bubble-forming gas were used:

The **Dynamic Autoclave Piston Corer I (DAPC I)** has been designed and built to recover, preserve, and analyze sediment cores under the *in situ* conditions of the deep sea. Its main use is to quantify gas and gas hydrate contents preserved in the cores. During incremental degassing of the cores, subsamples of the released gas can be taken for analyses of their chemical compositions (Chap. 12). DAPC I has been successfully deployed and continuously improved during several previous cruises (SO 174; TTR-15; M70/3) since 2003.

The **Dynamic Autoclave Piston Corer II (DAPC II)** consists of a tool system, which includes an autoclave corer similar to the DAPC I and a set of individual pressure chambers and associated manipulators. It is an advancement of DAPC I with the aim of recovering and cutting sediment cores and transferring the core segments into smaller, manageable pressure chambers while still under pressure. In contrast to the pressure chamber of DAPC I, these pressure chambers allow for visualization and determination of gas, gas hydrate and sediment amounts by computer tomography (CT, Chap. 10.3), prior to incremental degassing. The whole system is a new development within the project METRO and made its first deployments during this cruise.

The ROV-based **Gas Bubble Sampler (GBS)** was primarily developed to collect free gas escaping from the seafloor, but it allows for the sampling of gas hydrates generated in the water column from ascending gas bubbles or of pure seawater, as well. Further, the GBS allows for estimations of gas flux rates by visual observations during ROV dives and by quantitative degassing upon its recovery on deck. Due to its handling with the ROV, samples can be taken very close to the seabottom, e.g. above discrete gas outlets. The GBS first launch was during cruise M70/3 and it has been routinely used during M72/3a.

9.2 Materials and methods

The **DAPC I** (Fig. 90) is a sediment pressure-core sampling device of 7.2 m total length and 500 kg total weight. It was designed to cut sediment cores from the seafloor surface to a maximum length of 2.5 m and to preserve them at *in situ* pressure. The certified pressure is 140 bar corresponding to water depths of down to 1400 m. Nevertheless, the DAPC I is equipped with a pressure control valve, which allows the deployment down to 5000 m

Fig. 90: Deployment of DAPC I from on board R/V METEOR. The pressure chamber (*top*) and the core cutting barrel (*bottom*) are shown.

water depth. An *in situ* pressure up to 200 bar can be preserved, and higher pressures up to 500 bar will be released down to 200 bar. The core cutting barrel, which is relatively short (2.7 m) hits the seafloor with strong impact. Therefore, it is especially suitable for sampling layered gas hydrate-bearing sediment. The device allows various analytical approaches such as quantitative analyses of gases and subsampling for chemical investigations. The pressure chamber consists of glass-fiber reinforced plastic (GRP), aluminum alloys, seawater resistant steel, and aluminum bronze. The pressure chamber is 2.6 m long and weighs about 230 kg. All parts of the pressure chamber exposed to seawater are suitable for long-term storage of cores under pressure for several weeks. The DAPC I is to be deployed from a research vessel on the deep sea cable. It can be released from variable heights (1-5 m) due to the resistance of the seafloor and penetrates in free fall. The pressure chamber was checked and approved by the Berlin TÜV (Technischer Überwachungsverein, technical inspection authority of Germany).

The **DAPC II** in detail is a tool system consisting of the pressure core sampling device, a set of pressure chambers and two manipulators (Fig. 91). The pressure core sampling device is in its physical dimensions similar to the DAPC I, but the total length is 7.6 m and the certified pressure is 200 bar. The process of tool preparation, deployment, and recovery is the same as for DAPC I. Upon recovery, many single steps have to be done consecutively such as disconnection of the core catcher, transfer of core material, connection and disconnection of pressure chambers. All these processes are actually very complicated and need great accuracy for success and security. When successfully transferred, the pressurized core segments can be analyzed using CT-technique, degassing (Chap. 12), and geochemical investigations (Chap. 11).

Fig. 91: The DAPC II: A = pressure coring tool, B = pressure chamber, C = manipulator.

Deployments of DAPC I and -II from R/V METEOR were similar to those of conventional piston corers, but without a core depositing frame. Both penetrate the seafloor in a free-fall mode using the release mechanism developed by Kullenberg (1947).

The **GBS** (Fig. 92) is a ROV-operated *in situ* pressure sampling device, which in principle consists of a steel tube with valves on each end. The valve on one end is connected to a funnel and is operated by the ROV manipulator via a handle. The other valve is used to release gas kept in the GBS upon its recovery on deck. Before deployment, both valves are closed preserving atmospheric pressure. While at the seafloor the content of the funnel (water, gas or gas hydrate) is sucked into the steel tube when the valve is opened due to the pressure difference. The valve is only shortly opened for sample collection. At maximum, two GBS were deployed during a single ROV dive.

Fig. 92:
Picture showing the gas bubble sampler with funnel, ball valve handle and pressure-resistant steel tube.

During cruise M72/3, 23 DAPC and 8 deployments of the GBS were carried out (Tabs. 13 and 14).

Table 13: Deployment statistics of the dynamic autoclave piston corer I (DAPC I) and the dynamic autoclave piston corer II (DAPC II). USBL = Ultra-short base line (Posidonia Unterwater positioning system).

GeoB	Instru-ment	Instru-ment No.	Area	Lat. [°N]	Long. [°E]	Water Depth [m]	Pres-sure [bar]	Gas released [mL]	Core recovery, remarks
11901	DAPC I	DAPC-01	BS	41:57.410	41:17.344	851	68	231.200	USBL; recovery 260 cm
11903	DAPC I	DAPC-02	BS	41:57.472	41:17.266	850	72	46.280	USBL; degassing stopped due to clogging of system. 260 cm core, 100 cm recovery
11906	DAPC I	DAPC-03	BS	41:57.465	41:17.270	843	64	40.700	USBL; recovery 83 cm
11920	DAPC I	DAPC-09	BS	41:57.454	41:17.545	844	81	100.550	USBL; recovery 259 cm
11937	DAPC I	DAPC-12	BS	41:57.489	41:17.462	842	52	8.000	recovery 41 cm
11958	DAPC I	DAPC-15	BS	41:57.448	41:17.446	845	87	137.450	recovery 146 cm
11963	DAPC I	DAPC-16	BS	41:57.410	41:17.278	853	27	30.700	recovery 169 cm
11922	DAPC I	DAPC-10	CS	41:58.071	41:06.214	1126	125	69.500	n.a.
11909	DAPC I	DAPC-04	DMV	44:16.906	34:59.066	2056	n.d.	0	USBL; device did not release, no recovery
11911	DAPC I	DAPC-05	DMV	44:16.972	34:59.215	2058	1	n.d.	USBL; Autoclave did not close; 251 cm recovery
11914	DAPC I	DAPC-06	DMV	44:16.987	34:59.097	2058	185	108.550	USBL; recovery 256 cm
11916	DAPC I	DAPC-07	DMV	44:16.896	34:58.789	2057	185	100.850	USBL; recovery 253 cm
11999	DAPC I	DAPC-23	DMV	44:16.892	34:58.902	2049	185	130.550	USBL; recovery 256 cm
11981	DAPC I	DAPC-19	VMV	44:17.650	35:01.979	2037	192	3.950	recovery 78 cm
11991	DAPC I	DAPC-20	VMV	44:17.625	35:01.949	2052	n.d.	n.d.	no recovery
11992	DAPC I	DAPC-21	VMV	44:17.630	35:01.932	2055	10	39.750	USBL; recovery 177 cm
11918	DAPC II	DAPC-08	BS	41:57.547	41:17.427	840	88	253.200	**first deployment of DAPC II;** recovery 233 cm
11935	DAPC II	DAPC-11	BS	41:57.549	41:17.425	843	n.d.	0	device lost pressure; no recovery
11944	DAPC II	DAPC-13	BS	41:57.554	41:17.654	841	n.d.	0	device lost pressure, no recovery
11951	DAPC II	DAPC-14	BS	41:57.546	41:17.431	840	79	103.250	recovery 137 cm
11972	DAPC II	DAPC-17	BS	41:57.541	41:17.428	841	n.d.	0	device did not release, no recovery
11973	DAPC II	DAPC-18	BS	41:57.544	41:17.430	840	n.r.*)	n.a.	device maintained pressure
11994	DAPC II	DAPC-22	DMV	44:16.995	34:59.096	1994	n.r.*)	n.a.	recovery 250 cm **core-transfer under pressure**

Pressure = pressure upon recovery. BS = Batumi seep, DMV = Dvurechenskii mud volcano, CS = Colkheti seep, VMV = Vodyanitskii mud volcano. n.d. = not detected; n.a. = not analysed.; n.r.*) material dedicated for core transfer, visual observations of pressure but no precise recording

Table 14: Deployment statistics of the gas bubble sampler (GBS).

GeoB	Instrument No.	Area	Lat. [°N]	Long. [°E]	Water Depth [m]	Pressure upon recovery [bar]	Gas released [mL]
11902-1	GBS-1	CS	41:58.071	41:06.197	1112	105	48.330,0
11904-7	GBS-2	BS	41:57.529	41:17.272	835	n.d.	0,0
11904-16	GBS-3	BS	41:57.541	41:17.413	833	78	24.690,0
11907-2	GBS-4	BS	41:57.543	41:17.529	834	74	28.450,0
11907-5	GBS-5	BS	41:57.544	41:17.472	835	1	50,0
11917-1	GBS-6	VMV	44:17.656	34:01.992	2032	175	69.150,0
11919-2	GBS-7	BS	41:57.533	41:17.268	833	75	32.850,0
11921-1	GBS-8	BS	41:57.530	41:17.266	844	75	33.300,0

CS = Colkheti seep, BS = Batumi seep, VMV = Vodyanitskii mud volcano. n.d. = not detected.

9.3 Preliminary results

9.3.1 DAPC I deployments

In total 16 deployments of DAPC I were conducted during M72/3. At 12 stations, the pressure inside the tool was sufficient to preserve the sampling material within the gas hydrate stability field. Immediately upon recovery, those cores were incrementally degassed in order to determine the total amounts of gas preserved and to take gas subsamples for further analyses (Chap. 12). Sediment cores were subjected to sedimentological descriptions (Chap. 10.2) and pore water sampling (Chap. 11). At two stations, DAPC I did not release and no sediments were recovered.

The DAPC I again has proven to be completely functional. The device has been deployed to a maximum pressure level of 200 bar without any technical concern or failure. Minor problems occurred with a sealing ring in the bottom ball valve due to cold temperatures. A pressure accumulator system balanced the pressure loss in most cases.

9.3.2 DAPC II deployments

The newly developed DAPC II pressure coring system including the pressure chambers and the manipulators was deployed for the first time during M72/3 (GeoB 11918, DAPC-08). In total 7 deployments of the DAPC II were conducted during the cruise. After the first deployments and necessary advancements, the system proved its full function within the pressure range of up to 200 bars. At two stations (GeoB 11918, DAPC-08; GeoB 11951, DAPC-14), it has been used for simply degassing similar to DAPC I.

A challenging task was the core transfer. After some problems concerning the sealing system and more precisely the interaction of the core liner and the pressure chamber, the core transfer was executed by a modification of the sealing system which was newly developed for this process. Two core segments (GeoB 11994-1 and -2) of 50 cm length each were cut and transferred under pressure. Subsequently, computer tomography scans were performed on these segments (Chap. 10.3).

The DAPC II is completely applicable for recovering pressurized cores similar to DAPC I. Nevertheless, some improvements have to be done: the bearings of the pressure chamber ball valves have to be enhanced for reducing the force which is necessary to operate the ball under pressure, the handling of the core transfer must be simplified, and a concerted and fixed tool carrying system has to be developed.

9.3.3 GBS deployments

For sampling of near-bottom gas escaping the seafloor within the gas hydrate stability field, two ROV-based GBS were operated 8 times during six dives over the course of M72/3a. Pressurized gas was recovered successfully from six sites while at one station the gas was completely lost due to leakage from the system. At one station, a partial loss of pressure due to handling problems during sampling occurred. However, since some pressure was preserved, the gas could be subsampled for chemical analysis.

The GBS are completely functional within the pressure range of 250 bars and are ready for further deployments.

10 Geological sampling and sedimentology

10.1 Geological sampling equipment

(S.A. Klapp, F. Abegg, A. Bahr, H.-J. Hohnberg, B. Domeyer, G. von Halem, A.H. Mai, K. Dehning)

Recovering geological samples was a major objective during R/V METEOR cruise M72/3. Several goals needed to be accomplished, for which different tools were suitable: For recovering cores of up to 6 meters length, gravity coring was conducted, while relatively short cores with undisturbed sediment-water interface were taken by use of multicorer or minicorer (Tabs. 15 and 16). For recovery of pressurized sediment cores the Dynamic Autoclave Piston Corers I and II were deployed (Chap. 9).

Gravity cores (GC) were either taken with a 6-m-core barrel or with a 3.5-m-core barrel. The outer diameter of the barrel is 14 cm and the inner diameter is 13.2 cm. The coring was conducted either with a PVC liner or with a soft plastic hose inside. The soft plastic hose allows for fast access to the sampled material and was commonly used for sampling gas hydrate-bearing sediments. Besides sedimentological and geochemical analyses, standard PVC liner were also used for cores which were intended to be scanned by computer-tomography (CT) in a frozen state (Chap. 10.3). For this purpose, the liners were pre-cut into segments of 55 cm and later to 50 cm due to the CT scanner's capabilities. Before deployment of the GC, the segments were carefully taped together. Upon recovery, the connecting tapes were cut off and the segments were closed with caps and immediately frozen in liquid nitrogen. This process has proved to be very fast, which is a necessity in order to avoid extended dissociation of gas hydrate.
On R/V METEOR, winch W11 was used for the deployment of the gravity corer. The winch speed was commonly set to 1.0 m/s to slack or heave the GC in the water column. For coring, the speed was sometimes set to 1.5 m/s. During the cruise, the gravity corer was used with reduced weight due to extended overpenetration during M72/2. The head was equipped with approx. 800 kg of lead.

The **multicorer (MUC)** was used to sample undisturbed top sediment layers. The tool was equipped with a head for the deployment of 8 liners with a diameter of 10 cm and 4 liners with diameters of 6 cm, all of them with a length of 50 cm. For the deployment again R/V METEOR's winch W11 was used.

The slacking was set to 0.8 m/s and lifting speed was set to 1.0 m/s; depending on the sediment the coring speed varied from 0.3 m/s to 0.7 m/s. The multicorer did not work properly: the lock of the liners only partially released. Several attempts to improve the coring results did not avail, and the problem could not be fixed onboard. For this reason, we switched to the **minicorer (MIC)**, a small version of the MUC, during Leg M72/3b. The MIC comes with four liners of 6 cm diameter and 60 cm length. For the deployment onboard R/V METEOR, winch W2 or W3 was used with a slacking speed of 0.5 m/s until a depth of 700 m is reached, further downwards the speed was set to 0.7 m/s. The low speed down to 700 m is necessary to avoid an overhauling of the MIC by the down-moving deep-sea cable, because the MIC is a very light sampling tool that without any attached weights only weighs about 30 kg. The coring speed was set to 0.3 m/s, the device is heaved with 1.0 m/s.

All GC, MUC, and MIC stations were run with POSIDONIA (USBL) underwater navigation if available.

Table 15: Overview of gravity corer (GC) and multicorer (MUC) stations.

GeoB	GC-No.	Area	Lat [°N]	Long [°]E	Water Depth [m]	Comment
11913	GC-1	Vodyanitskiy MV	44:17.621	35:01.946	2048	USBL; recovery 138 cm
11923	GC-2	Colkheti seep	41:58.120	41:06.250	1088	USBL; 6 m; plastic bag
11924	GC-3	Colkheti seep	41:58.068	41:06.195	1056	USBL; 6 m; plastic bag; recovery 698 cm
11925	GC-4	Batumi seep	41.57.431	41:17.347	844	USBL; 6 m; plastic bag; recovery 215 cm
11926	GC-5	Batumi seep	41:57.416	41:17.345	849	USBL; 6 m; plastic bag
11927	GC-6	Batumi seep	41:57.410	41:17.324	856	USBL; 6 m; plastic bag; recovery 413 cm
11933	GC-7	Gudauta High	42:40.262	40:22.631	690	USBL; recovery 380 cm
11936	GC-8	Batumi seep	41:57.563	41:17.430	844	USBL; PVC-liner Segments for CT analysis (6 m); recovery 193 cm
11938	GC-9	Iberia mound	41:52.340	41:10.036	982	USBL; recovery 134 cm
11941	GC-10	Pechori mound	41:58.962	41:02.404	1014	USBL; recovery 83 cm
11942	GC-11	Pechori mound	41:59.008	41:07.400	1024	USBL; no recovery
11945	GC-12	Batumi seep	41:57.345	41:17.456	848	USBL; no recovery
11946	GC-13	Batumi seep	41:57.532	41:17.582	842	USBL; PVC-liner Segments; recovery 302 cm
11949	GC-14	Batumi seep	41:57.550	41:17.175	842	USBL
11952	GC-15	Pechori mound	41:58.955	41:07.539	1019	USBL; plastic hose (6 m), no recovery
11953	GC-16	Pechori mound	41:58.958	41:07.543	1015	USBL; PVC liner segments for CT analysis (3 m); recovery 335 cm
11955	GC-17	Pechori mound	41:58.963	41:07.540	1012	USBL; PVC-liner (3 m); recovery 144 cm
11956	GC-18	Batumi seep	41:57.450	14:17.436	843	USBL; PVC-liner Segments for CT analysis (3 m); recovery 110 cm
11957	GC-19	background Batumi seep	41:57.803	41:18.001	844	USBL; PCV liner Segments (1 m) for home analysis (6 m total)
11967	GC-20	Batumi seep	41:57.530	41:17.268	843	USBL; no recovery; some carbonate pieces in core catcher
11971	GC-21	Colkheti seep	41:58.069	41:06.199	1124	USBL; PVC-liner (3 m); recovery 151 cm
11974	GC-22	Reference Station	41:57.428	41:16.803	884	USBL; PVC-liner (6 m), recovery 697 cm; reference station near Batumi Seep
11975	GC-23	Batumi seep	41:57.528	41:17.588	844	USBL; plastic hose (3 m); recovery 304 cm
11980	GC-24	Vodyanitskiy MV	44:17.659	35:01.965	2039	USBL; PVC-liner Segments; recovery 131 cm
11987	GC-25	Kerch Strait	44:37.138	35:42.249	894	USBL; recovery 157 cm
11988	GC-26	Kerch Strait	44:37.207	35:42.291	889	USBL; recovery 293 cm
11989	GC-27	Kerch Strait	44:37.203	35:42.260	888	USBL; recovery 289 cm
11990	GC-28	Vodyanitskiy MV	44:17.623	35:01.946	2061	USBL; recovery 153 cm
11998	GC-29	Dvurechenskii MV	44:16.998	34:59.090	2052	USBL
11905-1	MUC-1	near Batumi seep	41:57.249	41:16.716	895	device did not release
11905-2	MUC-2	near Batumi seep	41:57.432	41:16.798	877	recovery 60 cm
11912	MUC-3	Dvurechenskii MV	44:17.015	34:58.885	2053	recovery 60 cm
11928	MUC-4	Shallow Ridge	41:42.332	41:28.174	379	device did not release
11929	MUC-5	Shallow Ridge	41:42.374	41:28.059	367	device did not release
11930	MUC-6	Shallow Ridge	41:42.386	41:27.938	382	device did not release
11931	MUC-7	Batumi seep	41:47.838	41:16.842	839	8 MUC-liners completely filled
11934	MUC-8	Gudauta High	42:40.260	40:22.678	701	USBL; recovery 57 cm
11939	MUC-9	Iberia mound	41:52.739	41:10.025	989	USBL; recovery 60 cm
11943	MUC-10	Pechori mound	41:58.659	41:07.428	1014	USBL, no recovery
11947	MUC-11	Batumi seep	41:57.531	41:17.585	841	USBL; device did not release
11948	MUC-12	Batumi seep	41:57.531	41:17.578	843	USBL; device did not release
11950	MUC-13	Batumi seep	41:57.542	41:17.424	840	USBL; device did not release

USBL = Ultra-short base line (Posidonia underwater positioning system); recovery = core recovery

Table 16: Overview of minicorer (MIC) stations.

GeoB-No.	Device/ No.	Area	Lat [°N]	Long [°]E	Water Depth [m]	Comment
11954	MIC-1	Pechori mound	41:58.964	41:07.541	1024	USBL; recovery 57 cm
11959	MIC-2	Batumi seep	41:57.533	41:17.568	840	USBL; recovery 58 cm
11960	MIC-3	Offshore Kobuleti	42:00.351	41:27.997	523	USBL; recovery 59 cm
11962	MIC-4	Batumi seep	41:57.548	41:17.435	838	USBL; 1 liner filled
11964	MIC-5	Batumi seep	41:57.414	41:17.360	847	USBL failed; 51 cm recovery
11965	MIC-6	Batumi seep	41:57.447	41:17.437	843	USBL failed; 27cm recovery
11966	MIC-7	Batumi seep	41:57.614	41:17.512	847	No USBL; 4 liners recovery
11968	MIC-8	Pechori mound	41:58.961	41:07.543	1022	USBL; device did not release; recovery 43 cm
11969	MIC-9	Pechori mound	41:58.962	41:07.541		USBL; recovery 41 cm
11970	MIC-10	Colkheti seep	41:58.069	41:06.191	1118	USBL; 3 liners full; recovery 34 cm
11976	MIC-11	Dvurechenskii MV	44.16.807	34:58.906	2052	No USBL; ship position; target ca. 12 meter sw'; recovery 46 cm
11977	MIC-12	Dvurechenskii MV	44:16.885	34:58.906	2052	No USBL; ship position; target ca. 12 meter sw'; recovery 52 cm
11978	MIC-13	Dvurechenskii MV	44.16.944	34:58.902	2050	No USBL; ship position; target ca. 12 meter sw'; recovery 56 cm
11979	MIC-14	Dvurechenskii MV	44.17.025	34:58.879	2048	No USBL; ship position; target ca. 12 meter sw'; recovery 40 cm
11983	MIC-15	Kerch Strait	44:39.607	35:42.519	747	USBL; liner full
11984	MIC-16	Kerch Strait	44:29.999	35:49.998	1341	USBL; liner full
11985	MIC-17	Kerch Strait	44:45.008	36:09.995	95	USBL; liner full
11986	MIC-18	Kerch Strait	44:46.007	36:01.998	173	USBL; liner full
11993	MIC-19	Vodyanitskiy MV	44:17.627	35:01.948	2067	USBL; liner full
11995	MIC-20	Dvurechenskii MV	44:17.034	34:58.951	1977	USBL; liner full
11997	MIC-21	Dvurechenskii MV	44:17.060	34:59.036	2050	USBL; liner full

USBL = Ultra-short base line (Posidonia underwater positioning system); recovery = core recovery

10.2 Sedimentological core descriptions

(A. Bahr, E. Kozlova)

During the R/V METEOR 72/3 cruise, three main areas (the Batumi seep area on the Georgian continental margin, the Sorokin Trough on the Ukrainian continental margin, and an area south of the Kerch Strait) were sampled by autoclave piston corers (DAPC I and II), multicorer (MUC), minicorer (MiC), gravity corer (GC), and pushcorer during the ROV dives (Tab. A 4 and Plate A 1 in the Appendix). Cores were mostly taken in places characterized by gas seepage or mud volcanic activity and were therefore dominated by gas-saturated sediments. According to the specific conditions, the sediments can be divided into those of hemipelagic or mud volcanic origin.

The reference station GeoB 11974, near the Batumi seep area, represents the late Pleistocene to Holocene hemipelagic sedimentation in the Black Sea (Figs. 93 and 94): At the top finely (sub-mm scale) laminated coccolith ooze (Unit 1 after Ross and Degens, 1974) overlays a finely (< mm) laminated sapropel (Unit 2 after Ross and Degens, 1974) with a series of aragonite laminae at the base of the otherwise dark sapropel (Fig. 95).

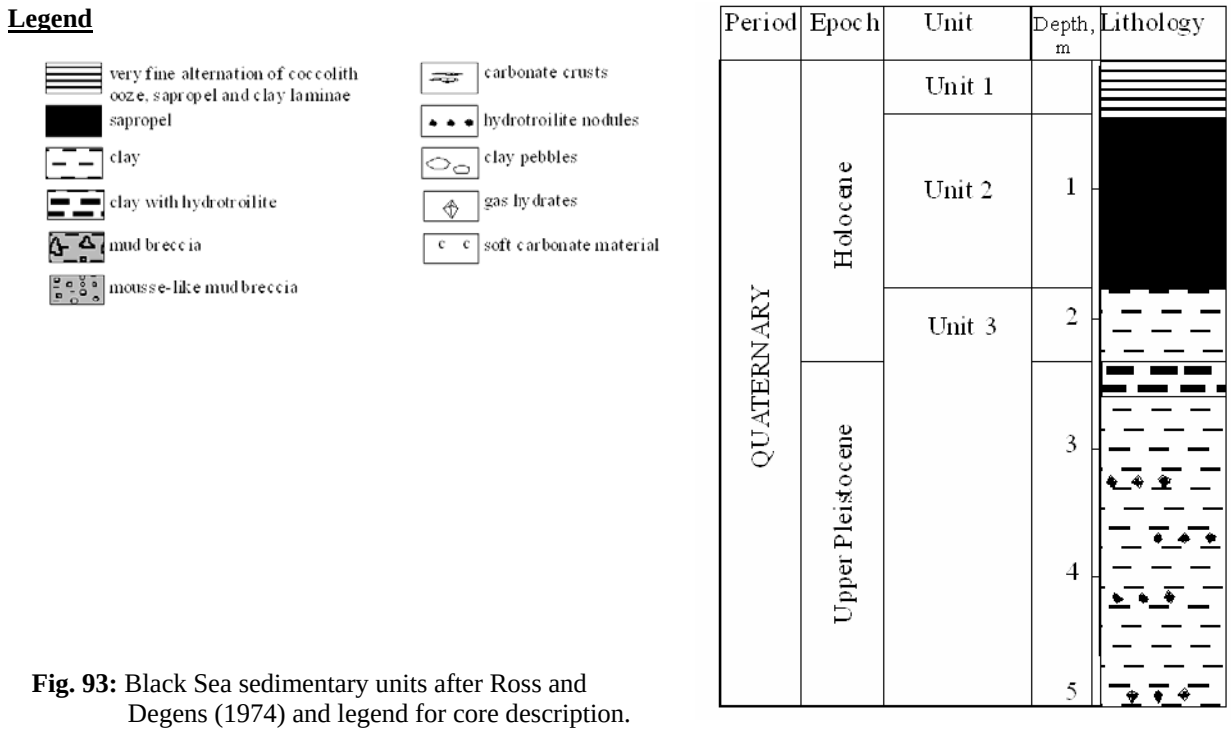

Fig. 93: Black Sea sedimentary units after Ross and Degens (1974) and legend for core description.

Both, Unit 1 and 2, are of marine origin and were deposited when the present anoxic conditions developed in the Black Sea basin some time after the inflow of marine water from the Mediterranean Sea started ca. 9.4 kyrs calBP (Major et al., 2006). The base of Unit 2 has an age of 8.0 kyrs calBP (Lamy et al., 2006), while the first coccolith layers of Unit 1 were deposited around 2.7 kyrs calBP (Jones and Gagnon, 1994). Below the sapropel, GeoB 11974 entirely consists of clayey mud belonging to Unit 3 after Ross and Degens (1974). These sediments were deposited in the lacustrine Black Sea during the last glacial to early Holocene. A characteristic feature of Unit 3 is a distinct black interval (in 301 to 364 cm core depth in GeoB 11974), which is rich in amorphous Fe-sulfides (Neretin et al., 2004), often termed „hydrotroilite“ (Limonov et al., 1994), that were precipitated as a result of the migration of a sulfidization front. The black color is lost within a few hours if the core is opened, since these Fe-sulfides are unstable and oxidate rapidly.

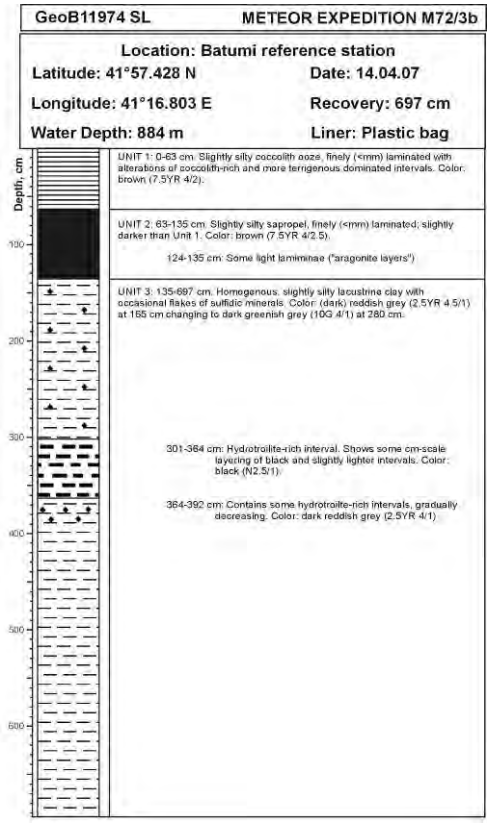

Fig. 94: Background sedimentation in the Batumi seep area (reference station GeoB 11974).

Mud volcanic deposits consist of matrix supported, gas-saturated mud breccia with rock clasts up to a few cm in diameter. On the basis of the matrix consistency and the matrix/ clasts ratio, the retrieved mud breccia was subdivided into two subgroups: the mousse-like mud breccia (very soupy and moussy mud with stiff pebbles of lithified clay) and the typical mud breccia (matrix supported, gas-saturated with numerous rock clasts). Sediments retrieved at Pechori and Colkheti seeps were also derived

from expelled mud with higher sand content than the common hemipelagic sediments, but lack gravel or rock-sized components.

In the Sorokin Trough and Batumi seep area, direct (visual) or indirect (sediment structure, gas content, CT-imaging) evidence for gas hydrates have been found. The dissociation of clathrates leaves characteristic sediment textures called „soupy“ (sediment with very high water content and completely destroyed primary structure) and „moussy“ (many small degassing vesicles, stiffer than the soupy sediments, primary structures are also almost totally destroyed). Especially in sediment cores with soupy sediment textures, the exact determinations of stratigraphic boundaries are difficult and might have an uncertainty of ±5 cm. In the following sections, a more detailed description of the sediments found at the various research areas will be given.

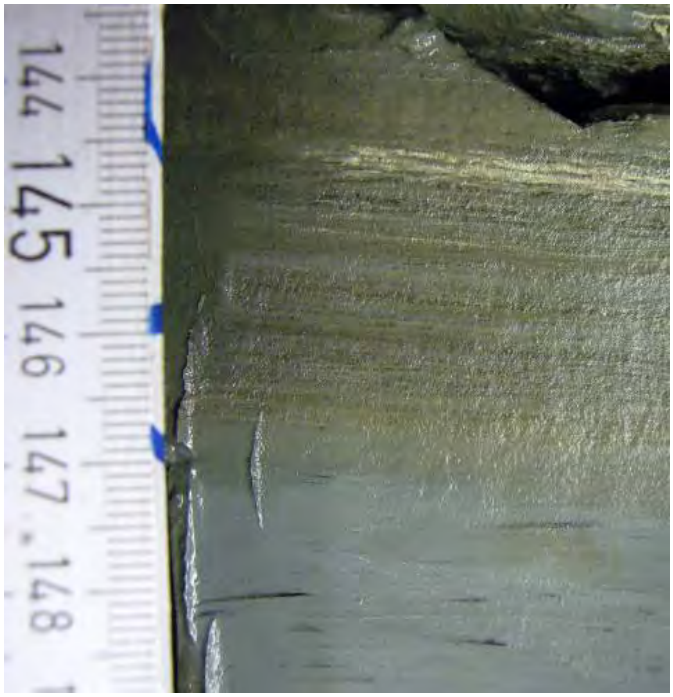

Fig. 95: Transition limnic (Unit 3, grey sediments) – marine (Unit 2, finely laminated sapropel) in GeoB 11974. The light laminae are aragonite layers typically found at the base of the sapropel.

10.2.1 Batumi Seep Area

The cores retrieved at the Batumi seep area (gravity cores: GeoB 11925, 11927, 11936, 11946, 11956, 11975; DAPCs: GeoB 11901, 11903, 11906, 11920, 11951, 11958, 11963; MUCs: GeoB 11905; MiCs: GeoB 11959, 11960, 11964, 11965) entirely consist of hemipelagic sediments without mudvolcanic deposits. The cores recovered show some variability regarding the thickness of the stratigraphic units and the occurrence of carbonates and gas hydrates (Fig. 96 shows a selection of some of the retrieved cores). The thickness of the marine Units 1 and 2 varies from ca. 75 (GeoB 11951) to more than 170 cm (GeoB 11963) or even 250 cm (GeoB 11920) indicating a variable sedimentation regime depending on the environmental conditions (morphology, local current regime, seep activity) of the respective location.

Gas hydrates were present in cores GeoB 11920, 11925, 11927, 11936, 11937, 11946, 11951, 11951, 11956, 11963 and 11975 from direct (visual observation) or indirect evidence (CT scanning, sediment texture). While in GeoB 11925, 11927, 11965, and 11975 gas hydrates are confined to Unit 3 and start to occur directly beneath the base of the sapropel. This distinction is not as obvious in the other hydrate-bearing cores. In GeoB 11936 they were detected by means of CT-scanning in the lacustrine deposits and lowermost sapropel, however a moussy texture was observed througout the entire core. The same holds true for GeoB 11936, 11963, and 11951, where the latter seems to have incorporated more hydrate within Unit 3 than in Unit 1 and 2 based on the soupy texture found in the lacustrine deposits. It seems therefore that the sediment in Unit 3 is more prone to the formation of massive clathrates than Unit 1 and 2, which maybe depends on the available pore space.

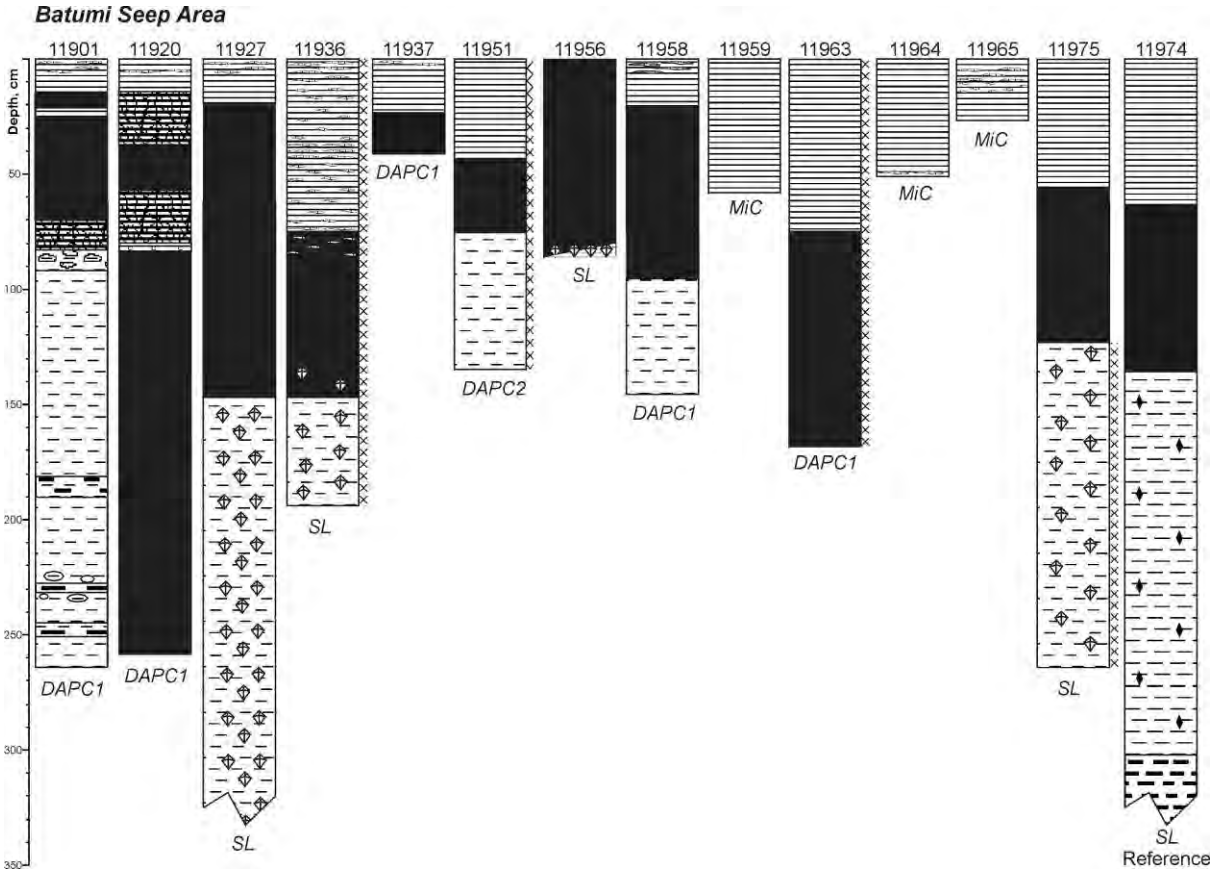

Fig. 96: Overview of some cores retrieved in the Batumi seep area. See Fig. 93 for legend.

Carbonates were retrieved in the upper sections (i.e. in the coccolith ooze layers) of GeoB cores 11901, 11920, 11925, 11927, 11936, 11937, 11958, and 11965. They consist of lithified plates of coccolith ooze laminae (Fig. 97), and were formed as a by-product of the anaerobic oxidation of methane, which increases alkalinity in the pore waters. Thicker and more rigid carbonate precipitates were only retrieved in the core catcher at the failed gravity core station GeoB 11967.

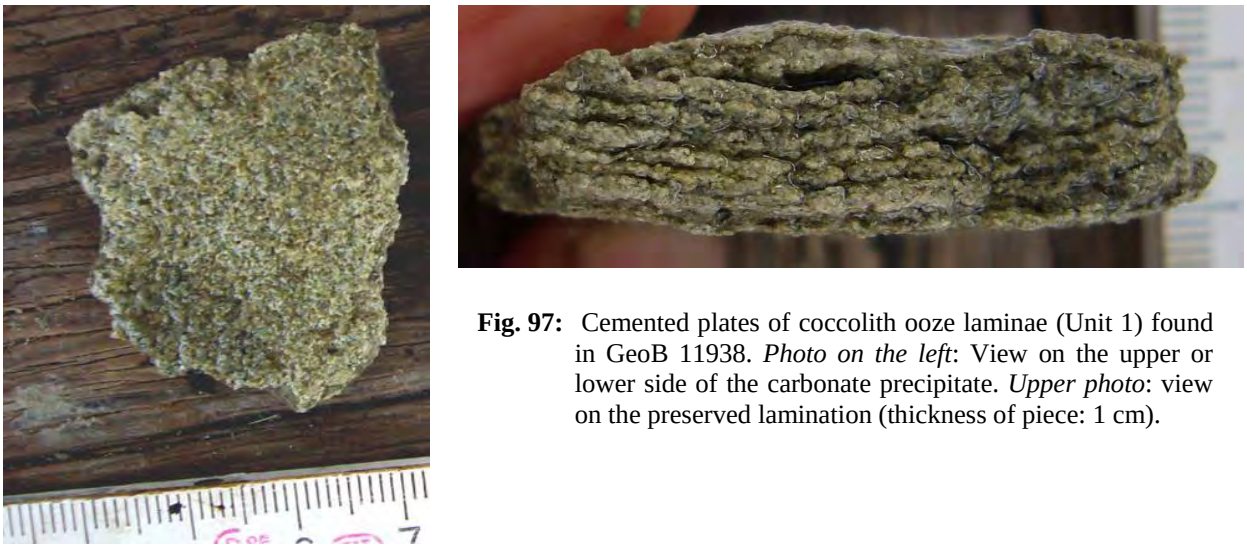

Fig. 97: Cemented plates of coccolith ooze laminae (Unit 1) found in GeoB 11938. *Photo on the left*: View on the upper or lower side of the carbonate precipitate. *Upper photo*: view on the preserved lamination (thickness of piece: 1 cm).

10.2.2 Iberia Mound

In the Iberia mound area, two cores (gravity core GeoB 11938 and MUC GeoB 11939) were successfully retrieved (Fig. 98). Both contained the common hemipelagic sediments expected in this area, coccolith ooze and sapropel (only in the longer gravity core). Thicknesses of Unit 1 and 2 are in the range of those observed in the Batumi seep area, indicating similar sedimentation rates in both areas. Carbonates were found in both cores as tabular, calcified layers of coccolith ooze within Unit 1 and more irregular tabular or nodular concretions in the sapropel. The gravity core sediments below 60 cm were oil-stained. Gas hydrates leaving a soupy texture were observed in core GeoB 11938 in the lower part of the coccolith ooze.

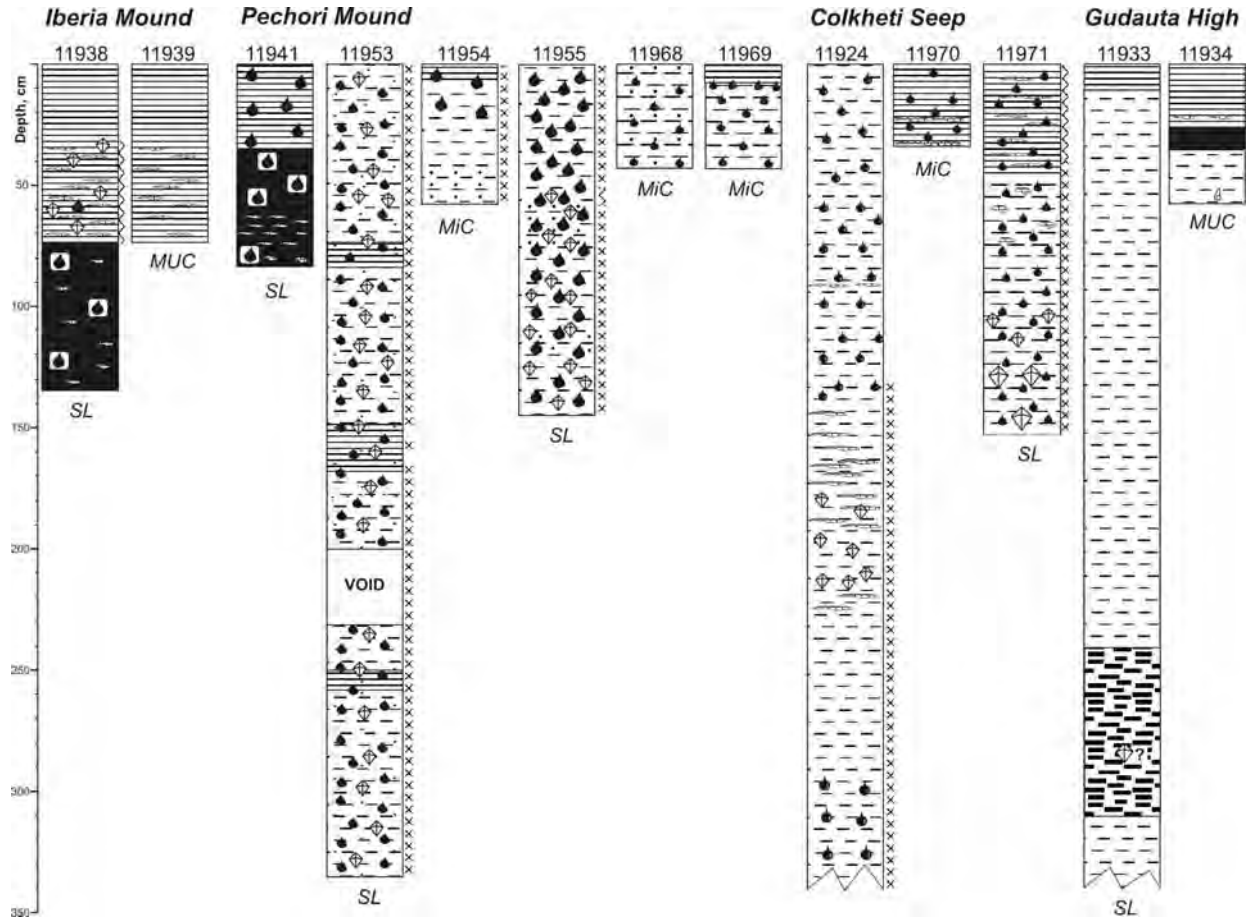

Fig. 98: Overview of cores retrieved at Iberia mound, Colkheti seep and on the Gudauta High. See Fig. 93 for legend. Oil-staining is shown by black drops.

10.2.3 Pechori Mound

The sediments retrieved from the Pechori mound (Fig. 98) are mostly different to those from Iberia mound. The dominant sediments are slightly sandy muds, which seem to be originated from expelled mud flows (mud breccia). With the exception of gravity core GeoB 11941, which consists of oil-stained Unit 1 and 2 with some carbonates in the sapropel, these mud breccia deposits occur at the other stations (gravity cores GeoB 11953, 11955; MiCs GeoB 11954, 11968, 11969). Badly preserved, laminated intervals of coccolith ooze or sapropel are found in GeoB 11953 and cover the tops of cores GeoB 11954 and 11969. They represent episodes where the mud-extrusion was not reaching the core position. All cores are oil-stained (Fig. 99), usually more oil is present in the more porous mud breccia deposits than in the less permeable laminated intervals.

In three cores, evidence for the presence of gas hydrates could be found (sampled throughout GeoB 11953 and the lower part of GeoB 11955, moussy texture in GeoB 11954). Carbonates were not retrieved in those cores dominated by mud breccia.

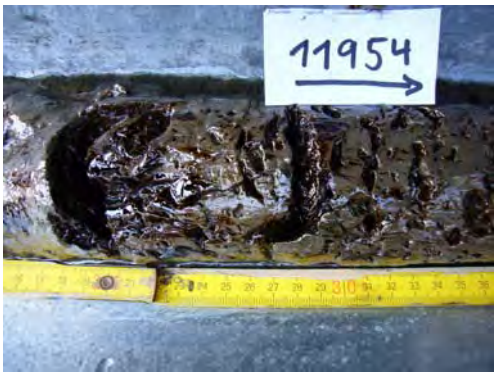

Fig. 99: Oil-stained sediment in a MiC (GeoB 11954) from Pechori mound.

10.2.4 Colkheti Seep

At the Colkheti seep, sediment was successfully recovered for three stations: a MiC (GeoB 11970) and two gravity cores (GeoB 11924, 11971) (Fig. 98). A thin coccolith ooze cover is present in GeoB 11970 and 11971. At station GeoB 11971, Unit 1 is underlain by homogeneous clay, which might represent the lacustrine Unit 3. Since this interval has been extremely disturbed due to decomposing hydrates (moussy texture) and extensive sampling, a secure assignement whether this section represents Unit 2 or 3 will be done with microfossil analyses onshore.

All cores were oil-stained and contained lithified coccolith ooze layers and slightly calcified irregular clayey concretions in Unit 1 (GeoB 11970, 11971) and further downcore (GeoB 11924, 11971). Fairly big gas hydrates were retrieved from the lower part of GeoB 11971, and between 130-344 cm in GeoB 11924, but soupy and moussy textures indicate that (finely dispersed) hydrates might have been present in a greater depth interval.

10.2.5 Gudauta High

Two cores, a MUC (GeoB 11934) and a gravity core (GeoB 11933), were retrieved from this newly discovered seepsite (Fig. 98). In both cores, the uppermost part is composed of coccolith ooze, which in GeoB 11934 is underlain by ca. 10 cm of sapropel, but, the dominating part is homogenous lacustrine clay. The thin or absent sapropel indicates that during or after the period of sapropel deposition an erosive regime prevailed, and sedimentation resumed only during the latest Holocene. Hydrates were potentially present in 280-290 cm core depth in GeoB 11933, where bubbling from dissociating clathrates was detectable after opening the core. In GeoB 11934, small plates of lithified coccolith ooze laminae have been found in Unit 1.

10.2.6 Sorokin Trough

The cores GeoB 11911, 11914, 11916, 11996 (DAPC), 11912 (MUC), 11976-11979, and 11995 (MiC) were sampled from the Dvurechenskii mud volcano in the Sorokin Trough (3 of these 8 cores are shown in Fig. 100). All cores are quite similar, they contain soupy or moussy mud breccia, in some cases covered by a thin veneer of coccolith ooze, and in others without any pelagic cover. This indicates a recent mud expulsion activity.

Rock clasts vary in size and shape (irregular as e.g. in GeoB 11911 or well-rounded as in the MiCs GeoB 11976 to 11979) up to 3 cm and are represented by dark grey clay (35%), brown clay (25%), grey silty clay (30%), light brown marlstone (9%), and coarse-grained sandstone (1 %), which is possibly Maikopian in age (Oligocene-Lower Miocene) (Fig. 101). Based on the moussy to soupy sediment, hydrates must have been present in the mud breccia deposits, but not in the coccolith ooze cover. However, hydrates have only been recovered from GeoB 11995 (MiC).

Five cores (GeoB 11913, 11980, 11981, 11990, 11992) have been taken from the Vodyanitskii mud volcano. Typical examples for sediments from this mud volcano are those recovered by GeoB 11913, mousse-like mud breccia overlain by a thin layer of recent soupy sediment. The upper part of the soupy grey clay contains big clasts of sapropel and plenty of carbonaceous material from very soft, white patches of recent carbonate to flat hard carbonate crusts up to 9 cm in size (Fig. 102). The core catcher contained gas hydrates, which were flat and triangular in shape, up to 3 cm in diameter. A similar carbonate-rich sediment layer at the core top was found in GeoB 11980 and 11981, consisting entirely of fine-grained mud breccia. In contrast GeoB 11990 and 11992 did not retrieve mud breccia, but solely homogenous clay (Unit 3?). The extent of soupy or moussy textures suggest that hydrates were present in high amounts mostly below ca. 30-40 cm core depth. In GeoB 11913 and 11990 clathrates were directly observed as relatively small chunks in the core catcher and/ or lowermost section of the respective cores.

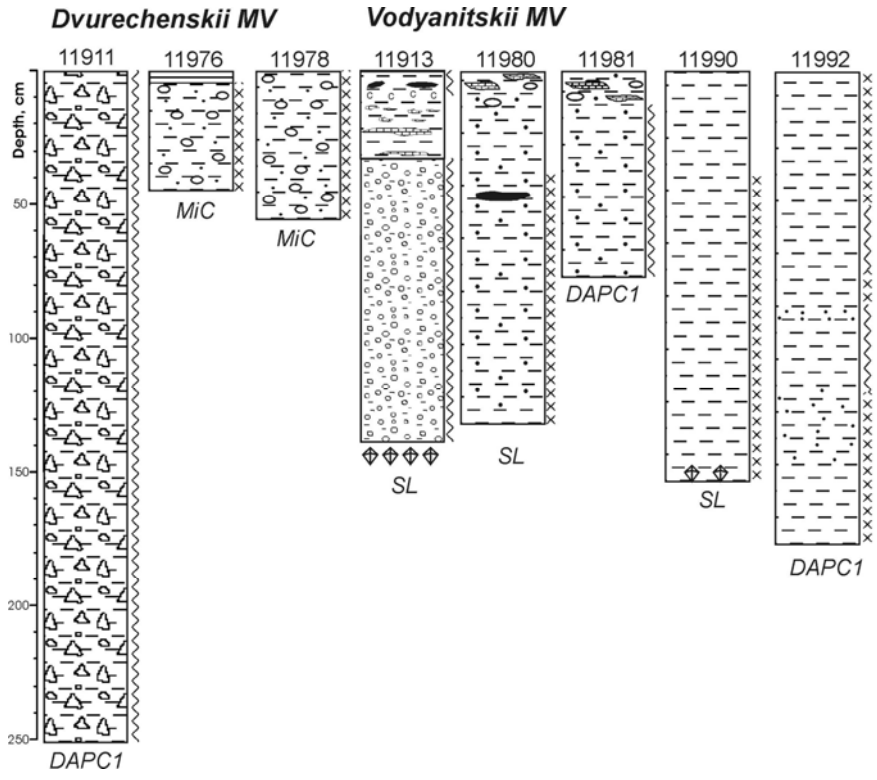

Fig. 100: Overview of cores sampled at the Dvurechenskii and Vodyanitskii mud volcanos in the Sorokin Trough. See Fig. 93 for legend.

Fig. 101: Three types of clasts found in a DAPC (GeoB 11911) from the Dvurechenskii mud volcano, probably derived from the Maikopian formation (Oligocene-Lower Miocene).

Fig. 102: Different types of carbonates recovered from the upper part of the gravity core GeoB 11913 from Vodyanitskii mud volcano.

10.2.7 Kerch Strait

East of the Crimean Peninsula, a total of 7 stations were sampled (Fig. 103). While GeoB 11983 - 11986 were taken for further analysis of terrigenous matter at non-seep sites along a transect over the outer shelf and slope, GeoB 11987-11989 were cored at a newly detected flare in ca. 900 m water depth. The deepest station of the slope transect, GeoB 11984 from 1341 m water depth, included coccolith ooze and lacustrine clay (Unit 3), but no sapropel. Since the coccolith ooze cover is relatively thin (17 cm), some erosion might have been taken place at this site. GeoB 11983 (747 m water depth) consists of undisturbed Unit 1 sediments. GeoB 11986 from 173 m, near the oxic/anoxic boundary, is also dominated by coccolith ooze, but here a gradual trend from (sub)oxic to the present fully anoxic conditions might be interpreted from the shift of relatively light colors at the base to the blackish coccolith ooze at the top. The MiC from 95 m water depth (GeoB 11985) is the only core retrieved during this cruise that has been taken in oxic waters. Here the clayey sediment is full of shells (disarticulated, but not fragmented) of juvenile *Dreissena spez.* (*D. polymorpha* or *bugensis*?) in a clayey matrix.

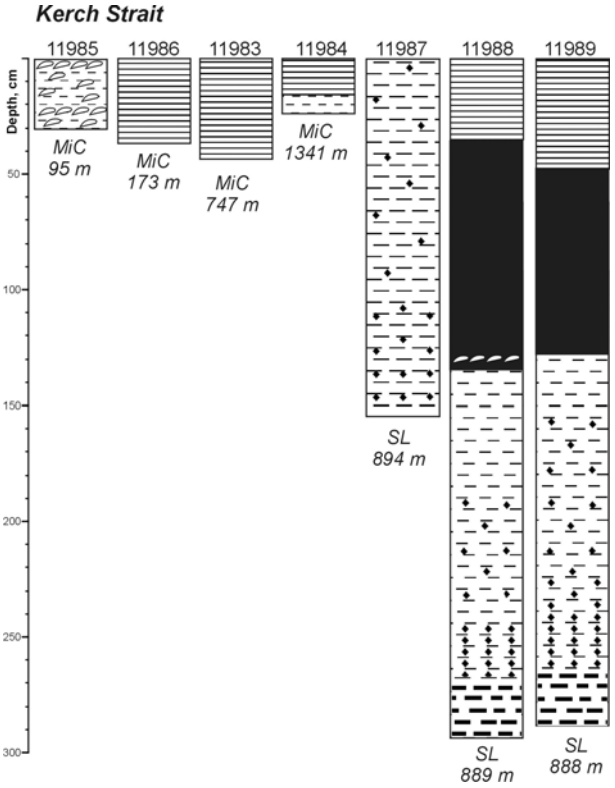

Fig. 103: Cores retrieved south of the Kerch Strait. See Fig. 93 for legend.

The three cores from the suspected flare site in 900 m water depth exhibit the common hemipelagic succession with some small gas-extension voids below 50 to 65 cm core depth, but no signs for the presence of gas hydrates. The lack of Unit 1 and 2 in GeoB 11987 is due to core-loss. An interesting aspect is the presence of two very thin layers at 118 and 120 cm core depth in GeoB 11988 covered with fragments of fragile mollusc shells smaller than 3 mm, ca. 3 cm above the base of the sapropel. These shell layers are missing in the well-preserved core GeoB 11989 taken virtually at the same position. Thus the sedimentary environment seems to be spatially very variable, as also indicated by the varying thickness of the sapropel.

10.3 Computerised tomography (CT) of gas-hydrate-bearing cores

(F. Abegg, K. Graef)

One of the tasks in gas hydrate research is the determination of its occurrences with depth and analyses of the gas hydrate fabric. Computerised Tomographic Imaging (CT) on board the research vessel, using X-ray beams to distinguish material of different densities, has three advantages fulfilling this task. Firstly, the cores can be investigated immediately upon recovery, no long storage or transportation is necessary. Secondly, the CT investigation of the cores allows a direct control of the core quality and content and makes an immediate decision about further investigations reasonable. And lastly, this method is non destructive and allows other investigations such as degassing, geochemical analyses, and sedimentological descriptions. Additionally, when using pressurised cores, the pressure vessels may be re-used after the analysis.

Gas hydrate is only stable at high pressure and low temperature. Standard coring devices such as gravity corers or multiple corers do not preserve either pressure or temperature during core recovery. For this reason, decomposition of gas hydrate begins when the sample leaves its stability field during recovery. The depth of this boundary depends on parameters such as gas composition, pore water salinity, and temperature. For the recovery of gas hydrate samples, autoclave sampling tools have been developed and applied (Chap. 9). Especially, the DAPC II has been designed to allow subsampling of the core while maintaining the pressure chain. The design of the pressure chambers allows computerised tomographic imaging of the materials inside. Primarily based on density contrasts between the materials, free gas, gas hydrate, sediment, and carbonate, the distribution and fabric of the constituents inside the core liner can be visualised. Besides investigations of cores for gas hydrate, they may also be investigated for sedimentary structures.

To avoid periodic port calls for using a CT in a local hospital we used a mobile CT unit. The CT scanner, a General Electric (GE) Pro Speed SX Power, was mounted in a double axial trailer of 13 m length. The trailer was 4 m high, 2.5 m wide and has a weight of 22 tons. The trailer was sent from Germany to Trabzon by truck and then craned on the strengthened deck of R/V METEOR (Figs. 104 and 105). The GE scanner was a single slice system with a hard disk capacity of approx. 3500 slices. Because the expected number of slices for the cruise exceeded this limit, a network was installed to externally save the data. The power requirement of the scanner was 400V, 125 Amp, and 50 Hz which could be served by the ship. The scanner was able to scan slices with 1, 2, 3, 5 and 10 mm thickness. We mostly used 1 mm slices with a 512 x 512 data matrix to achieve a very high resolution. The table load was limited to 180 kg.

Fig. 104: CT-Trailer on deck of R/V METEOR.

Fig. 105: Lab-transfer-chamber inside the CT scanner.

Sampling of gas hydrates has been done mostly using the gravity corer with pre-cut and taped PVC-liner. Upon recovery, the liner segments were closed with caps and immediately frozen in liquid nitrogen. The time from leaving the gas hydrate stability field during core recovery until placing all core segments in liquid nitrogen was measured to be less then 25 minutes. The second type of sampling tool was the newly developed DAPC II. For an extended description of the tool see Chap. 9. Additionally, some subsamples from gravity cores used with plastic hoses and a background core were investigated. All scanned samples are listed in Table 17.

Table 17: List of scanned samples. Abbreviations: GC = gravity corer, DAPC = dynamic autoclave piston corer.

GeoB	Instrument	Area	Subsample No.	No. of slices	Slice thickness	Description
11918	DAPC-8 (II)	Batumi seep	-	5	1 mm	Test
11925	GC-4	Batumi seep	increment	83	1 mm	
11927	GC-6	Batumi seep	increment	157	1 mm	frozen, GH
11936-1	GC-8	Batumi seep	no. 1	188	1 mm	frozen segm., GH
11936-2			no. 2	520	1 mm	frozen segm., GH
11936-3			no. 3	539	1 mm	frozen segm.
11936-4			no. 4	529	1 mm	frozen segm.
11936-5			no. 5	192	1 mm	frozen segm.
11936-1-A	GC-8	Batumi seep	increment	100	1 mm	frozen, GH
11944	DAPC-13 (II)	Batumi seep	transfer test	55	1 mm	non pressurized
11946-1	GC-13	Batumi seep	no. 1	420	1 mm	frozen segm., GH
11946-2			no. 2	495	1 mm	frozen segm., GH
11946-3			no. 3	495	1 mm	frozen segm., GH
11946-4			no. 4	481	1 mm	frozen segm., GH
11946-5			no. 5	492	1 mm	frozen segm.
11946-6			no. 6	500	1 mm	frozen segm.

Table 17, continuation: List of scanned samples. Abbreviations: GC = gravity corer, DAPC = dynamic autoclave piston Corer.

GeoB	Instrument	Area	Subsample No.	No. of slices	Slice thickness	Description
11949-A	GC-14	Batumi seep	increment 1	127	1 mm	frozen, GH
11949-B			increment 2	128	1 mm	frozen, GH
11949-C			increment 3	73	1 mm	frozen, GH
11949-D			increment 4	71	1 mm	frozen, GH
11949-E			increment 5	66	1 mm	frozen, GH
11953-1	GC-16	Pechori mound	no. 1	172	2 mm	frozen segm., GH
11953-2			no. 2	222	2 mm	frozen segm., GH
11953-3			no. 3	125	2 mm	frozen segm., GH
11953-4			no. 4	250	2 mm	frozen segm., GH
11953-5			no. 5	249	2 mm	frozen segm., GH
11953-6			no. 6	244	2 mm	frozen segm., GH
11953-7			no. 7	91	2 mm	frozen segm., GH
11956-1	GC-18	Batumi seep	no. 1	199	2 mm	frozen segm., GH
11956-2			no. 2	181	2 mm	frozen segm.
11956-3			no. 3	56		frozen segm.
11956-1			no.1	106	2+3 mm	test scanns
11957	GC-19	Batumi, background	12 subsamples	overviews	various	scanned for sedimentology
11971	GC-21	Colkheti mound	increment	147	1 mm	frozen, GH
11973	DAPC-18 (II)	Batumi seep		4	1 mm	test
11975-1	GC-23	Batumi seep	increment 1	83	1 mm	frozen, GH
11975-1B			increment 2	210	1 mm	frozen, GH
11980-1	GC-24	Vodyanitskiy MV	no. 1	469	1 mm	frozen segm.
11980-2			no. 2	519	1 mm	frozen segm.
11980-3			no. 3	268	1 mm	frozen segm.
11994-1	DAPC-22 (II)	Dvurechenskii MV	no. 1	596	1 mm	pressurized, gas
11994-2			no. 2	200	2 mm	pressurized, gas

The mobile CT unit proved to work reliably within certain limits. Due to the age of the scanning system and limitations set by the software, we could only scan segments of up to 50 cm length. When the cores exceeded this length they had to be replaced. The second limit was the sensitivity of the scanning system to vibrations caused by the ships propulsion system. When the ships speed exceeded 6 knots, the scanner stopped. Wave driven failures have not been noticed due to the very calm conditions during the cruise. Maximum wind was measured to be 8 m/s with wave heights up to 1.5 m, which did not constrict scanning. The last limitation we noticed during the cruise was the heating of the X-ray tube. Due to the large amount of slices, many breaks had to be included. which resulted in approx. 3 hours of time needed for scanning one 50 cm core segments in 1 mm slices.

First results of the gas hydrate-bearing cores are discussed in Chap. 10.4.1. Here we show first results of the pressurized DAPC II sub-cores of GeoB 11994 taken at the Dvurechenskii mud volcano. The first section (GeoB 11994-1) contains the lowermost part of the core taken with the DAPC II. The left image in Fig. 106 represents the place where the core catcher was removed. The core section appears disturbed for a length of 6 cm. Above this, the sediment looks quite undisturbed although it still does not completely fill the liner. Interestingly, the sediment contains a lot of gas bubbles of various sizes (right image in Fig. 106).

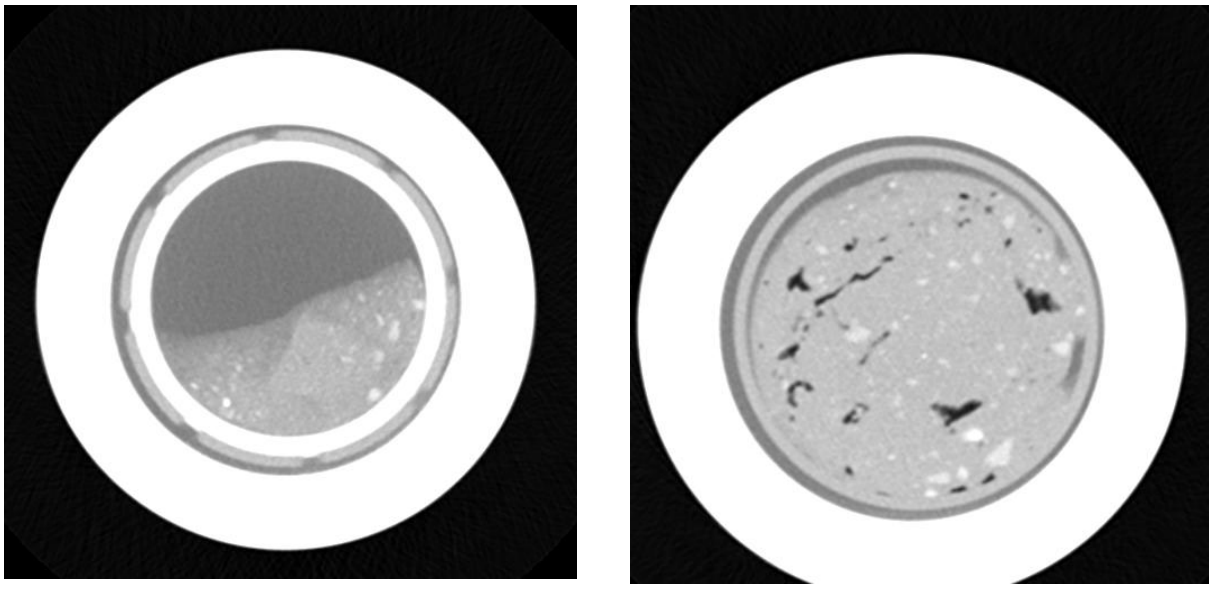

Fig. 106: *Left*: Thick white ring outside: pressure barrel, dark grey = water, light grey ring with interruptions = PVC liner, thin white ring inside = piston holding the liner, medium grey = slumped sediment. *Right*: black dots and lines = free gas inside the sediment.

10.4 Visualization, sampling, and on-board analyses of gas hydrates – Preliminary results

(F. Abegg, S.A. Klapp, T. Pape)

During M72/3, numerous gas hydrate bearing samples and gas hydrate pieces were taken from gravity cores for computer tomography scanning and gas chemical analyses on board (see below), and for shore-based examinations.

10.4.1 Gas hydrate distribution and fabrics analysed by computerised tomographic imaging

Due to the dissociation of gas hydrate at atmospheric temperature and pressure, the cores which were taken for the investigation of the distribution and structure of gas hydrate have been frozen upon recovery as described in Chap. 10.1. Most of those cores and most of the subsampled increments of gas hydrates taken during the cruise originate from the Batumi seep site (Tab. 17; Chap. 10.3). The detailed scanning of the frozen core segments gives a first impression of the core quality and reveals the gas hydrate content and fabric within the sediment.

The first core taken for CT-investigation at the Batumi seep site was core GeoB11936. The core had a length of 196 cm with gas hydrates detected deeper than 125 cm below seafloor (cm bsf). They seem to form irregular coatings of gas filled fractures and also contain free gas themselves (Fig. 107). The bottom most part of the core was disturbed and contained chunks of gas hydrate. Presumably, the gravity corer stopped penetration here due to massive gas hydrates.

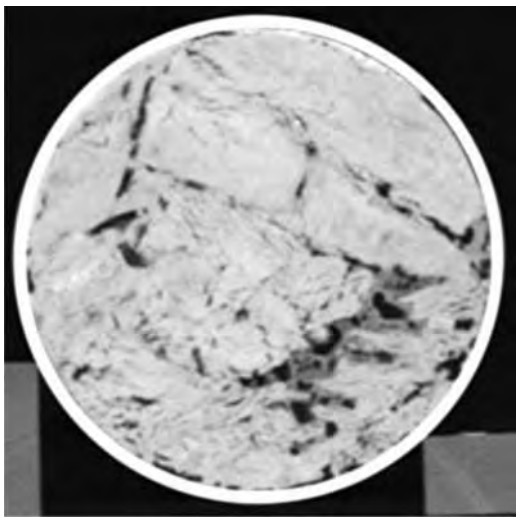

Fig. 107: Slice from core GeoB 11936. Black: air/gas, dark grey: gas hydrate, light grey: sediment.

The second core from the Batumi seep site was GeoB 11946 (Fig. 108). This is the longest core with a length of 289 cm. Gas hydrates were found in this core deeper than116 cm bsf. The gas hydrate extends from that depth downwards with a layer of 12 cm thickness. Below this layer, it contains an extended network of veinlets and veins. The massive gas hydrate encloses many gas filled fractures and an uncounted number of smaller bubbles. Above the massive hydrate, many gas filled fractures appear in the sediment.

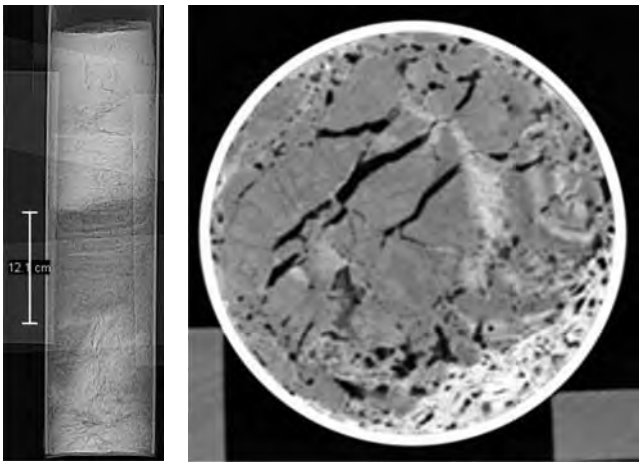

Fig. 108: *Left:* overview of core GeoB 11946. The location of the massive gas hydrate layer is indicated on the left side. *Right*: single slice from the massive hydrate showing fractures and bubbles inside.

The core GeoB 11956 only recovered a core length of 87 cm (Fig. 109). We found gas hydrate in the lowermost part of the deepest section, below 79 cm bsf. At the top of the gas hydrate layer, a piece of wood was found. Above, we noticed a large amount of gas-filled fractures. Due to the fact that this core was not pressurized, it is not quite clear whether these fractures are generated by dissociation of gas hydrate. We could not detect such large fractures in other cores and dissociation mostly starts at the outer margin of the cores and is identified by the generation of many small bubbles. These large fractures may also be caused by free gas, which under *in situ* conditions only claims very small open space and due to the pressure reduction it appears in the scans with this large size.

Fig. 109: Cross section of core GeoB 11956. At the bottom the gas hydrate is visible by lower density. Above the network of gas filled fractures in black begins and spans until the top of the core segment.

Further cores have been taken at the Pechori mound and at the Vodyanitskii mud volcano (VMV). The core from the Pechori mound overpenetrated so that the surface was lost. The recovered length was 270 cm with gas hydrate distributed over the whole core. The main hydrate fabrics found in this core are again networks of veins and veinlets. The core from the VMV does not contain any gas hydrate, but only shows small fractures caused by degassing.

10.4.2 Sampling strategy of gas hydrate specimen

Most gas hydrates were sampled from plastic hose liners, which are easily opened. In addition, a few gas hydrate specimen were also subsampled from PVC liners. For on-board gas chemical investigations, most samples were taken from the core catchers. Table 18 lists the gas hydrate samples taken on Leg M72/3. For on-shore analyses much attention was paid to adequate long-term storage, since gas hydrates rapidly decompose when brought outside the gas hydrate stability field. Therefore, the samples were immediately

transferred into liquid nitrogen dewars, which assures long-term preservation of the samples due to deep-freezing. Further, only relatively large pieces of several centimetres in diameter were taken, since the risk of gas hydrate destabilization during recovery and transfer into liquid nitrogen increases with decreasing size. In addition, some comparatively large gas hydrate samples of several centimetres size were recovered from PVC liner segments after they were visualized by computerized X-ray tomography (CT; Chap. 10.3; Table 17). The respective liner segments were opened in a cold temperature laboratory (4 °C – dry air) and the gas hydrate pieces were transferred into liquid nitrogen for long-term storage. All stored gas hydrate samples were transported to the University of Bremen. Further investigations include phase analyses, several experiments on synchrotron beam lines, and controlled destabilization for gas chemical analysis as well as stable isotope ($^{13}C/^{12}C$, D/H) investigations.

Table 18: Gas hydrate samples for shore based analyses.

GeoB No.	Area	Lat [°N]	Long [°E]	Water depth [m]	CT
11913	Vodyanitskii MV	44:17.621	35:01.946	2048	-
11923	Colkheti seep	41:58.120	41:06.250	1088	-
11924	Colkheti seep	41:58.068	41:06.195	1056	-
11971	Colkheti seep	41:58.069	41:06.199	1124	+
11925	Batumi seep	41.57.431	41:17.347	844	+
11927	Batumi seep	41:57.410	41:17.324	856	+
11936	Batumi seep	41:57.563	41:17.430	844	+
11946	Batumi seep	41:57.532	41:17.582	842	+
11949	Batumi seep	41:57.550	41:17.175	842	+
11956	Batumi seep	41:57.450	41:17.436	843	+
11975	Batumi seep	41:57.528	41:17.588	844	+
11938	Iberia mound	41:52.340	41:10.036	982	-
11953	Pechori mound	41:58.958	41:07.543	1015	+
11953	Pechori mound	41:58.958	41:07.543	1015	+
11955	Pechori mound	41:58.963	41:07.540	1012	-

CT = Computerized tomography (+ = analysed; - = not analysed).
MV = Mud volcano

10.4.3 Gas chemical compositions

13 gas hydrate pieces sampled by conventional gravity coring at gas and oil seep sites offshore Georgia as well as at the Vodyanitskii mud volcano (VMV) were analysed for the chemical composition of hydrate-bound volatiles. Immediately upon recovery, the pieces were thoroughly cleaned with purified ice-cooled water, filled into gas tight syringes, and stored at room temperature for dissolution. The released gases were transferred into glass vials and subsamples were taken from head space for compositional analyses.

For all samples, methane was found to be the prevailing gas hydrate-bound low-molecular-weight hydrocarbon (LMWHC, C_1 through C_6), constituting between 97.01 to 99.97 mol-% (Fig. 110). However, considerable differences in the total amounts of C_{2+}-components were observed for the samples from different sites. For example, ethane and propane, which were present in all samples, strongly varied in their relative abundances. While non-oil seep associated gas hydrates (e.g. Batumi seep area, VMV) were characterized by a clear ethane over propane preference (C_2/C_3 ratio = 13 to 31), much higher relative abundances of propane were found for the oil-associated samples (C_2/C_3 ratio = 1.6 to 4.6). For one sample from the Colkheti seep (GeoB 11923-1), propane was even more abundant than ethane (C_2/C_3 ratio = 0.6). Furthermore, small amounts of *i*-butane and *n*-butane were found in gas hydrates associated with the oil-seeps (Iberia mound, Colkheti seep, Pechori mound) and the VMV, but were absent in samples from the Batumi seep area. Interestingly, for all samples carbon dioxide was found in higher proportions than ethane.

Onshore, comprehensive chemical analysis of gases released from gas hydrate pieces will be carried out subsequent to investigations on the hydrate crystal structures (see also Chap. 10.4.4) in order to clarify the relationships between crystallographic properties and encaged volatiles in gas hydrates from the Black Sea.

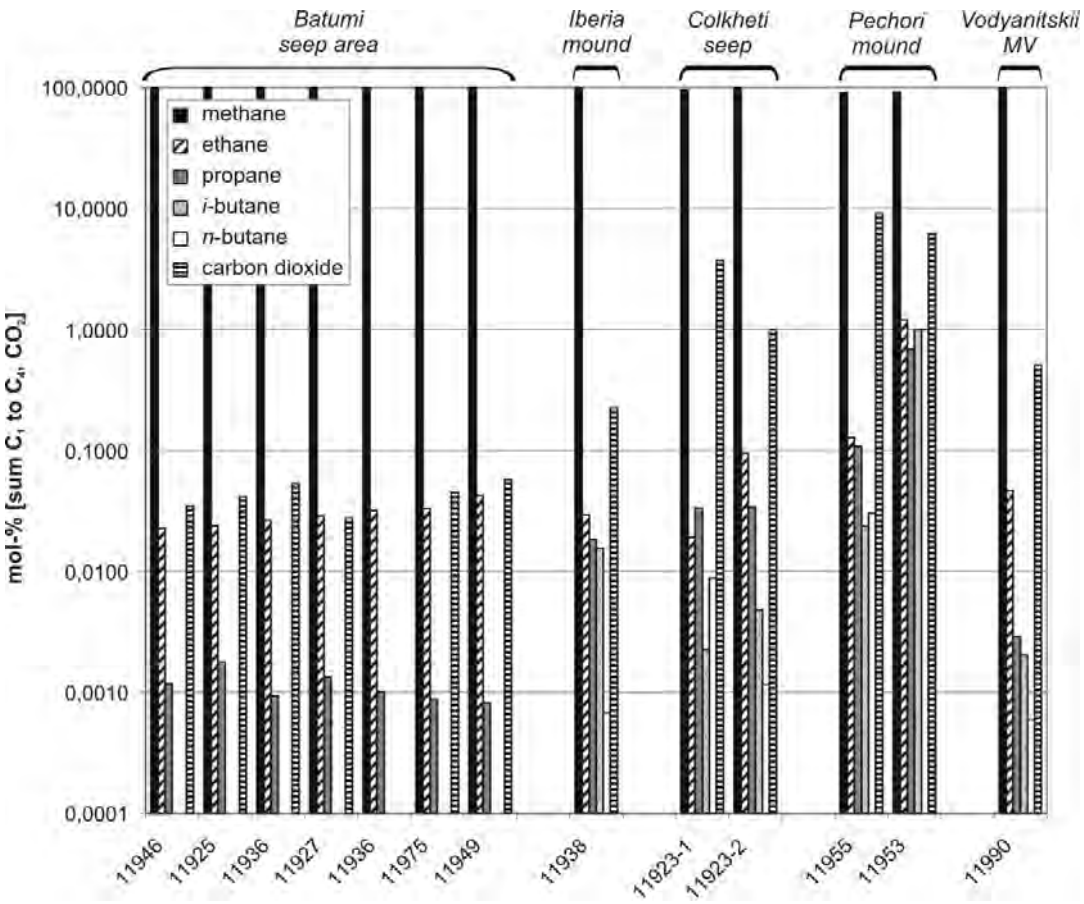

Fig. 110: Relative abundances of C_1 to C_4 hydrocarbons and carbon dioxide (Σ C_1 to C_4 and CO_2) in gas hydrate pieces sampled and dissociated on board during M72/3. Note the logarithmic scale. Numbers refer to cruise station (GeoB) numbers.

10.4.4 Theoretical stability of gas hydrates at the working areas

Due to thermodynamic prerequisites, gas hydrates demand cold temperatures and high pressures to form and be stable. Also, high salinity in hydrate-forming water negatively affects hydrate formation. Commonly, the bottom water temperature in the Black Sea is about 9 °C and the salinity is about 2.0-2.1 % of dissolved NaCl. Because of these specific geochemical parameters in the Black Sea, gas hydrates are generally not observed at depths shallower than 720 m water depth, which is equivalent to about 72 bars. In the sediment, methane (CH_4) has been identified as the major hydrate forming gas (Chap. 10.4.3). However, local differences in the hydrate formation conditions and in gas composition are significant and thus affect gas hydrate stability. Based on the local geochemical parameters, hypothetic stabilities of different gas hydrate crystallographic structures can be calculated (Fig. 111) by using commercially available software packages. For instance, at the Dvurechenskii mud volcano (DMV), high salinar fluids (Chap. 11) in shallow sediment depths shift the threshold of hydrate formation to much lower temperatures.

Another important factor for gas hydrate stabilities is their crystallographic structure (e.g. Sloan, 1998). Gas hydrate structure I is the dominant structure at pressures and temperatures in question for the M72/3 working areas, as revealed from structure analysis of gas hydrate samples retrieved offshore Georgia during TTR-15 (unpublished results). Methane is the most frequent gas (Chap. 12) and also is the major structure I former. However, if hydrocarbons of higher molecular weight (C_{2+}) are available and incorporated in the hydrate cages, gas hydrates of the structure type II are more stable and form gas hydrates.

At oil seeps offshore Georgia, pore water salinity is much lower than at the DMV (roughly 350 mmol; Chap.11). Although CH_4 concentrations are generally higher than 99 mol-% (of C_1 to C_6 hydrocarbons), C_{2+} hydrocarbons are more abundant than e.g. at the DMV and are incorporated in the gas hydrates (Chap. 10.4.3). Propane (C_3H_8), *i*- and *n*-butane (C_4H_{10}) are not incorporated in structure-I-gas hydrates, but instead, induce the formation of gas hydrate structure type II. Due to low concentrations of such gases in the hydrates, pure structure-II-gas hydrates are very unlikely, and instead mixed hydrate structures are more probable.

Fig. 111 depicts the stability curves (calculated on basis of P/T conditions, salinities, and gas hydrate gas chemical compositions measured during M72/3) for gas hydrate samples from the Colkheti oil seep, the Batumi seep area, and the DMV. Intersections of the water column temperature curves with the stability curves yielded for the different working areas point to the upper limit of gas hydrate stability at a given site. For example, the stability curve calculated for structure II gas hydrates at the Colkheti oil seep (about 1120 m water depth) based on their gas chemical composition demonstrates that at this site pure structure II gas hydrate might be stable in water depths below about 570 m (corresponding to about 57 bars). At the Batumi seep area (about 840 m water depths), structure-II hydrate could hardly occur at the P/T conditions prevailing, since the hydrostatic pressure is too low for the formation of structure II gas hydrates as sourced by the specific gas composition (Chap. 10.4.3). Instead, structure-I gas hydrate is the more stable hydrate structure.

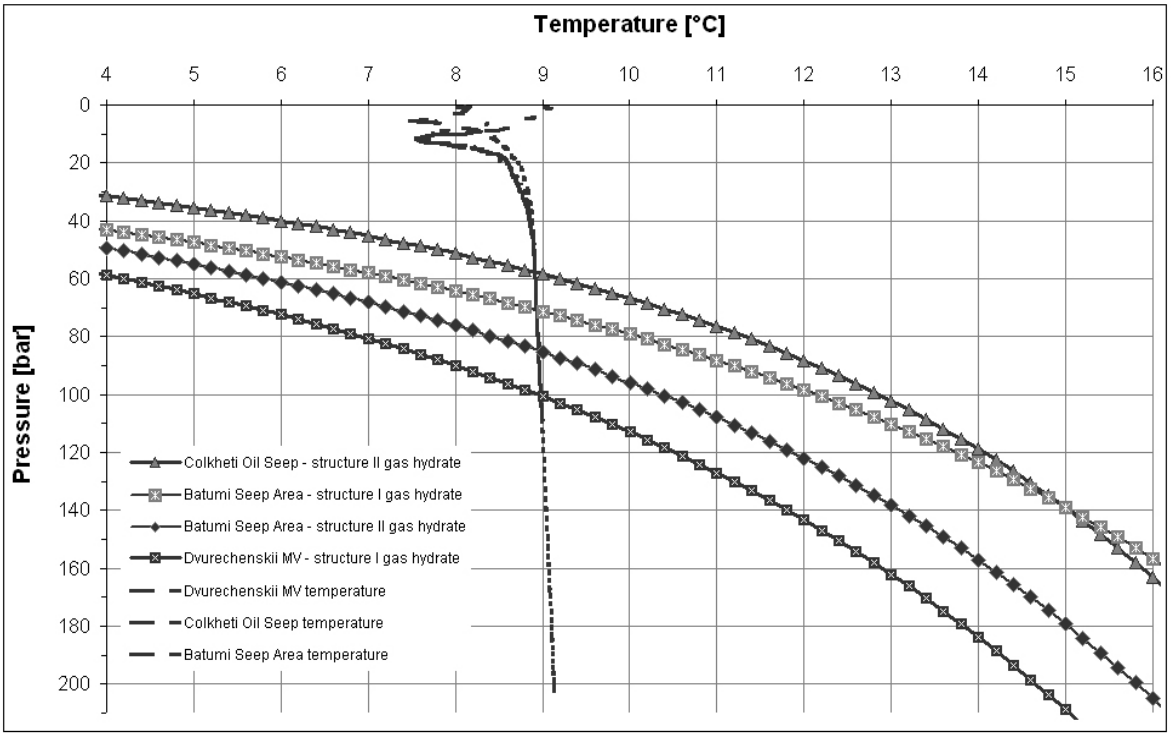

Fig. 111:
Calculated gas hydrate stability curves at different methane-enriched sites in the Black Sea. Gas compositions of the hydrate forming gases were determined for a DAPC-core (DAPC-7, GeoB 11916; Dvurechenskii MV) and gas bubble sampler (Colkheti seep, GeoB 11902-1; Batumi seep, GeoB 11904-16). Pressure and temperature were taken from CTD recording during ROV Dive 160 (GeoB 11915) and salinities were calculated from push core sampling during Dive 159 (GeoB 11910) and Dive 160 (GeoB 11915). The data were modelled using the Heriot-Watt-Hydrate (HWHYD) software and suggest for example a dissociation pressure of ca. 100 bar (1000 m water depth) at the Dvurechenskii mud volcano.

At the Batumi seep area (about 840 m water depths), structure-II hydrate could hardly occur at the P/T conditions prevailing, since the hydrostatic pressure is too low for the formation of structure II gas hydrates as sourced by the specific gas composition (Chap. 10.4.3). Instead, structure-I gas hydrate is the more stable hydrate structure.

At the DMV, structure I gas hydrate is only stable below 1000 m water depth. Hence, gas hydrates occurred at the locations visited during the M72/3 cruise in the Black Sea under diverse stability conditions. This implies that gas hydrates cannot be expected at the same water depths at any location in the Black Sea. Since the stability of gas hydrates is affected by the gas hydrate structure or structure mixtures, which in turn are the results of the site-specific environmental parameters, shore-based phase analyses of recovered gas hydrates will reveal the proportions of co-occurring gas hydrate structures.

11 Pore water geochemistry

(K. Wallmann, A. Bleyer, D. Karaca, V. Mavromatis, B. Domeyer, R. Surberg, M. Bausch, F. Scholz)

11.1 Introduction

Pore water was separated from sediments by squeezing at 2-4 bars and 4-6°C. The pressure was applied from an argon gas bottle and the pore water was passed through 0.2 µm membrane filters. Additional sediment subsamples were taken for the determination of methane concentrations and physical properties. The pore water was analyzed for dissolved nutrients (ammonia, silicate, phosphate) and total dissolved sulfide applying standard photometric procedures. Dissolved chloride and total alkalinity were determined via titration using $AgNO_3$ and HCl solutions. A detailed description of the applied methods can be found at the IFM-GEOMAR homepage.

Sediments were retrieved via push coring (PC) during ROV dives and by the Dynamic Autoclave Piston Corers (DAPC), the multicorer (MUC), the minicorer (MIC), and the gravity corer (GC) at stations listed in Tab.19.

Table 19: Sediment cores taken for pore water analysis. BS = Batumi seep area, DMV = Dvurechenskii mud volcano, VMV = Vodyanitskii mud volcano, CS = Colkheti seep, GH = Gudauta High, IM = Iberia mound, PM = Pechori mound, KS = Kerch Strait

GeoB	St. No.	Area	Date	Lat. [°N]	Long. [°E]	Water Depth [m]	Recovery/ Remark
11901	DAPC-1	BS	19.3.07	41:57.410	41:17.344	851	14 samples
11903	DAPC-2	BS	21.3.07	41:57.472	41:17.266	850	5 samples
11904	ROV-2	BS	21.3.07				
11904-13	PC			41:57.529	41:17.270	835	No. 47, 20 cm from large bubble hole, 8 samples
11904-15	PC			41:57.541	41:17.413	833	No. 46, 2 cm from small bubble hole, 13 samples
11905-2	MUC-2	Ref. station next to BS	22.3.07	41:57.432	41:16.798	877	24 samples, no bottom water
11906	DAPC-3	BS	22.3.07	41:57.465	41:17.270	843	5 samples
11907	ROV-3	BS	22.3.07				
11907-7	PC			41:57.542	41:17.413	833	No. 38, 2 cm from small bubble hole, 13 samples
11907-8	PC			41:57.543	41:17.413	833	No. 46, 20 cm from small bubble hole, 13 samples
11907-9	PC			41:57.545	41:17.413	833	No. 67, 60 cm from small bubble hole, 8 samples
11907-10	PC			41:57.542	41:17.413	833	No. 68, 100 cm from small bubble hole, 11 samples
11910	ROV-5	DMV	25.3.07			~2050	
11910-3	PC			44:16.929	34:59.232		No. 16, rim of DMV, 12 samples
11910-6	PC			44:16.976	34:59.084		No. 50/60, 9 samples
11910-8	PC			44:17.006	34:58.974		No. 47, 9 samples
11910-11	PC			44:17.029	34:58.880		No. 48, center of DMV, core lost during retrieval
11911	DAPC-5	DMV	26.3.07	44:16.972	34:59.215	2058	14 samples
11912	MUC-3	DMV	26.3.07	44:17.015	34:58.885	2053	Center of DMV, 15 samples
11913	GC-1	VMV	26.3.07	44:17.621	35:01.946	2048	Center of VMV, 7 samples
11914	DAPC-6	DMV	27.3.07	44:16.987	34:59.097	2058	14 samples
11915	ROV-6	DMV	27.3.07			~2050	
11915-8	PC			44:17.023	34:58.610		No. 47, bacterial mat, 9 samples
11915-12	PC			44:17.092	34:58.676		No. 67, rim of DMV, 10 samples
11915-15	PC			44:17.061	34:58.760		No. 46, 11 samples
11915-16	PC			44:17.007	34:58.896		No. 54, center of DMV, 9 samples
11915-23	PC			44:17.051	34:58.836		No. 26, 10 samples

Table 19, continuation: Sediment cores taken for pore water analysis.

GeoB	St. No.	Area	Date	Lat. [°N]	Long. [°E]	Water Depth [m]	Recovery/ Remark
11916	DAPC-7	DMV	28.3.07	44:16.896	34:58.789	2057	12 samples
11917	ROV-7		28.3.07				
11917-3	PC	VMV		44:17.658	35:01.992	2032	No. 38, next to bubble site, 8
11918	DAPC-8	BS	30.3.07	41:57.547	41:17.427	840	12 samples
11920	DAPC-9	BS	31.3.07	41:57.454	41:17.545	844	13 samples
11924	GC-3	CS	01.4.07	41:58.068	41:06.195	1056	Oil-bearing sediments, 12 samples
11933	GC-7	GH	06.4.07	42:40.262	40:22.631	690	14 samples
11934	MUC-8	GH	06.4.07	42:40.260	40:22.678	701	28 samples, no bottomwater
11937	DAPC-12	BS	07.4.07	41:57.489	41:17.462	842	3 samples
11938	GC-9	IM	07.4.07	41:52.340	41:10.036	982	10 samples, gashydrates
11939	MUC-9	IM	07.4.07	41:52.739	41:10.025	989	23 samples
11941	GC-10	PM	08.4.07	41:58.962	41:02.404	1014	7 samples
11951	DAPC-14	BS	09.4.07	41:57.546	41:17.431	840	11 samples
11954	MIC-1	PM	11.4.07	41:58.964	41:07.541	1024	18 samples, no bottomwater
11955	GC-17	PM	11.4.07	41:58.963	41:07.540	1012	9 samples
11958	DAPC-15	BS	11.4.07	41:57.448	41:17.446	845	13 samples
11959	MIC-2	BS	11.4.07	41:57.533	41:17.568	840	19 samples, TTR-15 (AP 351)
11962	MIC-4	BS	12.4.07	41:57.548	41:17.435	838	16 samples, DAPC-8
11963	DAPC-16	BS	12.4.07	41:57.410	41:17.278	853	14 samples
11964	MIC-5	BS	12.4.07	41:57.414	41:17.360	847	19 samples
11965	MIC-6	BS	12.4.07	41:57.447	41:17.437	843	14 samples
11966	MIC-7	BS	12.4.07	41:57.614	41:17.512	847	17 samples
11969	MIC-9	PM	13.4.07	41:58.962	41:07.541	1011	18 samples, no bottomwater
11970	MIC-10	CS	13.4.07	41:58.069	41:06.191	1118	12 samples
11971	GC-21	CS	13.4.07	41:58.069	41:06.199	1124	13 samples
11974	GC-22	Ref.-Station	13.4.07	41:57.428	41:16.803	884	18 samples, near BS
11976	MIC-11	DMV	16.4.07	44:16.807	34:58.906	2052	17 samples
11977	MIC-12	DMV	16.4.07	44:16.885	34:58.906	2052	17 samples
11978	MIC-13	DMV	16.4.07	44:16.944	34:58.902	2050	17 samples
11979	MIC-14	DMV	16.4.07	44:17.025	34:58.879	2048	14 samples
11981	DAPC-19	VMV	16.4.07	44 :17.650	35 :01.979	2037	7 samples
11988	GC-26	KS	19.4.07	44:37.207	35:42.291	889	13 samples
11990	GC-28	VMV	20.4.07	44 :17.623	35 :01.946	2061	11 samples
11992	DAPC-21	VMV	20.4.07	44 :17.630	35 :01932	2055	12 samples
11993	MIC-19	VMV	20.4.07	44 :17.627	35 :01.948	2067	9 samples
11994	DAPC-22	DMV	20.4.07	44:16.995	34:59.096	1994	7 samples
11995	MIC-20	DMV	20.4.07	44 :17.034	34 :58.951	1977	15 sampls
11997	MIC-21	DMV	21.4.07	44:17.060	34:59.036	2050	17 samples
11999	DAPC-23	DMV	21.4.07	44:16.892	34:58.902	2049	14 samples

11.2 Results and discussion

In the following, we present and discuss initial results obtained at the Dvurechinskii mud volcano (DMV) and in the Batumi seep area.

11.2.1 Dvurechenskii Mud Volcano

During ROV Dive 160 (GeoB 11915), 4 push cores were taken in a transect across the DMV (Figs. 112 and 113). The first core (GeoB 11915-12, PC 67), taken at the northwestern rim, showed a gentile and almost linear increase in dissolved chloride and ammonia with depth, which is caused by the slow ascent of deep brines strongly enriched in ammonia. The steep gradients in total dissolved sulfide (TH_2S) and total alkalinity (TA) are caused by the anaerobic oxidation of methane (AOM). Steep dissolved silica (SiO_2) gradients indicate the rapid dissolution of biogenic opal in surface sediments. The next core taken within the DMV (GeoB 11915-15, PC 46) showed steeper gradients in dissolved chloride and ammonia indicating elevated rates of upward fluid flow. TH_2S, TA, and SiO_2 gradients were, however, diminished. This observation might indicate slower rates of AOM and opal dissolution. The following core taken

towards the center of the DMV (GeoB 11915-23, PC 26) had even steeper chloride and ammonia gradients. The highest dissolved chloride and ammonia values were, however, found in core GeoB 11915-16, PC 54 taken directly in the center of the DMV. The regular increase in dissolved chloride and ammonia towards the center of the DMV clearly indicates that the center is the most active part of the DMV in terms of fluid flow and dissolved methane release. A preliminary evaluation of the chloride data indicates that the velocity of upward fluid flow is only 2 cm/yr at the rim and increases to 50 cm/yr in the center of the DMV.

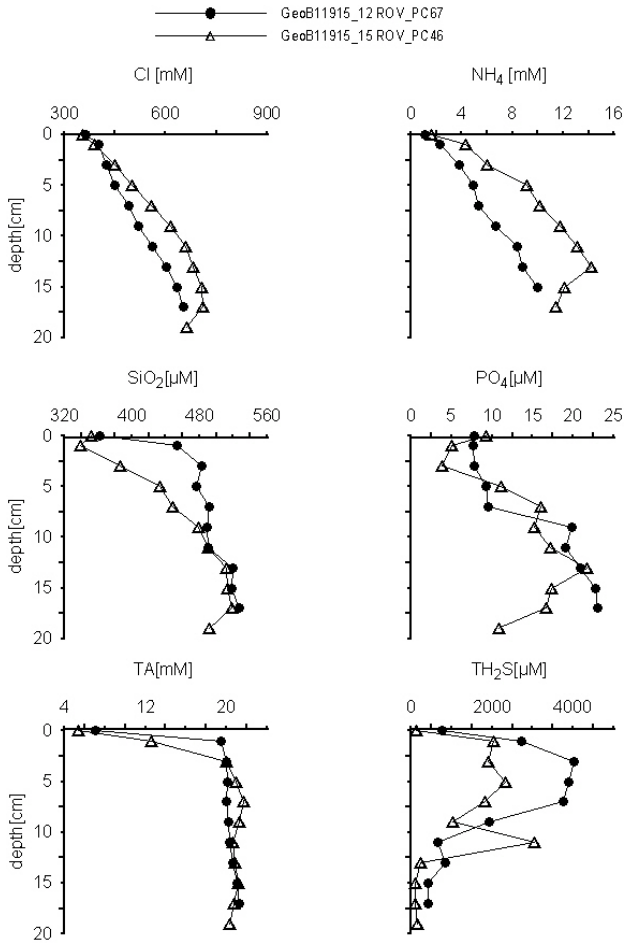

Fig. 112: Push cores taken at the rim of the DMV.

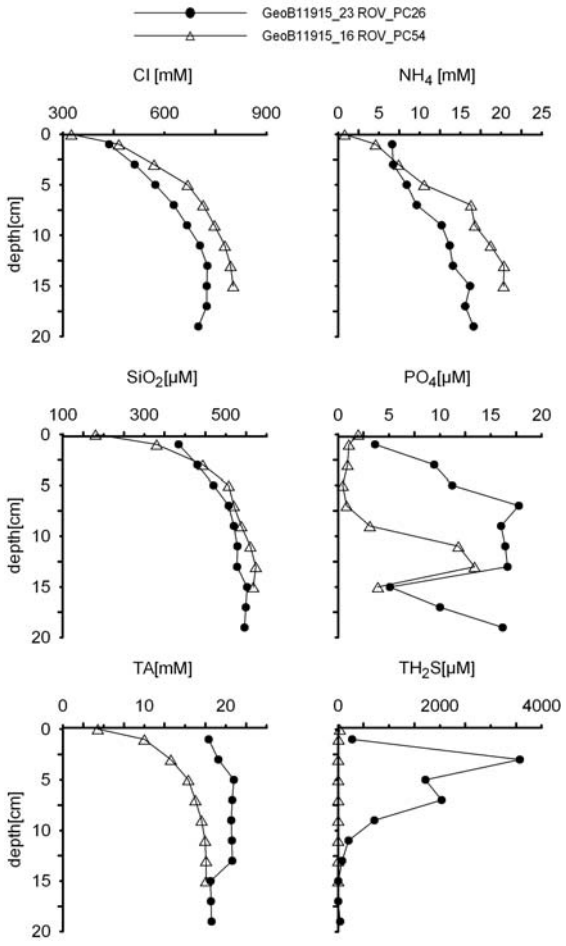

Fig. 113: Push cores taken at the center of the DMV.

TH_2S and TA values showed a reverse trend with low values in the center and high concentrations at the rim. This observation suggests that AOM rates are diminished in the center. Since dissolved sulfate from ambient bottom waters serves as terminal electron acceptor in the anaerobic oxidation of methane, the AOM decrease towards the center could be related to the flushing of surface sediments by ascending brines. AOM rates may, thus, be diminished by the decrease in dissolved sulfate concentrations in surface sediments caused by the ascent of sulfate-free fluids. An additional push core was taken at a location within the DMV where the seafloor was covered with whitish to grayish material (GeoB 11915-8, PC 47). Visual inspection of the recovered core indicated that the surface sediments contained large amounts of authigenic carbonates and microbial biomass. The dissolved chloride gradient points towards a moderately

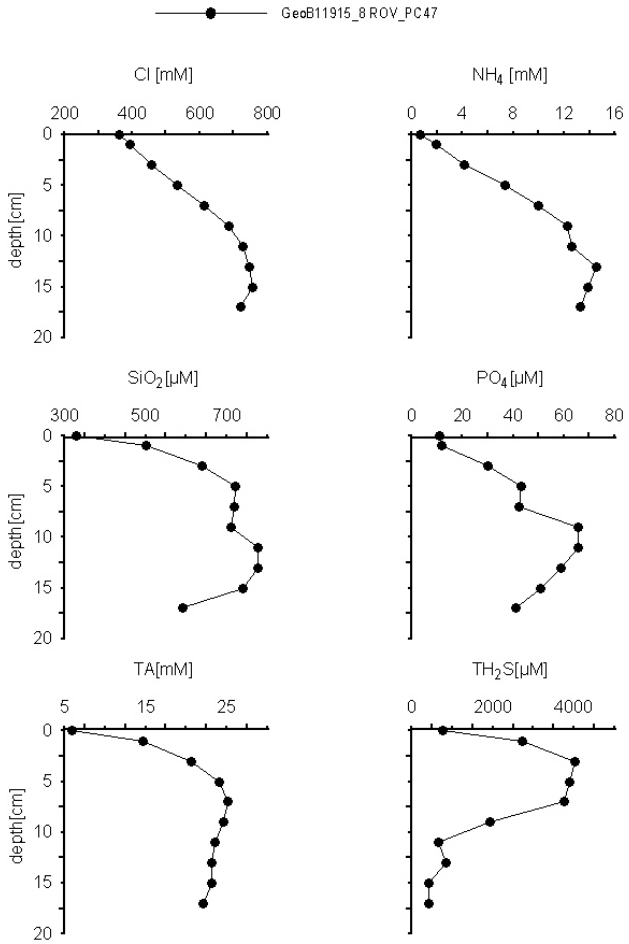

Fig. 114: Push core taken within the DMV at a bacterial site.

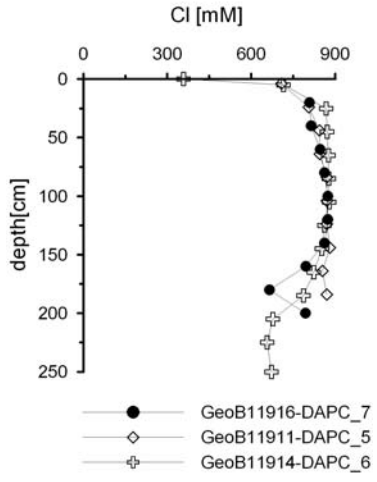

Fig. 115: Dissolved chloride concentrations in DAPC cores taken at the DMV.

high rate of upward fluid flow (25 cm yr^{-1}), while intense AOM is suggested by the very high TA and TH_2S values (Fig. 114). The material retrieved at this station will be further evaluated to better understand the unusual accumulation of microbial biomass and carbonates at this specific location.

Sediments retrieved with the DAPC were first degassed to quantify the amount of hydrate enclosed in the autoclave. Subsequently, the core was removed from the autoclave and processed for pore water analysis. The dissolved chloride concentrations in the three DAPC cores taken within the DMV showed constant chloride values between 50 and 150 cm sediment depths (Fig. 112). Below that depth, dissolved chloride was diluted by the melting of gas hydrates during the degassing procedure. The decrease in dissolved chloride can be taken as a measure for the original hydrate content. Thus, the hydrate content can be estimated from both the total gas volumes and the chloride values.

Dissolved salts, that are enriched in pore fluids during hydrate formation, may either remain within the sediments (closed system) or may be flushed from the sediments by ascending fluids (open system). In an open system the two independent methods should yield the same results while the chloride method would underestimate the hydrate contents for closed systems. The chloride values shown in Fig. 115 may thus be used to determine the amount of salt that was retained within the sediments after hydrate formation if the hydrate contents, independently derived from the gas volume data, were significantly larger than the chloride-based estimates.

Sediments from the Vodyanitskiy mud volcano located in the immediate vicinity of the DMV were sampled by push coring and with the gravity corer. The pore fluids retrieved from these sediments showed the same composition as the DMV fluids with elevated concentrations of dissolved chloride and ammonia. These two adjacent mud volcanoes are apparently linked to the same deep source region, which may extend over a larger area than previously assumed.

11.2.2 Batumi Seep Area

Several push cores were taken close to bubble vent sites within the Batumi seep area. Two of these cores (GeoB 11904-15 PC46, GeoB 11907-07 PC38) showed much higher concentrations of total alkalinity and dissolved sulfide than a multicorer taken at a reference station (GeoB 11912, MUC3). The dissolved nutrient concentrations were, however, much higher at the reference site (Fig. 116). This pattern may be explained by the bubble tube that contains not only elevated concentrations of gaseous and dissolved methane, but also bottom water which is mixed into the bubble tube by eddy-diffusive processes induced by the gas bubble stream. Methane and possibly also dissolved sulfate enters the adjacent sediments via lateral diffusion, while nutrients are lost to the bubble tube by the same diffusive exchange process. The AOM rates are probably extremely high because dissolved sulfate from the overlying bottom water enters the methane-charged surface sediments both by vertical and lateral diffusion.

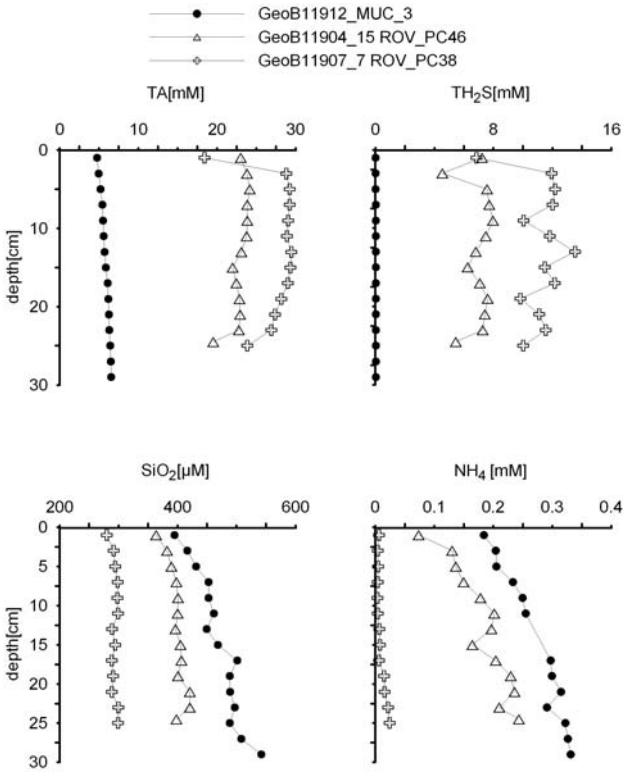

Fig. 116: Push cores taken close to bubble vent sites in the Batumi seep area and a multicorer taken at an adjacent reference station.

DAPC cores taken at the Batumi seep area show strong chloride depletions below 50 cm sediment depth. Only core GeoB 11918 was depleted at a shallower depth (Fig. 117). A gradual decrease in dissolved chloride is also seen at reference stations were no hydrates occur. It is caused by old formation fluids from a more lacustrine phase of the Black Sea. This non-linear background has to be considered in the quantification of hydrate contents. The Batumi hydrates are found at shallower sediment depths than the DMV hydrates. It thus seems that the vigorous gas seepage in the Batumi seep area favors hydrate formation at shallow depths, whereas the slow fluid seepage at the DMV induces hydrate formation at greater sediment depths.

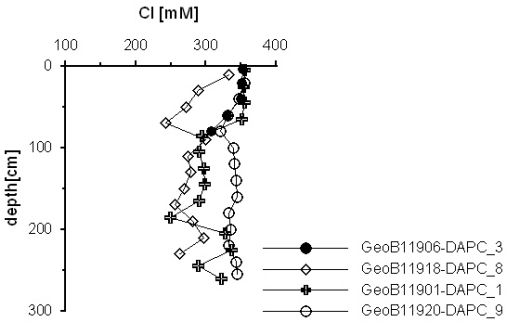

Fig. 117: Dissolved chloride concentrations in DAPC cores taken at the Batumi seep area.

12 Gas chemical compositions

(T. Pape, J. Rethemeyer, S. Kusch, H.-J. Hohnberg)

12.1 Introduction

The deeper, anoxic part of the Black Sea water column is characterized by extremely high concentrations of low-molecular-weight hydrocarbons (LMWHCs, C_1 through C_6) predominantly brought along by seep structures at the seafloor, like cold seeps (Kessler et al., 2006) and mud volcanoes (Bohrmann et al., 2003; Greinert et al., 2006). Provided that the seeping sites are located within the gas hydrate stability field, near-surface buried gas hydrates can generally form in associated deposits (Chap. 10.4). The chemical composition of the source gas, in general, affects the crystal structure of the gas hydrates generated. However, gas hydrate formation and decomposition, and thus, the amount of hydrate-bound hydrocarbons, is strongly controlled by the dynamic advective transport of gases and heat from greater depth. Further, preferential incorporation of specific LMWHCs into the gas hydrate cages leads to compound fractionation processes of the ascending gas. When discharged into the water column, LMWHCs are either dissolved in the water or form bubbles of free uprising gas as controlled by their compound-specific solubility.

The major objectives of the onboard gas analytical works during M72/3 were to determine the spatial variability of LMWHC concentrations in gas- and hydrate-rich sediments at the Eastern Black Sea. For the quantification of *in situ* gas abundances, autoclave technology was applied, which, unlike conventional sampling tools, enables us to maintain the ambient pressure and, thus, prevents degassing of the sampled material (Chap. 9; Abegg et al., subm.). The chemical composition of the gases contained in near-surface gas hydrates, interstitial waters, and bubbles of free gas in the water column was followed in order to determine the source type(s) and to characterize compound fractionations during advective transport in the sediment and gas hydrate formation.

Primary sites of gas chemical investigations during Legs M72/3a and 3b were cold seep structures and a mud volcano area. The seep area offshore Georgia comprises several individual gas seeps, which in some cases are characterized by additional oil seeps. Near-surface gas hydrates, high concentrations of LMWHCs in interstitial waters as well as gas flares in the water column are known from several sites of this area (Heeschen et al., 2006; Klaucke et al., 2006; Wagner-Friedrichs, 2007). At several mud volcanoes east off the Krimean Peninsula, the presence of gas hydrates and high concentrations of LMWHCs were proven during previous cruises (MARGASCH I, Bohrmann et al., 2003; Blinova et al., 2003; TTR-11, Stadnitskaia et al., 2005).

12.2 Samples

In order to determine the *in situ* amounts of LMWHCs present in gas-laden sediments and to elucidate stripping effects during upward migration and gas hydrate generation, the first leg's work was focussed on the quantitative degassing and subsampling of sediment cores retrieved with the dynamic autoclave piston corer (DAPC I). During Leg M72/3b, core GeoB 11994 was recovered with the DAPC II and smaller core segments were prepared under pressure (Chap. 9). Selected core segments were subject to incremental degassing immediately upon scanning by computerized tomography (CT, Chap. 10.3).

Gases were retrieved from 16 DAPC stations and a total of 242 gas subsamples were obtained by incremental degassing during Legs M72/3a and 3b. The sample set was completed by I) gas bubble samples retrieved with the GBS, II) by gas released by controlled dissociation of gas hydrate pieces recovered with gravity cores, and III) by gases obtained from sediments sampled with gravity and push cores (Tab. 20).

Table 20: List of samples taken for gas chemical measurements during Legs M72/3a and 3b. DAPC: dynamic autoclave piston corer; GBS: gas bubble sampler (ROV-based); GC: gravity corer;
Note: DAPC I was used for incremental degassing of pressurized sediment cores, while the DAPC II system was primarily applied for preparations of core segments.

GeoB No.	Tool	Lat. [°N]	Long. [°E]	Water depth [m]	Type of sample	No. of samples
Batumi seep area						
11901	DAPC I	41:57.410	41:17.344	851	gas released	40
11903	DAPC I	41:57.472	41:17.266	850	gas released	7
11906	DAPC I	41:57.465	41:17.270	843	gas released	9
11918	DAPC II	41:57.547	41:17.427	840	gas released	32
11920	DAPC I	41:57.454	41:17.545	844	gas released	19
11937	DAPC I	41:57.489	41:17.462	842	gas released	6
11951	DAPC II	41:57.546	41:17.431	840	gas released	17
11958	DAPC I	41:57.448	41:17.446	847	gas released	17
11963	DAPC I	41:57.410	41:17.278	853	gas released	7
11904-16	GBS	41:57.541	41:17.413	833	gas released	5
11907-2	GBS	41.57.543	41.17.529	834	gas released	5
11907-5	GBS	41.57.544	41.17.472	835	gas released	1
11919-2	GBS	41:57.533	41:17.268	833	gas released	6
11921-1	GBS	41:57.530	41:17.266	844	gas released	2
11925	GC	41.57.431	41:17.347	844	gas hydrate	1
11927	GC	41:57.410	41:17.324	856	gas hydrate	3
11936	GC	41:57.563	41:17.430	844	gas hydrate	3
11946	GC	41:57.532	41:17.582	842	gas hydrate	3
11949	GC	41:57.550	41:17.175	842	gas hydrate	3
11956	GC	41:57.450	41:17.436	843	gas hydrate	1
11975	GC	41:57.528	41:17.588	844	gas hydrate	2
Colkheti seep area						
11922	DAPC I	41:58.071	41:06.214	1126	gas released	14
11902-1	GBS	41:58.071	41:06.197	1112	gas released	5
11923-1	GC	41:58.120	41:06.250	1088	gas hydrate	1
11923-2	GC	41:58.120	41:06.250	1088	gas hydrate	1
11971	GC	41:58.069	41:06.199	1124	gas hydrate	3
11902-4	GC	41:58.071	41:06.197	1112	sediment	1
11924	GC	41:58.068	41:06.195	1056	sediment, gas	3
Pechori mound						
11953	GC	41:58.958	41:07.543	1015	gas hydrate	1
11955	GC	41:58.963	41:07.540	1012	gas hydrate	4
Iberia mound						
11938	GC	41:52.340	41:10.036	982	gas hydrate	3
Gudauta High						
11933	GC	42:40.262	40:22.631	690	sediment	3
Dvurechenskii mud volcano						
11911	DAPC I	44:16.972	34:59.215	2058	gas released	7
11914	DAPC I	44:16.987	34:59.097	2058	gas released	24
11916	DAPC I	44:16.896	34:58.789	2057	gas released	21
11994-1*)	DAPC II	44:16.995	34:59.096	1994	gas released	5
11994-3*)	DAPC II	44:16.995	34:59.096	1994	gas released	7
11999	DAPC I	44:16.892	34:58.902	2049	gas released	12
Vodyanitskii mud volcano						
11981	DAPC I	44:17.650	35:01.979	2037	gas released	3
11992	DAPC I	44:17.630	35:01.932	2055	gas released	7
11917-1	GBS	44:17.656	34:01.992	2032	gas released	9
11913	GC	44:17.621	35:01.946	2048	gas hydrate	1
11990	GC	44:17.623	35:01.946	2061	gas hydrate	2
					Total	**330**

*) gas released from core sections no. GeoB 11994-1 (lowermost section, degassing subsequent to computerized tomography scanning) and no. GeoB 11994-3 (top section) prepared from a sediment core retrieved with DAPC II.

The overall gas volumes preserved in DAPC cores and core segements were specified by incremental degassing (Heeschen et al., in press). During the procedure, the pressure preserved inside the DAPC was monitored and subsamples were taken at selected time points and transferred into 20 mL glass vials pre-filled with concentrated NaCl solution I) for immediate analyses of the gas chemical composition on board and II) for storage and further measurements on shore.

Gas bubbles discharged from the seafloor were caught during 6 ROV dives in the Batumi seep area, at the Colkheti oil seep, and at the Vodyanitskii mud volcano with the GBS (Chaps. 7 and 9). The GBS was degassed quantitatively upon recovery using the same technique as for DAPC cores.

12.3 Gas analyses

For onboard measurements of gas chemical compositions, the samples were analyzed with a two-channel 6890N (Agilent Technologies) gas chromatograph (GC). Low-molecular-weight hydrocarbons (C_1 to C_6) were separated, detected, and quantified with a capillary column (OPTIMA-5; 5 µM film thickness; 0.32 mm ID, 50 m length, carrier gas: N_2) connected to a Flame Ionisation Detector (FID), while permanent gases (O_2, N_2, CO_2) as well as C_1 and C_2 hydrocarbons were determined using a packed (Molecular sieve, carrier gas: He) stainless steel column coupled to a Thermal Conductivity Detector (TCD). The GC oven temperature program was: initial 45°C held for 4 min; heating with a rate of 15°C min^{-1} up to 155°C (constant for 2 min), 25°C min^{-1} up to 240°C (7 min). A PC-operated integration system (GC Chemstation, Agilent Technologies) was used for recording and calculation of the data. Calibrations and performance checks of the analytical system were conducted daily using commercial pure gas standards and gas mixtures (AIR LIQUIDE). The coefficient of variation determined for the analytical procedure was lower than 2 %.

For onshore determination of stable isotope ratios ($^1H/D$, $^{12}C/^{13}C$) of volatile hydrocarbons by GC-Isotope-Ratio-Mass-Spectrometry (GC-IRMS), gas samples were stored in sealed glass vials filled with NaCl-saturated water.

12.4 Preliminary results

A total of 330 gas samples recovered by DAPC coring and by the GBS, as well as gas samples retrieved by dissolution of gas hydrate pieces, were analyzed on board for their gas compositions (Tab. 20). Using GC-FID analyses about 10 individual hydrocarbons were detected in the C_1 to C_6 range. Structural identifications of unidentified hydrocarbons are subject to experiments in the home lab.

Significant trends in the hydrocarbon compositions of gases during release from the DAPC were found. For an overview, only compositions of a selected subsample retrieved during intermediate stages of degassing are presented. Average contributions of air (sum of N_2, O_2 and Ar) were found to be less than 2.5 mol-% for all gas samples retrieved with the DAPC and the GBS.

12.4.1 Seep areas offshore Georgia

Batumi Seep Area

The Batumi seep area was intensively studied for gas contents and composition during Legs M72/3a and 3b. Samples of pressurized sediment cores, gas and gas hydrates were retrieved at 7 DAPC I stations, 2 DAPC II stations, 6 applications of the GBS, and at 6 gravity core stations. The gas volumes retrieved by incremental degassing of DAPC ranged between 3.3 and 20.3 L per L sediment (Tab. 21).

Table 21: Accumulated gas volumes and calculated gas-sediment ratios of gas samples retrieved by the DAPC systems in the *Batumi seep area*.

GeoB No.	Device	Core volume [mL]	Gas volumes released [mL]	Gas volume / volume wet sediment [mL / mL]
11901	DAPC I	13,892	231,200	16.6
11903	DAPC I	5,343 *	46,280 *	8.7 *
11906	DAPC I	4,435	40,700	9.2
11918	DAPC II	12,449	253,200	20.3
11920	DAPC I	13,892	100,550	7.2
11937	DAPC I	2,458	8,000	3.3
11951	DAPC II	7,320	103,250	14.1
11958	DAPC I	7,801	137,450	17.6
11963	DAPC I	9,030	30,700	3.4

*)Degassing experiment was aborted due to clogging of the DAPC gas openings. Since the upper sediment core was partially lost during abrupt pressure release, the core recovery was estimated for calculations.

Gas subsamples obtained with the DAPC were strongly dominated by methane (99.946 to 99.976 mol-% of LMWHCs, Fig. 118), followed by ethane (0.023 to 0.052 mol-%) and propane (0.0006 to 0.0012 mol-%). When present, C_{3+} hydrocarbons (*i*-C_4, *n*-C_4, and C_5- and C_6-derivatives) were found in smaller amounts. In the course of degassing, CH_4/CO_2 ratios varied considerably between about 300 and 11.500.

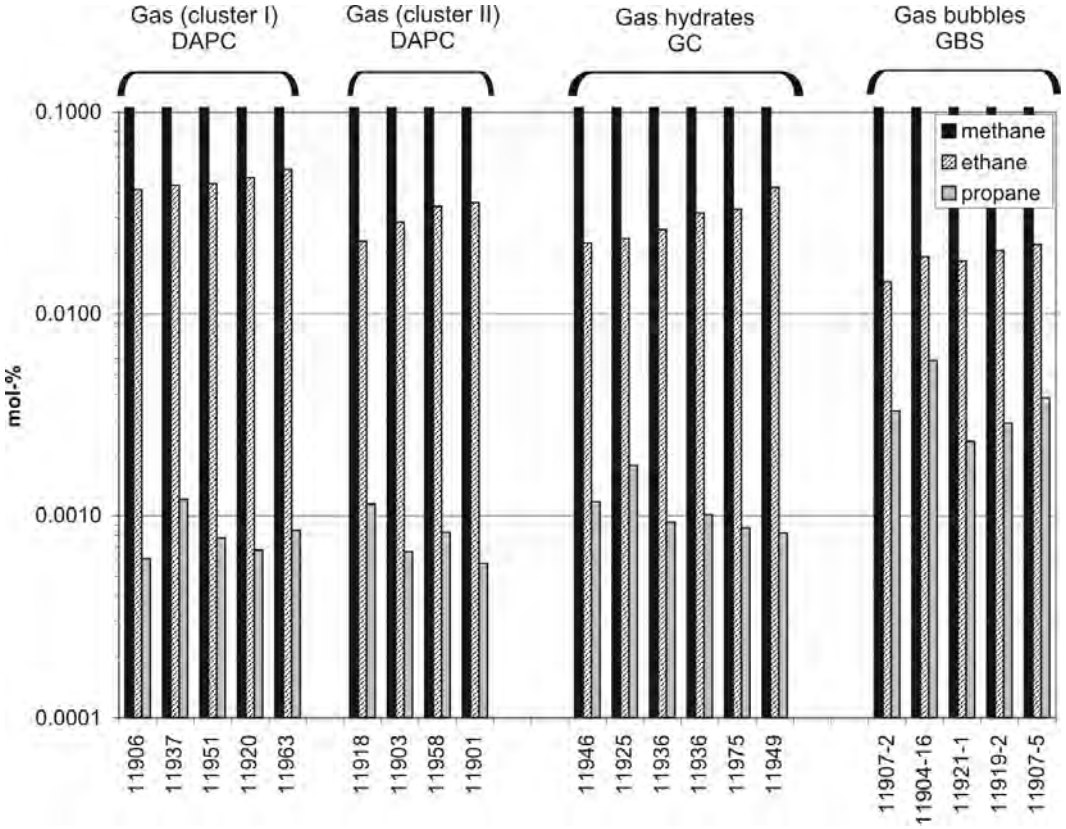

Fig. 118: C_1 to C_3 hydrocarbon composition of gases retrieved by the DAPC, the GBS, and by decomposition of gas hydrates from the Batumi seep area. Numbers of samples refer to GeoB station numbers. As an overview concentrations are only shown in the 0.0001 to 0.1 mol-% range. Based on different C_1/C_{2+} ratios, gases of two distinct compositions (cluster I + II) were recognized for DAPC samples. Note: For comparison only values for subsamples retrieved during intermediate stages of the DAPC degassing experiments are shown.

For preliminary characterizations of gas compositions, molar ratios between methane and higher homologues (commonly expressed as $R = C_1 / (C_2 + C_3)$; Bernard et al., 1978) were calculated. Remarkably, *R* of subsamples from pressurized sediments taken with the DAPC in the Batumi seep area clustered in two distinct groups ranging from I) 1,665 to 2,515 (cluster I) and II) from 2,603 to 5,413 (cluster II). In general, a predominance of biogenic LMWHCs can be inferred from these values (Bernard et al., 1978). However, it was found that DAPC cores releasing cluster I gas, mainly consisted of the stratigraphic units 1 and 2, while cluster II gas was derived from cores additionally containing significant amounts of unit 3 material (Chap. 10.2).
Except for one sample, gases released from decomposing gas hydrates (n = 6) were similar in LMWHC compositions to those of cluster II gases obtained from the DAPC, exhibiting the molar ratio, *R*, ranging from 2,318 to 4,091. Bubble forming gases obtained with the ROV-based GBS were slightly depleted in ethane, but enriched in propane (*R* = 3,250 to 5,383). These yielded the lowest ethane to propane ratios (3.3 to 7.8) observed for the Batumi samples.
Based on the chemical similarities between gas hydrate-bound gases and DAPC cluster II gases, a preferential occurrence of gas hydrates below the stratigraphic units 1 and 2 (predominantly below about 50 - 80 cm bsf; Chap. 10.2) might be assumed for the Batumi seep area. Further support for this assumption comes from the fact that highest gas amounts were released from cores of relatively high core recovery, by the prevalence of gas hydrates predominantly in deeper GC core sections, and by steep gradients of dissolved chloride in specific depths of DAPC and GC cores (Chap. 11).

Colkheti Seep, Pechori Mound, and Iberia Mound

Three gas- and oil-seep areas, the Colkheti seep, the Pechori mound, and the Iberia mound offshore Georgia, were sampled for LMWHC containing material. While the DAPC and GBS were only deployed at the Colkheti seep area, gas hydrates embedded in partially oil-contaminated sediments were retrieved at six GC stations covering all oil-seep sites (Chap. 10.2).
Generally, more complex LMWHC distribution patterns were found for the oil-seep samples compared to samples from the Batumi seep area. Altough methane dominated by far the fraction of all samples obtained from the three oil seeps, further individual LMWHCs and considerably higher portions of C_{2+}-compounds in general were found. Further, most oil seep gas samples were characterized by relatively high CO_2 portions.

At Colkheti seep, the only DAPC station carried out at an oil seep site (GeoB 11922), yielded about 70 L of gas. The sampled material consisted of small amounts of sediment suspended in a huge volume of water. This mixture was strongly contaminated with oil slicks. LMWHCs released by the degassing procedure consisted of about 99.366 mol-% CH_4, 0.546 mol-% C_2H_6 and small amounts of C_3H_8 (0.00349 mol-%), *i*-C_4, *n*-C_4, and C_5- and C_6-derivatives. C_1/C_{2+} ratios of < 200 were found for gases retrieved with the DAPC and for gas bubbles, which indicate the prevalence of thermogenic gases (Bernard et al., 1978) sourcing the Colkheti seep. CH_4/CO_2 values varied between 9.9 and 374. Remarkably, gas kept with the GBS showed a C_3-over-C_2 predominance.

12.4.2 Mud volcanoes in the Sorokin Trough

Dvurechenskii Mud Volcano

For collecting pressurized sediment cores from the Dvurechenskii mud volcano (DMV), five DAPC stations were carried out at the outer rim of the DMV (Table 22). Gas flares in the water column as well as gas escaping from the seafloor were not observed during Leg M72/3a, and thus, gas bubbles could not be collected in the DMV area.

For one station (GeoB 11994) sampled with the DAPC II, we succeeded to quantitatively degas a pressurized segment of the lowermost part of a sediment core (GeoB 11994-1) subsequent to the non-destructive, high-resolution computerized tomography scanning (Chaps. 9.3.2 and 10.3). Thus, during Leg M72/3b a three-dimensional imaging of the gas hydrate fabric in a pressurized sediment core and its *in situ* gas inventory could be correlated for the first time. Further, the preservation of this core segment for degassing proved the complete applicability of the DAPC II system.

However, for the intermediate section of the core (GeoB 11994-2), which also was successfully cut and transferred into a smaller pressure chamber, the degassing experiment had to be aborted due to severe clogging of its gas openings. The core top section (GeoB 11994-3) was left in the DAPC II pressure chamber and degassed quantitatively without preceding CT imaging.

Table 22: Gas volumes and calculated gas-sediment ratios of samples retrieved by use of the DAPC at the Dvurechenskii mud volcano.

GeoB No.	Instrument	Core volume [mL]	Gas volumes released [mL]	Gas volume / wet sediment volume [mL / mL]
11911	DAPC I	13,892	n.d.	n.d.
11914	DAPC I	13,678	108,550	7.9
11916	DAPC I	13,518	100,850	7.5
11994-1	DAPC II	3,259	21,350	6.6
11994-3	DAPC II	3,633	24,050	6.6
11999	DAPC I	13,678	130,550	9.5

From DAPC I cores, 108.6 L of gas corresponding to 7.9 L gas per L wet sediment were retrieved at maximum at a station ENE from the center (GeoB 11914). CH_4 (99.933 to 99.967 mol-% of LMWHCs) was the prevailing constituent of the LMWHCs, followed by C_2H_6 (0.031 to 0.066 mol-%) and C_3H_8 ($\leq$ 0.001 mol-%). During degassing, C_1/C_{2+} ratios varied between 1,487 and 3,010 pointing to the prevalence of volatiles from biogenic sources. Traces of *i*-C_4H_{10} (< 0.001 mol-%) were only found in samples of station GeoB11916 and higher homologues were below detection limit. Also during degassing, CH_4/CO_2 values varied between 17.0 and 8,245.

Vodyanitskii Mud Volcano

In contrast to observations from the DMV area, active gas escape into the water column was recognized at the Vodyanitskii mud volcano (VMV) during M72/3. At VMV, two DAPC station were performed, and gas hydrate bearing sediments and ascending gas bubbles were collected using gravity corers and the GBS.

For DAPC core GeoB 11981, about 0.9 L gas per L sediment was determined, while for DAPC core GeoB 11992 no accurate data are available (min. 4.2 L gas per L sediment) since pressure was partially lost during recovery of the core. However, CH_4 contributed 99.945 to 99.961 mol-% of LMWHC, and C_2H_6 (0.038 to 0.054 mol-%) and C_3H_8 ($\leq$ 0.001 mol-%) were less abundant. C_1/C_{2+} ratios ranged between 1,360 and 2,607 and CH_4/CO_2 values varied between 138 and 1,626. For near-seafloor gas bubbles a slight

enrichment of C_2H_6 (0.058 mol-%) and C_3H_8 compared to gases retrieved from pressurized sediments was observed.

12.5 Conclusions

During M72/3a and 3b, a comprehensive set of gaseous samples was retrieved from sediments and waters of gas-enriched settings in the Black Sea by use of conventional and novel deep-sea sampling tools. On-board, gas chemical analyses of selected samples showed a strong predominance of volatile hydrocarbons in the gases.

Considerable variations in the hydrocarbon distribution patterns were observed for the sample set. These variations point to molecular differentiation processes during fluid migration through the sediment, gas hydrate crystallization, and preferential gas release from specific hydrocarbon reservoirs during increental degassing of autoclave sediment cores.

Future onshore work combining methodological approaches (computer tomography scanning, cryo-scaning electron microscopy, isotope-ratio-monitoring mass spectrometry, X-ray diffractometry) will help to clarify the type(s) of the source gas(es), as well as the internal dynamics during accumulation in and discharge from gas- and gas hydrate bearing sediments. Gas hydrate structure(s) will be determined in order to characterize the source gas – hydrate interrelationships prevailing at cold seeps and mud volcanoes in the Black Sea.

13 Distribution and carbon isotopic composition of lipid biomarkers

(J. Rethemeyer, S. Kusch)

13.1 Introduction

Paleoenvironmental studies are often based on the analysis of source-specific organic compounds, so-called biomarkers, e.g. the reconstruction of sea surface temperatures (SST) via long-chain, unsaturated alkenones (UK'37) derived from marine coccolithophorids. A prerequisite for such studies is the identical age of all compounds deposited within the same sediment layer. Postdepositional processes as well as the contribution of terrigenous organic matter however, can significantly affect the reliability of the sediment record. There is strong evidence for the selective degradation of organic compounds in marine sediments that seems mainly dependent on biomarker exposure to oxygen. The Black Sea, being the world's largest basin with both well-oxygenated and permanently oxygen-deficient conditions, provides ideal conditions for investigating the effect of the selective degradation of different lipid biomarkers as well as the contribution of terrestrial organic matter to Black Sea surface sediments delivered from nearby rivers.

The objective of our research is to study the degradation/preservation of different organic compounds by comparing their abundance and radiocarbon concentration in surface sediments from oxygen-replete and oxygen-depleted sites in the Black Sea taken on a slope transect. Compound-specific ^{14}C analysis will also be used to differentiate between recently produced marine and pre-aged terrestrial organic compounds and to estimate the timescales of organic carbon transport from the continent to the ocean. In addition, we will use the new branched versus isoprenoid tetraether lipid (BIT) index as an indicator for the relative fluvial contribution of terrigenous organic matter to marine sediments (Hopmans et al., 2004). A further goal is to evaluate the applicability of the UK'37 SST proxy, which was found to give unrealistically low results with strong spatial and down-core variations questioning the applicability of UK'37 in the Black Sea (e.g. Freemann and Wakeham, 1992). Alkenone derived SSTs will be compared with temperature estimates determined with the new TEX86 proxy that is based on the distribution of glycerol dialkyl glycerol tetraethers (GDGTs) from marine Crenarchaeota (Schouten et al., 2002).The radiocarbon concentrations of di- and tri-alkenones and GDGTs will give us information on their degradation/preservation under oxic and anoxic conditions.

13.2 Samples and methods

During cruise M72/3a and 3b, near-surface sediments from eight different sites were sampled with a multicorer or a minicorer (Tab. 23). The multicorer (MUC) was equipped with 8 large tubes (9.9 cm outer diameter, 9.5 cm inner diameter) and the minicorer (MIC) with 4 tubes (6.3cm outer diameter, 5.7 cm inner diameter) each being 60 cm long. GeoB 11905-2 was recovered from 877 m water depth near the Batumi seep area. One MUC core was taken at the temperature maximum of the Dvurechenskii mud volcano and will serve us as reference material for lipid extraction and radiocarbon analysis. For the study of terrigenous organic matter input and preservation of organic biomarkers at slopes and depocenters, a transect consisting of three MUC/MIC stations was run near Batumi at 41°47.838'N, 41°16.842'E, 42°40.260'N, 40°22.618'E, and 42°00.351'N, 41°27.997'E from 838.7 m to 523m water depth. Selective degradation of biomarkers will also be studied in a transect S/E of the Crimean peninsula consisting of four MIC stations. The stations were located (i) in the oxygenated zone at 95 m water depth, (ii) in the transition zone of oxic/anoxic conditions at 173 m water depth, and in the anoxic part (iii) at 747 m and (iv) 1341 m water depth.

At each station one core was used for the sedimentological description and one or two cores were immediately sampled. Sediment cores were pushed carefully out of the tubes using a piston. The upper 2 to 6 cm consisting of unconsolidated, fluffy material was sampled with a spoon. If possible, sediment cores were cut into 1 cm segments throughout the entire core length for high resolution analysis. Because of the high water content of the upper sediment section, most cores were cut into 2 cm segments within the first 15 cm core length and the remaining 15 to about 50 cm were sampled in 5 cm intervals. All samples were filled into pre-combusted glass jars. Until further processing in the laboratory, samples were kept frozen at –18°C and shipped frozen by air cargo to Bremen.

Table 20: Samples taken for lipid analysis. MUC = multicorer, MIC = minicorer.

GeoB No.	Tool	Lat. [°N]	Long. [°E]	Water depth [m]	Sampled core length [cm]	No. of sub-samples
11905-2a	MUC	41:57.432	41:16.798	877	49	14
11905-2b	MUC	41:57.432	41:16.798	877	46	14
11912	MUC	44:17.015	34:58.885	2053	20	4
11934	MUC	42:40.260	40:22.618	701	57	39
11960-1	MIC	42:00.351	41:27.997	523	52	37
11960-2	MIC	42:00.351	41:27.997	523	53	28
11983	MIC	44:39.607	35:42.519	747	45	26
11984	MIC	44:29.999	35:49.998	1341	24	14
11985	MIC	44:45.008	36:09.995	95	26	14
11986	MIC	44:46.007	36:01.998	173	50	26

In Bremen, all sediment samples will be freeze-dried in the laboratory. Aliquots of samples will be taken for analysis of bulk parameters such as total organic carbon content, water content, etc. Sediment samples will then be extracted with organic solvents using a soxhlet extractor to recover total extractable lipids. Total lipids will be separated into different compound classes such as alkanes, ketones, fatty acids, and alcohols using standard methods (Fig 119). Individual compounds will subsequently be isolated by capillary gas-chromatography (GC) and high performance liquid-chromatography (HPLC). Suitable compounds (e.g., long-chain n-fatty acids) that occur in sufficient quantities for radiocarbon analysis (>100 µg C of each individual compound), will be isolated using preparative GC and HPLC and purified for radiocarbon analyses using accelerator mass spectrometry.

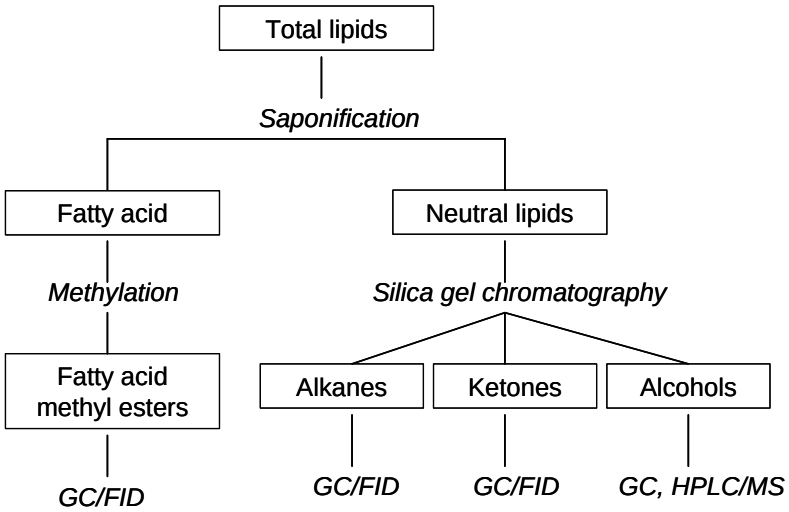

Fig. 119: Lipid extraction scheme. GC = capillary gas chromatography, FID = flame ionization detector, HPLC/MS = high performance liquid chromatography mass spectrometry.

14 References

Abegg F., Freitag J., Bohrmann G., Brueckmann W., Eisenhauer A., Amann H., Hohnberg H.-J. (2003) Free gas bubbles in the hydrate stability zone: evidence from CT investigation under in situ conditions. *Geophysical Research Abstracts* 5, EAE03-A-10342.

Abegg F., Hohnberg H.-J., Bohrmann G., Freitag J. (submitted). Development and application of pressure core sampling systems for the investigation of gas and gas hydrate bearing sediments. *Deep Sea Research Part I: Oceanographic Research Papers.*

Artemov Y.G. (2006) Software support for investigation of natural methane seeps by hydroacostic method., *Marine Ecological Journal* N1, 57-71.

Artemov Y.G., Egorov V.N., Polikarpov G.G., Gulin S.B. (2007) Methane emission to the hydro - and atmosphere by gas bubble streams in the Dnieper paleo-delta, the Black Sea. *Reports of the National Academy of Science of Ukraine* 5, 110 - 116 (in Russian).

Bernard B.B., Brooks J.M., Sackett W.M. (1978) Light hydrocarbons in recent Texas continental shelf and slope sediments. *Journal of Geophysical Research* 83, 4053-4061.

Blinova V., Ivanov M., Bohrmann G., (2003) Hydrocarbon gases in deposits from mud volcanoes in the Sorokin Trough, north-eastern Black Sea. *Geo-Marine Letters* 23, 250-257.

Bohrmann G., Ivanov M., Foucher J.-P., Spiess V., Bialas J., Greinert J., Weinrebe W., Abegg F., Aloisi G., Artemov Y., Blinova V., Drews M., Heidersdorf F., Krabbenhöft A., Klaucke I., Krastel S., Leder T., Polikarpov I., Saburova M., Schmale O., Seifert R., Volkonskaya A., Zillmer M., (2003) Mud volcanoes and gas hydrates in the Black Sea: new data from Dvurechenskii and Odessa mud volcanoes. *Geo-Marine Letters* 23, 239-249.

Bouriak S.V., Akhmetjanov A.M. (1998) Origin of gas hydrate accumulations on the continental slope of the Crimea from geophysical studies. In: J.-P. Henriet and J. Mienert (eds.), Gas hydrates: Relevance to world margin stability and climate change. Geological Society, London., special publications 137, 215-222.

Çifçi G., Dondurur D., Ergün M. (2003) Deep and shallow structures of large pockmarks in the Turkish shelf, Eastern Black Sea. *Geo-Marine Letters* 23, 311-322.

Egorov V., Polikarpov G.G., Gulin S.B., Artemov Y.G., Stokozov N.A., Kostova S.K. (2003) Present-day views on the environment-forming and ecological role of the Black Sea methane gas seeps. *Marine Ecological Journal*, 2, 5-26 (in Russian).

Ershov A.V., Brunet M.-F., Nikishin A.M., Bolotov S.N., Nazarevich B.P., Korotaev M.V. (2003) Northern Caucasus basin: thermal history and synthesis of subsidence models. *Sedimentary Geology* 156, 95-118.

Freeman K.H., Wakeham S.G. (1992) Variations in the distributions and isotopic compositions of alkenons in Black Sea particles and sediments. *Organic Geochemistry*, 19, 277-285.

Greinert J., Nützel B. (2004) Hydroacoustic experiments to establish a method for the determination of methane bubble fluxes at cold seeps. *Geo-Marine Letters*, 24, 75-85.

Greinert J., Artemov Y.G., Egorov V., De Batist M., McGinnis D. (2006) 1300-m-high rising bubbles from mud volcanoes at 2080 m in the Black Sea: Hydroacoustic characteristics and temporal variability. *Earth and Planetary Science Letters* 244(1-2), 1-15.

Heeschen K.U., Hohnberg H.-J., Haeckel M., Abegg F., Drews M., Bohrmann G. (in press). *In-situ* hydrocarbon concentrations from pressurized cores in surface sediments, Northern Gulf of Mexico. *Marine Chemistry*.

Heeschen K.U., Hohnberg H.-J., Abegg F., Mohr T., Haeckel M., Sahling H., Haas A., Bohrmann G. (2006) Pressure core sampling in the Eastern Black Sea. Poster during 1st statusseminar "Methane in the Geo/Bio-System" in the frame of the R&D-Program GEOTECHNOLOGIEN, Kiel 07 – 08 March, 2006.

Hopmans E.C., Weijers J.W.H., Schefuß E., Herfort L., Sinninghe Damsté J.S., Schouten S. (2004) A novel proxy for terrestrial organic matter in sediments based on branched and isoprenoid tetraether lipids. *Earth and Planetary Science Letters* 224, 107-116.

Ivanov M.K., Limonov A.M., Woodside J.M. (1998) Extensive deep fluid flux through the sea fllor on the Crimean continental margin (Black Sea). In: J.-P. Henriet and J. Mienert (eds.), Gas hydrates: Relevance to world margin stability and climate change. Geological Society, London., special publications 137, 195-214.

Jones G.A., Gagnon A.R. (1994) Radiocarbon chronology of Black Sea sediments. *Deep-Sea Research* 41, 531–557.

Judd A.G. (2003) The global importance and context of methane escape from the seabed. *Geo-Marine Letters* 23, 147-154.

Kessler J.D., Reeburgh W.S., Southon J., Seifert R., Michaelis W., Tyler S.C. (2006) Basin-wide estimates of the input of methane from seeps and clathrates to the Black Sea. *Earth and Planetary Science Letters* 243(3-4), 366-375.

Klaucke I., Sahling H., Bürk D., Weinrebe W., and Bohrmann G. (2005) Mapping deep-water gas emissions with sidescan sonar. EOS, *Transactions,* 86, 341-352.

Klaucke I., Sahling H., Weinrebe W., Blinova V., Burk D., Lursmanashvili N., Bohrmann G. (2006) Acoustic investtigation of cold seeps offshore Georgia, eastern Black Sea. *Marine Geology* 231, 51-67.

Kullenberg B. (1947) The Piston Core Sampler. *Svenska Hydrografisk-Biologiska Kommissionens Skrifter*, tredje ser.1, S. 2.

Kvenvolden, K.A. (1998). A primer on the geological occurrence of gas hydrate. In: J.-P. Henriet and J. Mienert (eds.), Gas hydrates: Relevance to world margin stability and climate change. Geological Society, London., special publications 137, 9-30.

Lamy F., Arz H., Bond G., Bahr A., Pätzold J. (2006) Multicentennial-scale hydrological changes in the Black Sea and northern Red Sea during the Holocene and the Arctic/North Atlantic Oscillation. *Paleoceanography* 21, PA1008.

Limonov A.F., Woodside J.M., Ivanov M.K. (1994) Mud volcanism in the Mediterranean and Black seas and shallow structure of the Eratosthenes Seamount. UNESCO reports in marine science 64, 173 pp.

Major C.O., Goldstein S.L., Ryan W.B.F., Lericolais G., Piotrowski A.M., Hajdas I., (2006) The co-evolution of Black Sea level and composition through the last deglaciation and its paleoclimatic significance. *Quaternary Science Reviews* 25, 2031-2047.

Neretin L.N., Böttcher M.E., Jørgensen B.B., Volkov I.I., Lüschen H., Hilgenfeld K. (2004) Pyritization processes and greigite formation in the advancing sulfidization front in the Upper Pleistocene sediments of the Black Sea. *Geochimica et Cosmochimica Acta* 68 (9), 2081-2093.

Nikishin A.M., Korotaev M.V., Ershov A.V., Brunet M.-F. (2003) The Black Sea basin: tectonic history and Neogene-Quaternary rapid subsidence modelling. *Sedimentary Geology* 156, 149-168.

Rangin C., Bader A.G., Pascal G., Ecevitoglu B., Gorur N. (2002) Deep structure of the Mid Black Sea High (offshore Turkey) imaged by multi-channel seismic survey (BLACKSIS cruise). *Marine Geology* 182, 265-278.

Reilinger R.E., McClusky S.C., Oral M.B., King R.W., Toksoz M.N., Barka A.A., Kinik I., Lenk O., Sanli I. (1997) Global positioning system measurements of present-day crustal movements in the Arabia– Africa –Eurasia plate collision zone. *Journal of Geophysical Research* 102, 9983- 9999.

Reitner J., Peckmann J., Reimer A., Schumann G., Thiel V. (2005) Methane-derived carbonate build-ups and associated microbial communities at cold seeps on the lower Crimean shelf (Black Sea). *Facies* 51, 66-79.

Robinson A.G. (1997) Regional and Petroleum geology on the Black Sea and surrounding region. *American Association of Petroleum Geologists*. 385 pp..

Ross D.A., Degens E.T. (1974) Recent sediments of the Black Sea. In: Degens E.T., Ross D.A. (Eds.), The Black Sea-Geology, Chemistry, and Biology. *American Association of Petroleum Geologists*, pp. 183– 199.

Schouten S., Hopmans E.C., Schefuβ E., Sinninghe Damsté J.S. (2002) Distributional variations in marine crenarchaeotal membrane lipids: a new organic proxy for reconstructing ancient sea water temperatures? *Earth and Planetary Science Letters*, 204, 265-274.

Stadnitskaia A., Muyzer G., Abbas B., Coolen M.J.L., Hopmans E.C., Baas M., van Weering T.C.E., Ivanov M.K., Poludetkina E., Sinninghe Damsté J.S. (2005) Biomarker and 16S rDNA evidence for anaerobic oxidation of methane and related carbonate precipitation in deep-sea mud volcanoes of the Sorokin Trough, Black Sea. *Marine Geology* 217, 67-96.

Sloan E.D. (1998) Clathrate hydrates of natural gases. 2nd ed. Marcel Dekker Inc., New York, 705 pp.

Tugolesov D.A., Gorshkov A.S., Meysner L.B., Soloviov V.V., Khakhalev E.M., Akilova Y.V., Akentieva G.P., Gabidulina T.I., Kolomeytseva S.A., Kochneva T.Y., Pereturina I.G., Plashihina I.N. (1985) Tectonics of the Mesozoic Sediments of the Black Sea Basin, Nedra, Moscow. 215 pp., (in Russian).

Wagner-Friedrichs M. (2007) Cold vents in the Black Sea: Acoustic characterization of mud volcanoes and gas seepages offshore Crimea and Georgia correlated to diapiric structures and gas/gas hydrates occurrences. Ph.D. thesis. University of Bremen.

Wessel P., Smith W.H.F (1998) New, improved version of Generic Mapping Tool released, *EOS, Transactions, American Geophysical Union* 79, 579.

Woodside J.M., Ivanov M.K., Limonov A.F. (1997) Neotectonics and fluid flow through seafloor sediments in the Eastern Mediterranean and Black Seas, Part II: Black Sea, Intergovernmental Oceanographic Commission technical series, UNESCO, 48.

Yefremova A.G., Zhizhchenko B.P. (1974) Occurrence of crystal hydrates of gases in the sediments of modern marine basins. *Doklady Akademii Nauk SSSR Earth Science Section* 214, 219-220.

Table A 1: Station list

R/V METEOR cruise M72/3a+b (Istanbul-Trabzon-Istanbul)														
Date	St. No.				Start Sci.	End Sci.	Begin / on seafloor			End / off seafloor			Recovery	
	GeoB	St. No.	Instruments	Location	Program	Program	Latitude N°	Longitude E°	Water depth (m)	Latitude N°	Longitude E°	Water depth (m)	Recovery	Remarks
M73/3a														
19.03.07	**11901**	DAPC-1	DAPC (I)	Batumi Seep	18.44	19:16	41:57.410	41:17.344	851	--	--	--	USBL; recovery 260 cm	
20.03.07	**11902**	ROV-1	ROV-155	Colkheti Seep	07:52	17:08	41:57.946	41:06.193	1071	41:58.073	41:06.191	1072		
	11902-1	GBS-1		Colkheti Seep	10:20		41:58.071	41:06.197	1112				Gas bubble sampler I	
	11902-2	T-stick-1		Colkheti Seep	11:28		41:58.071	41:06.197	1112				Temperature measurement	
	11902-3	T-stick-2		Colkheti Seep	11:42		41:58.072	41:06.197	1112				Temperature measurement	
	11902-4	Sediment-1		Colkheti Seep	16:37		41:58.071	41:06.197	1112				oily gas-rich sediment, no carbonates	
21.03.07	**11903**	DAPC-2	DAPC (I)	Batumi Seep	05:08	05:39	41:57.472	41:17.266	860				USBL; degassing stopped due to clogging of system. 260 cm core, 100 cm recovery	
	11904	ROV-2	ROV-156	Batumi Seep	08:23	18:10	41:57.529	41:17.108	812	41:57.565	41:17.507	824		
	11904-1	BC small		Batumi Seep	12:17		41:57.529	41:17.272	835				bubble catcher	
	11904-2	BC small		Batumi Seep	12:47		41:57.529	41:17.272	835				bubble catcher	
	11904-3	BC small		Batumi Seep	12:50		41:57.530	41:17.271	835				bubble catcher	
	11904-4	BC small		Batumi Seep	12:52		41:57.530	41:17.273	835				bubble catcher	
	11904-5	BC small		Batumi Seep	12:56		41:57.529	41:17.272	835				bubble catcher	
	11904-6	BC small		Batumi Seep	13:01		41:57.529	41:17.271	835				Sampled chimneys	
	11904-7	GBS-2		Batumi Seep	13:17		41:57.529	41:17.272	835				Gas bubble sampler II	
	11904-8	BC large		Batumi Seep	13:43		41:57.529	41:17.272	835				bubble catcher	
	11904-9	BC large		Batumi Seep	13:54		41:57.529	41:17.273	835				Sampled chimneys	
	11904-10	T-stick-1		Batumi Seep	14:15		41:57.529	41:17.271	835				T-stick in bubble flow	
	11904-11	T-stick-2		Batumi Seep	14:27		41:57.528	41:17.270	835				T-stick in bubble flow	
	11904-12	T-stick-3		Batumi Seep	14:35		41:57.529	41:17.271	835				T-stick 0,5 m from bubble hole	
	11904-13	Push core-1		Batumi Seep	15:02		41:57.529	41:17.270	835				Push Core No. 47; 20 cm from gas bubble hole	
	11904-14	Marker-1		Batumi Seep	15:16		41:57.528	41:17.271	835				Marker	
	11904-15	Push core-2		Batumi Seep	16:49		41:57.540	41:17.414	833				Push core 46	
	11904-16	GBS-3		Batumi Seep	17:33		41:57.541	41:17.413	833				Gas bubble sampler I	
22.03.07	**11905-1**	MUC-1	MUC	near Batumi Seep	05:29		41:57.249	41:16.716	895				no TV; liners empty	
	11905-2	MUC-2	MUC	near Batumi Seep	06:33		41:57.432	41:16.798	877				no TV	
	11906	DAPC-3	DAPC (I)	Batumi Seep	07:58		41:57.465	41:17.270	843				USBL; recovery 83 cm	
	11907	ROV-3	ROV-157	Batumi Seep	11:48	20:30	41:57.520	41:17.101	836	41:57.542	41:17.413	833		
	11907-1	BC small		Batumi Seep	16:02		41:57.542	41:17.529	834				small Bubble catcher (1 l/10 min)	
	11907-2	GBS-4		Batumi Seep	16:30		41:57.543	41:17.529	834				Gas bubble sampler (yellow)	
	11907-3	T-stick-1		Batumi Seep	16:51		41:57.543	41:17.529	834				T-stick (15 min duration)	
	11907-4	BC small		Batumi Seep	18:21		41:57.546	41:17.473	835				small Bubble catcher (1 l/12 min)	
	11907-5	GBS-5		Batumi Seep	18:33		41:57.544	41:17.472	835				Gas bubble sampler (red)	
	11907-6	Marker-2		Batumi Seep	18:59		41:57.544	41:17.472	835				Marker No. 2	
	11907-7	Push core-3		Batumi Seep	19:52		41:57.542	41:17.413	833				Push core 38	
	11907-8	Push core-4		Batumi Seep	19:58		41:57.543	41:17.413	833				Push core 46	
	11907-9	Push core-5		Batumi Seep	20:03		41:57.545	41:17.413	833				Push core 67	
	11907-10	Push core-6		Batumi Seep	20.13		41:57.542	41:17.413	833				Push core 68	
	11907-11	Marker-3		Batumi Seep	20:16		41:57.542	41:17.413	833				Marker No. 3	
24.03.07	11908	ROV-4	ROV-158	Egorov MV	14:52	18:55	44:23.548	35:15.499	1803	44:23.7491	35:15.964	1792		

Table A 1, continuation: Station list

R/V METEOR cruise M72/3a+b (Istanbul-Trabzon-Istanbul)														
Date	St. No.	St. No.			Start Sci:	End Sci:	Begin / on seafloor			End / off seafloor			Recovery	
	GeoB		Instruments	Location	Program	Program	N°	E°	depth (m)	N°	E°	depth (m)	Remarks	
25.03.07	**11909**	DAPC-4	DAPC (I)	Dvurechenskii MV	05:18		44:16.906	34:59.066	2056				USBL; no recovery (decive did not release)	
	11910	ROV-5	ROV-159	Dvurechenskii MV	08:04	17:57	44:16.901	34:59.292	2045	44:16.946	34:58.850	2042		
	11910-1	T-stick-1		Dvurechenskii MV	08:30		44:16.900	34:59.293	2046					
	11910-2	T-stick-2		Dvurechenskii MV	09:18		44:16.929	34:59.233	2045					
	11910-3	Push core-7		Dvurechenskii MV	09:21		44:16.929	34:59.232	2045				Push core No. 16	
	11910-4	T-stick-3		Dvurechenskii MV	09:54		44:16.946	34:59.175	2044					
	11910-5	T-stick-4		Dvurechenskii MV	10:45		44:16.977	34:59.085	2042					
	11910-6	Push core-8		Dvurechenskii MV	10:48		44:16.976	34:59.084	2042				Push core No. 60	
	11910-7	T-stick-5		Dvurechenskii MV	11:36		44:17.006	34:58.974	2042					
	11910-8	Push core-9		Dvurechenskii MV	11:41		44:17.006	34:58.974	2042				Push core No. 47	
	11910-9	T-stick-6		Dvurechenskii MV	12:27		44:17.019	34:58.929	2041					
	11910-10	T-stick-7		Dvurechenskii MV	13:14		44:17.029	34:58.880	2040					
	11910-11	Push core-10		Dvurechenskii MV	13:25		44:17.029	34:58.880	2040				Push core No. 46	
	11910-12	T-string-1		Dvurechenskii MV	16:55		44:16.972	34:58.910	2036				Thermistor temperature string recovered from mooring station	
	11910-13	T-stick 8		Dvurechenskii MV	17:39		44:16.947	34:58.850	2042					
26.03.07	**11911**	DAPC-5	DAPC (I)	Dvurechenskii MV	05:36		44:16.972	34:59.215	2058				USBL; Autoclave did not close; 251 cm recovery	
	11912	MUC-3	MUC	Dvurechenskii MV	13:50		44:17.015	34:58.885	2053					
	11913	GC-1	GC	Vodyanitskii MV	16:22		44:17.621	35:01.946	2048				USBL; Gas hydrates	
27.03.07	**11914**	DAPC-6	DAPC (I)	Dvurechenskii MV	05:28		44:16.987	34:59.097	2058				USBL; recovery 256 cm	
	11915	ROV-6	ROV-160	Dvurechenskii MV	08:08	16:46	44:16.803	34:58.606	2050	44:17.090	34:58.968	2016		
	11915-1	T-stick-1		Dvurechenskii MV	08:31		44:16.802	34:58.596	2052					
	11915-2	T-stick-2		Dvurechenskii MV	09:04		44:16.838	34:58.596	2043					
	11915-3	T-stick-3		Dvurechenskii MV	09:37		44:16.893	34:58.709	2043					
	11915-4	T-stick-4		Dvurechenskii MV	10:04		44:16.954	34:58.784	2041					
	11915-5	T-stick-5		Dvurechenskii MV	10:39		44:17.002	34:58.889	2040					
	11915-6	T-stick-6		Dvurechenskii MV	11:14		44:16.995	34:58.736	2042					
	11915-7	T-stick-7		Dvurechenskii MV	11:49		44:17.024	34:58.612	2042					
	11915-8	Push core-11		Dvurechenskii MV	11:57		44:17.023	34:58.610	2042				Push core No. 47	
	11915-9	Gas catcher-1		Dvurechenskii MV	12:12		44:17.021	34:58.613	2042				sediment sample (bacteria mat or carbonate)	
	11915-10	T-stick-8		Dvurechenskii MV	12:52		44:17.093	34:58.673	2043					
	11915-11	Push core-12		Dvurechenskii MV	12:59		44:17.090	34:58.674	2043				Push core No. 38	
	11915-12	Push core-13		Dvurechenskii MV	13:06		44:17.092	34:58.676	2043				Push core No. 67	
	11915-13	T-stick-9		Dvurechenskii MV	14:21		44:17.054	34:58.759	2042					
	11915-14	Push core-14		Dvurechenskii MV	14:26		44:17.061	34:58.760	2042				Push core No. 46	
	11915-15	Push core-15		Dvurechenskii MV	14:31		44:17.062	34:58.759	2042				Push core No. 16	
	11915-16	T-stick-10		Dvurechenskii MV	15:12		44:17.005	34:58.896	2040					
	11915-17	Push core-16		Dvurechenskii MV	15:14		44:17.007	34:58.896	2040				Push core No. 54	
	11915-18	Push core-17		Dvurechenskii MV	15:16		44:17.008	34:58.891	2040				Push core No. 46	
	11915-19	Push core-18		Dvurechenskii MV	15:21		44:17.008	34:58.895	2040				Push core No. 68	
	11915-20	T-stick-11		Dvurechenskii MV	15:45		44:17.052	34:58.842	2041					
	11915-21	Push core-19		Dvurechenskii MV	15:48		44:17.051	34:58.836	2041				Push core No. 55	
	11915-22	Push core-20		Dvurechenskii MV	15.51		44:17.052	34:58.845	2041				Push core No. 26	

Table A 1, continuation: Station list

R/V METEOR cruise M72/3a+b (Istanbul-Trabzon-Istanbul)							Begin / on seafloor			End / off seafloor			
Date	St. No.	St. No.			Start Sci.	End Sci.	Latitude	Longitude	Water	Latitude	Longitude	Water	Recovery
	GeoB		Instruments	Location	Program	Program	N°	E°	depth (m)	N°	E°	depth (m)	Remarks
28.03.07	**11916**	DAPC-7	DAPC (I)	Dvurechenskii MV	10:17		44:16.896	34:58.789	2057				USBL; recovery 253 cm
	11917	ROV-7	ROV-161	Vodyanitskii MV	13:28	21:57	44:17.618	35:01.942	1925	44:17.668	35:01.993	2031	
	11917-1	GBS-6		Vodyanitskii MV	16:35		44:17.656	34:01.992	2032				Gas bubble sampler-yellow
	11917-2	T-stick-1		Vodyanitskii MV	18:02		44:17.657	35:01.995	2032				
	11917-3	Push core-21		Vodyanitskii MV	18:12		44:17.658	35:01.992	2032				
30.03.07	**11918**	DAPC-8	DAPC (II)	Batumi Seep	10:30		41:57.547	41:17.427	840				USBL; first time DAPC-II used; recovery 233 cm
	11919	ROV-8	ROV-162	Batumi Seep	12:44	19:05	41:57.547	41:17.330	812	41:57.402	41:17.269	818	No Orion arm
	11919-1	Gas catcher-1		Batumi Seep	15:12		41:57.543	41:17.337	833				Small gas catcher
	11919-2	GBS-7		Batumi Seep	18:10		41:57.533	41:17.268	833				Gas bubble sampler
31.03.07	**11920**	DAPC-9	DAPC (I)	Batumi Seep	04:12		41:57.454	41:17.545	844				USBL failed; recovery 259 cm
	11921	ROV-9	ROV-163	Batumi Seep	05:55	19:24	41:57.400	41:17.267	844	41:57.542	41:17.840	833	No Orion arm
	11921-1	GBS-8		Batumi Seep	18:07		41:57.530	41:17.266	844				Gas bubble sampler
01.04.07	**11922**	DAPC-10	DAPC (I)	Colkheti Seep	05:53		41:58.071	41:06.214	1126				USBL
	11923	GC-2	GC	Colkheti Seep	07:47		41:58.120	41:06.250	1088				USBL; 6 m; plastic bag
	11924	GC-3	GC	Colkheti Seep	09:09		41:58.068	41:06.195	1056				USBL; 6 m; plastic bag
	11925	GC-4	GC	Batumi Seep	11:26		41:57.431	41:17.347	844				USBL; 6 m; plastic bag
	11926	GC-5	GC	Batumi Seep	12:28		41:57.416	41:17.345	849				USBL; 6 m; plastic bag
	11927	GC-6	GC	Batumi Seep	13:56		41:57.410	41:17.324	856				USBL; 6 m; plastic bag
02.04.07	**11928**	MUC-4	MUC	Shallow Ridge	13:39		41:42.332	41:28.174	379				no sediments in liners; devide did not release
	11929	MUC-5	MUC	Shallow Ridge	14:06		41:42.374	41:28.059	367				no sediments in liners; devide did not release
	11930	MUC-6	MUC	Shallow Ridge	14:51		41:42.386	41:27.938	382				no sediments in liners; devide did not release
	11931	MUC-7	MUC	Batumi Seep	16:50		41:47.838	41:16.842	839				8 MUC-liners completely filled
End Station work M72/3a													

Start station work M 72/3b													
05.04.07	07-001	Seismics	Gudauta High	16:03	16:28	42:47.854	42:46.421		40:09.671	40:09.890	1557		
	07-002A	Seismics	Gudauta High	16:40	19:57	42:45.923	42:39.318	1557	40:10.592	40:24.832	955		
	07-002B	Seismics	Gudauta High	21:12	21:40	42:37.90	42:38.29		40:27.90	40:28.98			
	07-003	Seismics	Gudauta High	21:46	22:46	42:38.475	42:41.021		40:28.877	40:26.602			
	11932	DTS-1	DTS	Gudauta High	23:00	06.04.07 / 05:18	42:41.250	40:25.730	1048	42:43.207	40:23.154	741	
	07-004	Seismics	Gudauta High	23:02	01:31	42:41.230	42:38.434		40:25.644	40:16.905			
06.04.07	07-005	Seismics	Gudauta High	02:26	05:03	42:38.055	42:42.892		40:18.284	40:22.558			
	07-006	Seismics	Gudauta High	06:34	07:45	42:42.613	42:38.135		40:23.620	40:19.818			
	11933	GC-7	GC	Gudauta High	10:31		42:40.262	40:22.631	690				USBL; recovery 380 cm
	11934	MUC-8	MUC	Gudauta High	11:37		42:40.260	40:22.678	701				USBL; recovery 57 cm
	07-007	Seismics	Batumi Seep	23:38	07.04.07 / 00:18	42:06.572	42:04.651		41:42.581	41:08.111			
07.04.07	07-008	Seismics	Batumi Seep	00:20	03:29	42:45.398	41:53.495		41:06.286	41:22.777			
	07-009	Seismics	Batumi Seep	03:46	04:49	41:52.846	41:56.486		41:22.167	41:17.276			
	07-010	Seismics	Batumi Seep	04:56	05:24	41:56.990	41:59.089		41:17.118	41:18.080			
	11935	DAPC-11	DAPC (II)	Batumi Seep	07:48		41:57.549	41:17.425	843				USBL; device lost pressure; no recovery

Table A 1, continuation: Station list

R/V METEOR cruise M72/3a+b (Istanbul-Trabzon-Istanbul)														
Date	St. No.	St. No.			Start Sci:	End Sci:	Begin / on seafloor			End / off seafloor				Recovery
	GeoB		Instruments	Location	Program	Program	N°	E°	depth (m)	N°	E°	depth (m)		Remarks
	11936	GC-8	GC	Batumi Seep	09:12		41:57.563	41:17.430	844					USBL; PVC-liner Segments for CT analysis (6 m); recovery 193 cm
	11937	DAPC-12	DAPC (I)	Batumi Seep	10:56		41:57.489	41:17.462	842					USBL; 41 cm recovery
	11938	GC-9	GC	Iberia Mound	12:55		41:52.340	41:10.036	982					USBL; recovery 134 cm
	11939	MUC-9	MUC	Iberia Mound	13:58		41:52.739	41:10.025	989					USBL; recovery 60 cm
08.04.07	**11940**	DTS-2	DTS	Batumi Seep	19:53	08.04.2007 / 09:18	41:57.647	41:17.247	854	41:58.75	41:20.68	885	USBL	
	11941	GC-10	GC	Pechori Mound	13:51		41:58.962	41:02.404	1014					USBL; recovery 83 cm
	11942	GC-11	GC	Pechori Mound	15:25		41:59.008	41:07.400	1024					USBL; no recovery
	11943	MUC-10	MUC	Pechori Mound	16:40		41:58.659	41:07.428	1014					USBL, no recovery
	11944	DAPC-13	DAPC (II)	Batumi Seep	19:04		41:57.554	41:17.654	841					USBL; device lost pressure
	11945	GC-12	GC	Batumi Seep	20:12		41:57.345	41:17.456	848					USBL; no recovery
		07-011	Seismics	Pechori Mound	22:27	23:03	41:58.573	41:12.48	1090	41:59.35	41:08.16	1262		
		07-012	Seismics	Pechori Mound	23:18	23:53	41:59.028	41:08.16	1282	41:57.21	41:04.28	1264		
09.04.07		07-013	Seismics	Pechori Mound	00:15	00:57	41:57.513	41:04.28	1264	41:59.78	41:09.78	1195		
		07-014	Seismics	Pechori Mound	01:14	02:03	41:59.781	41:09.78	1195	41:57.80	41:04.60	1307		
		07-015	Seismics	Pechori Mound	02:18	02:52	41:57.735	41:04.48	1282	41:59.61	41:08.61	1300		
		07-016	Seismics	Pechori Mound	02:57	03:19	41:59.641	41:08.61	1300	42:00.97	41:06.96	1328		
		07-017	Seismics	Pechori Mound	03:26	03:34	42:00.956	41:06.96	1328	42:00.46	41:06.21	1344		
		07-018	Seismics	Pechori Mound	03:41	04:18	42:00.258	41:06.21	1344	41:57.81	41:09.02			
		07-019	Seismics	Pechori Mound	04:30	05:19	41:57.885	41:09.02	--	42:01.05	41:06.31			
		07-020	Seismics	Pechori Mound	05:35	06:10	42:00.061	41:05.92	--	41:57.29	41:08.60			
		07-021	Seismics	Pechori Mound	06:20	07:08	41:57.608	41:08.86	--	42:00.89	41:06.01			
		07-022	Seismics	Pechori Mound	07:22	07:45	42:0.281	41:05.74	--	41:59.34	41:03.39			
	11946	GC-13	GC	Batumi Seep	10:52		41:57.532	41:17.582	842					USBL; PVC-liner Segments for CT analysis (6 m)
	11947	MUC-11	MUC	Batumi Seep	11:21		41:57.531	41:17.585	841					USBL; device did not release
	11948	MUC-12	MUC	Batumi Seep	12:20		41:57.531	41:17.578	843					USBL; device did not release
	11949	GC-14	GC	Batumi Seep	13:28		41:57.550	41:17.175	842					USBL; recovery
	11950	MUC-13	MUC	Batumi Seep	16:10		41:57.542	41:17.424	840					USBL; device did not release
	11951	DAPC-14	DAPC (II)	Batumi Seep	17:26		41:57.546	41:17.431	840					USBL; recovery 137 cm
	11952	GC-15	GC	Pechori Mound	19:27		41:58.955	41:07.539	1019					USBL; plastic hose (6 m), no recovery
	11953	GC-16	GC	Pechori Mound	20:32		41:58.958	41:07.543	1015					USBL; PVC liner segments for CT analysis (3 m); recovery 335 cm
		07-023	Seismics	Batumi Seep	22:32	22:47	41:56.202	41:55.671		41:15.533	41:17.109			3D-Seismics Batumi, Part 1
		07-024	Seismics	Batumi Seep	22:55	23:26	41:55.922	41:58.206		41:17.752	41:19.338			
		07-025	Seismics	Batumi Seep	23:43	10.04.07 / 00:02:00	41:58.330	41:56.964		41:18.291	41:17.345			
10.04.07		07-026	Seismics	Batumi Seep	00:13	00:47	41:56.806	41:59.270		41:18.050	41:19.803			
		07-027	Seismics	Batumi Seep	00:55	01:38	41:59.653	41:56.943		41:19.541	41:16.988			
		07-028	Seismics	Batumi Seep	01:55	02:17	41:56.958	41:58.404		41:17.982	41:18.962			
		07-029	Seismics	Batumi Seep	02:32	02:51	41:58.513	41:57.072		41:18.000	41:16.999			
		07-030	Seismics	Batumi Seep	03:03	03:24	41:56.804	41:58.472		41:17.647	41:18.812			
		07-031	Seismics	Batumi Seep	03:37	03:58	41:58.687	41:57.101		41:17.922	41:16.821			

Table A 1, continuation: Station list

R/V METEOR cruise M72/3a+b (Istanbul-Trabzon-Istanbul)						Begin / on seafloor			End / off seafloor			
Date	St. No.	St. No.		Start Sci:	End Sci:	Latitude	Longitude	Water	Latitude	Longitude	Water	Recovery
	GeoB		Instruments	Location	Program	Program	N°	E°	depth (m)	N°	E°	depth (m)	Remarks
		07-032	Seismics	Batumi Seep	04:10	04:35	41:56.823	41:58.532		41:17.522	41:18.752		
		07-033	Seismics	Batumi Seep	04:48	05:09	41:58.793	41:57.230		41:17.787	41:16.706		
		07-034	Seismics	Batumi Seep	05:23	05:40	41:57.081	41:58.429		41:17.707	41:18.582		
		07-035	Seismics	Batumi Seep	05:56	06:16	41:58.731	41:57.224		41:17.542	41:16.505		
		07-036	Seismics	Batumi Seep	06:32	06:50	41:57.277	41:58.621		41:17.380	41:18.303		
		07-037	Seismics	Batumi Seep	07:01	07:24	42:00.281	41:03.505		41:59.405	41:05.543		
		07-038	Seismics	Batumi Seep	07:35	07:57	41:56.202	41:17.28		41:55.672	41:18.39		
		07-039	Seismics	Batumi Seep	08:09	08:30	41:55.922	41:17.81		41:58.206	41:16.75		
		07-040	Seismics	Batumi Seep	08:43	09:03	41:58.330	41:17.47		41:56.964	41:18.53		
		07-041	Seismics	Batumi Seep	09:14	09:36	41:56.806	41:17.97		41:59.270	41:16.89		
		07-042	Seismics	Batumi Seep	09:46	10:07	41:59.653	41:17.49		41:56.943	41:18.57		
		07-043	Seismics	Batumi Seep	10:18	10:39	41:56.958	41:18.01		41:58.405	41:16.90		
		07-044	Seismics	Batumi Seep	10:53	11:13	41:58.513	41:17.57		41:57.072	41:18.59		
		07-045	Seismics	Batumi Seep	11:25	11:46	41:56.804	41:18.04		41:58.473	41:17.00		
		07-046	Seismics	Batumi Seep	11:59	12:20	41:58.687	41:17.65		41:57.102	41:18.65		
		07-047	Seismics	Batumi Seep	12:32	12:54	41:56.823	41:18.11		41:58.533	41:14.05		
		07-048	Seismics	Batumi Seep	13:06	13:27	41:58.793	41:17.68		41:57.230	41:18.77		
		07-049	Seismics	Batumi Seep	13:37	14:00	41:57.081	41:18.17		41:58.429	41:17.00		
		07-050	Seismics	Batumi Seep	14:11	14:31	41:58.732	41:17.71		41:57.224	41:18.80		
		07-051	Seismics	Batumi Seep	14:43	15:06	41:57.277	41:17.94		41:58.621	41:16.81		
		07-052	Seismics	Batumi Seep	15:15	15:36	41:57.02	41:17.46		41:58.66	41:18.57		
		07-053	Seismics	Batumi Seep	15:46	16:07	41:58.66	41:17.87		41:57.15	41:16.81		
		07-054	Seismics	Batumi Seep	16:17	16:38	41:57.06	41:17.40		41:58.70	41:18.49		
		07-055	Seismics	Batumi Seep	16:48	17:09	41:58.68	41:17.84		41:57.11	41:16.74		
		07-056	Seismics	Batumi Seep	17:20	17:20	41:56.99	41:17.29		41:48.63	41:18.43		
		07-057	Seismics	Batumi Seep	17:51	18:12	41:58.71	41:17.76		41:57.21	41:16.71		
		07-058	Seismics	Batumi Seep	18:21	18:42	41:57.04	41:17.24		41:58.61	41:18.33		
		07-059	Seismics	Batumi Seep	18:53	19:13	41:58.72	41:17.72		41:57.21	41:16.65		
		07-060	Seismics	Batumi Seep	19:22	19:43	41:57.05	41:17.17		41:58.64	41:18.29		
		07-061	Seismics	Batumi Seep	19:53	20:14	41:58.79	41:17.70		41:57.24	41:16.63		
		07-062	Seismics	Batumi Seep	20:26	20:44	41:57.17	41:17.11		41:58.67	41:18.15		
		07-063	Seismics	Batumi Seep	20:54	21:15	41:58.78	41:17.62		41:57.29	41:16.58		
		07-064	Seismics	Batumi Seep	21:27	21:46	41:57.13	41:17.14		41:58.63	41:18.16		
		07-065	Seismics	Batumi Seep	21:58	22:20	41:59.78	41:17.61		41:57.28	41:16.55		
		07-066	Seismics	Batumi Seep	22:33	22:54	41:57.11	41:17.16		41:58.63	41:18.31		
		07-067	Seismics	Batumi Seep	23:07	23:29	41:58.79	41:17.67		41:57.26	41:16.59		
		07-068	Seismics	Batumi Seep	23:41	00:02	41:57.10	41:17.18		41:58.63	41:18.25		
		07-069	Seismics	Batumi Seep	00:14	00:36	41:58.76	41:17.66		41:57.26	41:16.63		
		07-070	Seismics	Batumi Seep	00:49	01:09	41:57.13	41:17.25		41:58.23	41:18.02		
		07-071	Seismics	Batumi Seep	01:20	01:41	41:58.76	41:17.70		41:57.21	41:16.63		
		07-072	Seismics	Batumi Seep	01:53	02:13	41:57.12	41:17.29		41:58.65	41:18.34		
		07-073	Seismics	Batumi Seep	02:26	02:46	41:58.74	41:17.71		41:57.21	41:16.67		
		07-074	Seismics	Batumi Seep	02:58	03:18	41:57.07	41:17.30		41:58.63	41:18.37		

Table A 1, continuation: Station list

R/V METEOR cruise M72/3a+b (Istanbul-Trabzon-Istanbul)														
Date	St. No.	St. No.			Start Sci:	End Sci:	Begin / on seafloor			End / off seafloor			Recovery	
	GeoB		Instruments	Location	Program	Program	N°	E°	depth (m)	N°	E°	depth (m)	Remarks	
		07-075	Seismics	Batumi Seep	03:29	03:49	41:58.73	41:17.76		41:57.20	41:16.69			
		07-076	Seismics	Batumi Seep	04:01	04:21	41:57.06	41:17.33		41:58.59	41:18.40			
		07-077	Seismics	Batumi Seep	04:33	04:54	41:58.68	41:17.75		41:57.18	41:16.74			
11.04.07	11954	MIC-1	MIC	Pechori Mound	07:18		41:58.964	41:07.541	1024				USBL; recovery 57 cm	
	11955	GC-17	GC	Pechori Mound	08:25		41:58.963	41:07.540	1012				USBL; PVC-liner (3 m); recovery 144 cm	
	11956	GC-18	GC	Batumi Seep	10:14		41:57.450	14:17.436	843				USBL; PVC-liner Segments for CT analysis (3 m); recovery 110 cm	
	11957	GC-19	GC	background Batumi Seep	11:28		41:57.803	41:18.001	844				USBL; PCV liner Segments (1 m) for home analysis (6 m total)	
	11958	DAPC-15	DAPC (I)	Batumi Seep	13:09		41:57.448	41:17.446	845				USBL; recovery 146 cm	
	11959	MIC-2	MIC	Batumi Seep	15:32		41:57.533	41:17.568	840				USBL; recovery 58 cm	
	11960	MIC-3	MIC	Offshore Kobuleti	18:03		42:00.351	41:27.997	523				USBL; recovery 59 cm	
	11961	DTS-3	DTS	Batumi Seep	20:50	12.04.07 / 09:26	41:58.080	41:19.370	911	42:03.866	41:03.557	1372	410 kHz survey on Batumi continued (GeoB 11940)	
12.04.07	11962	MIC-4	MIC	Batumi Seep	11:22		41:57.548	41:17.435	838				USBL; 1 liner filled	
	11963	DAPC-16	DAPC (I)	Batumi Seep	13:49		41:57.410	41:17.278	853				USBL failed; 169 cm recovery	
	11964	MIC-5	MIC	Batumi Seep	15:27		41:57.414	41:17.360	847				USBL failed; 51 cm recovery	
	11965	MIC-6	MIC	Batumi Seep	16:31		41:57.447	41:17.437	843				USBL failed; 27cm recovery	
	11966	MIC-7	MIC	Batumi Seep	17:23		41:57.614	41:17.512	847				No USBL; 4 liners recovery	
	11967	GC-20	GC	Batumi Seep	18:51		41:57.530	41:17.268	843				USBL; no recovery; some carbonate pieces in core catcher	
		07-078	Seismics	Batumi Seep	20:29	20:49	41:57.04	41:17.36		41:58.56	41:18.40		3D-Seismics Batumi, part 2	
		07-079	Seismics	Batumi Seep	20:59	21:21	41:58.71	41:17.82		41:57.19	41:16.78			
		07-080	Seismics	Batumi Seep	21:33	21:52	41:57.00	41:17.37		41:58.54	41:18.42			
		07-081	Seismics	Batumi Seep	22:03	22:24	41:58.70	41:17.86		41:57.16	41:16.81			
		07-082	Seismics	Batumi Seep	22:36	22:56	41:57.00	41:17.41		41:58.52	41:18.45			
		07-083	Seismics	Batumi Seep	23:09	23:29	41:58.67	41:17.90		41:57.16	41:16.84			
		07-084	Seismics	Batumi Seep	23:41	13.04.07 / 00:02:00	41:57.00	41:17.44		41:58.51	41:18.49			
13.04.07		07-085	Seismics	Batumi Seep	00:14	00:35	41:58.64	41:17.91		41:57.14	41:16.86			
		07-086	Seismics	Batumi Seep	00:47	01:08	41:56.99	41:17.48		41:58.58	41:18.58			
		07-087	Seismics	Batumi Seep	01:21	01:40	41:58.59	41:17.90		41:57.13	41:16.89			
		07-088	Seismics	Batumi Seep	01:51	02:11	41:56.98	41:17.53		41:58.51	41:18.59			
		07-089	Seismics	Batumi Seep	02:24	02:46	41:58.66	41:18.01		41:57.10	41:16.91			
		07-090	Seismics	Batumi Seep	02:57	03:18	41:56.97	41:17.57		41:58.54	41:18.65			
		07-091	Seismics	Batumi Seep	03:30	03:50	41:58.64	41:18.03		41:57.09	41:16.97			
		07-092	Seismics	Batumi Seep	04:01	04:21	41:56.94	41:17.57		41:58.50	41:18.64			
		07-093	Seismics	Batumi Seep	04:35	04:56	41:58.61	41:18.06		41:57.08	41:16.99			
		07-094	Seismics	Batumi Seep	05:03	05:23	41:57.28	41:16.80		41:58.78	41:17.85			
		07-095	Seismics	Batumi Seep	05:36	05:57	41:58.63	41:18.16		41:57.04	41:17.08			
		07-096	Seismics	Batumi Seep	06:14	07:37	41:56.46	41:16.56		41:52.15	41:09.08			
		07-097	Seismics	Batumi Seep	07:41	07:53	41:51.8	41:09.05		41:51.57	41:10.39			
		07-098	Seismics	Batumi Seep	08:04	08:28	41:51.69	41:10.99		41:53.42	41:09.65			
		07-099	Seismics	Batumi Seep	08:37	09:04	41:53.21	41:09.35		41:51.22	41:10.74			

Table A 1, continuation: Station list

R/V METEOR cruise M72/3a+b (Istanbul-Trabzon-Istanbul)														
Date	St. No.	St. No.			Start Sci:	End Sci:	Begin / on seafloor			End / off seafloor			Recovery	
	GeoB		Instruments	Location	Program	Program	Latitude N°	Longitude E°	Water depth (m)	Latitude N°	Longitude E°	Water depth (m)	Remarks	
		07-100	Seismics	Batumi Seep	09:23	11:03	41:51.57	41:10.74		41:59.41	41:05.26			
		07-101	Seismics	Batumi Seep	11:24	11:53	41:59.27	41:05.19		41:56.88	41:06.86			
	11968	MIC-8	MIC	Pechori Mound	14:05		41:58.961	41:07.543	1022				USBL; device did not release; recovery 43 cm	
	11969	MIC-9	MIC	Pechori Mound	15:39		41:58.962	41:07.541					USBL; recovery 41 cm	
	11970	MIC-10	MIC	Colkheti Seep	17:18		41:58.069	41:06.191	1118				USBL; 3 liners full; recovery 34 cm	
	11971	GC-21	GC	Colkheti Seep	18:22		41:58.069	41:06.199	1124				USBL; PVC-liner (3 m); recovery 151 cm	
	11972	DAPC-17	DAPC (II)	Batumi Seep	20:32		41:57.541	41:17.428	841				USBL; device did not release	
	11973	DAPC-18	DAPC (II)	Batumi Seep	21:21		41:57.544	41:17.430	840				USBL; decive maintained pressure	
	11974	GC-22	GC	Reference Station	22:36		41:57.428	41:16.803	884				USBL; PVC-liner (6 m), recovery 697 cm; reference station near Batumi Seep	
14.04.07	11975	GC-23	GC	Batumi Seep	00:05		41:57.528	41:17.588	844				USBL; plastic hose (3 m); recovery 304 cm	
15.04.07		07-102	Seismics	Andrusov Ridge	00:24	05:14	42:27.85	36:48.85		42:46.99	36:29.77			
		07-103	Seismics	Andrusov Ridge	05:29	06:16	42:46.29	36:30.67						
		07-104	Seismics	Dvurechenskii MV	18:07	18:36	44:13.49	35:01.40		44:15.04	34:59.00			
		07-105	Seismics	Dvurechenskii MV	18:36	19:20	44:15.04	34:59.00		44:18.70	34:59.01			
		07-106	Seismics	Dvurechenskii MV	19:34	20:04	44:18.44	34:59.95		44:15.95	35:00.00			
		07-107	Seismics	Dvurechenskii MV	20:24	20:48	44:16.00	34:58.24		44:18.00	34:58.24			
		07-108	Seismics	Dvurechenskii MV	21:01	21:26	44:17.97	34°58.67		44:15.98	34:58.75			
		07-109	Seismics	Dvurechenskii MV	21:41	22:06	44:16.00	34:59.23		44:17.99	34:5925			
		07-110	Seismics	Dvurechenskii MV	22:25	22:49	44:17.98	34:58.05		44:15.97	34:58.48			
		07-111	Seismics	Dvurechenskii MV	23:05	23:31	44:16.01	34:59.12		44:18.02	34:59.11			
		07-112	Seismics	Dvurechenskii MV	23:46	00:11	44:17.98	34:58.62		44:15.96	34:58.61			
16.04.07		07-113	Seismics	Dvurechenskii MV	00:23	00:48	44:16.00	34:59.04		44:18.00	34:59.04			
		07-114	Seismics	Dvurechenskii MV	01:04	01:30	44:17.86	34:58.38		44:15.77	34:58.36			
		07-115	Seismics	Dvurechenskii MV	01:45	02:10	44:16.12	34:58.97		44:18.25	34:58.96			
		07-116	Seismics	Dvurechenskii MV	02:25	02:50	44:18.00	34:58.12		44:15.76	34:58.11			
		07-117	Seismics	Dvurechenskii MV	03:06	03:33	44:16.00	34:58.85		44:18.25	34:58.85			
		07-118	Seismics	Dvurechenskii MV	03:46	04:15	44:17.96	34:58.43		44:15.77	34:58.45			
		07-119	Seismics	Dvurechenskii MV	04:27	04:53	44:15.99	34:58.92		44:18.21	34:58.91			
		07-120	Seismics	Dvurechenskii MV	05:07	05:34	44:17.98	34:58.56		44:15.90	34:58.57			
		07-121	Seismics	Dvurechenskii MV	05:46	06:11	44:16.15	34:59.18		44:18.19	34:59.18			
		07-122	Seismics	Dvurechenskii MV	06:20	06:46	44:17.96	34:58.68		44:15.79	34:58.692			
		07-123	Seismics	Dvurechenskii MV	06:57	07:23	44:16.06	34:59.30		44:18.20	34:59.29			
		07-124	Seismics	Dvurechenskii MV	07:33	07:58	44:17.98	34:58.79		44:15.67	34:58.79			
	11976	MIC-11	MIC	Dvurechenskii MV	10:28		44:16.807	34:58.906	2052				No USBL; ship position; target ca. 12 meter sw'; recovery 46 cm	
	11977	MIC-12	MIC	Dvurechenskii MV	12:33		44:16.885	34:58.906	2052				No USBL; ship position; target ca. 12 meter sw'; recovery 52 cm	
	11978	MIC-13	MIC	Dvurechenskii MV	14:30		44:16.944	34:58.902	2050				No USBL; ship position; target ca. 12 meter sw'; recovery 56 cm	
	11979	MIC-14	MIC	Dvurechenskii MV	16:31		44:17.025	34:58.879	2048				No USBL; ship position; target ca. 12 meter sw'; recovery 40 cm	
	11980	GC-24	GC	Vodyanitskii MV	18:55		44:17.659	35:01.965	2039				USBL; PVC-liner Segments for CT analysis (3 m)	

Table A 1, continuation: Station list

R/V METEOR cruise M72/3a+b (Istanbul-Trabzon-Istanbul)														
Date	St. No.	St. No.			Start Sci.	End Sci.	Begin / on seafloor			End / off seafloor			Recovery	
	GeoB		Instruments	Location	Program	Program	Latitude N°	Longitude E°	Water depth (m)	Latitude N°	Longitude E°	Water depth (m)	Remarks	
	11981	DAPC-19	DAPC (I)	Vodyanitskii MV	21:04		44:17.650	35:01.979	2037				USBL; recovery 78 cm	
17.04.07		07-125	Seismics	Kerch Strait	07:23	09:17	44:48.04	36:03.16		44:41.10	35:53.90			
		07-126	Seismics	Kerch Strait	09:36	11:31	44:40.63	35:55.06		44:45.72	36:06.10			
		07-127	Seismics	Kerch Strait	11:35	13:24	44:45.71	36:06.55		44:39.75	36:15.95			
		07-128	Seismics	Kerch Strait	13:24	14:29	44:39.75	36:15.95		44:37.40	36:23.33			
		07-129	Seismics	Kerch Strait	14:29	17:18	44:37.40	36:23.33		44:23.01	36:28.27			
		07-130	Seismics	Kerch Strait	17:18	20:30	44:23.01	36:28.27		44:28.82	36:07.41			
		07-131	Seismics	Kerch Strait	20:36	22:35	44:26.61	36:07.02		41:19.46	36:10.14			
		07-132	Seismics	Kerch Strait	22:38		44:19.59	36:10.28						
18.04.07		07-133	Seismics	Kerch Strait	2:45	4:43	44:37.31	36:21.64		44:27.50	36:18.46			
	11982	DTS-3	DTS	Kerch Strait	06:58	08:27	44:28.011	36:18.800	724	44:26.803	36:22.681	767	USBL; DTS failed	
		07-134	Seismics	Kerch Strait	07:27	07:49	44:27.52	36:20.09		44:28.25	36:21.01			
		07-135	Seismics	Kerch Strait	07:49	10:30	44:28.25	36:21.01		44:25.23	36:29.06			
		07-136	Seismics	Kerch Strait	15:07	17:32	44:34.55	36:48.26		44:44.29	35:40.23			
		07-137	Seismics	Kerch Strait	17:41	18:10	44:44.25	35:39.08		44:43.73	35:35.91			
		07-138	Seismics	Kerch Strait	18:13	20:14	44:43.12	35:35.75		44:34.99	35:44.71			
		07-139	Seismics	Kerch Strait	20:20	21:46	44:34.71	35:44.49		44:36.07	35:35.21			
		07-140	Seismics	Kerch Strait	21:52	00:01	44:36.22	35:35.06		44:40.40	35:48.63			
19.04.07		07-141	Seismics	Kerch Strait	00:22	1:31	44:39.12	35°48.15		44:36.77	35:40.78			
		07-142	Seismics	Kerch Strait	2:01	2:10	44:37.40	35:42.30		44:38.06	35:42.67			
	11983	MIC-15	MIC	Kerch Strait	03:39		44:39.607	35:42.519	747				USBL; liner full	
	11984	MIC-16	MIC	Kerch Strait	06:03		44:29.999	35:49.998	1341				USBL; liner full	
	11985	MIC-17	MIC	Kerch Strait	09:12		44:45.008	36:09.995	95				USBL; liner full	
	11986	MIC-18	MIC	Kerch Strait	10:19		44:46.007	36:01.998	173				USBL; liner full	
	11987	GC-25	GC	Kerch Strait	13:10		44:37.138	35:42.249	894				USBL; recovery 157 cm	
	11988	GC-26	GC	Kerch Strait	15:17		44:37.207	35:42.291	889				USBL; recovery 293 cm	
		07-143	Seismics	Kerch Strait	17:11	17:26	44:38.42	35:42.25		44:38.32	35:43.63			
		07-144	Seismics	Kerch Strait	17:30	18:58	44:38.14	35:43.92		44:31.94	35:48.25			
		07-145	Seismics	Kerch Strait	19:05	20:13	44:31.70	35:47.72		44:33.64	35:40.18			
		07-146	Seismics	Kerch Strait	20:17	20:50	44:33.90	35:40.08		44:36.49	35:40.60			
		07-147	Seismics	Kerch Strait	20:55	21:30	44:36.66	35:40.18		44:37.12	35:36.30			
		07-148	Seismics	Kerch Strait	21:33	23:15	44:37.17	35:36.51		44:40.48	35:46.62			
		07-149	Seismics	Kerch Strait	23:26	00:19	44:40.86	35:45.96		44:38.86	35:39.48			
20.04.07		07-150	Seismics	Kerch Strait	00:26	00:42	44:38.47	35:39.59		44:37.49	35:40.82			
		07-151	Seismics	Kerch Strait	00:46	00:56	44:37.49	35:41.19		44:37.85	35:42.20			
		07-152	Seismics	Kerch Strait	00:59	01:26	44:38.03	35:42.39		44:39.87	35:40.70			
		07-153	Seismics	Kerch Strait	01:38	02:08	44:40.19	35:41.63		44:37.90	35:43.50			
		07-154	Seismics	Kerch Strait	02:10	02:20	44:37.91	35:43.68		44:38.29	35:44.32			
		07-155	Seismics	Kerch Strait	02:23	02:43	44:38.50	35:44.18		44:40.05	35:43.12			
		07-156	Seismics	Kerch Strait	02:55	03:22	44:39.75	35:42.82		44:38.01	35:44.01			
	11989	GC-27	GC	Kerch Strait	06:21		44:37.203	35:42.260	888				USBL; recovery 289 cm	
	11990	GC-28	GC	Vodyanitskii MV	10:59		44:17.623	35:01.946	2061				USBL; recovery 153 cm	
	11991	DAPC-20	DAPC (I)	Vodyanitskii MV	12:58		44:17.625	35:01.949	2052				USBL; no recovery	
	11992	DAPC-21	DAPC (I)	Vodyanitskii MV	14:49		44:17.630	35:01.932	2055				USBL; recovery 177 cm	

Table A 1, continuation: Station list

R/V METEOR cruise M72/3a+b (Istanbul-Trabzon-Istanbul)													
Date	St. No.	St. No.			Start Sci:	End Sci:	Begin / on seafloor			End / off seafloor			Recovery
	GeoB		Instruments	Location	Program	Program	Latitude N°	Longitude E°	Water depth (m)	Latitude N°	Longitude E°	Water depth (m)	Remarks
	11993	MIC-19	MIC	Vodyanitskii MV	17:10		44:17.627	35:01.948	2067				USBL; liner full
	11994	DAPC-22	DAPC (II)	Dvurechenskii MV	19:33		44:16.995	34:59.096	1994				USBL
	11995	MIC-20	MIC	Dvurechenskii MV	22:21		44:17.034	34:58.951	1977				USBL; liner full
21.04.07	**11996**	DTS-4	DTS	Sorokin Trough	02:19	07:42	44:18.768	35:06.141	1982	44:17.50	34:45.24		USBL failed during the survey
	11997	MIC-21	MIC	Dvurechenskii MV	12:59		44:17.060	34:59.036	2050				USBL; liner full
	11998	GC-29	GC	Dvurechenskii MV	14:41		44:16.998	34:59.090	2052				USBL; to be opened
	11999	DAPC-23	DAPC-(I)	Dvurechenskii MV	17:07		44:16.892	34:58.902	2049				USBL; recovery 256 cm

Abbreviations:

GC: Gravity corer

DAPC (I): Dynamic autoclave piston corer I

DAPC (II): Dynamic autoclave piston corer II

MUC: Multicorer

MIC: Minicorer

ROV: Remotely operated vehicle QUEST

DTS: Sidescan Sonar

Seismics: Seismics

USBL: Ultra-short base line (Underwater positioning system)

ROV samples / tools:

Push core 1,2,3…

Pressure sampler

T-stick 1,2,3

Gas bubble sampler (GBS) 1-2

Bubble catcher (BC) small (s), large (l)

Table A 2.1: Positions of Gudauta seeps detected during M72/3b.

No.	Date	Time	Lat. [°N]	Lon. [°N]	Water Depth [m]	Height [m]
1	05.04.2007	09:41:10	42:40.500	40:22.518	676.95	299.57
2	05.04.2007	09:43:31	42:40.465	40:22.498	671.77	175.07
3	05.04.2007	09:44:51	42:40.443	40:22.485	666.58	299.57
4	05.04.2007	09:45:13	42:40.438	40:22.480	667.88	405.91
5	05.04.2007	09:46:22	42:40.418	40:22.468	669.17	508.36
6	05.04.2007	09:47:19	42:40.403	40:22.457	666.58	408.51
7	05.04.2007	09:48:05	42:40.390	40:22.448	666.58	504.47
8	05.04.2007	09:49:35	42:40.365	40:22.428	665.28	404.62
9	05.04.2007	09:50:43	42:40.345	40:22.413	661.39	377.38
10	05.04.2007	09:52:35	42:40.312	40:22.387	660.10	448.71
11	05.04.2007	09:53:36	42:40.293	40:22.370	663.99	403.32
12	05.04.2007	09:54:47	42:40.273	40:22.350	669.17	523.93
13	05.04.2007	11:01:24	42:39.073	40:19.542	693.81	232.14
14	05.04.2007	11:02:41	42:39.108	40:19.452	684.74	287.90
15	05.04.2007	11:03:13	42:39.123	40:19.413	682.14	182.86
16	05.04.2007	18:42:20	42:41.035	40:21.148	579.69	152.09
17	05.04.2007	19:01:55	42:40.593	40:21.993	630.27	143.95
18	05.04.2007	19:03:40	42:40.555	40:22.070	638.05	475.94
19	05.04.2007	19:04:07	42:40.545	40:22.090	639.35	442.23
20	05.04.2007	19:04:52	42:40.530	40:22.125	640.64	437.04
21	05.04.2007	19:06:14	42:40.498	40:22.187	647.13	462.98
22	05.04.2007	19:06:44	42:40.490	40:22.210	648.42	429.26
23	05.04.2007	19:07:21	42:40.477	40:22.238	651.02	402.02
24	05.04.2007	19:07:53	42:40.465	40:22.263	652.31	343.66
25	05.04.2007	19:09:10	42:40.437	40:22.320	662.69	351.45
26	05.04.2007	19:10:01	42:40.417	40:22.358	660.10	440.93
27	05.04.2007	19:11:01	42:40.397	40:22.405	670.47	508.36
28	05.04.2007	19:11:47	42:40.380	40:22.440	666.58	418.88
29	05.04.2007	19:13:18	42:40.350	40:22.512	666.58	482.43
30	05.04.2007	19:14:36	42:40.323	40:22.573	676.95	521.33
31	05.04.2007	19:15:37	42:40.303	40:22.622	678.25	386.46
32	05.04.2007	19:15:56	42:40.298	40:22.638	676.95	387.76
33	05.04.2007	19:17:33	42:40.267	40:22.718	684.74	198.42

Table A 2.2: Positions of Pechori seeps detected during M72/3b.

No.	Date	Time	Lat. [°N]	Lon. [°N]	Water Depth [m]	Height [m]
1	08.04.2007	23:18:15	41:59.017	41:07.690	1012.31	577.11
2	08.04.2007	23:18:54	41:58.988	41:07.633	1004.74	692.53
3	08.04.2007	23:20:11	41:58.933	41:07.517	1014.20	686.86
4	08.04.2007	23:21:15	41:58.887	41:07.420	1008.52	626.31
5	08.04.2007	23:35:01	41:58.282	41:06.210	1114.48	565.76
6	08.04.2007	23:35:56	41:58.242	41:06.132	1116.38	571.43
7	08.04.2007	23:37:19	41:58.182	41:06.015	1118.27	497.64
8	09.04.2007	00:24:45	41:57.968	41:06.242	1097.45	427.63
9	09.04.2007	02:26:42	41:58.163	41:05.985	1122.05	543.05
10	09.04.2007	02:27:54	41:58.223	41:06.097	1112.59	412.49
11	09.04.2007	02:29:00	41:58.278	41:06.202	1112.59	633.87
12	09.04.2007	02:41:21	41:58.870	41:07.423	1008.52	544.94
13	09.04.2007	02:41:54	41:58.897	41:07.477	1014.20	618.74
14	09.04.2007	02:43:03	41:58.950	41:07.590	999.06	569.54
15	09.04.2007	02:43:55	41:58.992	41:07.675	1012.31	437.09
16	09.04.2007	03:58:05	41:59.022	41:07.377	1002.85	537.38
17	09.04.2007	03:58:27	41:58.995	41:07.398	1004.74	618.74
18	09.04.2007	03:59:08	41:58.943	41:07.438	1008.52	459.80
19	09.04.2007	03:59:47	41:58.897	41:07.477	1010.42	696.32
20	09.04.2007	04:00:45	41:58.825	41:07.533	1008.52	728.48
21	09.04.2007	05:49:31	41:58.970	41:07.092	1072.86	410.60
22	09.04.2007	06:40:10	41:58.910	41:07.780	1023.66	372.76
23	09.04.2007	06:41:05	41:58.973	41:07.732	1017.98	596.03
24	09.04.2007	06:41:44	41:59.017	41:07.697	1014.20	357.62

Table A 2.3: Positions of Kerch Strait seeps during M72/3a and 3b.

No.	Date	Time	Lat. [°N]	Lon. [°N]	Water Depth [m]	Height [m]
1	23.03.2007	23:31:01	44:33.477	36:22.467	362.5	158.8
2	23.03.2007	23:32:00	44:33.573	36:22.443	362.5	266.0
3	23.03.2007	23:35:00	44:33.910	36:22.365	349.8	50.7
4	23.03.2007	23:51:01	44:36.158	36:21.827	247.5	83.8
5	23.03.2007	23:57:01	44:36.967	36:21.630	166.6	41.9
6	24.03.2007	00:26:00	44:40.673	36:20.785	107.2	52.6
7	24.03.2007	01:23:01	44:39.903	36:11.900	297.2	115.0
8	24.03.2007	01:27:00	44:39.710	36:11.160	414.1	106.2
9	24.03.2007	01:35:00	44:39.398	36:09.828	491.1	40.0
10	24.03.2007	01:42:00	44:39.060	36:08.468	560.3	98.4
11	24.03.2007	01:46:00	44:38.895	36:07.670	573.9	249.5
12	24.03.2007	01:48:00	44:38.817	36:07.365	571.0	170.5
13	24.03.2007	01:49:00	44:38.747	36:07.117	587.6	110.1
14	24.03.2007	01:51:00	44:38.627	36:06.718	628.5	248.5
15	24.03.2007	01:53:00	44:38.562	36:06.448	649.0	213.4
16	24.03.2007	01:53:00	44:38.535	36:06.327	655.8	217.3
17	24.03.2007	02:11:00	44:37.693	36:02.967	735.7	178.3
18	24.03.2007	02:13:00	44:37.602	36:02.582	737.6	137.4
19	24.03.2007	02:15:00	44:37.528	36:02.277	731.8	52.6
20	24.03.2007	03:01:00	44:41.158	36:00.008	686.0	139.3
21	24.03.2007	03:06:00	44:41.887	36:00.003	653.8	196.8
22	24.03.2007	03:07:00	44:41.967	35:59.997	626.6	228.0
23	24.03.2007	03:07:00	44:42.038	35:59.993	614.9	199.8
24	24.03.2007	03:08:00	44:42.190	35:59.990	582.7	154.0
25	24.03.2007	03:09:00	44:42.283	35:59.987	555.4	170.5
26	24.03.2007	03:11:00	44:42.542	35:59.975	493.1	194.9
27	24.03.2007	03:14:00	44:42.960	35:59.970	407.3	249.5
28	24.03.2007	03:22:00	44:43.902	35:59.975	297.2	78.0
29	24.03.2007	03:48:00	44:45.477	35:58.160	229.0	83.8
30	24.03.2007	03:50:00	44:45.363	35:57.700	263.1	70.2
31	24.03.2007	03:52:00	44:45.245	35:57.317	273.8	116.0
32	24.03.2007	03:56:00	44:45.037	35:56.705	244.6	64.3
33	24.03.2007	03:56:00	44:45.002	35:56.600	238.7	97.4
34	24.03.2007	04:02:00	44:44.717	35:55.578	331.3	32.2
35	24.03.2007	04:03:01	44:44.645	35:55.288	353.7	174.4
36	24.03.2007	04:16:01	44:43.902	35:52.990	544.7	53.6
37	24.03.2007	04:27:00	44:43.338	35:51.070	551.5	298.2
38	24.03.2007	04:36:00	44:42.872	35:49.542	539.8	299.2
39	24.03.2007	04:42:01	44:42.523	35:48.392	611.9	143.2
40	24.03.2007	04:47:00	44:42.310	35:47.647	592.5	251.4
41	24.03.2007	04:47:00	44:42.285	35:47.562	602.2	397.6
42	24.03.2007	04:48:00	44:42.253	35:47.463	612.9	116.9
43	24.03.2007	05:10:00	44:41.028	35:43.398	541.8	53.6
44	24.03.2007	05:11:00	44:40.953	35:43.155	567.1	375.2
45	24.03.2007	05:14:00	44:40.828	35:42.730	566.1	154.9
46	24.03.2007	05:15:00	44:40.753	35:42.477	565.2	193.9
47	24.03.2007	05:16:00	44:40.723	35:42.378	570.0	297.2
48	24.03.2007	05:16:00	44:40.698	35:42.292	567.1	305.0
49	24.03.2007	05:25:00	44:40.227	35:40.708	614.9	86.7
50	24.03.2007	05:37:00	44:39.547	35:38.435	551.5	230.0
51	24.03.2007	05:38:00	44:39.512	35:38.313	581.7	222.2
52	24.03.2007	05:45:00	44:39.158	35:37.118	661.6	175.4
53	24.03.2007	05:50:00	44:38.868	35:36.155	668.5	102.3
54	17.04.2007	03:04:59	44:39.307	35:28.093	664.4	370.0
55	17.04.2007	03:08:07	44:39.423	35:28.653	647.5	301.8
56	17.04.2007	03:17:24	44:39.782	35:30.325	603.5	245.1
57	17.04.2007	03:17:41	44:39.792	35:30.373	603.5	122.6
58	17.04.2007	03:30:42	44:40.330	35:32.738	659.0	191.9

Table A 2.3, continuation: Positions of Kerch Strait seeps during M72/3a and 3b.

No.	Date	Time	Lat. [°N]	Lon. [°N]	Water Depth [m]	Height [m]
59	17.04.2007	03:32:22	44:40.400	35:33.043	583.9	163.0
60	17.04.2007	03:32:41	44:40.412	35:33.100	568.9	227.8
61	17.04.2007	03:33:04	44:40.428	35:33.170	553.8	113.3
62	17.04.2007	03:34:15	44:40.477	35:33.388	548.0	175.7
63	17.04.2007	03:37:59	44:40.630	35:34.072	653.3	167.7
64	17.04.2007	03:46:01	44:40.960	35:35.522	491.3	240.5
65	17.04.2007	03:49:27	44:41.152	35:36.157	395.7	131.6
66	17.04.2007	03:50:06	44:41.192	35:36.278	367.9	135.7
67	17.04.2007	03:50:21	44:41.207	35:36.328	346.3	30.8
68	17.04.2007	03:51:09	44:41.255	35:36.478	313.5	126.4
69	17.04.2007	03:52:26	44:41.330	35:36.718	280.6	136.7
70	17.04.2007	03:53:03	44:41.363	35:36.833	285.7	84.3
71	17.04.2007	03:53:21	44:41.380	35:36.892	288.8	95.6
72	17.04.2007	03:54:04	44:41.418	35:37.025	279.5	68.9
73	17.04.2007	03:54:15	44:41.428	35:37.058	272.3	119.2
74	17.04.2007	03:55:23	44:41.488	35:37.275	272.3	67.8
75	17.04.2007	03:55:35	44:41.498	35:37.313	285.2	53.2
76	17.04.2007	03:55:52	44:41.512	35:37.365	293.7	61.7
77	17.04.2007	03:58:22	44:41.635	35:37.838	309.1	86.3
78	17.04.2007	03:58:30	44:41.642	35:37.862	314.5	129.5
79	17.04.2007	04:00:01	44:41.717	35:38.148	308.3	94.8
80	17.04.2007	04:00:19	44:41.732	35:38.205	303.7	67.8
81	17.04.2007	04:00:33	44:41.742	35:38.247	309.1	80.9
82	17.04.2007	04:00:47	44:41.755	35:38.293	316.8	99.4
83	17.04.2007	04:01:24	44:41.783	35:38.407	337.6	53.2
84	17.04.2007	04:01:48	44:41.803	35:38.480	350.7	47.0
85	17.04.2007	04:01:57	44:41.812	35:38.512	357.7	212.0
86	17.04.2007	04:02:18	44:41.828	35:38.577	373.1	82.5
87	17.04.2007	04:06:07	44:42.022	35:39.280	325.1	55.9
88	17.04.2007	04:06:41	44:42.050	35:39.383	334.7	136.2
89	17.04.2007	04:07:29	44:42.092	35:39.528	359.7	86.1
90	17.04.2007	04:07:59	44:42.117	35:39.620	380.9	52.7
91	17.04.2007	04:08:30	44:42.143	35:39.718	405.4	82.9
92	17.04.2007	04:10:19	44:42.237	35:40.050	416.9	59.7
93	17.04.2007	04:12:09	44:42.330	35:40.387	364.9	119.5
94	17.04.2007	04:12:32	44:42.350	35:40.455	350.1	114.4
95	17.04.2007	04:13:38	44:42.407	35:40.658	324.4	75.8
96	17.04.2007	04:14:08	44:42.432	35:40.750	317.3	107.9
97	17.04.2007	04:14:41	44:42.462	35:40.853	300.6	118.2
98	17.04.2007	04:14:51	44:42.468	35:40.883	301.3	157.4
99	17.04.2007	04:15:06	44:42.482	35:40.930	309.6	123.3
100	17.04.2007	04:16:56	44:42.577	35:41.268	296.0	161.1
101	17.04.2007	04:17:02	44:42.582	35:41.288	296.0	124.1
102	17.04.2007	04:17:34	44:42.608	35:41.387	310.6	108.7
103	17.04.2007	04:18:11	44:42.640	35:41.500	339.9	171.9
104	17.04.2007	04:18:32	44:42.658	35:41.565	342.2	205.0
105	17.04.2007	04:19:19	44:42.698	35:41.708	363.1	124.9
106	17.04.2007	04:20:17	44:42.747	35:41.887	371.5	111.0
107	17.04.2007	04:20:47	44:42.773	35:41.978	376.9	145.7
108	17.04.2007	04:21:41	44:42.818	35:42.145	409.3	105.6
109	17.04.2007	04:22:14	44:42.847	35:42.245	432.4	90.2
110	17.04.2007	04:28:49	44:43.190	35:43.450	474.8	46.3
111	17.04.2007	04:35:20	44:43.533	35:44.620	497.3	162.8
112	17.04.2007	04:38:52	44:43.712	35:45.242	564.8	118.7
113	17.04.2007	04:41:51	44:43.845	35:45.773	481.1	105.2
114	17.04.2007	04:45:49	44:44.013	35:46.487	397.5	246.4
115	17.04.2007	04:46:45	44:44.055	35:46.653	368.7	113.3
116	17.04.2007	04:46:56	44:44.063	35:46.687	362.4	102.5
117	17.04.2007	04:47:15	44:44.078	35:46.740	356.1	168.2

Table A 2.3, continuation: Positions of Kerch Strait seeps during M72/3a and 3b.

No.	Date	Time	Lat. [°N]	Lon. [°N]	Water Depth [m]	Height [m]
118	17.04.2007	04:47:35	44:44.093	35:46.800	350.7	142.1
119	17.04.2007	04:50:27	44:44.240	35:47.307	355.2	153.8
120	17.04.2007	04:51:03	44:44.272	35:47.412	378.6	75.5
121	17.04.2007	04:51:30	44:44.297	35:47.490	394.8	227.5
122	17.04.2007	04:56:56	44:44.562	35:48.462	359.7	165.5
123	17.04.2007	04:57:15	44:44.577	35:48.518	348.0	180.8
124	17.04.2007	04:58:31	44:44.638	35:48.747	323.8	160.1
125	17.04.2007	04:58:50	44:44.655	35:48.803	322.0	98.0
126	17.04.2007	04:59:32	44:44.688	35:48.925	320.2	116.0
127	17.04.2007	05:01:05	44:44.768	35:49.198	305.8	140.3
128	17.04.2007	05:01:29	44:44.790	35:49.272	302.2	55.8
129	17.04.2007	05:02:19	44:44.832	35:49.418	310.3	153.8
130	17.04.2007	05:07:15	44:45.078	35:50.287	394.8	151.1
131	17.04.2007	05:09:29	44:45.185	35:50.683	396.6	125.9
132	17.04.2007	05:10:48	44:45.252	35:50.915	420.0	98.0
133	17.04.2007	05:11:35	44:45.292	35:51.053	426.3	98.0
134	17.04.2007	05:13:13	44:45.372	35:51.340	411.0	177.2
135	17.04.2007	05:19:37	44:45.687	35:52.465	364.2	151.1
136	17.04.2007	05:19:47	44:45.695	35:52.492	357.0	150.2
137	17.04.2007	05:20:00	44:45.705	35:52.530	351.6	80.9
138	17.04.2007	05:20:19	44:45.720	35:52.587	360.6	103.4
139	17.04.2007	05:20:31	44:45.730	35:52.623	363.3	75.5
140	17.04.2007	05:20:45	44:45.742	35:52.663	365.1	40.5
141	17.04.2007	05:20:59	44:45.753	35:52.705	371.4	214.0
142	17.04.2007	05:23:18	44:45.867	35:53.113	358.8	84.5
143	17.04.2007	05:23:37	44:45.882	35:53.170	358.8	80.0
144	17.04.2007	05:25:07	44:45.958	35:53.433	326.4	54.9
145	17.04.2007	05:26:20	44:46.020	35:53.647	292.3	135.8
146	17.04.2007	05:26:31	44:46.030	35:53.682	300.4	123.2
147	17.04.2007	05:28:01	44:46.105	35:53.945	319.3	62.1
148	17.04.2007	07:13:30	44:48.778	36:03.680	87.1	64.0
149	17.04.2007	07:43:55	44:46.772	36:01.488	100.2	85.6
150	17.04.2007	08:05:10	44:45.473	35:59.750	150.7	22.4
151	17.04.2007	08:05:19	44:45.465	35:59.737	152.2	80.9
152	17.04.2007	08:05:28	44:45.457	35:59.725	151.1	79.0
153	17.04.2007	08:05:38	44:45.447	35:59.712	152.2	80.6
154	17.04.2007	08:05:49	44:45.435	35:59.697	150.3	91.7
155	17.04.2007	08:06:18	44:45.405	35:59.657	156.9	100.2
156	17.04.2007	08:06:30	44:45.393	35:59.643	157.6	90.2
157	17.04.2007	08:06:44	44:45.378	35:59.623	157.6	17.0
158	17.04.2007	08:13:13	44:44.983	35:59.097	180.4	54.7
159	17.04.2007	08:13:29	44:44.967	35:59.075	180.4	34.7
160	17.04.2007	08:13:47	44:44.950	35:59.052	179.6	63.2
161	17.04.2007	08:13:53	44:44.943	35:59.042	180.4	45.5
162	17.04.2007	08:14:57	44:44.878	35:58.955	196.6	49.3
163	17.04.2007	08:15:37	44:44.838	35:58.902	223.5	71.7
164	17.04.2007	08:15:47	44:44.828	35:58.888	225.9	62.4
165	17.04.2007	08:16:47	44:44.767	35:58.805	246.7	46.3
166	17.04.2007	08:17:28	44:44.725	35:58.750	255.9	96.6
167	17.04.2007	08:17:43	44:44.712	35:58.732	261.0	115.1
168	17.04.2007	08:19:23	44:44.610	35:58.597	278.5	131.6
169	17.04.2007	08:19:39	44:44.593	35:58.577	281.6	96.6
170	17.04.2007	08:20:13	44:44.558	35:58.530	297.0	126.4
171	17.04.2007	08:22:13	44:44.438	35:58.368	330.9	110.0
172	17.04.2007	08:22:45	44:44.405	35:58.323	341.2	79.1
173	17.04.2007	08:24:14	44:44.317	35:58.203	366.9	25.7
174	17.04.2007	08:26:50	44:44.158	35:57.997	395.7	150.1
175	17.04.2007	08:29:10	44:44.017	35:57.810	439.4	217.4
176	17.04.2007	10:25:40	44:42.747	35:59.645	442.4	168.0

Table A 2.3, continuation: Positions of Kerch Strait seeps during M72/3a and 3b.

No.	Date	Time	Lat. [°N]	Lon. [°N]	Water Depth [m]	Height [m]
177	17.04.2007	10:26:04	44:42.763	35:59.683	436.3	112.5
178	17.04.2007	10:27:01	44:42.805	35:59.772	419.3	177.3
179	17.04.2007	12:39:45	44:42.217	36:12.000	115.9	34.0
180	17.04.2007	13:02:22	44:40.978	36:13.923	120.7	108.9
181	17.04.2007	13:03:23	44:40.920	36:14.013	120.7	84.3
182	17.04.2007	13:03:56	44:40.890	36:14.060	121.3	63.5
183	17.04.2007	13:04:40	44:40.848	36:14.125	121.5	53.3
184	17.04.2007	13:05:18	44:40.812	36:14.180	121.5	75.9
185	17.04.2007	13:05:29	44:40.802	36:14.198	121.8	19.7
186	17.04.2007	13:05:42	44:40.790	36:14.217	122.1	14.2
187	17.04.2007	13:06:23	44:40.750	36:14.278	122.1	52.2
188	17.04.2007	13:16:00	44:40.208	36:15.147	126.0	80.1
189	17.04.2007	13:16:26	44:40.183	36:15.187	126.3	76.6
190	17.04.2007	13:16:37	44:40.173	36:15.200	126.5	114.7
191	17.04.2007	13:22:08	44:39.847	36:15.692	132.6	110.8
192	17.04.2007	13:39:10	44:39.242	36:17.558	125.7	91.6
193	17.04.2007	13:40:37	44:39.202	36:17.728	123.1	99.2
194	17.04.2007	13:41:08	44:39.185	36:17.788	123.4	92.1
195	17.04.2007	13:42:17	44:39.142	36:17.915	122.6	63.5
196	17.04.2007	13:43:02	44:39.108	36:17.992	122.6	13.7
197	17.04.2007	13:43:08	44:39.103	36:18.003	121.8	30.5
198	17.04.2007	13:43:41	44:39.078	36:18.060	122.6	102.4
199	17.04.2007	13:43:48	44:39.073	36:18.072	122.1	102.6
200	17.04.2007	13:43:59	44:39.063	36:18.090	122.1	101.1
201	17.04.2007	13:44:04	44:39.060	36:18.098	122.1	45.1
202	17.04.2007	13:44:14	44:39.052	36:18.117	122.1	82.2
203	17.04.2007	13:44:33	44:39.038	36:18.150	122.6	54.6
204	17.04.2007	13:44:43	44:39.030	36:18.167	122.3	93.2
205	17.04.2007	13:45:39	44:38.992	36:18.267	121.8	91.3
206	17.04.2007	13:46:02	44:38.977	36:18.308	121.5	57.0
207	17.04.2007	13:48:00	44:38.908	36:18.528	122.3	45.1
208	17.04.2007	13:49:50	44:38.853	36:18.735	122.6	90.0
209	17.04.2007	13:52:01	44:38.778	36:18.980	122.3	72.4
210	17.04.2007	13:57:08	44:38.597	36:19.570	122.8	92.4
211	17.04.2007	13:57:58	44:38.570	36:19.667	121.8	44.9
212	17.04.2007	13:58:26	44:38.553	36:19.722	122.3	26.0
213	17.04.2007	13:58:42	44:38.545	36:19.755	122.3	22.3
214	17.04.2007	14:00:19	44:38.490	36:19.943	121.5	70.6
215	17.04.2007	14:00:41	44:38.477	36:19.987	121.8	81.4
216	17.04.2007	14:00:48	44:38.472	36:20.000	122.8	79.8
217	17.04.2007	14:00:55	44:38.468	36:20.013	122.3	52.2
218	17.04.2007	14:01:06	44:38.462	36:20.035	122.6	61.7
219	17.04.2007	14:02:32	44:38.410	36:20.200	122.6	34.7
220	17.04.2007	14:03:10	44:38.385	36:20.273	122.6	76.6
221	17.04.2007	14:12:24	44:38.052	36:21.348	129.9	105.3
222	17.04.2007	14:14:13	44:37.992	36:21.568	130.7	58.0
223	17.04.2007	14:15:10	44:37.958	36:21.682	130.2	113.4
224	17.04.2007	14:15:41	44:37.940	36:21.743	131.2	23.1
225	17.04.2007	14:15:47	44:37.937	36:21.755	130.7	31.5
226	17.04.2007	14:15:57	44:37.930	36:21.775	131.0	24.4
227	17.04.2007	14:16:11	44:37.922	36:21.802	131.0	100.0
228	17.04.2007	14:16:56	44:37.893	36:21.890	130.7	71.9
229	17.04.2007	14:51:17	44:35.530	36:23.963	313.5	150.0
230	17.04.2007	14:53:30	44:35.338	36:24.033	322.0	50.4
231	17.04.2007	15:45:34	44:30.708	36:25.622	535.5	103.8
232	17.04.2007	15:45:58	44:30.675	36:25.635	533.2	133.9
233	17.04.2007	15:46:21	44:30.643	36:25.648	534.0	238.5
234	17.04.2007	15:47:03	44:30.583	36:25.673	532.4	237.7
235	18.04.2007	02:08:37	44:35.278	36:19.793	262.2	58.7

Table A 2.3, continuation: Positions of Kerch Strait seeps during M72/3a and 3b.

No.	Date	Time	Lat. [°N]	Lon. [°N]	Water Depth [m]	Height [m]
236	18.04.2007	02:16:42	44:35.905	36:20.177	227.1	61.5
237	18.04.2007	02:21:46	44:36.290	36:20.432	209.0	31.9
238	18.04.2007	02:40:52	44:37.578	36:21.505	136.0	22.9
239	18.04.2007	02:41:49	44:37.547	36:21.595	136.4	17.3
240	18.04.2007	03:05:26	44:35.690	36:20.758	255.7	90.2
241	18.04.2007	03:07:06	44:35.558	36:20.703	261.3	53.6
242	18.04.2007	03:13:13	44:35.063	36:20.570	286.7	46.7
243	18.04.2007	03:13:43	44:35.022	36:20.560	289.9	105.0
244	18.04.2007	16:30:40	44:39.897	35:43.893	672.3	343.6
245	18.04.2007	16:32:16	44:40.013	35:43.798	654.3	428.5
246	18.04.2007	16:32:58	44:40.063	35:43.757	642.3	215.8
247	18.04.2007	16:33:20	44:40.090	35:43.735	635.3	116.9
248	18.04.2007	16:34:23	44:40.167	35:43.673	629.3	48.0
249	18.04.2007	16:35:25	44:40.242	35:43.613	620.3	153.8
250	18.04.2007	16:35:58	44:40.282	35:43.580	614.3	30.0
251	18.04.2007	16:36:34	44:40.327	35:43.545	607.3	72.9
252	18.04.2007	16:37:37	44:40.402	35:43.482	604.3	89.9
253	18.04.2007	16:39:53	44:40.565	35:43.343	601.3	272.7
254	18.04.2007	16:41:54	44:40.710	35:43.215	594.3	196.8
255	18.04.2007	16:47:29	44:41.118	35:42.865	539.4	172.8
256	18.04.2007	16:48:23	44:41.187	35:42.810	527.4	196.8
257	18.04.2007	16:51:15	44:41.402	35:42.640	486.5	178.8
258	18.04.2007	16:52:41	44:41.507	35:42.557	472.5	92.9
259	18.04.2007	16:55:32	44:41.723	35:42.375	482.5	250.7
260	18.04.2007	16:56:39	44:41.808	35:42.305	477.5	128.9
261	18.04.2007	16:57:39	44:41.885	35:42.242	469.5	64.9
262	18.04.2007	17:00:11	44:42.075	35:42.085	442.5	17.0
263	18.04.2007	17:02:21	44:42.233	35:41.950	420.5	64.9
264	18.04.2007	17:02:53	44:42.270	35:41.918	410.5	75.9
265	18.04.2007	17:03:26	44:42.310	35:41.885	402.6	125.9
266	18.04.2007	17:06:11	44:42.510	35:41.722	372.6	91.9
267	18.04.2007	17:08:16	44:42.657	35:41.600	343.6	160.8
268	18.04.2007	17:09:45	44:42.762	35:41.512	306.7	45.0
269	18.04.2007	17:11:13	44:42.863	35:41.427	288.7	86.9
270	18.04.2007	17:12:21	44:42.943	35:41.362	285.7	86.9
271	18.04.2007	17:12:50	44:42.977	35:41.333	288.7	103.9
272	18.04.2007	17:13:16	44:43.005	35:41.308	284.7	112.9
273	18.04.2007	17:14:00	44:43.055	35:41.268	292.7	111.9
274	18.04.2007	17:15:55	44:43.187	35:41.158	293.7	45.0
275	18.04.2007	17:16:45	44:43.242	35:41.112	278.7	56.9
276	18.04.2007	17:18:28	44:43.357	35:41.017	252.1	53.3
277	18.04.2007	17:18:47	44:43.378	35:40.998	250.4	47.6
278	18.04.2007	17:22:01	44:43.595	35:40.815	231.4	55.3
279	18.04.2007	17:22:12	44:43.607	35:40.805	225.1	48.6
280	18.04.2007	17:22:26	44:43.622	35:40.792	215.8	46.6
281	18.04.2007	17:22:51	44:43.648	35:40.765	204.8	49.6
282	18.04.2007	17:23:20	44:43.680	35:40.738	200.4	59.3
283	18.04.2007	17:24:26	44:43.755	35:40.673	189.5	77.3
284	18.04.2007	18:29:42	44:42.072	35:37.013	222.1	15.7
285	18.04.2007	18:34:30	44:41.733	35:37.382	293.0	105.7
286	18.04.2007	18:42:55	44:41.145	35:38.022	376.3	67.3
287	18.04.2007	18:43:20	44:41.117	35:38.053	381.6	127.2
288	18.04.2007	18:43:47	44:41.085	35:38.087	386.9	134.5
289	18.04.2007	18:44:12	44:41.057	35:38.118	392.2	79.9
290	18.04.2007	18:47:07	44:40.857	35:38.340	423.5	251.1
291	18.04.2007	18:47:27	44:40.832	35:38.368	424.9	129.2
292	18.04.2007	18:48:19	44:40.770	35:38.433	436.9	50.6
293	18.04.2007	18:49:43	44:40.670	35:38.537	446.8	147.2
294	18.04.2007	18:50:13	44:40.633	35:38.575	450.2	221.8

Table A 2.3, continuation: Positions of Kerch Strait seeps during M72/3a and 3b.

No.	Date	Time	Lat. [°N]	Lon. [°N]	Water Depth [m]	Height [m]
295	18.04.2007	18:52:09	44:40.495	35:38.718	462.8	90.6
296	18.04.2007	18:52:36	44:40.462	35:38.753	460.2	195.8
297	18.04.2007	18:55:10	44:40.282	35:38.950	478.8	149.8
298	18.04.2007	18:56:02	44:40.218	35:39.022	486.8	91.2
299	18.04.2007	18:56:19	44:40.198	35:39.045	489.5	124.5
300	18.04.2007	18:56:38	44:40.175	35:39.070	494.1	120.5
301	18.04.2007	18:57:25	44:40.120	35:39.132	502.1	16.7
302	18.04.2007	18:57:55	44:40.083	35:39.172	508.1	178.5
303	18.04.2007	18:59:35	44:39.967	35:39.302	532.1	140.5
304	19.04.2007	22:47:21	44:39.472	35:43.843	701.3	167.5
305	19.04.2007	22:47:51	44:39.490	35:43.900	707.1	202.2
306	19.04.2007	23:44:03	44:40.202	35:43.823	640.1	439.0
307	19.04.2007	23:44:34	44:40.183	35:43.758	634.3	321.2
308	19.04.2007	23:44:59	44:40.167	35:43.708	629.7	73.9
309	19.04.2007	23:47:08	44:40.088	35:43.450	642.4	234.5
310	20.04.2007	00:11:32	44:39.177	35:40.468	674.7	78.6
311	20.04.2007	00:15:56	44:39.022	35:39.942	663.2	176.8
312	20.04.2007	00:17:28	44:38.963	35:39.758	668.9	425.2
313	20.04.2007	00:18:03	44:38.940	35:39.687	666.6	82.0
314	20.04.2007	00:19:29	44:38.875	35:39.525	671.3	219.5
315	20.04.2007	00:19:46	44:38.857	35:39.497	672.4	162.9
316	20.04.2007	00:20:24	44:38.818	35:39.443	679.3	161.8
317	20.04.2007	00:21:55	44:38.708	35:39.362	703.6	311.9
318	20.04.2007	01:23:56	44:39.682	35:40.885	677.0	84.3
319	20.04.2007	01:25:02	44:39.760	35:40.812	671.3	147.9
320	20.04.2007	01:26:13	44:39.842	35:40.730	664.3	164.1
321	20.04.2007	01:27:14	44:39.915	35:40.673	657.4	295.8
322	20.04.2007	01:29:57	44:40.098	35:40.707	610.0	223.0
323	20.04.2007	02:39:13	44:39.748	35:43.340	679.3	239.2
324	20.04.2007	02:44:22	44:40.145	35:43.058	663.2	26.6
325	20.04.2007	02:46:43	44:40.250	35:42.842	629.6	298.1
326	19.04.2007	01:11:45	44:37.440	35:42.928	927.4	149.6
327	19.04.2007	01:17:20	44:37.242	35:42.313	884.6	323.4
328	19.04.2007	01:17:58	44:37.217	35:42.245	881.8	518.5

Table A 2.4: Positions of Dvurechenskii seeps detected during M72/3b.

No.	Date	Time	Lat. [°N]	Lon. [°N]	Water Depth [m]	Height [m]
1	21.04.2007	18:51:27	44:16.947	34:58.472	2023.13	955.76
2	21.04.2007	19:31:40	44:17.042	34:58.848	2025.99	1156.07

Table A 3: MTU seismic survey profile list.

Profile No.*	Start Date	Start Time	End Time**	Start Lat. (N)	End Lat. (N)	Start Lon. (E)	End Lon. (E)	GI 4.1	GI 0.4	WG	Profile length (km)
Gudauta area, Georgia											
GeoB07-001	05.04.2007	16:01	16:32	42°48,00	42°46,10	40°09,00	40°10,10		x		3,823
GeoB07-002A	05.04.2007	16:32	19:57	42°46,10	42°39,30	40°10,10	40°24,90		x		23,753
GeoB07-002B*	05.04.2007	21:12	21:40	42°37,90	42°38,29	40°27,90	40°28,98		x		1,639
GeoB07-003*	05.04.2007	21:40	22:46	42°38,29	42°41,03	40°28,98	40°26,59		x		6,029
GeoB07-004*	05.04.2007	22:56	01:27 +	42°41,26	42°38,49	40°26,01	40°17,05		x		13,237
GeoB07-005*	06.04.2007	02:15	05:11	42°37,97	42°43,10	40°18,00	40°22,90		x		11,609
GeoB07-006	06.04.2007	06:37	07:39	42°42,40	42°38,40	40°23,40	40°20,00		x		8,736
Batumi											
GeoB07-007	06.04.2007	23:38	00:20 +	42°06,54	42°04,53	41°04,33	41°08,34	x	x		6,650
GeoB07-008	07.04.2007	00:20	03:38	42°04,53	41°52,77	41°08,34	41°22,77	x			29,480
GeoB07-009	07.04.2007	03:38	04:53	41°52,77	41°56,77	41°22,77	41°17,09	x			10,778
GeoB07-010	07.04.2007	04:53	05:27	41°56,77	41°59,30	41°17,09	41°18,26	x			4,955
Pechori											
GeoB07-011	08.04.2007	22:27	23:08	41°58,57	41°59,35	41°12,48	41°08,16	x			6,120
GeoB07-012	08.04.2007	23:08	00:03 +	41°59,35	41°57,21	41°08,16	41°04,28	x			6,652
GeoB07-013	09.04.2007	00:03	01:02	41°57,21	41°59,78	41°04,28	41°09,78	x			8,944
GeoB07-014	09.04.2007	01:02	02:06	41°59,78	41°57,80	41°09,78	41°04,60	x			8,019
GeoB07-015	09.04.2007	02:09	02:56	41°57,50	41°59,61	41°04,48	41°08,61		x		6,900
GeoB07-016	09.04.2007	02:56	03:25	41°59,61	42°00,97	41°08,61	41°06,96	x			3,391
GeoB07-017	09.04.2007	03:25	03:37	42°00,97	42°00,46	41°06,96	41°06,21	x			1,399
GeoB07-018	09.04.2007	03:37	04:28	42°00,46	41°57,81	41°06,21	41°09,02	x			6,249
GeoB07-019	09.04.2007	04:28	05:19	41°57,81	42°01,05	41°09,02	41°06,31	x			7,065
GeoB07-020	09.04.2007	05:27	06:13	42°00,68	41°57,29	41°05,92	41°08,60	x			7,282
GeoB07-021	09.04.2007	06:20	07:10	41°57,63	42°00,89	41°08,86	41°06,01	x			7,200
GeoB07-022	09.04.2007	07:18	07:45	42°04,02	41°59,34	41°05,74	41°03,39	x			9,251
Batumi 3D											
GeoB07-023	09.04.2007	22:32	22:49	41°56,12	41°55,62	41°15,82	41°17,34		x	x	2,290
GeoB07-024	09.04.2007	22:54	23:26	41°55,90	41°58,21	41°17,74	41°19,34		x	x	4,812
GeoB07-025	09.04.2007	23:40	00:01 +	41°58,51	41°56,97	41°18,38	41°17,34		x	x	3,191
GeoB07-026	10.04.2007	00:12	00:49	41°56,77	41°59,47	41°18,03	41°19,86		x	x	5,599
GeoB07-027	10.04.2007	00:52	01:39	41°59,62	41°56,78	41°19,78	41°16,89		x	x	6,595
GeoB07-028	10.04.2007	01:53	02:19	41°56,83	41°58,62	41°17,90	41°19,04		x	x	3,668
GeoB07-029	10.04.2007	02:30	02:50	41°58,59	41°57,07	41°18,06	41°16,99		x	x	3,177
GeoB07-030	10.04.2007	03:04	03:25	41°56,89	41°58,57	41°17,73	41°18,86		x	x	3,479
GeoB07-031	10.04.2007	03:37	03:59	41°58,68	41°57,00	41°17,81	41°16,76		x	x	3,431
GeoB07-032	10.04.2007	04:12	04:36	41°56,99	41°58,65	41°17,65	41°18,79		x	x	3,452
GeoB07-033	10.04.2007	04:48	05:10	41°58,75	41°56,99	41°17,76	41°16,64		x	x	3,606
GeoB07-034	10.04.2007	05:22	05:42	41°57,07	41°58,66	41°17,70	41°18,66		x	x	3,228
GeoB07-035	10.04.2007	05:55	06:16	41°58,73	41°57,14	41°17,54	41°16,45		x	x	3,305
GeoB07-036	10.04.2007	06:23	06:50	41°56,75	41°58,62	41°16,74	41°18,31		x	x	4,083
GeoB07-037	10.04.2007	07:01	07:24	41°58,77	41°57,03	41°17,64	41°16,47		x	x	3,603
GeoB07-038	10.04.2007	07:35	07:57	41°57,06	41°58,63	41°17,28	41°18,39		x	x	3,285
GeoB07-039	10.04.2007	08:09	08:30	41°58,87	41°57,19	41°17,81	41°16,75		x	x	3,437
GeoB07-040	10.04.2007	08:43	09:03	41°57,03	41°58,52	41°17,47	41°18,53		x	x	3,122
GeoB07-041	10.04.2007	09:14	09:36	41°58,63	41°57,11	41°17,97	41°16,89		x	x	3,184
GeoB07-042	10.04.2007	09:46	10:07	41°56,99	41°58,23	41°17,49	41°18,57		x	x	2,736
GeoB07-043	10.04.2007	10:18	10:39	41°58,64	41°57,10	41°18,01	41°16,90		x	x	3,236
GeoB07-044	10.04.2007	10:53	11:13	41°57,03	41°58,49	41°17,57	41°18,59		x	x	3,047
GeoB07-045	10.04.2007	11:25	11:46	41°58,64	41°57,13	41°18,04	41°17,00		x	x	3,142
GeoB07-046	10.04.2007	11:59	12:20	41°57,05	41°58,48	41°17,65	41°18,65		x	x	2,985
GeoB07-047	10.04.2007	12:32	12:54	41°58,61	41°57,09	41°18,11	41°17,05		x	x	3,171
GeoB07-048	10.04.2007	13:06	13:27	41°56,93	41°58,77	41°17,68	41°18,77		x	x	3,724
GeoB07-049	10.04.2007	13:37	14:00	41°58,57	41°56,90	41°18,17	41°17,00		x	x	3,487
GeoB07-050	10.04.2007	14:11	14:31	41°56,92	41°58,49	41°17,71	41°18,80		x	x	3,272
GeoB07-051	10.04.2007	14:43	15:06	41°58,65	41°57,01	41°17,94	41°16,81		x	x	3,413
GeoB07-052	10.04.2007	15:15	15:36	41°57,02	41°58,66	41°17,46	41°18,57		x	x	3,400
GeoB07-053	10.04.2007	15:46	16:07	41°58,66	41°57,15	41°17,87	41°16,81		x	x	3,155
GeoB07-054	10.04.2007	16:17	16:38	41°57,06	41°58,70	41°17,40	41°18,49		x	x	3,388
GeoB07-055	10.04.2007	16:48	17:09	41°58,68	41°57,11	41°17,84	41°16,74		x	x	3,279
GeoB07-056	10.04.2007	17:20	17:46	41°56,99	41°58,63	41°17,29	41°18,43		x	x	3,419
GeoB07-057	10.04.2007	17:51	18:12	41°58,71	41°57,21	41°17,76	41°16,71		x	x	3,132
GeoB07-058	10.04.2007	18:21	18:42	41°57,04	41°58,61	41°17,24	41°18,33		x	x	3,272
GeoB07-059	10.04.2007	18:53	19:13	41°58,72	41°57,21	41°17,72	41°16,65		x	x	3,161
GeoB07-060	10.04.2007	19:22	19:43	41°57,05	41°58,64	41°17,17	41°18,29		x	x	3,324
GeoB07-061	10.04.2007	19:53	20:14	41°58,79	41°57,24	41°17,70	41°16,63		x	x	3,227

Table A 3 continuation: MTU seismic survey profile list.

Profile No.*	Start Date	Start Time	End Time**	Start Lat. (N)	End Lat. (N)	Start Lon. (E)	End Lon. (E)	GI 4.1	GI 0.4	WG	Profile length (km)
GeoB07-062	10.04.2007	20:26	20:44	41°57,17	41°58,67	41°17,11	41°18,15		x	x	3,125
GeoB07-063	10.04.2007	20:54	21:15	41°58,78	41°57,29'	41°17,62	41°16,58'		x	x	3,109
GeoB07-064	10.04.2007	21:27	21:46	41°57,13	41°58,63	41°17,14	41°18,16		x	x	3,113
GeoB07-065	10.04.2007	21:58	22:20	41°58,78	41°57,28	41°17,61	41°16,55		x	x	3,138
GeoB07-066	10.04.2007	22:33	22:54	41°57,11	41°58,63	41°17,16	41°18,31		x	x	3,230
GeoB07-067	10.04.2007	23:07	23:29	41°58,79	41°57,26	41°17,67	41°16,59		x	x	3,200
GeoB07-068	10.04.2007	23:41	00:02 +	41°57,10	41°58,63	41^17,18	41°18,25		x	x	3,194
GeoB07-069	11.04.2007	00:14	00:36	41°58,76	41°57,26	41°17,66	41°16,63		x	x	3,119
GeoB07-070	11.04.2007	00:49	01:09	41°57,13	41°58,23	41°17,25	41°18,02		x	x	2,297
GeoB07-071	11.04.2007	01:20	01:41	41°58,76	41°57,21	41°17,70	41°16,63		x	x	3,227
GeoB07-072	11.04.2007	01:53	02:13	41°57,12	41°58,65	41°17,29	41°18,34		x	x	3,181
GeoB07-073	11.04.2007	02:26	02:46	41°58,74	41°57,21	41°17,71	41°16,67		x	x	3,175
GeoB07-074	11.04.2007	02:58	03:18	41°57,07	41°58,63	41°17,30	41°18,37		x	x	3,243
GeoB07-075	11.04.2007	03:29	03:49	41°58,73	41°57,20	41°17,76	41°16,69		x	x	3,194
GeoB07-076	11.04.2007	04:01	04:21	41°57,06	41°58,59	41°17,33	41°18,40		x	x	3,194
GeoB07-077	11.04.2007	04:33	04:54	41°58,68	41°57,18	41°17,75	41°16,74		x	x	3,107
GeoB07-078	12.04.2007	20:29	20:49	41°57,04	41°58,56	41°17,36	41°18,40		x	x	3,158
GeoB07-079	12.04.2007	20:59	21:21	41°58,71	41°57,19	41°17,82	41°16,78		x	x	3,158
GeoB07-080	12.04.2007	21.33	21:52	41°57,00	41°58,54	41°17,37	41°18,42		x	x	3,198
GeoB07-081	12.04.2007	22:03	22:24	41°58,70	41°57,16	41°17,86	41°16,81		x	x	3,198
GeoB07-082	12.04.2007	22:36	22:56	41°57,00	41°58,52	41°17,41	41°18,45		x	x	3,158
GeoB07-083	12.04.2007	23:09	23:29	41°58,67	41°57,16	41°17,90	41°16,84		x	x	3,155
GeoB07-084	12.04.2007	23:41	00:02 +	41°57,00	41°58,51	41°17,44	41°18,49		x	x	3,148
GeoB07-085	13.04.2007	00:14	00:35	41°58,64	41°57,14	41°17,91	41°16,86		x	x	3,132
GeoB07-086	13.04.2007	00:47	01:08	41°56,99	41°58,58	41°17,48	41°18,58		x	x	3,311
GeoB07-087	13.04.2007	01:21	01:40	41°58,59	41°57,13	41°17,90	41°16,89		x	x	3,041
GeoB07-088	13.04.2007	01:51	02:11	41°56,98	41°58,51	41°17,53	41°18,59		x	x	3,187
GeoB07-089	13.04.2007	02:24	02:46	41°58,66	41°57,10	41°18,01	41°16,91		x	x	3,262
GeoB07-090	13.04.2007	02:57	03:18	41°56,97	41°58,54	41°17,57	41°18,65		x	x	3,266
GeoB07-091	13.04.2007	03:30	03:50	41°58,64	41°57,09	41°18,03	41°16,97		x	x	3,220
GeoB07-092	13.04.2007	04:01	04:21	41°56,94	41°58,50	41°17,57	41°18,64		x	x	3,243
GeoB07-093	13.04.2007	04:35	04:56	41°58,61	41°57,08	41°18,06	41°16,99		x	x	3,194
GeoB07-094	13.04.2007	05:03	05:23	41°57,28	41°58,78	41°16,80	41°17,85		x	x	3,132
GeoB07-095	13.04.2007	05:36	05:57	41°58,63	41°57,04	41°18,16	41°17,08		x	x	3,299
Iberia, Colkheti											
GeoB07-096	13.04.2007	06:14	07:37	41°56,46	41°52,15	41°16,56	41°09,08	x			13,039
GeoB07-097	13.04.2007	07:41	07:53	41°51,8	41°51,57	41°09,05	41°10,39	x			1,897
GeoB07-098	13.04.2007	08:04	08:28	41°51,69	41°53,42	41°10,99	41°09,65	x			3,699
GeoB07-099	13.04.2007	08:37	09:04	41°53,21	41°51,22	41°09,35	41°10,74	x			4,154
GeoB07-100	13.04.2007	09:23	11:03	41°51,57	41°59,41	41°10,74	41°05,26	x			16,366
GeoB07-101	13.04.2007	11:24	11:53	41°59,27	41°56,88	41°05,19	41°06,86	x			4,988
Andrusov Ridge											
GeoB07-102	15.04.2007	00:24	05:14	42°27,85	42°46,99	36°48,85	36°29,77	x			43,961
GeoB07-103	15.04.2007	05:29	06:16	42°46,29	42°42,71	36°30,67	36°28,49	x			7,263
Dvurechenskii MV											
GeoB07-104	15.04.2007	18:07	18:36	44°13,49	44°15,04	35°01,40	34°59,00		x	x	4,287
GeoB07-105	15.04.2007	18:36	19:20	44°15,04	44°18,70	34°59,00	34°59,01		x	x	6,778
GeoB07-106	15.04.2007	19:34	20:04	44°18,44	44°15,95	34°59,95	35°00,00		x	x	4,612
GeoB07-107	15.04.2007	20:24	20:48	44°16	44°18,00	34°58,24	34°58,24		x	x	3,704
GeoB07-108	15.04.2007	21:01	21:26	44°17,97	44°15,98	34^58,67	34°58,75		x	x	3,687
GeoB07-109	15.04.2007	21:41	22:06	44°16,00	44°17,99	34°59,23	34°59,25		x	x	3,686
GeoB07-110	15.04.2007	22:25	22:49	44°17,98	44°15,97	34°58,05	34°58,48		x	x	3,766
GeoB07-111	15.04.2007	23:05	23:31	44°16,01	44°18,02	34°59,12	34°59,11		x	x	3,723
GeoB07-112	15.04.2007	23:46	00:11 +	44°17,98	44°15,96	34°58,62	34°58,61		x	x	3,741
GeoB07-113	16.04.2007	00:23	00:48	44°16,00	44°18,00	34°59,04	34°59,04		x	x	3,704
GeoB07-114	16.04.2007	01:04	01:30	44°17,86	44°15,77	34°58,38	34°58,36		x	x	3,871
GeoB07-115	16.04.2007	01:45	02:10	44°16,12	44°18,25	34°58,97	34°58,96		x	x	3,945
GeoB07-116	16.04.2007	02:25	02:50	44°18,00	44°15,76	34°58,12	34°58,11		x	x	4,149
GeoB07-117	16.04.2007	03:06	03:33	44°16,00	44°18,25	34°58,85	34°58,85		x	x	4,167
GeoB07-118	16.04.2007	03:46	04:15	44°17,96	44°15,77	34°58,43	34°58,45		x	x	4,056
GeoB07-119	16.04.2007	04:27	04:53	44°15,99	44°18,21	34°58,92	34°58,91		x	x	4,111
GeoB07-120	16.04.2007	05:07	05:34	44°17,98	44°15,90	34°58,56	34°58,57		x	x	3,852
GeoB07-121	16.04.2007	05:46	06:11	44°16,15	44°18,19	34°59,18	34°59,18		x	x	3,778
GeoB07-122	16.04.2007	06:20	06:46	44°17,96	44°15,79	34°58,68	34°58,692		x	x	4,019
GeoB07-123	16.04.2007	06:57	07:23	44°16,06	44°18,20	34°59,30	34°59,29		x	x	3,963
GeoB07-124	16.04.2007	07:33	07:58	44°17,98	44°15,67	34°58,79	34°58,79		x	x	4,278

Table A 3 continuation: MTU seismic survey profile list.

Profile No.*	Start Date	Start Time	End Time**	Start Lat. (N)	End Lat. (N)	Start Lon. (E)	End Lon. (E)	GI 4.1	GI 0.4	WG	Profile length (km)
Kerch-Strait											
GeoB07-125	17.04.2007	07:23	09:17	44°48,04	44°41,10	36°03,16	35°53,90	x			17,708
GeoB07-126	17.04.2007	09:36	11:31	44°40,63	44°45,72	35°55,06	36°06,10	x			17,318
GeoB07-127	17.04.2007	11:35	13:24	44°45,71	44°39,75	36°06,55	36°15,95	x			16,580
GeoB07-128	17.04.2007	13:24	14:29	44°39,75	44°37,40	36°15,95	36°23,33	x			10,654
GeoB07-129	17.04.2007	14:29	17:18	44°37,40	44°23,01	36°23,33	36°28,27	x			27,437
GeoB07-130	17.04.2007	17:18	20:30	44°23,01	44°28,82	36°28,27	36°07,41	x			29,611
GeoB07-132	17.04.2007	20:36	22:35	44°28,61	44°19,46	36°07,02	36°10,14	x			17,441
GeoB07-133	17.04.2007	22:38	02:36 +	44°19,59	44°37,42	36°10,28	36°21,13	x			36,000
GeoB07-134	18.04.2007	02:45	04:43	44°37,31	44°27,50	36°21,64	36°18,46	x			18,647
GeoB07-135*	18.04.2007	07:27	07:49	44°27,52	44°28,25	36°20,09	36°21,01		x		1,818
GeoB07-136*	18.04.2007	07:49	10:30	44°28,25	44°25,23	36°21,01	36°29,06		x		12,024
GeoB07-137	18.04.2007	15:07	17:32	44°34,55	44°44,29	35°48,26	35°40,23	x			20,912
GeoB07-138	18.04.2007	17:41	18:10	44°44,25	44°43,73	35°39,08	35°35,91	x			4,280
GeoB07-139	18.04.2007	18:13	20:14	44°43,12	44°34,99	35°35,75	35°44,71	x			19,133
GeoB07-140	18.04.2007	20:20	21.46	44°34,71	44°36,07	35°44,49	35°35,21	x			12,496
GeoB07-141	18.04.2007	21:52	00:01 +	44°36,22	44°40,40	35°35,06	35°48,63	x			19,486
GeoB07-142	19.04.2007	00:22	01:31	44°39,12	44°36,77	35^48,15	35°40,78	x			10,644
GeoB07-143	19.04.2007	02:01	02:10	44°37,40	44°38,06	35°42,30	35°42,67	x			1,316
GeoB07-144	19.04.2007	17:11	17:26	44°38,42	44°38,32	35°42,25	35°43,63	x			1,828
GeoB07-145	19.04.2007	17:30	18:58	44°38,14	44°31,94	35°43,92	35°48,25	x			12,824
GeoB07-146	19.04.2007	19:05	20:13	44°31,70	44°33,64	35°47,72	35°40,18	x			10,581
GeoB07-147	19.04.2007	20:17	20:50	44°33,90	44°36,49	35°40,08	35°40,60	x			4,845
GeoB07-148	19.04.2007	20:55	21:30	44°36,66	44°37,12	35°40,18	35°36,30	x			5,186
GeoB07-149	19.04.2007	21:33	23:15	44°37,17	44°40,48	35°36,51	35°46,82	x			14,904
GeoB07-150	19.04.2007	23:26	00:19 +	44°40,86	44°38,86	35°45,96	35°39,48	x			9,305
GeoB07-151	20.04.2007	00:26	00:42	44°38,47	44°37,49	35°39,59	35°40,82	x			2,433
GeoB07-152	20.04.2007	00:46	00:56	44°37,49	44°37,85	35°41,19	35°42,20	x			1,489
GeoB07-153	20.04.2007	00:59	01:26	44°38,03	44°39,87	35°42,39	35°40,70	x			4,071
GeoB07-154	20.04.2007	01:38	02:08	44°40,19	44°37,90	35°41,63	35°43,50	x			4,905
GeoB07-155	20.04.2007	02:10	02:20	44°37,91	44°38,29	35°43,68	35°44,32	x			1,098
GeoB07-156	20.04.2007	02:23	02:43	44°38,50	44°40,05	35°44,18	35°43,12	x			3,192
GeoB07-157	20.04.2007	02:55	03:22	44°39,75	44°38,01	35°42,82	35°44,01	x			3,584

*: Profiles were recorded at a cruising speed of approx. 5 kn. Profiles marked * were acquired at 3 kn.
**: + behind end time denotes day change during profile
GI 4.1 - starboardside GI source, 4.1L
GI 0.4 - portside GI source, 0.4L
WG - portside watergun source, 0.16L

Table A 4: List of gravity corer (GC), Dynamic Autoclave Piston Corer (DAPC, I + II), multi corer (MUC), and mini corer (MiC) stations performed during cruise M72/3a+b.

Date	GeoB No.	Station-Nr.	Instru-ment	Location	Latitude [°N]	Longitude [°E]	Water Depth [m}	Core recovery
M73/3a								
18.03.07	11901	DAPC-1	DAPC I	Batumi seep	41:57.410	41:17.344	851	260 cm
20.03.07	11903	DAPC-2	DAPC I	Batumi seep	41:57.472	41:17.266	850	260 cm core, 100 cm
21.03.07	11905-1	MUC-1	MUC	near Batumi seep	41:57.249	41:16.716	895	-
21.03.07	11905-2	MUC-2	MUC	near Batumi seep	41:57.432	41:16.798	877	60 cm
21.03.07	11906	DAPC-3	DAPC I	Batumi seep	41:57.465	41:17.270	843	83 cm
24.03.07	11909	DAPC-4	DAPC I	Dvurechenskii MV	44:16.906	34:59.066	2056	-
25.03.07	11911	DAPC-5	DAPC I	Dvurechenskii MV	44:16.972	34:59.215	2058	60 cm
25.03.07	11912	MUC-3	MUC	Dvurechenskii MV	44:17.015	34:58.885	2053	60 cm
25.03.07	11913	GC-1	GC	Vodyanitskii MV	44:17.621	35:01.946	2048	138 cm
26.03.07	11914	DAPC-6	DAPC I	Dvurechenskii MV	44:16.987	34:59.097	2058	256 cm
27.03.07	11916	DAPC-7	DAPC I	Dvurechenskii MV	44:16.896	34:58.789	2057	253 cm
29.03.07	11918	DAPC-8	DAPC II	Batumi seep	41:57.547	41:17.427	840	233 cm
30.03.07	11920	DAPC-9	DAPC I	Batumi seep	41:57.454	41:17.545	844	259 cm
31.03.07	11922	DAPC-10	DAPC I	Colkheti seep	41:58.071	41:06.214	1126	-
31.03.07	11923	GC-2	GC	Colkheti seep	41:58.120	41:06.250	1088	-
31.03.07	11924	GC-3	GC	Colkheti seep	41:58.068	41:06.195	1056	698 cm
31.03.07	11925	GC-4	GC	Batumi seep	41.57.431	41:17.347	844	215 cm
31.03.07	11926	GC-5	GC	Batumi seep	41:57.416	41:17.345	849	-
31.03.07	11927	GC-6	GC	Batumi seep	41:57.410	41:17.324	856	413 cm
01.04.07	11928	MUC-4	MUC	Shallow ridge	41:42.332	41:28.174	379	-
01.04.07	11929	MUC-5	MUC	Shallow ridge	41:42.374	41:28.059	367	-
01.04.07	11930	MUC-6	MUC	Shallow ridge	41:42.386	41:27.938	382	-
01.04.07	11931	MUC-7	MUC	Batumi seep	41:47.838	41:16.842	839	60 cm
M73/3b								
06.04.07	11933	GC-7	GC	Gudauta High	42:40.262	40:22.631	690	380 cm
06.04.07	11934	MUC-8	MUC	Gudauta High	42 :40.260	40 :22.678	701	57 cm
07.04.07	11935	DAPC-11	DAPC II	Batumi seep	41:57.549	41:17.425	843	-
07.04.07	11936	GC-8	GC	Batumi seep	41:57.563	41:17.430	844	193 cm
07.04.07	11937	DAPC-12	DAPC I	Batumi seep	41:57.489	41:17.462	842	41 cm
07.04.07	11937	DAPC-12	DAPC I	Batumi seep	41:57.489	41:17.462	842	41 cm
07.04.07	11938	GC-9	GC	Iberia mound	41:52.340	41:10.036	982	134 cm
07.04.07	11939	MUC-9	MUC	Iberia mound	41:52.739	41:10.025	989	60 cm
08.04.07	11941	GC-10	GC	Pechori mound	41:58.962	41:02.404	1014	83 cm
08.04.07	11942	GC-11	GC	Pechori mound	41:59.008	41:07.400	1024	-
08.04.07	11943	MUC-10	MUC	Pechori mound	41:58.659	41:07.428	1014	-
08.04.07	11944	DAPC-13	DAPC II	Batumi seep	41:57.554	41:17.654	841	-
08.04.07	11945	GC-12	GC	Batumi seep	41:57.345	41:17.456	848	-
09.04.07	11946	GC-13	GC	Batumi seep	41:57.532	41:17.582	842	252 cm
09.04.07	11947	MUC-11	MUC	Batumi seep	41:57.531	41:17.585	841	-
09.04.07	11948	MUC-12	MUC	Batumi seep	41:57.531	41:17.578	843	-
09.04.07	11949	GC-14	GC	Batumi seep	41:57.550	41:17.175	842	-
09.04.07	11950	MUC-13	MUC	Batumi seep	41:57.542	41:17.424	840	-
09.04.07	11951	DAPC-14	DAPC II	Batumi seep	41:57.546	41:17.431	840	137 cm
09.04.07	11952	GC-15	GC	Pechori mound	41:58.955	41:07.539	1019	-
09.04.07	11953	GC-16	GC	Pechori mound	41:58.958	41:07.543	1015	335 cm
11.04.07	11954	MIC-1	MIC	Pechori mound	41:58.964	41:07.541	1024	57 cm
11.04.07	11955	GC-17	GC	Pechori mound	41:58.963	41:07.540	1012	144 cm
11.04.07	11956	GC-18	GC	Batumi seep	41:57.450	14:17.436	843	110 cm
11.04.07	11957	GC-19	GC	Reference Batumi	41:57.803	41:18.001	844	to be opened
11.04.07	11958	DAPC-15	DAPC I	Batumi seep	41:57.448	41:17.446	845	146 cm
11.04.07	11959	MIC-2	MIC	Batumi seep	41:57.533	41:17.568	840	58 cm
11.04.07	11960	MIC-3	MIC	Offshore Kobuleti	42:00.351	41:27.997	523	59 cm
12.04.07	11962	MIC-4	MIC	Batumi seep	41:57.548	41:17.435	838	for pore water
12.04.07	11963	DAPC-16	DAPC I	Batumi seep	41:57.410	41:17.278	853	169 cm
12.04.07	11964	MIC-5	MIC	Batumi seep	41:57.414	41:17.360	847	51 cm

Table A 4, continuation: List of gravity corer (GC), Dynamic Autoclave Piston Corer (DAPC, I + II), multi corer (MUC), and mini corer (MiC) stations performed during cruise M72/3a+b.

Date	GeoB No.	Station-Nr.	Instru-ment	Location	Latitude [°N]	Longitude [°E]	Water Depth [m]	Core recovery
12.04.07	11965	MIC-6	MIC	Batumi seep	41:57.447	41:17.437	843	27cm
12.04.07	11966	MIC-7	MIC	Batumi seep	41:57.614	41:17.512	847	-
12.04.07	11967	GC-20	GC	Batumi seep	41:57.530	41:17.268	843	-
13.04.07	11968	MIC-8	MIC	Pechori mound	41:58.961	41:07.543	1022	43 cm
13.04.07	11969	MIC-9	MIC	Pechori mound	41:58.962	41:07.541		41 cm
13.04.07	11970	MIC-10	MIC	Colkheti seep	41:58.069	41:06.191	1118	34 cm
13.04.07	11971	GC-21	GC	Colkheti seep	41:58.069	41:06.199	1124	151 cm
13.04.07	11972	DAPC-17	DAPC II	Batumi seep	41:57.541	41:17.428	841	-
13.04.07	11973	DAPC-18	DAPC II	Batumi seep	41:57.544	41:17.430	840	-
13.04.07	11974	GC-22	GC	Reference Batumi	41:57.428	41:16.803	884	697 cm
14.04.07	11975	GC-23	GC	Batumi seep	41:57.528	41:17.588	844	304 cm
16.04.07	11976	MIC-11	MIC	Dvurechenskii MV	44.16.807	34:58.906	2052	46 cm
16.04.07	11977	MIC-12	MIC	Dvurechenskii MV	44:16.885	34:58.906	2052	52 cm
16.04.07	11978	MIC-13	MIC	Dvurechenskii MV	44.16.944	34:58.902	2050	56 cm
16.04.07	11979	MIC-14	MIC	Dvurechenskii MV	44.17.025	34:58.879	2048	40 cm
16.04.07	11980	GC-24	GC	Vodyanitskiy MV	44:17.659	35:01.965	2039	132 cm
16.04.07	11981	DAPC-19	DAPC I	Vodyanitskiy MV	44:17.650	35:01.979	2037	78 cm
19.04.07	11983	MIC-15	MIC	Kerch strait	44:39.607	35:42.519	747	45 cm
19.04.07	11984	MIC-16	MIC	Kerch strait	44:29.999	35:49.998	1341	24 cm
19.04.07	11985	MIC-17	MIC	Kerch strait	44:45.008	36:09.995	95	30 cm
19.04.07	11986	MIC-18	MIC	Kerch strait	44:46.007	36:01.998	173	37 cm
19.04.07	11987	GC-25	GC	Kerch strait	44:37.138	35:42.249	894	157 cm
19.04.07	11988	GC-26	GC	Kerch strait	44:37.207	35:42.291	889	293 cm
20.04.07	11989	GC-27	GC	Kerch strait	44:37.203	35:42.260	888	289 cm
20.04.07	11990	GC-28	GC	Vodyanitskiy MV	44:17.623	35:01.946	2061	153 cm
20.04.07	11991	DAPC-20	DAPC I	Vodyanitskiy MV	44:17.625	35:01.949	2052	-
20.04.07	11992	DAPC-21	DAPC I	Vodyanitskiy MV	44:17.630	35:01.932	2055	177 cm
20.04.07	11993	MIC-19	MIC	Vodyanitskiy MV	44:17.627	35:01.948	2067	pore water
20.04.07	11994	DAPC-22	DAPC II	Dvurechenskii MV	44:16.995	34:59.096	1994	USBL;
20.04.07	11995	MIC-20	MIC	Dvurechenskii MV	44:17.034	34:58.951	1977	40 cm
21.04.07	11997	MIC-21	MIC	Dvurechenskii MV	44:17.060	34:59.036	2050	29 cm
21.04.07	11998	GC-29	GC	Dvurechenskii MV	44:16.998	34:59.090	2052	to be opened
21.04.07	11999	DAPC-23	DAPC I	Dvurechenskii MV	44:16.892	34:58.902	2049	ca. 300 cm (core loss)

Plate A 5: Sedimentological core descriptions

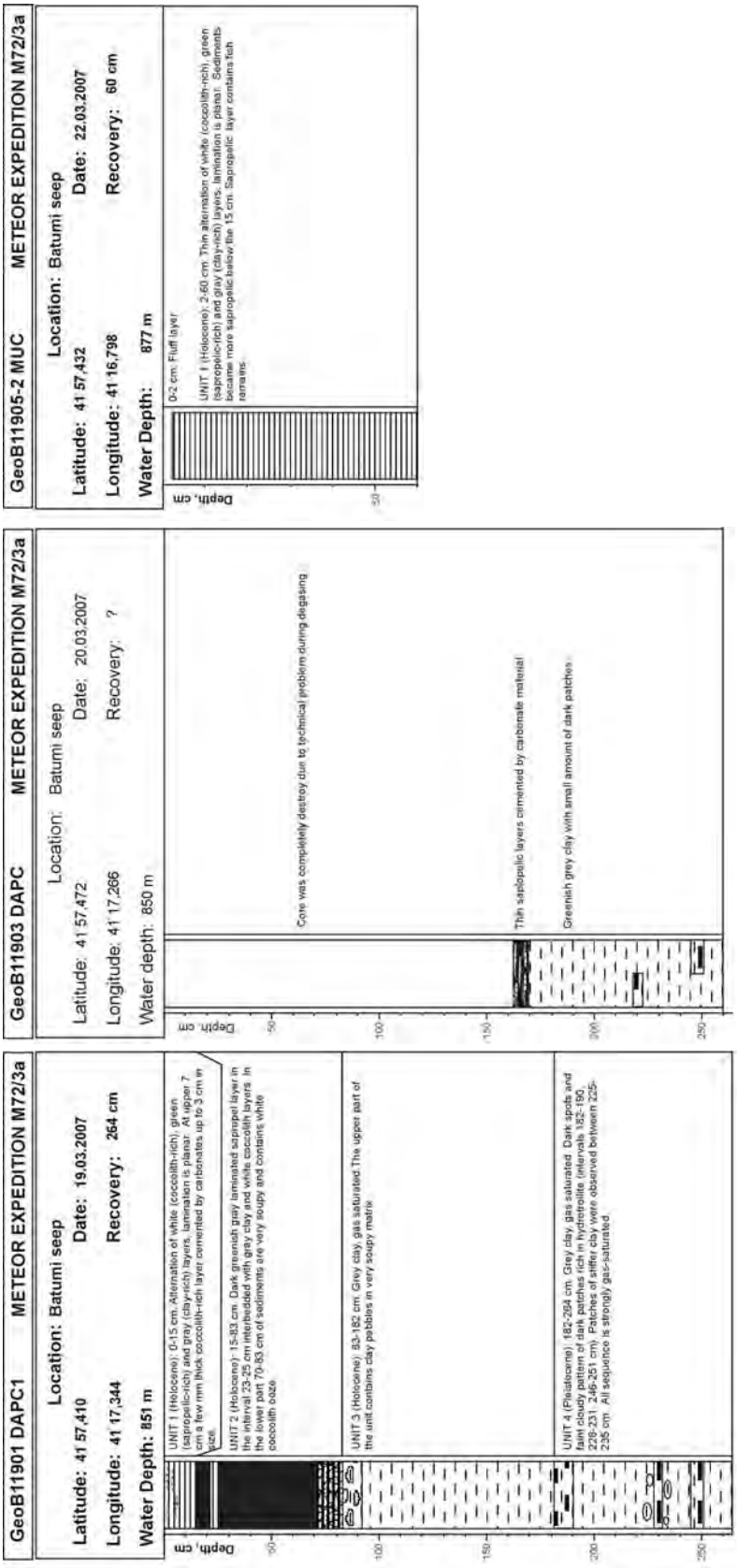

Plate A 5, continuation: Sedimentological core descriptions

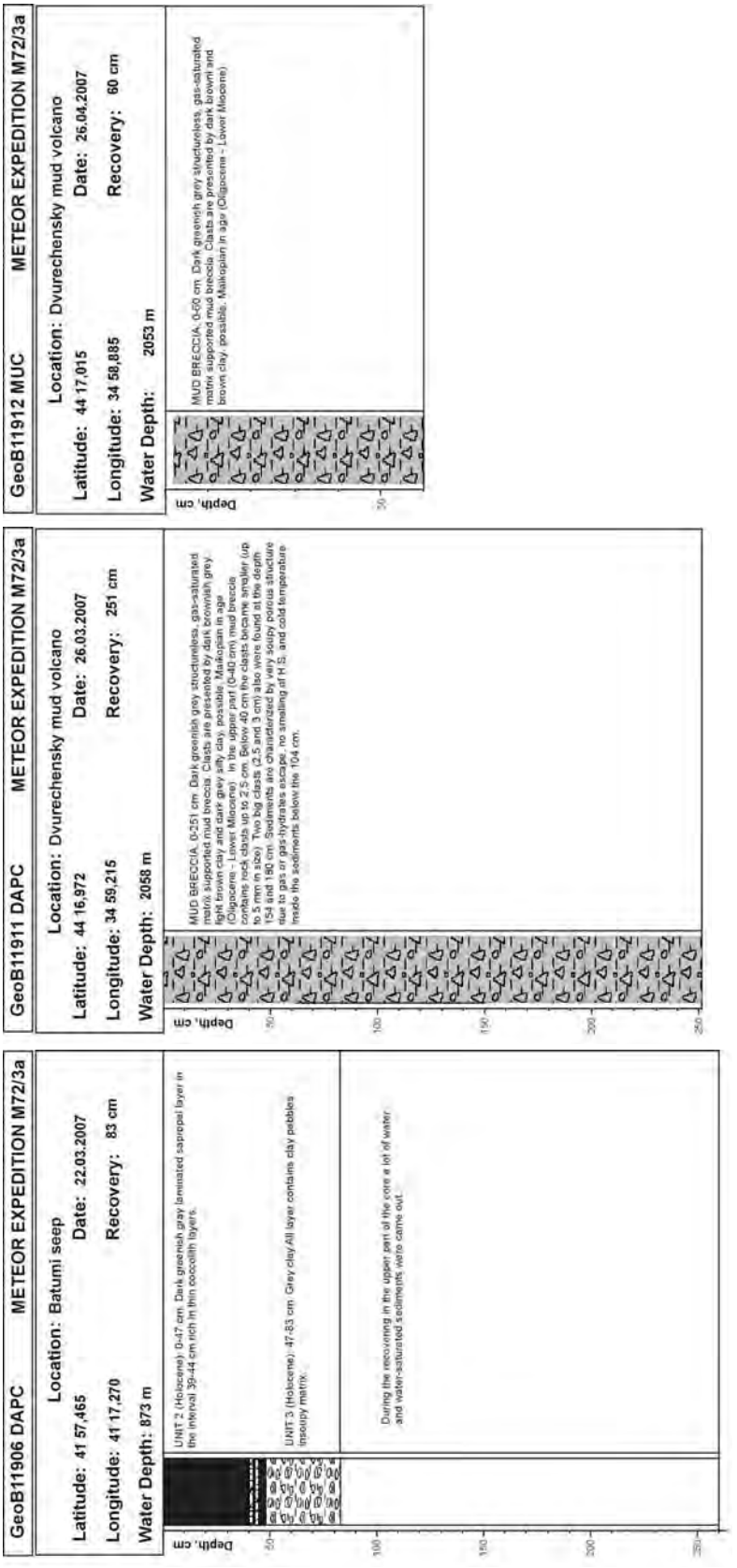

Plate A 5, continuation: Sedimentological core descriptions

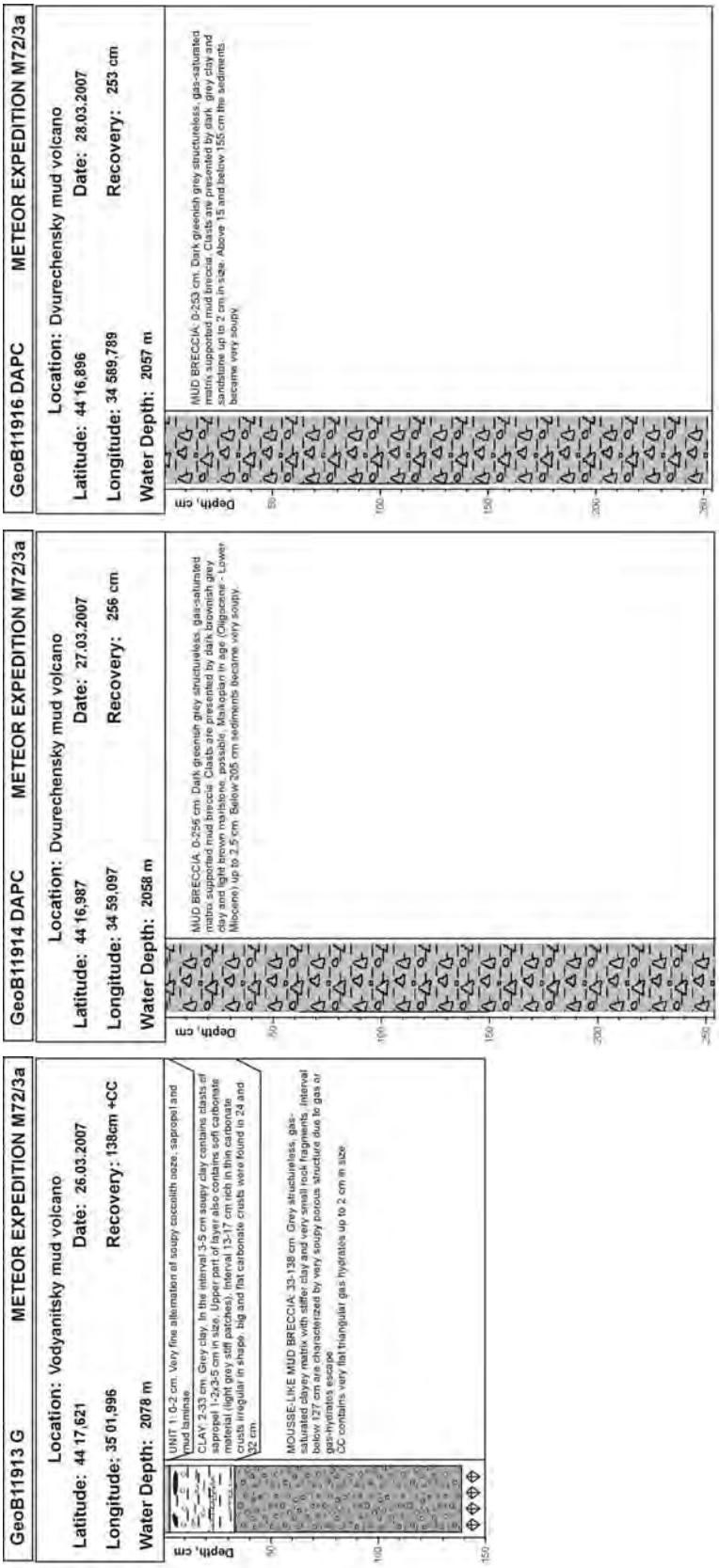

Plate A 5, continuation: Sedimentological core descriptions

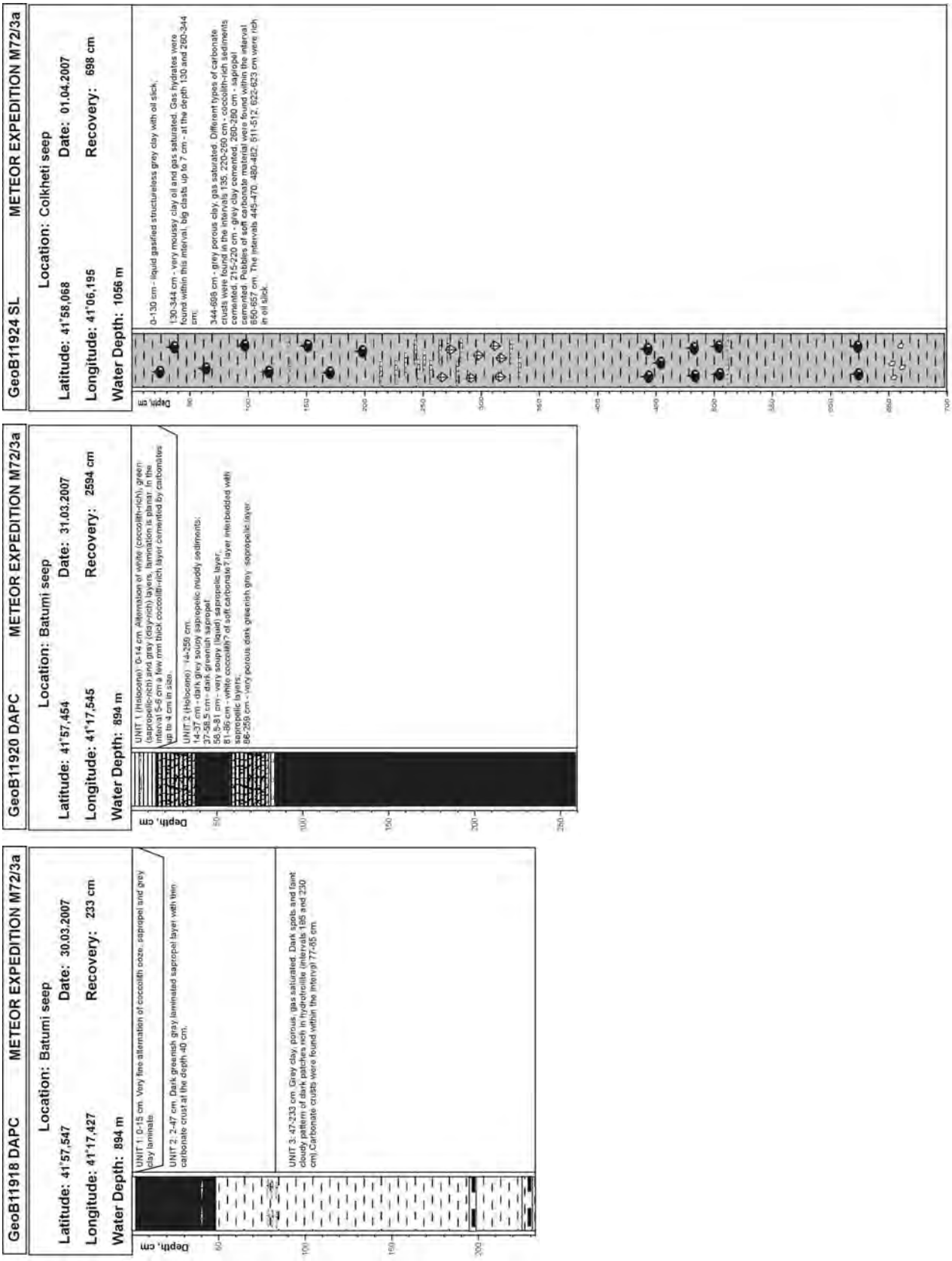

Plate A 5, continuation: Sedimentological core descriptions

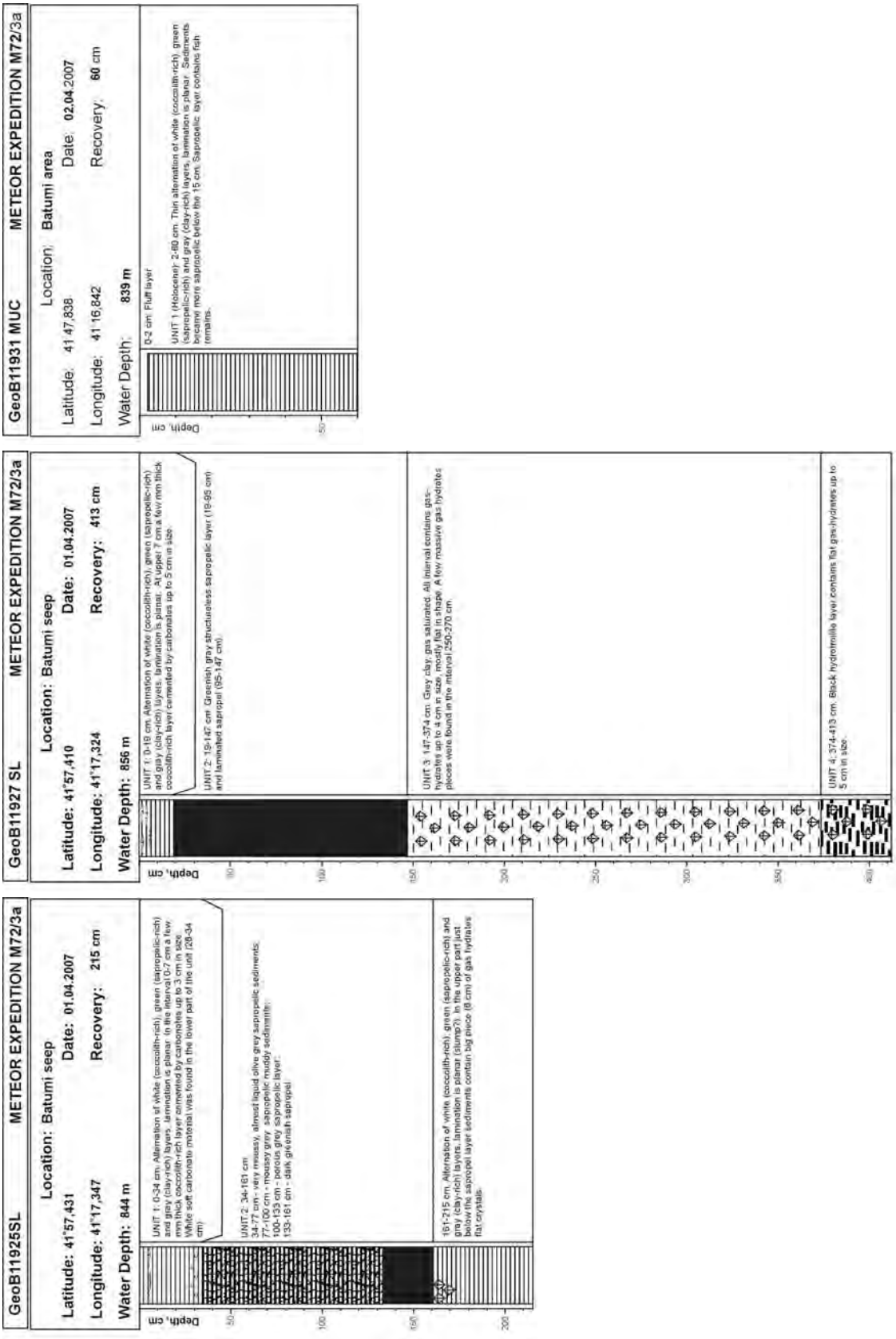

Plate A 5, continuation: Sedimentological core descriptions

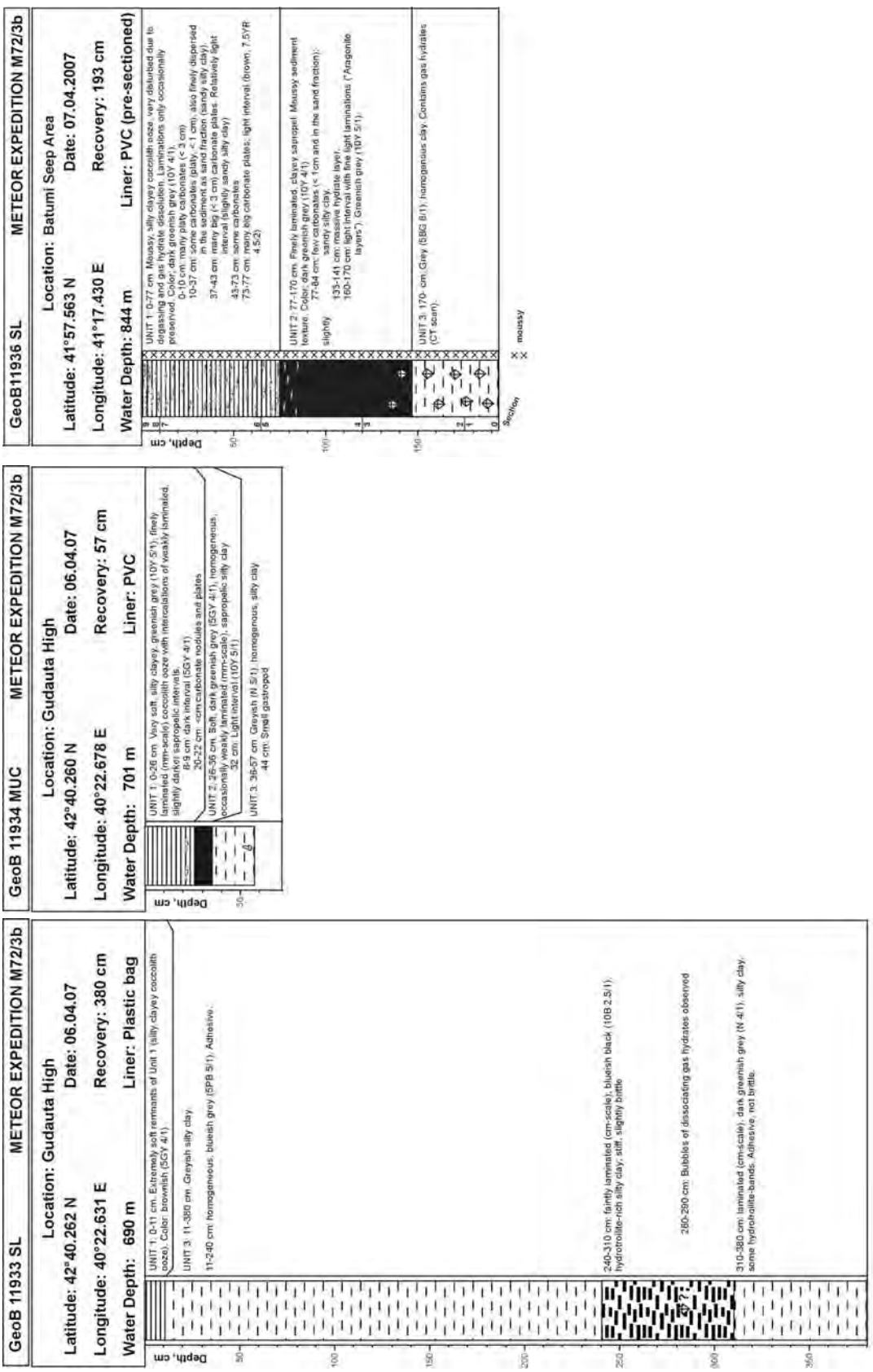

Plate A 5, continuation: Sedimentological core descriptions

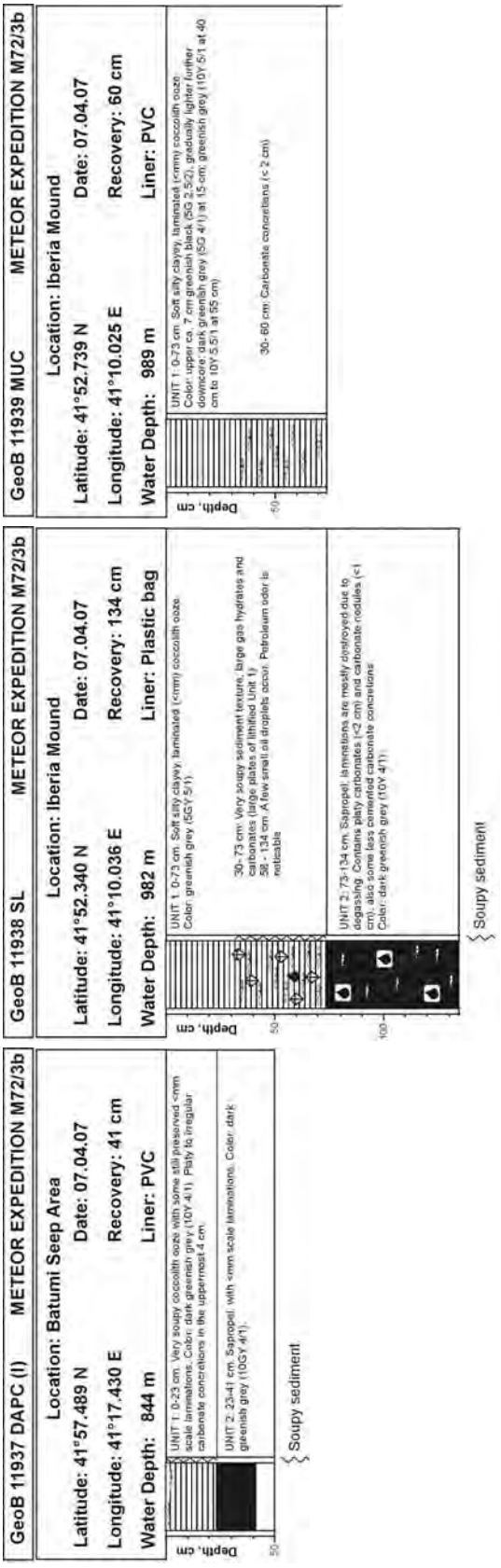

Plate A 5, continuation: Sedimentological core descriptions

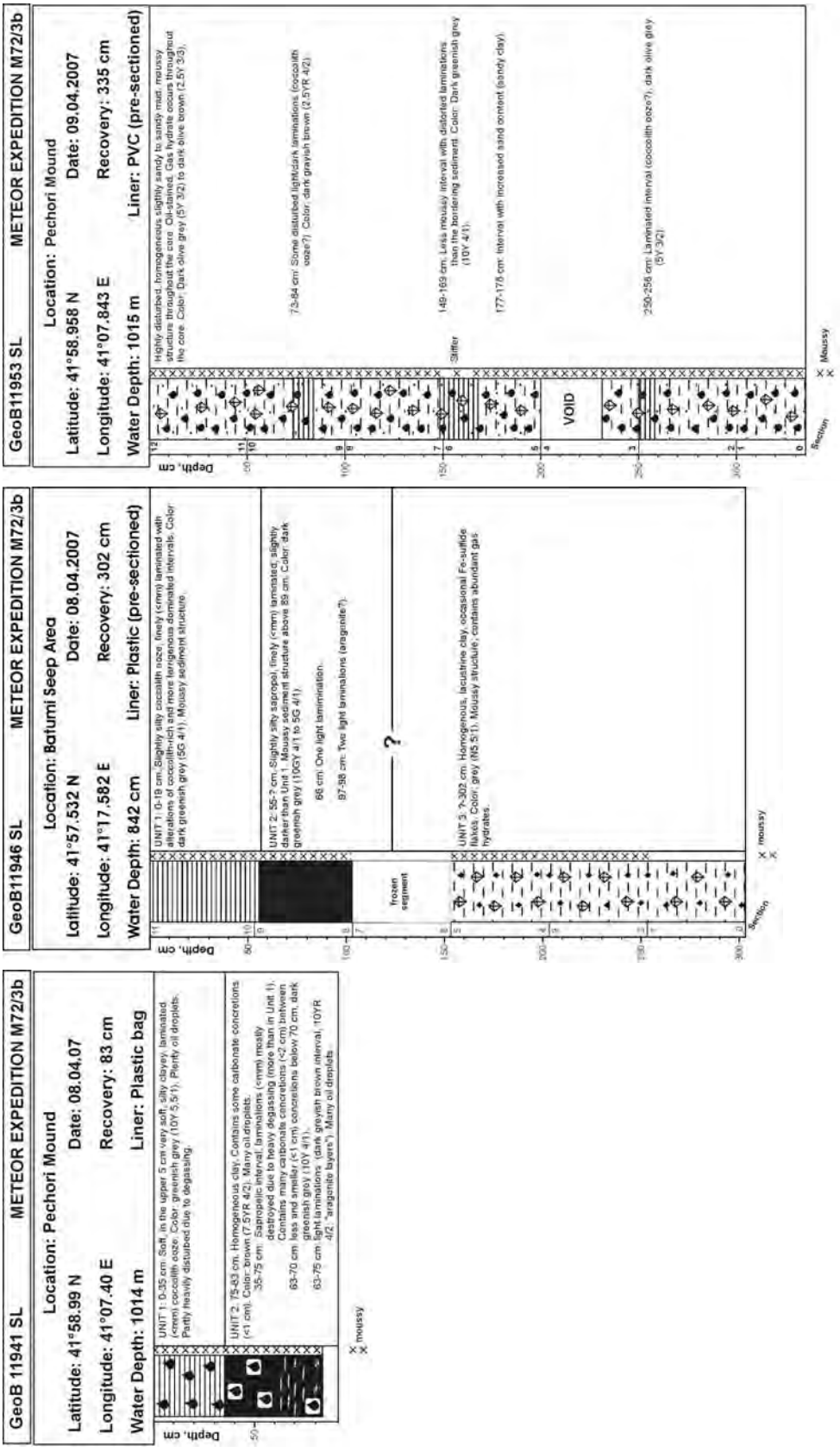

Plate A 5, continuation: Sedimentological core descriptions

Plate A 5, continuation: Sedimentological core descriptions

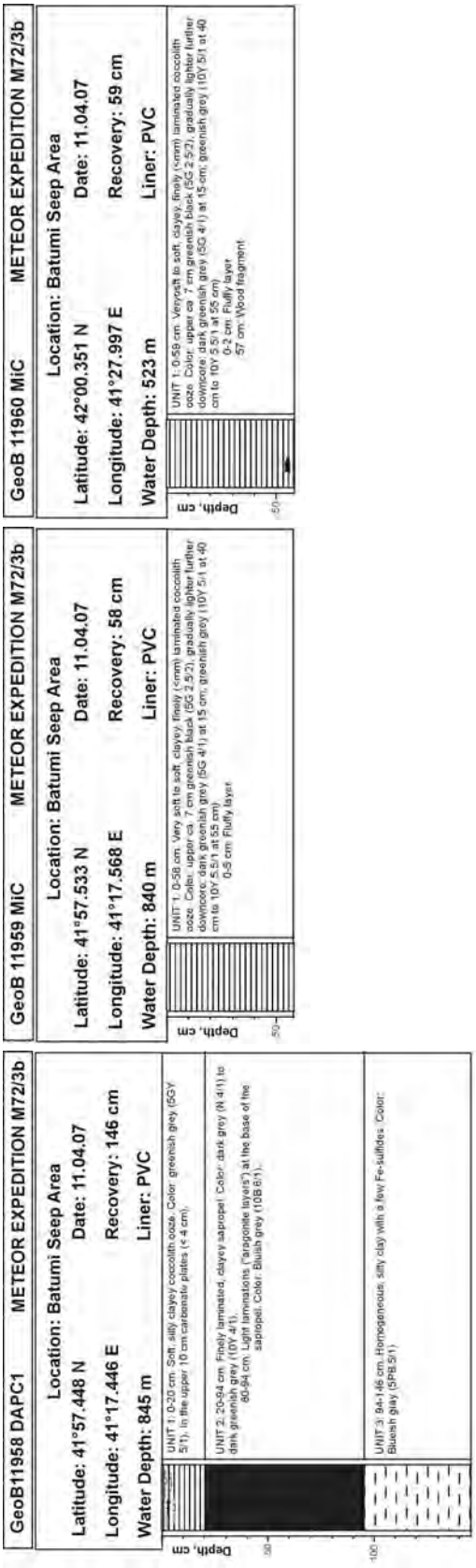

Plate A 5, continuation: Sedimentological core descriptions

Plate A 5, continuation: Sedimentological core descriptions

Plate A 5, continuation: Sedimentological core descriptions

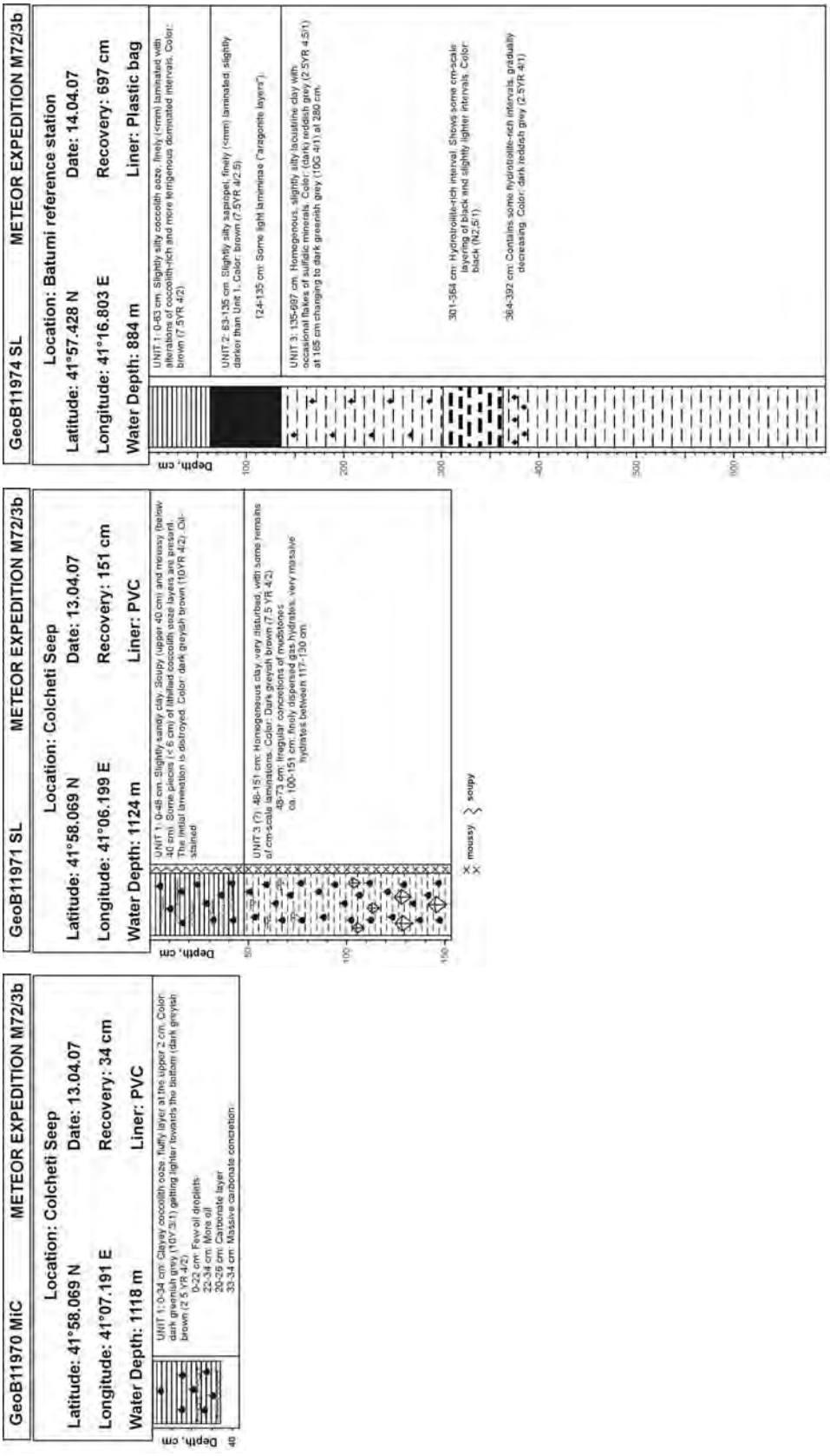

Plate A 5, continuation: Sedimentological core descriptions

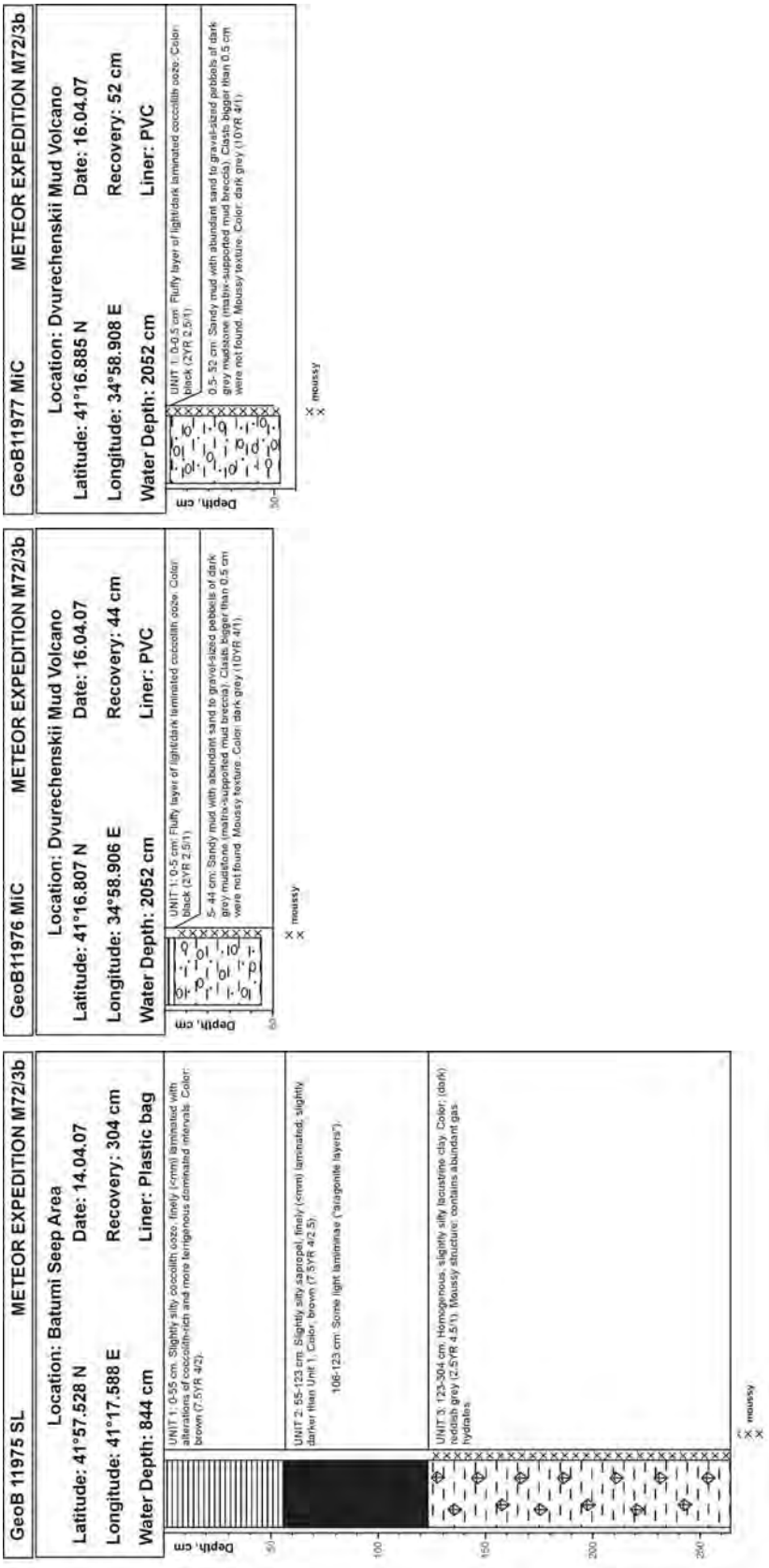

Plate A 5, continuation: Sedimentological core descriptions

Plate A 5, continuation: Sedimentological core descriptions

Plate A 5, continuation: Sedimentological core descriptions

Plate A 5, continuation: Sedimentological core descriptions

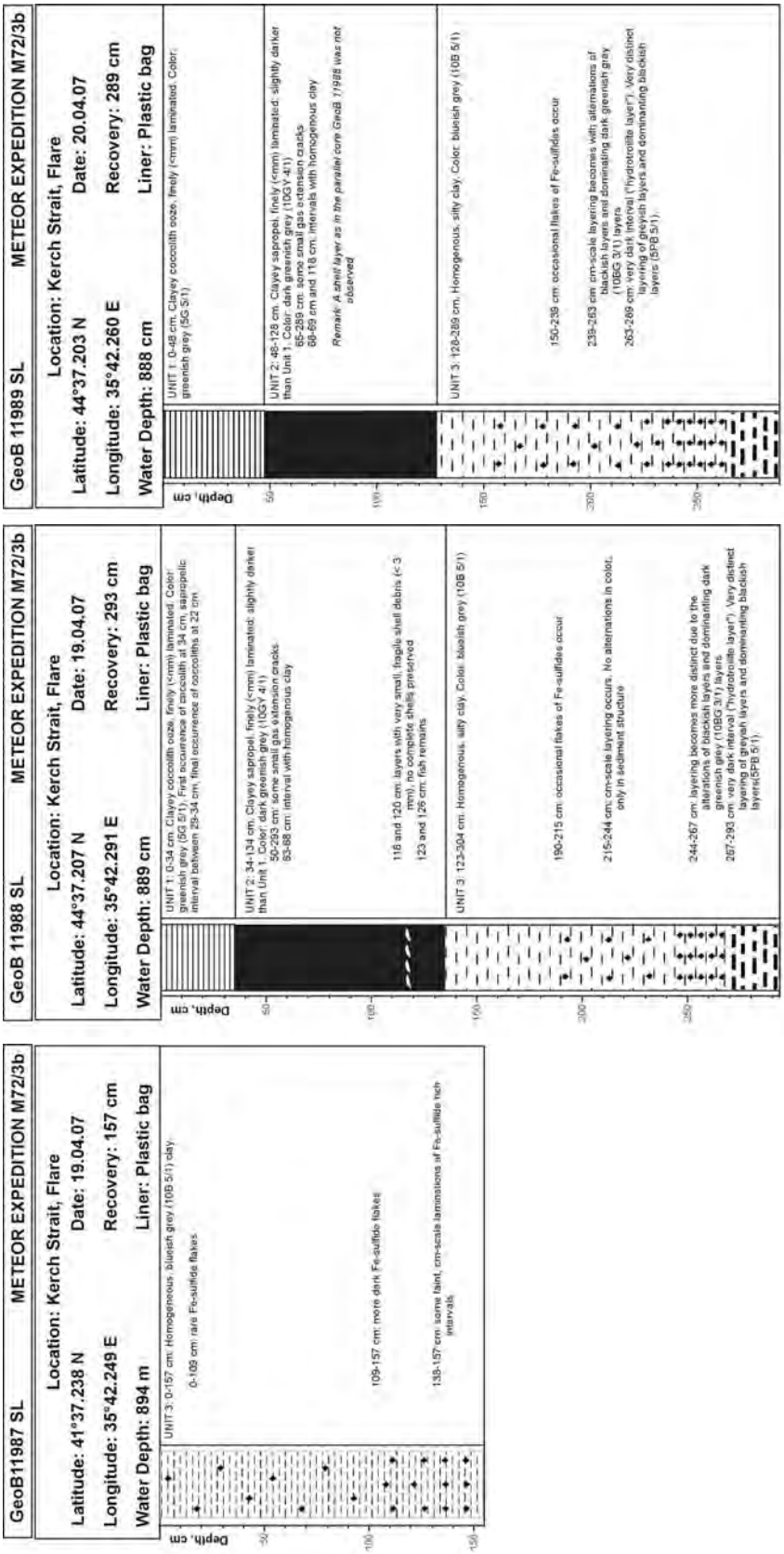

Plate A 5, continuation: Sedimentological core descriptions

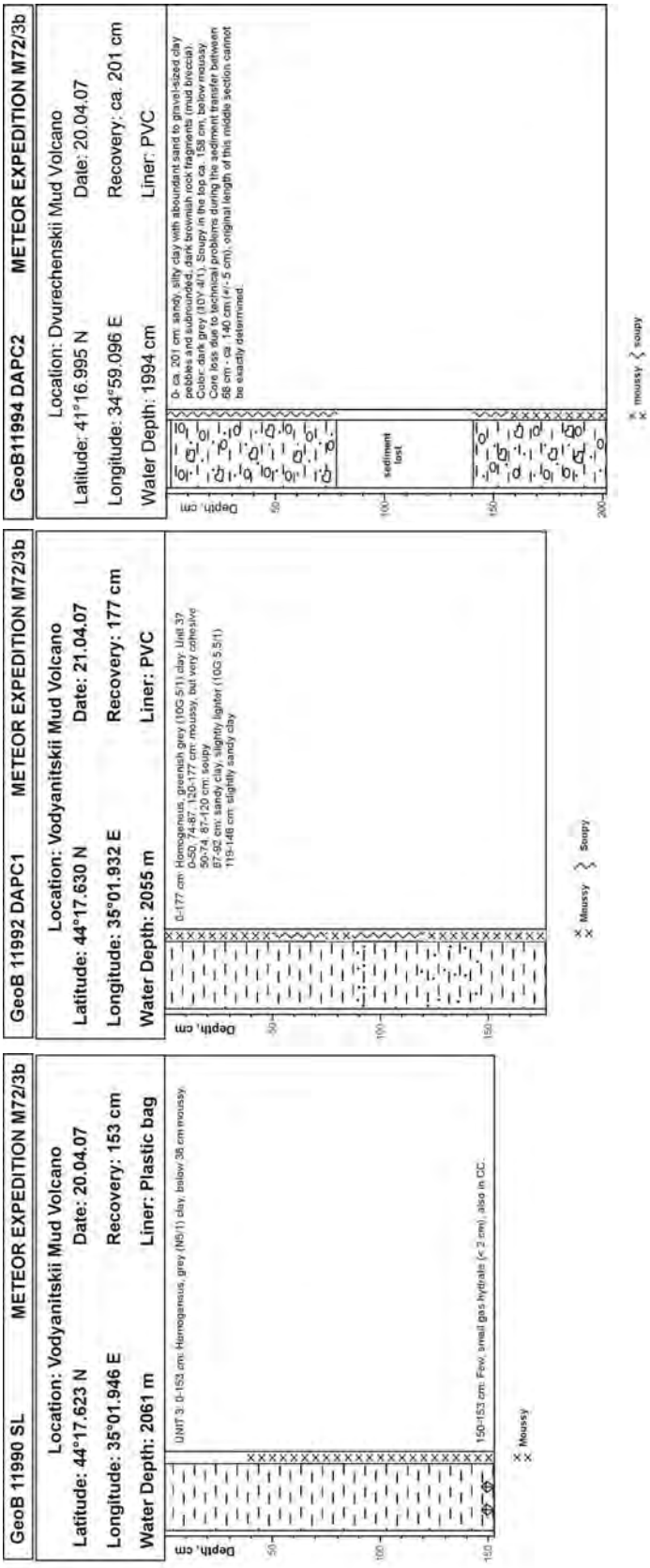

Plate A 5, continuation: Sedimentological core descriptions

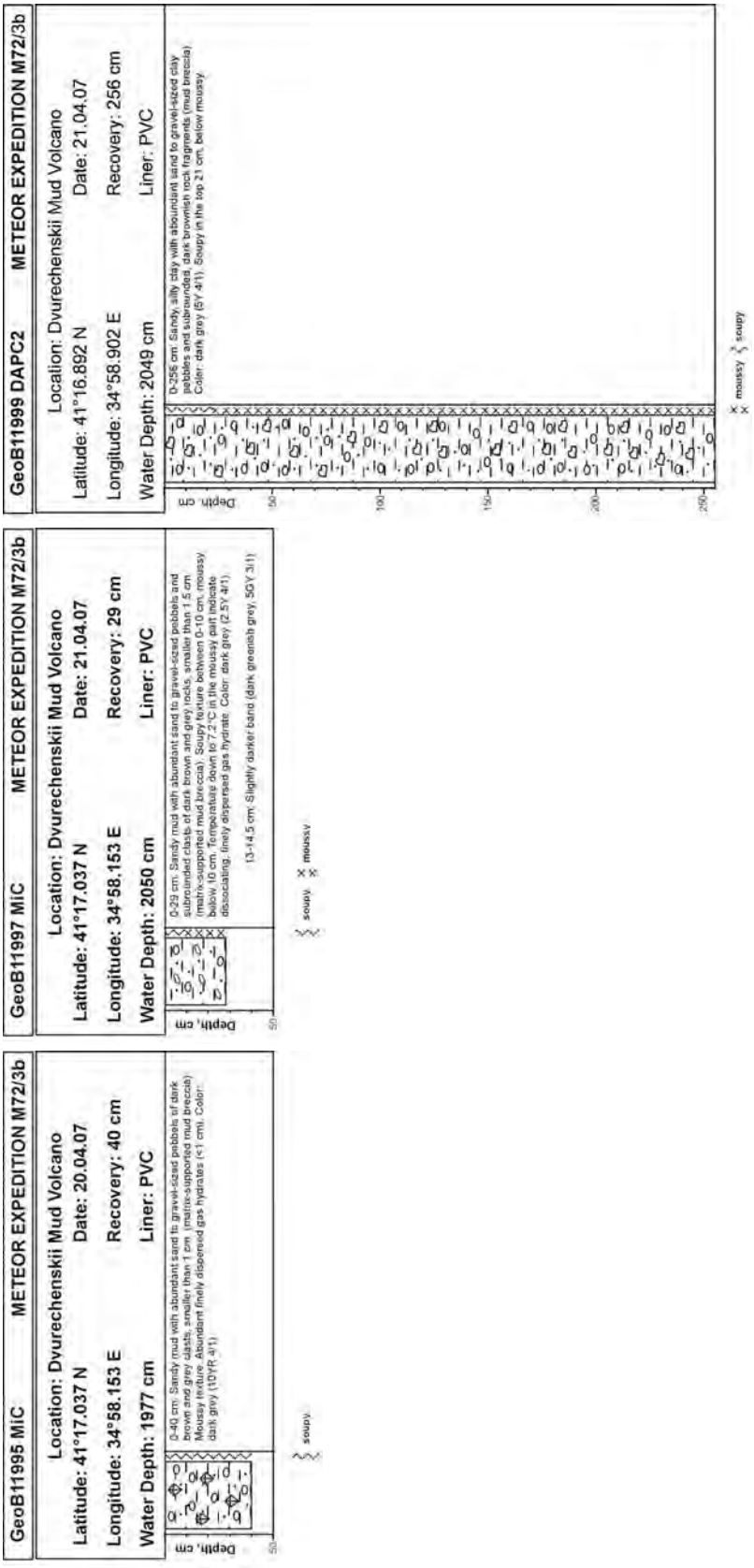

Publications of this series:

No. 1 **Wefer, G., E. Suess and cruise participants**
Bericht über die POLARSTERN-Fahrt ANT IV/2, Rio de Janeiro - Punta Arenas, 6.11. - 1.12.1985.
60 pages, Bremen, 1986.

No. 2 **Hoffmann, G.**
Holozänstratigraphie und Küstenlinienverlagerung an der andalusischen Mittelmeerküste.
173 pages, Bremen, 1988. (out of print)

No. 3 **Wefer, G. and cruise participants**
Bericht über die METEOR-Fahrt M 6/6, Libreville - Las Palmas, 18.2. - 23.3.1988.
97 pages, Bremen, 1988.

No. 4 **Wefer, G., G.F. Lutze, T.J. Müller, O. Pfannkuche, W. Schenke, G. Siedler, W. Zenk**
Kurzbericht über die METEOR-Expedition No. 6, Hamburg - Hamburg, 28.10.1987 - 19.5.1988.
29 pages, Bremen, 1988. (out of print)

No. 5 **Fischer, G.**
Stabile Kohlenstoff-Isotope in partikulärer organischer Substanz aus dem Südpolarmeer (Atlantischer Sektor). 161 pages, Bremen, 1989.

No. 6 **Berger, W.H. and G. Wefer**
Partikelfluß und Kohlenstoffkreislauf im Ozean.
Bericht und Kurzfassungen über den Workshop vom 3.-4. Juli 1989 in Bremen.
57 pages, Bremen, 1989.

No. 7 **Wefer, G. and cruise participants**
Bericht über die METEOR - Fahrt M 9/4, Dakar - Santa Cruz, 19.2. - 16.3.1989.
103 pages, Bremen, 1989.

No. 8 **Kölling, M.**
Modellierung geochemischer Prozesse im Sickerwasser und Grundwasser.
135 pages, Bremen, 1990.

No. 9 **Heinze, P.-M.**
Das Auftriebsgeschehen vor Peru im Spätquartär. 204 pages, Bremen, 1990. (out of print)

No. 10 **Willems, H., G. Wefer, M. Rinski, B. Donner, H.-J. Bellmann, L. Eißmann, A. Müller, B.W. Flemming, H.-C. Höfle, J. Merkt, H. Streif, G. Hertweck, H. Kuntze, J. Schwaar, W. Schäfer, M.-G. Schulz, F. Grube, B. Menke**
Beiträge zur Geologie und Paläontologie Norddeutschlands: Exkursionsführer.
202 pages, Bremen, 1990.

No. 11 **Wefer, G. and cruise participants**
Bericht über die METEOR-Fahrt M 12/1, Kapstadt - Funchal, 13.3.1990 - 14.4.1990.
66 pages, Bremen, 1990.

No. 12 **Dahmke, A., H.D. Schulz, A. Kölling, F. Kracht, A. Lücke**
Schwermetallspuren und geochemische Gleichgewichte zwischen Porenlösung und Sediment im Wesermündungsgebiet. BMFT-Projekt MFU 0562, Abschlußbericht. 121 pages, Bremen, 1991.

No. 13 **Rostek, F.**
Physikalische Strukturen von Tiefseesedimenten des Südatlantiks und ihre Erfassung in Echolotregistrierungen. 209 pages, Bremen, 1991.

No. 14 **Baumann, M.**
Die Ablagerung von Tschernobyl-Radiocäsium in der Norwegischen See und in der Nordsee.
133 pages, Bremen, 1991. (out of print)

No. 15 **Kölling, A.**
Frühdiagenetische Prozesse und Stoff-Flüsse in marinen und ästuarinen Sedimenten.
140 pages, Bremen, 1991.

No. 16 **SFB 261 (ed.)**
1. Kolloquium des Sonderforschungsbereichs 261 der Universität Bremen (14.Juni 1991):
Der Südatlantik im Spätquartär: Rekonstruktion von Stoffhaushalt und Stromsystemen.
Kurzfassungen der Vorträge und Poster. 66 pages, Bremen, 1991.

No. 17 **Pätzold, J. and cruise participants**
Bericht und erste Ergebnisse über die METEOR-Fahrt M 15/2, Rio de Janeiro - Vitoria,
18.1. - 7.2.1991. 46 pages, Bremen, 1993.

No. 18 **Wefer, G. and cruise participants**
Bericht und erste Ergebnisse über die METEOR-Fahrt M 16/1, Pointe Noire - Recife,
27.3. - 25.4.1991. 120 pages, Bremen, 1991.

No. 19 **Schulz, H.D. and cruise participants**
Bericht und erste Ergebnisse über die METEOR-Fahrt M 16/2, Recife - Belem, 28.4. - 20.5.1991.
149 pages, Bremen, 1991.

No. 20 **Berner, H.**
Mechanismen der Sedimentbildung in der Fram-Straße, im Arktischen Ozean und in der Norwegischen See. 167 pages, Bremen, 1991.

No. 21 **Schneider, R.**
Spätquartäre Produktivitätsänderungen im östlichen Angola-Becken: Reaktion auf Variationen im Passat-Monsun-Windsystem und in der Advektion des Benguela-Küstenstroms.
198 pages, Bremen, 1991. (out of print)

No. 22 **Hebbeln, D.**
Spätquartäre Stratigraphie und Paläozeanographie in der Fram-Straße. 174 pages, Bremen, 1991.

No. 23 **Lücke, A.**
Umsetzungsprozesse organischer Substanz während der Frühdiagenese in ästuarinen Sedimenten.
137 pages, Bremen, 1991.

No. 24 **Wefer, G. and cruise participants**
Bericht und erste Ergebnisse der METEOR-Fahrt M 20/1, Bremen - Abidjan, 18.11.- 22.12.1991.
74 pages, Bremen, 1992.

No. 25 **Schulz, H.D. and cruise participants**
Bericht und erste Ergebnisse der METEOR-Fahrt M 20/2, Abidjan - Dakar, 27.12.1991 - 3.2.1992.
173 pages, Bremen, 1992.

No. 26 **Gingele, F.**
Zur klimaabhängigen Bildung biogener und terrigener Sedimente und ihrer Veränderung durch die Frühdiagenese im zentralen und östlichen Südatlantik. 202 pages, Bremen, 1992.

No. 27 **Bickert, T.**
Rekonstruktion der spätquartären Bodenwasserzirkulation im östlichen Südatlantik über stabile Isotope benthischer Foraminiferen. 205 pages, Bremen, 1992. (out of print)

No. 28 **Schmidt, H.**
Der Benguela-Strom im Bereich des Walfisch-Rückens im Spätquartär. 172 pages, Bremen, 1992.

No. 29 **Meinecke, G.**
Spätquartäre Oberflächenwassertemperaturen im östlichen äquatorialen Atlantik.
181 pages, Bremen, 1992.

No. 30 **Bathmann, U., U. Bleil, A. Dahmke, P. Müller, A. Nehrkorn, E.-M. Nöthig, M. Olesch, J. Pätzold, H.D. Schulz, V. Smetacek, V. Spieß, G. Wefer, H. Willems**
Bericht des Graduierten Kollegs. Stoff-Flüsse in marinen Geosystemen.
Berichtszeitraum Oktober 1990 - Dezember 1992. 396 pages, Bremen, 1992.

No. 31 **Damm, E.**
Frühdiagenetische Verteilung von Schwermetallen in Schlicksedimenten der westlichen Ostsee.
115 pages, Bremen, 1992.

No. 32 **Antia, E.E.**
Sedimentology, Morphodynamics and Facies Association of a mesotidal Barrier Island Shoreface (Spiekeroog, Southern North Sea). 370 pages, Bremen, 1993.

No. 33 **Duinker, J. and G. Wefer (ed.)**
Bericht über den 1. JGOFS-Workshop. 1./2. Dezember 1992 in Bremen. 83 pages, Bremen, 1993.

No. 34 **Kasten, S.**
Die Verteilung von Schwermetallen in den Sedimenten eines stadtbremischen Hafenbeckens.
103 pages, Bremen, 1993.

No. 35 **Spieß, V.**
Digitale Sedimentographie. Neue Wege zu einer hochauflösenden Akustostratigraphie.
199 pages, Bremen, 1993.

No. 36 **Schinzel, U.**
Laborversuche zu frühdiagenetischen Reaktionen von Eisen (III) - Oxidhydraten in marinen Sedimenten.189 pages, Bremen, 1993.

No. 37 **Sieger, R.**
CoTAM - ein Modell zur Modellierung des Schwermetalltransports in Grundwasserleitern.
56 pages, Bremen, 1993. (out of print)

No. 38 **Willems, H. (ed.)**
Geoscientific Investigations in the Tethyan Himalayas. 183 pages, Bremen, 1993.

No. 39 **Hamer, K.**
Entwicklung von Laborversuchen als Grundlage für die Modellierung des Transportverhaltens von Arsenat, Blei, Cadmium und Kupfer in wassergesättigten Säulen. 147 pages, Bremen, 1993.

No. 40 **Sieger, R.**
Modellierung des Stofftransports in porösen Medien unter Ankopplung kinetisch gesteuerter Sorptions- und Redoxprozesse sowie thermischer Gleichgewichte. 158 pages, Bremen, 1993.

No. 41 **Thießen, W.**
Magnetische Eigenschaften von Sedimenten des östlichen Südatlantiks und ihre paläozeanographische Relevanz. 170 pages, Bremen, 1993.

No. 42 **Spieß, V. and cruise participants**
Report and preliminary results of METEOR-Cruise M 23/1, Kapstadt - Rio de Janeiro, 4.-25.2.1993. 139 pages, Bremen, 1994.

No. 43 **Bleil, U. and cruise participants**
Report and preliminary results of METEOR-Cruise M 23/2, Rio de Janeiro - Recife, 27.2.-19.3.1993 133 pages, Bremen, 1994.

No. 44 **Wefer, G. and cruise participants**
Report and preliminary results of METEOR-Cruise M 23/3, Recife - Las Palmas, 21.3. - 12.4.1993 71 pages, Bremen, 1994.

No. 45 **Giese, M. and G. Wefer (ed.)**
Bericht über den 2. JGOFS-Workshop. 18../19. November 1993 in Bremen. 93 pages, Bremen, 1994.

No. 46 **Balzer, W. and cruise participants**
Report and preliminary results of METEOR-Cruise M 22/1, Hamburg - Recife, 22.9. - 21.10.1992. 24 pages, Bremen, 1994.

No. 47 **Stax, R.**
Zyklische Sedimentation von organischem Kohlenstoff in der Japan See: Anzeiger für Änderungen von Paläoozeanographie und Paläoklima im Spätkänozoikum. 150 pages, Bremen, 1994.

No. 48 **Skowronek, F.**
Frühdiagenetische Stoff-Flüsse gelöster Schwermetalle an der Oberfläche von Sedimenten des Weser Ästuares. 107 pages, Bremen, 1994.

No. 49 **Dersch-Hansmann, M.**
Zur Klimaentwicklung in Ostasien während der letzten 5 Millionen Jahre: Terrigener Sedimenteintrag in die Japan See (ODP Ausfahrt 128). 149 pages, Bremen, 1994.

No. 50 **Zabel, M.**
Frühdiagenetische Stoff-Flüsse in Oberflächen-Sedimenten des äquatorialen und östlichen Südatlantik. 129 pages, Bremen, 1994.

No. 51 **Bleil, U. and cruise participants**
Report and preliminary results of SONNE-Cruise SO 86, Buenos Aires - Capetown, 22.4. - 31.5.93 116 pages, Bremen, 1994.

No. 52 **Symposium: The South Atlantic: Present and Past Circulation.**
Bremen, Germany, 15 - 19 August 1994. Abstracts. 167 pages, Bremen, 1994.

No. 53 **Kretzmann, U.B.**
^{57}Fe-Mössbauer-Spektroskopie an Sedimenten - Möglichkeiten und Grenzen. 183 pages, Bremen, 1994.

No. 54 **Bachmann, M.**
Die Karbonatrampe von Organyà im oberen Oberapt und unteren Unteralb (NE-Spanien, Prov. Lerida): Fazies, Zyklo- und Sequenzstratigraphie. 147 pages, Bremen, 1994. (out of print)

No. 55 **Kemle-von Mücke, S.**
Oberflächenwasserstruktur und -zirkulation des Südostatlantiks im Spätquartär. 151 pages, Bremen, 1994.

No. 56 **Petermann, H.**
Magnetotaktische Bakterien und ihre Magnetosome in Oberflächensedimenten des Südatlantiks. 134 pages, Bremen, 1994.

No. 57 **Mulitza, S.**
Spätquartäre Variationen der oberflächennahen Hydrographie im westlichen äquatorialen Atlantik. 97 pages, Bremen, 1994.

No. 58 **Segl, M. and cruise participants**
Report and preliminary results of METEOR-Cruise M 29/1, Buenos-Aires - Montevideo, 17.6. - 13.7.1994
94 pages, Bremen, 1994.

No. 59 **Bleil, U. and cruise participants**
Report and preliminary results of METEOR-Cruise M 29/2, Montevideo - Rio de Janiero 15.7. - 8.8.1994. 153 pages, Bremen, 1994.

No. 60 **Henrich, R. and cruise participants**
Report and preliminary results of METEOR-Cruise M 29/3, Rio de Janeiro - Las Palmas 11.8. - 5.9.1994. Bremen, 1994. (out of print)

No. 61 **Sagemann, J.**
Saisonale Variationen von Porenwasserprofilen, Nährstoff-Flüssen und Reaktionen in intertidalen Sedimenten des Weser-Ästuars. 110 pages, Bremen, 1994. (out of print)

No. 62 **Giese, M. and G. Wefer**
Bericht über den 3. JGOFS-Workshop. 5./6. Dezember 1994 in Bremen.
84 pages, Bremen, 1995.

No. 63 **Mann, U.**
Genese kretazischer Schwarzschiefer in Kolumbien: Globale vs. regionale/lokale Prozesse.
153 pages, Bremen, 1995. (out of print)

No. 64 **Willems, H., Wan X., Yin J., Dongdui L., Liu G., S. Dürr, K.-U. Gräfe**
The Mesozoic development of the N-Indian passive margin and of the Xigaze Forearc Basin in southern Tibet, China. – Excursion Guide to IGCP 362 Working-Group Meeting "Integrated Stratigraphy". 113 pages, Bremen, 1995. (out of print)

No. 65 **Hünken, U.**
Liefergebiets - Charakterisierung proterozoischer Goldseifen in Ghana anhand von Fluideinschluß - Untersuchungen. 270 pages, Bremen, 1995.

No. 66 **Nyandwi, N.**
The Nature of the Sediment Distribution Patterns in ther Spiekeroog Backbarrier Area, the East Frisian Islands. 162 pages, Bremen, 1995.

No. 67 **Isenbeck-Schröter, M.**
Transportverhalten von Schwermetallkationen und Oxoanionen in wassergesättigten Sanden. - Laborversuche in Säulen und ihre Modellierung -. 182 pages, Bremen, 1995.

No. 68 **Hebbeln, D. and cruise participants**
Report and preliminary results of SONNE-Cruise SO 102, Valparaiso - Valparaiso, 95.
134 pages, Bremen, 1995.

No. 69 **Willems, H. (Sprecher), U.Bathmann, U. Bleil, T. v. Dobeneck, K. Herterich, B.B. Jorgensen, E.-M. Nöthig, M. Olesch, J. Pätzold, H.D. Schulz, V. Smetacek, V. Speiß. G. Wefer**
Bericht des Graduierten-Kollegs Stoff-Flüsse in marine Geosystemen.
Berichtszeitraum Januar 1993 - Dezember 1995.
45 & 468 pages, Bremen, 1995.

No. 70 **Giese, M. and G. Wefer**
Bericht über den 4. JGOFS-Workshop. 20./21. November 1995 in Bremen. 60 pages, Bremen, 1996. (out of print)

No. 71 **Meggers, H.**
Pliozän-quartäre Karbonatsedimentation und Paläozeanographie des Nordatlantiks und des Europäischen Nordmeeres - Hinweise aus planktischen Foraminiferengemeinschaften.
143 pages, Bremen, 1996. (out of print)

No. 72 **Teske, A.**
Phylogenetische und ökologische Untersuchungen an Bakterien des oxidativen und reduktiven marinen Schwefelkreislaufs mittels ribosomaler RNA. 220 pages, Bremen, 1996. (out of print)

No. 73 **Andersen, N.**
Biogeochemische Charakterisierung von Sinkstoffen und Sedimenten aus ostatlantischen Produktions-Systemen mit Hilfe von Biomarkern. 215 pages, Bremen, 1996.

No. 74 **Treppke, U.**
Saisonalität im Diatomeen- und Silikoflagellatenfluß im östlichen tropischen und subtropischen Atlantik. 200 pages, Bremen, 1996.

No. 75 **Schüring, J.**
Die Verwendung von Steinkohlebergematerialien im Deponiebau im Hinblick auf die Pyritverwitterung und die Eignung als geochemische Barriere. 110 pages, Bremen, 1996.

No. 76 **Pätzold, J. and cruise participants**
Report and preliminary results of VICTOR HENSEN cruise JOPS II, Leg 6, Fortaleza - Recife, 10.3. - 26.3. 1995 and Leg 8, Vítoria - Vítoria, 10.4. - 23.4.1995.
87 pages, Bremen, 1996.

No. 77 **Bleil, U. and cruise participants**
Report and preliminary results of METEOR-Cruise M 34/1, Cape Town - Walvis Bay, 3.-26.1.1996.
129 pages, Bremen, 1996.

No. 78 **Schulz, H.D. and cruise participants**
Report and preliminary results of METEOR-Cruise M 34/2, Walvis Bay - Walvis Bay, 29.1.-18.2.96
133 pages, Bremen, 1996.

No. 79 **Wefer, G. and cruise participants**
Report and preliminary results of METEOR-Cruise M 34/3, Walvis Bay - Recife, 21.2.-17.3.1996.
168 pages, Bremen, 1996.

No. 80 **Fischer, G. and cruise participants**
Report and preliminary results of METEOR-Cruise M 34/4, Recife - Bridgetown, 19.3.-15.4.1996. 105 pages, Bremen, 1996.

No. 81 **Kulbrok, F.**
Biostratigraphie, Fazies und Sequenzstratigraphie einer Karbonatrampe in den Schichten der Oberkreide und des Alttertiärs Nordost-Ägyptens (Eastern Desert, N'Golf von Suez, Sinai). 153 pages, Bremen, 1996.

No. 82 **Kasten, S.**
Early Diagenetic Metal Enrichments in Marine Sediments as Documents of Nonsteady-State Depositional Conditions. Bremen, 1996.

No. 83 **Holmes, M.E.**
Reconstruction of Surface Ocean Nitrate Utilization in the Southeast Atlantic Ocean Based on Stable Nitrogen Isotopes. 113 pages, Bremen, 1996.

No. 84 **Rühlemann, C.**
Akkumulation von Carbonat und organischem Kohlenstoff im tropischen Atlantik: Spätquartäre Produktivitäts-Variationen und ihre Steuerungsmechanismen. 139 pages, Bremen, 1996.

No. 85 **Ratmeyer, V.**
Untersuchungen zum Eintrag und Transport lithogener und organischer partikulärer Substanz im östlichen subtropischen Nordatlantik. 154 pages, Bremen, 1996.

No. 86 **Cepek, M.**
Zeitliche und räumliche Variationen von Coccolithophoriden-Gemeinschaften im subtropischen Ost-Atlantik: Untersuchungen an Plankton, Sinkstoffen und Sedimenten. 156 pages, Bremen, 1996.

No. 87 **Otto, S.**
Die Bedeutung von gelöstem organischen Kohlenstoff (DOC) für den Kohlenstoffffluß im Ozean. 150 pages, Bremen, 1996.

No. 88 **Hensen, C.**
Frühdiagenetische Prozesse und Quantifizierung benthischer Stoff-Flüsse in Oberflächensedimenten des Südatlantiks. 132 pages, Bremen, 1996.

No. 89 **Giese, M. and G. Wefer**
Bericht über den 5. JGOFS-Workshop. 27./28. November 1996 in Bremen. 73 pages, Bremen, 1997.

No. 90 **Wefer, G. and cruise participants**
Report and preliminary results of METEOR-Cruise M 37/1, Lisbon - Las Palmas, 4.-23.12.1996. 79 pages, Bremen, 1997.

No. 91 **Isenbeck-Schröter, M., E. Bedbur, M. Kofod, B. König, T. Schramm & G. Mattheß**
Occurrence of Pesticide Residues in Water - Assessment of the Current Situation in Selected EU Countries. 65 pages, Bremen 1997.

No. 92 **Kühn, M.**
Geochemische Folgereaktionen bei der hydrogeothermalen Energiegewinnung. 129 pages, Bremen 1997.

No. 93 **Determann, S. & K. Herterich**
JGOFS-A6 "Daten und Modelle": Sammlung JGOFS-relevanter Modelle in Deutschland. 26 pages, Bremen, 1997.

No. 94 **Fischer, G. and cruise participants**
Report and preliminary results of METEOR-Cruise M 38/1, Las Palmas - Recife, 25.1.-1.3.1997, with Appendix: Core Descriptions from METEOR Cruise M 37/1. Bremen, 1997.

No. 95 **Bleil, U. and cruise participants**
Report and preliminary results of METEOR-Cruise M 38/2, Recife - Las Palmas, 4.3.-14.4.1997. 126 pages, Bremen, 1997.

No. 96 **Neuer, S. and cruise participants**
Report and preliminary results of VICTOR HENSEN-Cruise 96/1. Bremen, 1997.

No. 97 **Villinger, H. and cruise participants**
Fahrtbericht SO 111, 20.8. - 16.9.1996. 115 pages, Bremen, 1997.

No. 98 **Lüning, S.**
Late Cretaceous - Early Tertiary sequence stratigraphy, paleoecology and geodynamics of Eastern Sinai, Egypt. 218 pages, Bremen, 1997.

No. 99 **Haese, R.R.**
Beschreibung und Quantifizierung frühdiagenetischer Reaktionen des Eisens in Sedimenten des Südatlantiks. 118 pages, Bremen, 1997.

No. 100 **Lührte, R. von**
Verwertung von Bremer Baggergut als Material zur Oberflächenabdichtung von Deponien - Geochemisches Langzeitverhalten und Schwermetall-Mobilität (Cd, Cu, Ni, Pb, Zn). Bremen, 1997.

No. 101 **Ebert, M.**
Der Einfluß des Redoxmilieus auf die Mobilität von Chrom im durchströmten Aquifer. 135 pages, Bremen, 1997.

No. 102 **Krögel, F.**
Einfluß von Viskosität und Dichte des Seewassers auf Transport und Ablagerung von Wattsedimenten (Langeooger Rückseitenwatt, südliche Nordsee). 168 pages, Bremen, 1997.

No. 103 **Kerntopf, B.**
Dinoflagellate Distribution Patterns and Preservation in the Equatorial Atlantic and Offshore North-West Africa. 137 pages, Bremen, 1997.

No. 104 **Breitzke, M.**
Elastische Wellenausbreitung in marinen Sedimenten - Neue Entwicklungen der Ultraschall Sedimentphysik und Sedimentechographie. 298 pages, Bremen, 1997.

No. 105 **Marchant, M.**
Rezente und spätquartäre Sedimentation planktischer Foraminiferen im Peru-Chile Strom. 115 pages, Bremen, 1997.

No. 106 **Habicht, K.S.**
Sulfur isotope fractionation in marine sediments and bacterial cultures. 125 pages, Bremen, 1997.

No. 107 **Hamer, K., R.v. Lührte, G. Becker, T. Felis, S. Keffel, B. Strotmann, C. Waschkowitz, M. Kölling, M. Isenbeck-Schröter, H.D. Schulz**
Endbericht zum Forschungsvorhaben 060 des Landes Bremen: Baggergut der Hafengruppe Bremen-Stadt: Modelluntersuchungen zur Schwermetallmobilität und Möglichkeiten der Verwertung von Hafenschlick aus Bremischen Häfen. 98 pages, Bremen, 1997.

No. 108 **Greeff, O.W.**
Entwicklung und Erprobung eines benthischen Landersystemes zur *in situ*-Bestimmung von Sulfatreduktionsraten mariner Sedimente. 121 pages, Bremen, 1997.

No. 109 **Pätzold, M. und G. Wefer**
Bericht über den 6. JGOFS-Workshop am 4./5.12.1997 in Bremen. Im Anhang: Publikationen zum deutschen Beitrag zur Joint Global Ocean Flux Study (JGOFS), Stand 1/1998. 122 pages, Bremen, 1998.

No. 110 **Landenberger, H.**
CoTReM, ein Multi-Komponenten Transport- und Reaktions-Modell. 142 pages, Bremen, 1998.

No. 111 **Villinger, H. und Fahrtteilnehmer**
Fahrtbericht SO 124, 4.10. - 16.10.199. 90 pages, Bremen, 1997.

No. 112 **Gietl, R.**
Biostratigraphie und Sedimentationsmuster einer nordostägyptischen Karbonatrampe unter Berücksichtigung der Alveolinen-Faunen. 142 pages, Bremen, 1998.

No. 113 **Ziebis, W.**
The Impact of the Thalassinidean Shrimp *Callianassa truncata* on the Geochemistry of permeable, coastal Sediments. 158 pages, Bremen 1998.

No. 114 **Schulz, H.D. and cruise participants**
Report and preliminary results of METEOR-Cruise M 41/1, Málaga - Libreville, 13.2.-15.3.1998. Bremen, 1998.

No. 115 **Völker, D.J.**
Untersuchungen an strömungsbeeinflußten Sedimentationsmustern im Südozean. Interpretation sedimentechographischer Daten und numerische Modellierung. 152 pages, Bremen, 1998.

No. 116 **Schlünz, B.**
Riverine Organic Carbon Input into the Ocean in Relation to Late Quaternary Climate Change. 136 pages, Bremen, 1998.

No. 117 **Kuhnert, H.**
Aufzeichnug des Klimas vor Westaustralien in stabilen Isotopen in Korallenskeletten. 109 pages, Bremen, 1998.

No. 118 **Kirst, G.**
Rekonstruktion von Oberflächenwassertemperaturen im östlichen Südatlantik anhand von Alkenonen. 130 pages, Bremen, 1998.

No. 119 **Dürkoop, A.**
Der Brasil-Strom im Spätquartär: Rekonstruktion der oberflächennahen Hydrographie während der letzten 400 000 Jahre. 121 pages, Bremen, 1998.

No. 120 **Lamy, F.**
Spätquartäre Variationen des terrigenen Sedimenteintrags entlang des chilenischen Kontinentalhangs als Abbild von Klimavariabilität im Milanković- und Sub-Milanković-Zeitbereich. 141 pages, Bremen, 1998.

No. 121 **Neuer, S. and cruise participants**
Report and preliminary results of POSEIDON-Cruise Pos 237/2, Vigo – Las Palmas, 18.3.-31.3.1998. 39 pages, Bremen, 1998

No. 122 **Romero, O.E.**
Marine planktonic diatoms from the tropical and equatorial Atlantic: temporal flux patterns and the sediment record. 205 pages, Bremen, 1998.

No. 123 **Spiess, V. und Fahrtteilnehmer**
Report and preliminary results of RV SONNE Cruise 125, Cochin – Chittagong, 17.10.-17.11.1997. 128 pages, Bremen, 1998.

No. 124 **Arz, H.W.**
Dokumentation von kurzfristigen Klimaschwankungen des Spätquartärs in Sedimenten des westlichen äquatorialen Atlantiks. 96 pages, Bremen, 1998.

No. 125 **Wolff, T.**
Mixed layer characteristics in the equatorial Atlantic during the late Quaternary as deduced from planktonic foraminifera. 132 pages, Bremen, 1998.

No. 126 **Dittert, N.**
Late Quaternary Planktic Foraminifera Assemblages in the South Atlantic Ocean: Quantitative Determination and Preservational Aspects. 165 pages, Bremen, 1998.

No. 127 **Höll, C.**
Kalkige und organisch-wandige Dinoflagellaten-Zysten in Spätquartären Sedimenten des tropischen Atlantiks und ihre palökologische Auswertbarkeit. 121 pages, Bremen, 1998.

No. 128 **Hencke, J.**
Redoxreaktionen im Grundwasser: Etablierung und Verlagerung von Reaktionsfronten und ihre Bedeutung für die Spurenelement-Mobilität. 122 pages, Bremen 1998.

No. 129 **Pätzold, J. and cruise participants**
Report and preliminary results of METEOR-Cruise M 41/3, Vítoria, Brasil – Salvador de Bahia, Brasil, 18.4. - 15.5.1998. Bremen, 1999.

No. 130 **Fischer, G. and cruise participants**
Report and preliminary results of METEOR-Cruise M 41/4, Salvador de Bahia, Brasil – Las Palmas, Spain, 18.5. – 13.6.1998. Bremen, 1999.

No. 131 **Schlünz, B. und G. Wefer**
Bericht über den 7. JGOFS-Workshop am 3. und 4.12.1998 in Bremen. Im Anhang: Publikationen zum deutschen Beitrag zur Joint Global Ocean Flux Study (JGOFS), Stand 1/ 1999. 100 pages, Bremen, 1999.

No. 132 **Wefer, G. and cruise participants**
Report and preliminary results of METEOR-Cruise M 42/4, Las Palmas - Las Palmas - Viena do Castelo; 26.09.1998 - 26.10.1998. 104 pages, Bremen, 1999.

No. 133 **Felis, T.**
Climate and ocean variability reconstructed from stable isotope records of modern subtropical corals (Northern Red Sea). 111 pages, Bremen, 1999.

No. 134 **Draschba , S.**
North Atlantic climate variability recorded in reef corals from Bermuda. 108 pages, Bremen, 1999.

No. 135 **Schmieder, F.**
Magnetic Cyclostratigraphy of South Atlantic Sediments. 82 pages, Bremen, 1999.

No. 136 **Rieß, W.**
In situ measurements of respiration and mineralisation processes – Interaction between fauna and geochemical fluxes at active interfaces. 68 pages, Bremen, 1999.

No. 137 **Devey, C.W. and cruise participants**
Report and shipboard results from METEOR-cruise M 41/2, Libreville – Vitoria, 18.3. – 15.4.98. 59 pages, Bremen, 1999.

No. 138 **Wenzhöfer, F.**
Biogeochemical processes at the sediment water interface and quantification of metabolically driven calcite dissolution in deep sea sediments. 103 pages, Bremen, 1999.

No. 139 **Klump, J.**
Biogenic barite as a proxy of paleoproductivity variations in the Southern Peru-Chile Current. 107 pages, Bremen, 1999.

No. 140 **Huber, R.**
Carbonate sedimentation in the northern Northatlantic since the late pliocene. 103 pages, Bremen, 1999.

No. 141 **Schulz, H.**
Nitrate-storing sulfur bacteria in sediments of coastal upwelling. 94 pages, Bremen, 1999.

No. 142 **Mai, S.**
Die Sedimentverteilung im Wattenmeer: ein Simulationsmodell. 114 pages, Bremen, 1999.

No. 143 **Neuer, S. and cruise participants**
Report and preliminary results of Poseidon Cruise 248, Las Palmas - Las Palmas, 15.2.-26.2.1999.
45 pages, Bremen, 1999.

No. 144 **Weber, A.**
Schwefelkreislauf in marinen Sedimenten und Messung von *in situ* Sulfatreduktionsraten.
122 pages, Bremen, 1999.

No. 145 **Hadeler, A.**
Sorptionsreaktionen im Grundwasser: Unterschiedliche Aspekte bei der Modellierung des Transportverhaltens von Zink. 122 pages, 1999.

No. 146 **Dierßen, H.**
Zum Kreislauf ausgewählter Spurenmetalle im Südatlantik: Vertikaltransport und Wechselwirkung zwischen Partikeln und Lösung. 167 pages, Bremen, 1999.

No. 147 **Zühlsdorff, L.**
High resolution multi-frequency seismic surveys at the Eastern Juan de Fuca Ridge Flank and the Cascadia Margin – Evidence for thermally and tectonically driven fluid upflow in marine sediments. 118 pages, Bremen 1999.

No. 148 **Kinkel, H.**
Living and late Quaternary Coccolithophores in the equatorial Atlantic Ocean: response of distribution and productivity patterns to changing surface water circulation. 183 pages, Bremen, 2000.

No. 149 **Pätzold, J. and cruise participants**
Report and preliminary results of METEOR Cruise M 44/3, Aqaba (Jordan) - Safaga (Egypt) – Dubá (Saudi Arabia) – Suez (Egypt) - Haifa (Israel), 12.3.-26.3.-2.4.-4.4.1999. 135 pages, Bremen, 2000.

No. 150 **Schlünz, B. and G. Wefer**
Bericht über den 8. JGOFS-Workshop am 2. und 3.12.1999 in Bremen. Im Anhang:
Publikationen zum deutschen Beitrag zur Joint Global Ocean Flux Study (JGOFS), Stand 1/ 2000.
95 pages, Bremen, 2000.

No. 151 **Schnack, K.**
Biostratigraphie und fazielle Entwicklung in der Oberkreide und im Alttertiär im Bereich der Kharga Schwelle, Westliche Wüste, SW-Ägypten. 142 pages, Bremen, 2000.

No. 152 **Karwath, B.**
Ecological studies on living and fossil calcareous dinoflagellates of the equatorial and tropical Atlantic Ocean. 175 pages, Bremen, 2000.

No. 153 **Moustafa, Y.**
Paleoclimatic reconstructions of the Northern Red Sea during the Holocene inferred from stable isotope records of modern and fossil corals and molluscs. 102 pages, Bremen, 2000.

No. 154 **Villinger, H. and cruise participants**
Report and preliminary results of SONNE-cruise 145-1 Balboa – Talcahuana, 21.12.1999 – 28.01.2000.
147 pages, Bremen, 2000.

No. 155 **Rusch, A.**
Dynamik der Feinfraktion im Oberflächenhorizont permeabler Schelfsedimente. 102 pages, Bremen, 2000.

No. 156 **Moos, C.**
Reconstruction of upwelling intensity and paleo-nutrient gradients in the northwest Arabian Sea derived from stable carbon and oxygen isotopes of planktic foraminifera. 103 pages, Bremen, 2000.

No. 157 **Xu, W.**
Mass physical sediment properties and trends in a Wadden Sea tidal basin. 127 pages, Bremen, 2000.

No. 158 **Meinecke, G. and cruise participants**
Report and preliminary results of METEOR Cruise M 45/1, Malaga (Spain) - Lissabon (Portugal),
19.05. - 08.06.1999. 39 pages, Bremen, 2000.

No. 159 **Vink, A.**
Reconstruction of recent and late Quaternary surface water masses of the western subtropical Atlantic Ocean based on calcareous and organic-walled dinoflagellate cysts. 160 pages, Bremen, 2000.

No. 160 **Willems, H. (Sprecher), U. Bleil, R. Henrich, K. Herterich, B.B. Jørgensen, H.-J. Kuß, M. Olesch, H.D. Schulz,V. Spieß, G. Wefer**
Abschlußbericht des Graduierten-Kollegs Stoff-Flüsse in marine Geosystemen.
Zusammenfassung und Berichtszeitraum Januar 1996 - Dezember 2000. 340 pages, Bremen, 2000.

No. 161 **Sprengel, C.**
Untersuchungen zur Sedimentation und Ökologie von Coccolithophoriden im Bereich der Kanarischen Inseln: Saisonale Flussmuster und Karbonatexport. 165 pages, Bremen, 2000.

No. 162 **Donner, B. and G. Wefer**
Bericht über den JGOFS-Workshop am 18.-21.9.2000 in Bremen:
Biogeochemical Cycles: German Contributions to the International Joint Global Ocean Flux Study.
87 pages, Bremen, 2000.

No. 163 **Neuer, S. and cruise participants**
Report and preliminary results of Meteor Cruise M 45/5, Bremen – Las Palmas, October 1 – November 3, 1999. 93 pages, Bremen, 2000.

No. 164 **Devey, C. and cruise participants**
Report and preliminary results of Sonne Cruise SO 145/2, Talcahuano (Chile) - Arica (Chile), February 4 – February 29, 2000. 63 pages, Bremen, 2000.

No. 165 **Freudenthal, T.**
Reconstruction of productivity gradients in the Canary Islands region off Morocco by means of sinking particles and sediments. 147 pages, Bremen, 2000.

No. 166 **Adler, M.**
Modeling of one-dimensional transport in porous media with respect to simultaneous geochemical reactions in CoTReM. 147 pages, Bremen, 2000.

No. 167 **Santamarina Cuneo, P.**
Fluxes of suspended particulate matter through a tidal inlet of the East Frisian Wadden Sea (southern North Sea). 91 pages, Bremen, 2000.

No. 168 **Benthien, A.**
Effects of CO_2 and nutrient concentration on the stable carbon isotope composition of C37:2 alkenones in sediments of the South Atlantic Ocean. 104 pages, Bremen, 2001.

No. 169 **Lavik, G.**
Nitrogen isotopes of sinking matter and sediments in the South Atlantic. 140 pages, Bremen, 2001.

No. 170 **Budziak, D.**
Late Quaternary monsoonal climate and related variations in paleoproductivity and alkenone-derived sea-surface temperatures in the western Arabian Sea. 114 pages, Bremen, 2001.

No. 171 **Gerhardt, S.**
Late Quaternary water mass variability derived from the pteropod preservation state in sediments of the western South Atlantic Ocean and the Caribbean Sea. 109 pages, Bremen, 2001.

No. 172 **Bleil, U. and cruise participants**
Report and preliminary results of Meteor Cruise M 46/3, Montevideo (Uruguay) – Mar del Plata (Argentina), January 4 – February 7, 2000. Bremen, 2001.

No. 173 **Wefer, G. and cruise participants**
Report and preliminary results of Meteor Cruise M 46/4, Mar del Plata (Argentina) – Salvador da Bahia (Brazil), February 10 – March 13, 2000. With partial results of METEOR cruise M 46/2. 136 pages, Bremen, 2001.

No. 174 **Schulz, H.D. and cruise participants**
Report and preliminary results of Meteor Cruise M 46/2, Recife (Brazil) – Montevideo (Uruguay), December 2 – December 29, 1999. 107 pages, Bremen, 2001.

No. 175 **Schmidt, A.**
Magnetic mineral fluxes in the Quaternary South Atlantic: Implications for the paleoenvironment.
97 pages, Bremen, 2001.

No. 176 **Bruhns, P.**
Crystal chemical characterization of heavy metal incorporation in brick burning processes.
93 pages, Bremen, 2001.

No. 177 **Karius, V.**
Baggergut der Hafengruppe Bremen-Stadt in der Ziegelherstellung. 131 pages, Bremen, 2001.

No. 178 **Adegbie, A. T.**
Reconstruction of paleoenvironmental conditions in Equatorial Atlantic and the Gulf of Guinea Basins for the last 245,000 years. 113 pages, Bremen, 2001.

No. 179 **Spieß, V. and cruise participants**
Report and preliminary results of R/V Sonne Cruise SO 149, Victoria - Victoria, 16.8. - 16.9.2000.
100 pages, Bremen, 2001.

No. 180 **Kim, J.-H.**
Reconstruction of past sea-surface temperatures in the eastern South Atlantic and the eastern South Pacific across Termination I based on the Alkenone Method. 114 pages, Bremen, 2001.

No. 181 **von Lom-Keil, H.**
Sedimentary waves on the Namibian continental margin and in the Argentine Basin – Bottom flow reconstructions based on high resolution echosounder data. 126 pages, Bremen, 2001.

No. 182 **Hebbeln, D. and cruise participants**
PUCK: Report and preliminary results of R/V Sonne Cruise SO 156, Valparaiso (Chile) - Talcahuano (Chile), March 29 - May 14, 2001. 195 pages, Bremen, 2001.

No. 183 **Wendler, J.**
Reconstruction of astronomically-forced cyclic and abrupt paleoecological changes in the Upper Cretaceous Boreal Realm based on calcareous dinoflagellate cysts. 149 pages, Bremen, 2001.

No. 184 **Volbers, A.**
Planktic foraminifera as paleoceanographic indicators: production, preservation, and reconstruction of upwelling intensity. Implications from late Quaternary South Atlantic sediments. 122 pages, Bremen, 2001.

No. 185 **Bleil, U. and cruise participants**
Report and preliminary results of R/V METEOR Cruise M 49/3, Montevideo (Uruguay) - Salvador (Brasil), March 9 - April 1, 2001. 99 pages, Bremen, 2001.

No. 186 **Scheibner, C.**
Architecture of a carbonate platform-to-basin transition on a structural high (Campanian-early Eocene, Eastern Desert, Egypt) – classical and modelling approaches combined. 173 pages, Bremen, 2001.

No. 187 **Schneider, S.**
Quartäre Schwankungen in Strömungsintensität und Produktivität als Abbild der Wassermassen-Variabilität im äquatorialen Atlantik (ODP Sites 959 und 663): Ergebnisse aus Siltkorn-Analysen. 134 pages, Bremen, 2001.

No. 188 **Uliana, E.**
Late Quaternary biogenic opal sedimentation in diatom assemblages in Kongo Fan sediments. 96 pages, Bremen, 2002.

No. 189 **Esper, O.**
Reconstruction of Recent and Late Quaternary oceanographic conditions in the eastern South Atlantic Ocean based on calcareous- and organic-walled dinoflagellate cysts. 130 pages, Bremen, 2001.

No. 190 **Wendler, I.**
Production and preservation of calcareous dinoflagellate cysts in the modern Arabian Sea. 117 pages, Bremen, 2002.

No. 191 **Bauer, J.**
Late Cenomanian – Santonian carbonate platform evolution of Sinai (Egypt): stratigraphy, facies, and sequence architecture. 178 pages, Bremen, 2002.

No. 192 **Hildebrand-Habel, T.**
Die Entwicklung kalkiger Dinoflagellaten im Südatlantik seit der höheren Oberkreide. 152 pages, Bremen, 2002.

No. 193 **Hecht, H.**
Sauerstoff-Optopoden zur Quantifizierung von Pyritverwitterungsprozessen im Labor- und Langzeit-in-situ-Einsatz. Entwicklung - Anwendung – Modellierung. 130 pages, Bremen, 2002.

No. 194 **Fischer, G. and cruise participants**
Report and Preliminary Results of RV METEOR-Cruise M49/4, Salvador da Bahia – Halifax, 4.4.-5.5.2001. 84 pages, Bremen, 2002.

No. 195 **Gröger, M.**
Deep-water circulation in the western equatorial Atlantic: inferences from carbonate preservation studies and silt grain-size analysis. 95 pages, Bremen, 2002.

No. 196 **Meinecke,G. and cruise participants**
Report of RV POSEIDON Cruise POS 271, Las Palmas - Las Palmas, 19.3.-29.3.2001. 19 pages, Bremen, 2002.

No. 197 **Meggers, H. and cruise participants**
Report of RV POSEIDON Cruise POS 272, Las Palmas - Las Palmas, 1.4.-14.4.2001. 19 pages, Bremen, 2002.

No. 198 **Gräfe, K.-U.**
Stratigraphische Korrelation und Steuerungsfaktoren Sedimentärer Zyklen in ausgewählten Borealen und Tethyalen Becken des Cenoman/Turon (Oberkreide) Europas und Nordwestafrikas. 197 pages, Bremen, 2002.

No. 199 **Jahn, B.**
Mid to Late Pleistocene Variations of Marine Productivity in and Terrigenous Input to the Southeast Atlantic. 97 pages, Bremen, 2002.

No. 200 **Al-Rousan, S.**
Ocean and climate history recorded in stable isotopes of coral and foraminifers from the northern Gulf of Aqaba. 116 pages, Bremen, 2002.

No. 201 **Azouzi, B.**
Regionalisierung hydraulischer und hydrogeochemischer Daten mit geostatistischen Methoden.
108 pages, Bremen, 2002.

No. 202 **Spieß, V. and cruise participants**
Report and preliminary results of METEOR Cruise M 47/3, Libreville (Gabun) - Walvis Bay (Namibia), 01.06 - 03.07.2000. 70 pages, Bremen 2002.

No. 203 **Spieß, V. and cruise participants**
Report and preliminary results of METEOR Cruise M 49/2, Montevideo (Uruguay) - Montevideo, 13.02 - 07.03.2001. 84 pages, Bremen 2002.

No. 204 **Mollenhauer, G.**
Organic carbon accumulation in the South Atlantic Ocean: Sedimentary processes and glacial/interglacial Budgets. 139 pages, Bremen 2002.

No. 205 **Spieß, V. and cruise participants**
Report and preliminary results of METEOR Cruise M49/1, Cape Town (South Africa) - Montevideo (Uruguay), 04.01.2001 - 10.02.2001. 57 pages, Bremen, 2003.

No. 206 **Meier, K.J.S.**
Calcareous dinoflagellates from the Mediterranean Sea: taxonomy, ecology and palaeoenvironmental application. 126 pages, Bremen, 2003.

No. 207 **Rakic, S.**
Untersuchungen zur Polymorphie und Kristallchemie von Silikaten der Zusammensetzung $Me_2Si_2O_5$ (Me:Na, K). 139 pages, Bremen, 2003.

No. 208 **Pfeifer, K.**
Auswirkungen frühdiagenetischer Prozesse auf Calcit- und Barytgehalte in marinen Oberflächen-sedimenten. 110 pages, Bremen, 2003.

No. 209 **Heuer, V.**
Spurenelemente in Sedimenten des Südatlantik. Primärer Eintrag und frühdiagenetische Überprägung. 136 pages, Bremen, 2003.

No. 210 **Streng, M.**
Phylogenetic Aspects and Taxonomy of Calcareous Dinoflagellates. 157 pages, Bremen 2003.

No. 211 **Boeckel, B.**
Present and past coccolith assemblages in the South Atlantic: implications for species ecology, carbonate contribution and palaeoceanographic applicability. 157 pages, Bremen, 2003.

No. 212 **Precht, E.**
Advective interfacial exchange in permeable sediments driven by surface gravity waves and its ecological consequences. 131 pages, Bremen, 2003.

No. 213 **Frenz, M.**
Grain-size composition of Quaternary South Atlantic sediments and its paleoceanographic significance. 123 pages, Bremen, 2003.

No. 214 **Meggers, H. and cruise participants**
Report and preliminary results of METEOR Cruise M 53/1, Limassol - Las Palmas – Mindelo, 30.03.2002 - 03.05.2002. 81 pages, Bremen, 2003.

No. 215 **Schulz, H.D. and cruise participants**
Report and preliminary results of METEOR Cruise M 58/1, Dakar – Las Palmas, 15.04..2003 - 12.05.2003. Bremen, 2003.

No. 216 **Schneider, R. and cruise participants**
Report and preliminary results of METEOR Cruise M 57/1, Cape Town – Walvis Bay, 20.01. – 08.02.2003. 123 pages, Bremen, 2003.

No. 217 **Kallmeyer, J.**
Sulfate reduction in the deep Biosphere. 157 pages, Bremen, 2003.

No. 218 **Røy, H.**
Dynamic Structure and Function of the Diffusive Boundary Layer at the Seafloor. 149 pages, Bremen, 2003.

No. 219 **Pätzold, J., C. Hübscher and cruise participants**
Report and preliminary results of METEOR Cruise M 52/2&3, Istanbul – Limassol – Limassol, 04.02. – 27.03.2002. Bremen, 2003.

No. 220 **Zabel, M. and cruise participants**
Report and preliminary results of METEOR Cruise M 57/2, Walvis Bay – Walvis Bay, 11.02. – 12.03.2003. 136 pages, Bremen 2003.

No. 221 **Salem, M.**
Geophysical investigations of submarine prolongations of alluvial fans on the western side of the Gulf of Aqaba-Red Sea. 100 pages, Bremen, 2003.

No. 222 **Tilch, E.**
Oszillation von Wattflächen und deren fossiles Erhaltungspotential (Spiekerooger Rückseitenwatt, südliche Nordsee). 137 pages, Bremen, 2003.

No. 223 **Frisch, U. and F. Kockel**
Der Bremen-Knoten im Strukturnetz Nordwest-Deutschlands. Stratigraphie, Paläogeographie, Strukturgeologie. 379 pages, Bremen, 2004.

No. 224 **Kolonic, S.**
Mechanisms and biogeochemical implications of Cenomanian/Turonian black shale formation in North Africa: An integrated geochemical, millennial-scale study from the Tarfaya-LaAyoune Basin in SW Morocco. 174 pages, Bremen, 2004. Report online available only.

No. 225 **Panteleit, B.**
Geochemische Prozesse in der Salz- Süßwasser Übergangszone. 106 pages, Bremen, 2004.

No. 226 **Seiter, K.**
Regionalisierung und Quantifizierung benthischer Mineralisationsprozesse. 135 pages, Bremen, 2004.

No. 227 **Bleil, U. and cruise participants**
Report and preliminary results of METEOR Cruise M 58/2, Las Palmas – Las Palmas (Canary Islands, Spain), 15.05. – 08.06.2003. 123 pages, Bremen, 2004.

No. 228 **Kopf, A. and cruise participants**
Report and preliminary results of SONNE Cruise SO175, Miami - Bremerhaven, 12.11 - 30.12.2003. 218 pages, Bremen, 2004.

No. 229 **Fabian, M.**
Near Surface Tilt and Pore Pressure Changes Induced by Pumping in Multi-Layered Poroelastic Half-Spaces. 121 pages, Bremen, 2004.

No. 230 **Segl, M. , and cruise participants**
Report and preliminary results of POSEIDON cruise 304 Galway – Lisbon, 5. – 22. Oct. 2004. 27 pages, Bremen 2004

No. 231 **Meinecke, G. and cruise participants**
Report and preliminary results of POSEIDON Cruise 296, Las Palmas – Las Palmas, 04.04 - 14.04.2003. 42 pages, Bremen 2005.

No. 232 **Meinecke, G. and cruise participants**
Report and preliminary results of POSEIDON Cruise 310, Las Palmas – Las Palmas, 12.04 - 26.04.2004. 49 pages, Bremen 2005.

No. 233 **Meinecke, G. and cruise participants**
Report and preliminary results of METEOR Cruise 58/3, Las Palmas - Ponta Delgada, 11.06 - 24.06.2003. 50 pages, Bremen 2005.

No. 234 **Feseker, T.**
Numerical Studies on Groundwater Flow in Coastal Aquifers. 219 pages. Bremen 2004.

No. 235 **Sahling, H. and cruise participants**
Report and preliminary results of R/V POSEIDON Cruise P317/4, Istanbul-Istanbul , 16 October - 4 November 2004. 92 pages, Bremen 2004.

No. 236 **Meinecke, G. und Fahrtteilnehmer**
Report and preliminary results of POSEIDON Cruise 305, Las Palmas (Spain) - Lisbon (Portugal), October 28th – November 6th, 2004. 43 pages, Bremen 2005.

No. 237 **Ruhland, G. and cruise participants**
Report and preliminary results of POSEIDON Cruise 319, Las Palmas (Spain) - Las Palmas (Spain), December 6th – December 17th, 2004. 50 pages, Bremen 2005.

No. 238 **Chang, T.S.**
Dynamics of fine-grained sediments and stratigraphic evolution of a back-barrier tidal basin of the German Wadden Sea (southern North Sea). 102 pages, Bremen 2005.

No. 239 **Lager, T.**
Predicting the source strength of recycling materials within the scope of a seepage water prognosis by means of standardized laboratory methods. 141 pages, Bremen 2005.

No. 240 **Meinecke, G.**
DOLAN - Operationelle Datenübertragung im Ozean und Laterales Akustisches Netzwerk in der Tiefsee. Abschlußbericht. 42 pages, Bremen 2005.

No. 241 **Guasti, E.**
Early Paleogene environmental turnover in the southern Tethys as recorded by foraminiferal and organic-walled dinoflagellate cysts assemblages. 203 pages, Bremen 2005.

No. 242 **Riedinger, N.**
Preservation and diagenetic overprint of geochemical and geophysical signals in ocean margin sediments related to depositional dynamics. 91 pages, Bremen 2005.

No. 243 **Ruhland, G. and cruise participants**
Report and preliminary results of POSEIDON cruise 320, Las Palmas (Spain) - Las Palmas (Spain), March 08th - March 18th, 2005. 57 pages, Bremen 2005.

No. 244 **Inthorn, M.**
Lateral particle transport in nepheloid layers – a key factor for organic matter distribution and quality in the Benguela high-productivity area. 127 pages, Bremen, 2006.

No. 245 **Aspetsberger, F.**
Benthic carbon turnover in continental slope and deep sea sediments: importance of organic matter quality at different time scales. 136 pages, Bremen, 2006.

No. 246 **Hebbeln, D. and cruise participants**
Report and preliminary results of RV SONNE Cruise SO-184, PABESIA, Durban (South Africa) – Cilacap (Indonesia) – Darwin (Australia), July 08th - September 13th, 2005. 142 pages, Bremen 2006.

No. 247 **Ratmeyer, V. and cruise participants**
Report and preliminary results of RV METEOR Cruise M61/3. Development of Carbonate Mounds on the Celtic Continental Margin, Northeast Atlantic. Cork (Ireland) – Ponta Delgada (Portugal), 04.06. – 21.06.2004. 64 pages, Bremen 2006.

No. 248 **Wien, K.**
Element Stratigraphy and Age Models for Pelagites and Gravity Mass Flow Deposits based on Shipboard XRF Analysis. 100 pages, Bremen 2006.

No. 249 **Krastel, S. and cruise participants**
Report and preliminary results of RV METEOR Cruise M65/2, Dakar - Las Palmas, 04.07. - 26.07.2005. 185 pages, Bremen 2006.

No. 250 **Heil, G.M.N.**
Abrupt Climate Shifts in the Western Tropical to Subtropical Atlantic Region during the Last Glacial. 121 pages, Bremen 2006.

No. 251 **Ruhland, G. and cruise participants**
Report and preliminary results of POSEIDON Cruise 330, Las Palmas – Las Palmas, November 21th – December 03rd, 2005. 48 pages, Bremen 2006.

No. 252 **Mulitza , S. and cruise participants**
Report and preliminary results of METEOR Cruise M65/1, Dakar – Dakar, 11.06.- 1.07.2005. 149 pages, Bremen 2006.

No. 253 **Kopf, A. and cruise participants**
Report and preliminary results of POSEIDON Cruise P336, Heraklion - Heraklion, 28.04. – 17.05.2006. 127 pages, Bremen, 2006.

No. 254 **Wefer, G. and cruise participants**
Report and preliminary results of R/V METEOR Cruise M65/3, Las Palmas - Las Palmas (Spain), July 31st - August 10th, 2005. 24 pages, Bremen 2006.

No. 255 **Hanebuth, T.J.J. and cruise participants**
Report and first results of the POSEIDON Cruise P342 GALIOMAR, Vigo – Lisboa (Portugal), August 19th – September 06th, 2006. Distribution Pattern, Residence Times and Export of Sediments on the Pleistocene/Holocene Galician Shelf (NW Iberian Peninsula). 203 pages, Bremen, 2007.

No. 256 **Ahke, A.**
Composition of molecular organic matter pools, pigments and proteins, in Benguela upwelling and Arctic Sediments. 192 pages, Bremen 2007.

No. 257 **Becker, V.**
Seeper - Ein Modell für die Praxis der Sickerwasserprognose. 170 pages, Bremen 2007.

No. 258 **Ruhland, G. and cruise participants**
Report and preliminary results of Poseidon cruise 333, Las Palmas (Spain) – Las Palmas (Spain), March 1st – March 10th, 2006. 32 pages, Bremen 2007.

No. 259 **Fischer, G., G. Ruhland and cruise participants**
Report and preliminary results of Poseidon cruise 344, leg 1 and leg 2, Las Palmas (Spain) – Las Palmas (Spain), Oct. 20th –Nov 2nd & Nov. 4th – Nov 13th, 2006. 46 pages, Bremen 2007.

No. 260 **Westphal, H. and cruise participants**
Report and preliminary results of Poseidon cruise 346, MACUMA. Las Palmas (Spain) – Las Palmas (Spain), 28.12.2006 – 15.1.2007. 49 pages, Bremen 2007.

No. 261 **Bohrmann, G., T. Pape, and cruise participants**
Report and preliminary results of R/V METEOR Cruise M72/3, Istanbul – Trabzon – Istanbul, 17 March – 23 April, 2007. Marine gas hydrates of the Eastern Black Sea. 130 pages, Bremen 2007.